

AD623718

SEMI-ANNUAL TECHNICAL SUMMARY

for the period ending 30 SEPTEMBER 1965

to

ADVANCED RESEARCH PROJECTS AGENCY

RESEARCH ON ELECTROMAGNETICS FOR PROJECT DEFENDER

ARPA Order No. 529

Program Code No. 5730

CLEARINGHOUSE  
FOR FEDERAL SCIENTIFIC AND  
TECHNICAL INFORMATION

Hardcopy

Microfiche

\$5.00

\$1.25

1980

ARCHIVE COPY

Code 1

Report  
R-1295.1-65

for  
Office of Naval Research  
Contract Nonr-839 (38)

D.O.C.  
RECEIVED  
SEP 21 1965  
OFFICE OF THE  
DIRECTOR

POLYTECHNIC INSTITUTE OF BROOKLYN

**BEST  
AVAILABLE COPY**

SEMI-ANNUAL TECHNICAL SUMMARY

*for the period ending 30 SEPTEMBER 1965*

to

ADVANCED RESEARCH PROJECTS AGENCY

RESEARCH ON ELECTRO MAGNETICS FOR PROJECT DEFENDER

ARPA Order No. 529

Program Code No. 5730

Report  
R-1295.1-65

for  
Office of Naval Research  
Contract Nonr - 839 (38)

Submitted by: ERNST WEBER, President

Coordinated by: Rudolf G. E. Hutter,  
Professor of Electrophysics

**POLYTECHNIC INSTITUTE OF BROOKLYN**

PIBMRI-1295.1-65

ACKNOWLEDGEMENT

The work reported herein was sponsored by the Advanced Research Projects Agency, ARPA Order No. 529, Program Code No. 5730, and was monitored by the Office of Naval Research, Washington, D. C. under Contract No. Nonr-839(38).

ABSTRACT

In this semi-annual report progress on a fairly large number of projects is described. In general, these projects deal with electromagnetic phenomena in plasmas and plasma-like media, such as the properties of antennas, excitation of electromagnetic waves in plasmas, coupling of acoustic and electromagnetic waves, propagation through time varying, random media, electron densities in shock waves, basic kinetic theory of ionized media, instabilities in plasmas, properties of laboratory type plasmas, etc. A smaller group of projects deals with characteristics of transmitters and receivers for communication through randomly time varying media and with the problem of pattern recognition.

TABLE OF CONTENTS

	<u>Page</u>
ACKNOWLEDGEMENT	ii
ABSTRACT	iii
TABLE OF CONTENTS	iv
INTRODUCTION	1
1. PLASMAS	3
Introduction	3
1.1 The Plasma Laboratory	4
1.2 Resistive Instabilities in a Toroidal Plasma	6
1.3 Spectroscopic Study of a Toroidal Discharge	11
1.4 Magnetic Probing of a Toroidal Discharge	19
1.5 Experimental Study of the Screen Cathode Discharge	25
1.6 An Air Filled Discharge Chamber	32
1.7 Interaction of High Energy Electron Beams with a Plasma	35
1.8 Plasma Sheath Studies	37
1.9 Plasma Boundary Oscillations	41
1.10 Perturbation Procedure for Nonlinear Plasma Equations	46
1.11 Kinetic Theoretical Investigations of a Fully Ionized Gas	53
1.12 Kinetic Theory of Plasmas	55
2. ELECTROMAGNETICS	58
Introduction	58
2.1 Diffraction by a Half Plane in a Compressible Homogeneous Plasma	60
2.2 Slot Antenna in a Plasma	68
2.3 Coupling of Acoustic and Electromagnetic Waves	70
2.4 Group Velocity and Power Flow Relations for Surface Waves in Plane-Stratified Anisotropic Media	76
2.5 Diffraction by a Transparent Elliptical Cylinder	83
2.6 Cerenkov Radiation in Dielectric Media	90
2.6.1 Dielectric Filled Infinite Space, One Electron	90
2.6.2 Dielectric Filled Infinite Space, Finite Train of (N+1) Electrons	92
2.6.3 Dielectric in Cylindrical Waveguide, One Electron	93
2.6.4 Dielectric in Cylindrical Waveguide, Finite Train of (N+1) Electrons	94

TABLE OF CONTENTS (continued)

	<u>Page</u>
2.6.5 Dielectric Filled Cavity, One Electron	95
2.6.6 Dielectric Filled Waveguide, Finite Train of (N+1) Electrons	96
2.7 Cerenkov Radiation in a Infinite Magneto-Plasma	98
2.8 Transition Radiation	104
2.9 Radiation by a Uniformly Rotating Line Charge in a Plasma	107
2.10 Experimental Work in Connection with Cerenkov and Transition Radiation	108
2.10.1 The Rebatron	108
2.10.2 Beam Measurements	109
2.10.3 Planned Experiment with Plasma	109
2.10.4 Screen Discharge	110
2.11 Propagation of Waves in Plasma Waveguides	111
3. FLUID DYNAMICS	113
Introduction	113
3.1 Resonant Cavity Techniques for Measurement of Electron Density Collision Frequency of Hypersonic Flows	115
3.1.1 General Data	115
3.1.2 Preliminary Data on Cavity Measurement of Electron Density in the 5' Shock Tunnel	117
3.1.3 Design Data for Smooth Bore T. M. Diagnostic Cavities	120
3.1.4 Measurement of Electron Density and Collision Frequency of a Field Induced Plasma	132
3.2 Microwave Resonant Cavity Measurement of Shock Produced Electron Precursors	139
3.3 Electron Density and Relaxation Time Measurement Behind a Reflected Shock	146
3.4 Measurement of Time-Resolved Electron Density	153
3.5 An Experimental Investigation of the Near Wake of a Slender Cone at $M_{\infty} = 8$ and 12	156
3.6 Utilization of Hot-Wire Anemometer	157
3.7 Ion Beam Collision Studies	162
3.8 Similar Solution of the Steady Incompressible MHD Flow in a Slender Channel	164

TABLE OF CONTENTS (continued)

	<u>Page</u>
4. COMMUNICATIONS AND PATTERN RECOGNITION	166
Introduction	166
4.1 Extending the Phase Locked Loop Threshold	167
4.2 Fading Channels and Communication Through Fading	168
4.3 Analysis of an F. M. Discriminator with Fading Signal Plus Additive Gaussian Noise	169
4.4 Optimum Demodulation Using Bayes Criterion in Random Channels	171
4.5 Realizable Approximations to Optimum Analog Demodulators	173
4.6 Pattern Recognition Theory	175
5. EDUCATION, PARTICIPATION IN COMMITTEES, REPORTS AND PUBLICATIONS	184
5.1 Education	184
5.2 Participation in Committees	187
5.3 Reports and Publications	188
5.3.1 Reports	188
5.3.2 Published papers	189
DISTRIBUTION LIST	vii
DD FORM 1473	

## INTRODUCTION

The ARPA-Polytechnic program is an academically oriented effort directed to the satisfaction of both the teaching needs of the Polytechnic and some mission oriented needs of the ARPA. Faculty from several academic departments of the Institute have joined together in setting up a unified interdisciplinary program in keeping with the stated philosophy. As a preliminary goal, an attempt has been made to institute and coordinate research and teaching efforts relevant to phenomena associated with hypersonic objects moving through the upper atmosphere and their detection. To this end several departments have developed and are continuing to explore research and teaching programs bearing on physical, chemical, aerodynamic, electromagnetic, and communication problems relating to plasma, shock, wake, etc., phenomena associated with missile reentry.

More specifically, the Electrophysics department has reoriented some of its ongoing efforts in electromagnetics, microwaves, and plasmas in accord with overall planning for the ARPA-Polytechnic program. Effects of plasma sheaths on radiation from antennas on missile cones and scattering from reentry missile wakes, for example, pose basic problems whose understanding has given rise to a number of projects directed toward evolving adequate theoretical techniques and laboratory plasma facilities for their treatment. In a coordinated effort with the Aerospace and Applied Mechanics department, special microwave instrumentation and techniques for hypersonic flow measurements are being explored and appear to offer considerable promise. Furthermore, the latter department is directing its attention to the measurement and theory of a variety of plasma phenomena associated with hypersonic shocks and their reflection, in addition to studies of near wake flows. Members of the Physics department have concentrated on understanding the kinetic basis for plasma dynamics and through studies of Landau damping and diffusion phenomena have attempted to contribute toward the development of an acceptable set of plasma equations suitable for use in engineering problems -- no simple task in view of the complexity of the phenomena to be described. In its contribution to the ARPA program the Electrical Engineering department has concerned itself with fading,

random channels, optimum detection, etc., and in collaboration with the department of Electrophysics, with pattern recognition and the radar signature problem.

More detailed accounts of the above activities are presented in the body of this first semi-annual report. It should be recognized that a good deal of effort is being devoted to shaping up a unified program of relevance to DEFENDER; the present report still represents only a preliminary indication of what may ultimately develop. In appraising the current programmatic trend, one is struck by a definite inter-departmental endeavor of faculty versed in conventional electromagnetic, microwave, aerodynamic, etc., techniques to extend and modify this knowledgeability for application to the type of plasma phenomena encountered in many DEFENDER problems. Projects that appear to be of more direct significance in this connection are receiving emphasis, while others are being deemphasized or transferred to other Institute programs. By way of illustration, the communications projects reported below are in the near future to be supported by other than ARPA means. This process of shifting support depending on relevance to the DEFENDER program, since the ARPA program is budgetarily a little over 10% of the Institute research effort, is intended as a realistic administrative procedure for optimization of the Polytechnic contribution.

The development of course programs for interdisciplinary training of graduate engineers in areas of interest to DEFENDER and the participation of Polytechnic faculty in ARPA Committee activities should also be noted.

N. Marcuvitz  
Institute Professor

## 1. PLASMAS

### Introduction

The plasma dynamic phase of the ARPA program has the dual theme of creating viable laboratory plasmas with well-defined surfaces and of developing effective analytical tools for the description of dynamic phenomena within and on the surfaces of such plasma. A primary motivation hereby is the experimental and theoretical study of wave propagation along and scattering from plasma interfaces with particular relevance to the effect of plasma sheaths on radiation from antennas and of scattering from ionized wakes.

The utility of a laboratory plasma demands an understanding of the inner structure of the plasma, i. e. knowledge of the electron density, temperature, ionic constituents, homogeneity, anisotropy, etc. properties as well as dynamic and stability characteristics. In this respect two distinct plasma structures, the toroidal discharge and the screen cathode discharge, are being investigated and reported on below. Particular attention is being paid to the development of several diagnostic techniques for the measurement of static plasma parameters. In addition, the presence of dynamic instabilities within and on the surface of laboratory plasmas makes their study essential; the dynamic structure and oscillations within the plasma sheath are receiving detailed consideration and are reported on.

The analytical understanding of plasma phenomena is of course dependent upon an unobjectionable and workable set of plasma equations descriptive of the dynamical and electromagnetic properties of a real plasma. Studies of the BBGKY hierarchy derived from the Liouville equation, the validity and approximate nature of the Boltzmann-Landau equation, and the coarser approximations of the macroscopic transport plus Maxwell equations continue to occupy the attention of a number of the faculty. In these terms Landau damping, diffusion, electro-plasma waves, electron beam excitation in plasmas are being studied in both the linear and nonlinear regime. A general study of nonlinear techniques for the solution of a class of nonlinear plasma problems is also reported upon.

N. Marcuvitz  
Institute Professor

### 1.1 The Plasma Laboratory

Many of the problems concerning electromagnetic and acoustic wave phenomena in plasmas discussed in this report require theoretical as well as experimental efforts if their solutions are designed to apply to phenomena in real plasmas. It is therefore necessary to develop and study a number of plasma configurations that can be produced in a laboratory. Through such studies it becomes possible to evaluate the applicability of certain theoretical assumptions and thus to determine the validity of theoretical predictions.

Starting about a year ago from a number of nuclei, a plasma laboratory has been organized and developed which is now supporting a range of experimental projects. In addition to carrying out specific experimental studies, which are described in parts of this report, the laboratory offers the opportunity for training students in experimental techniques such as arising from the use of vacuum systems, microwave measuring techniques, spectroscopic techniques, etc.

The laboratory is equipped with a variety of vacuum stations, high-power pulse sources, electronic, optical, and microwave measuring instruments as well as a dark room for photographic work. In addition, a glass-blowing shop, a model shop and a chemical laboratory provide supporting services for the laboratory. Another microwave measurements laboratory is also available for preliminary work which does not require the facilities of the plasma laboratory.

Two general views of some of the facilities are shown in Figs. 1 and 2. Studies on the toroidal discharge, described in Sections 1.2 to 1.4, are carried out on the set-up shown in Fig. 3. Langmuir probe studies of the screen cathode discharge are conducted on the apparatus shown in Fig. 4 and are reported in Section 1.5. A microwave measurement bench is shown in Fig. 5 which was used in connection with experiments on Tonks-Dattner resonances described in Section 2.3.

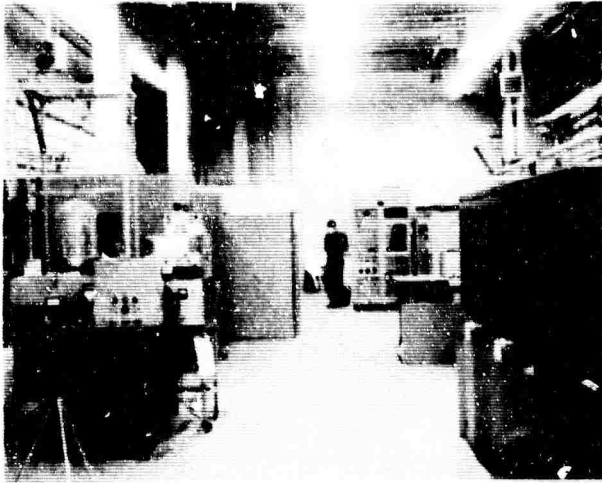


FIG. 1 (1-1)-GENERAL VIEW

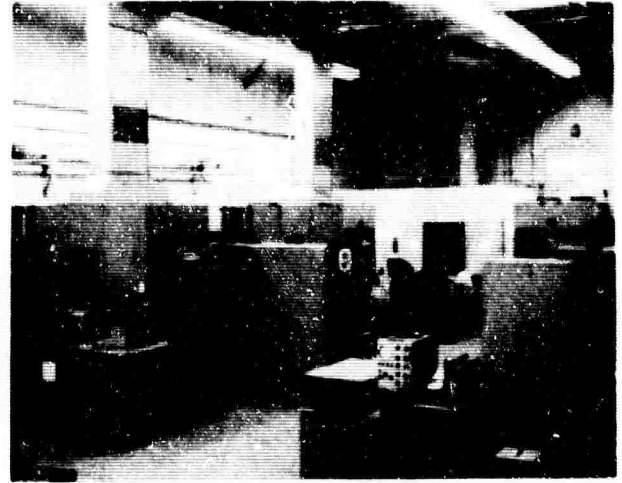


FIG. 2 (1-2) -GENERAL VIEW

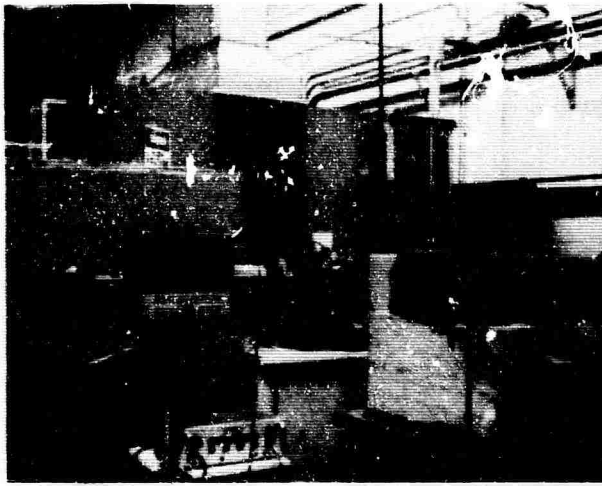


FIG. 3 (1-3)-SET-UP FOR TOROIDAL DISCHARGE

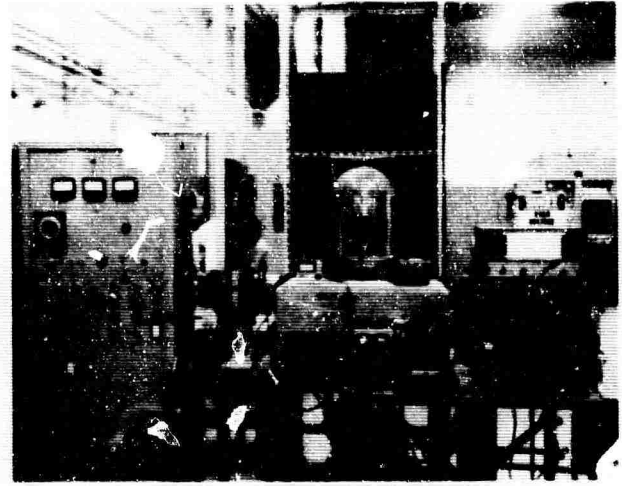


FIG. 4 (1-4)-SCREENED CATHODE DISCHARGE STUDIES

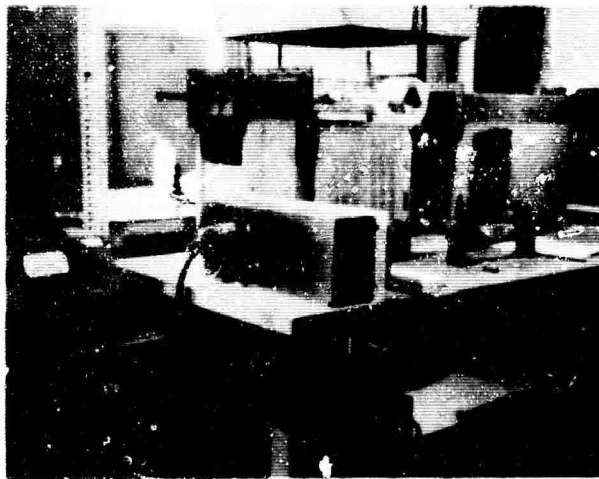


FIG. 5 (1-5)-TONKS-DATTNER RESONANCES SET-UP

The rebatron discussed in Section 2.10 and shown as Fig. 1 in Section 2.10.1 is also part of the plasma laboratory.

H. Farber  
Electrophysics Department

1.2 Resistive Instabilities in a Toroidal Plasma

Introduction

This report describes the observations of two instabilities found within a toroidal plasma which is illustrated in Fig. 1. The instabilities appear to be the

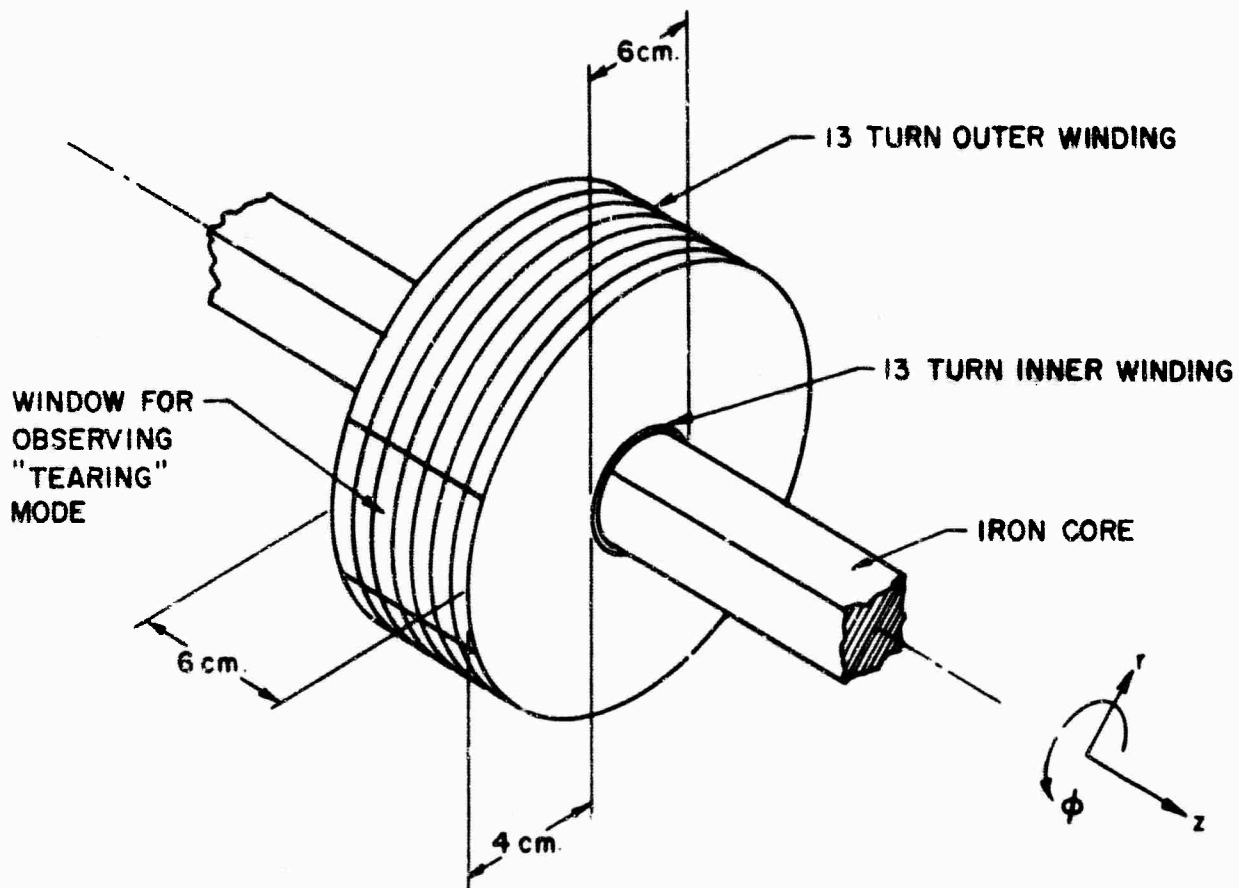


Fig. 1 (1-6) - Toroidal plasma bottle

resistive "tearing" and "gravitational" (Rayleigh-Taylor) modes described theoretically by Furch, Killeen, and Rosenbluth<sup>1</sup> and Coppi, Greene and Johnson.<sup>2</sup> The "tearing" mode has been observed experimentally by Bodin<sup>3</sup>, and of course many experimenters have witnessed the "gravitational" mode. For various drive currents and neutral pressures of hydrogen gas either the "tearing" mode can be observed along the z-axis or the "gravitational" mode can be observed along the r-axis.

Physically, a null or zero in the confining magnetic field is required to excite the "tearing" mode. For the "gravitational" mode to be excited, a small mass and a large magnetic field which is capable of accelerating the mass is required.

Our effort has been concentrated on the tearing mode since there is much current theoretical interest in this mode and the critical null in magnetic field can be detected experimentally with little difficulty.

#### The "Tearing Mode"

The theory presented in references 1 and 2 relate the instability to  $\tau_R$ , a resistive diffusion time, and  $\tau_H$ , a magnetohydrodynamic transit time. The characteristic growth time is  $\tau_R^{-3/5} \tau_H^{-2/5}$  where

$$\tau_R = \frac{4\pi a^2}{\langle \eta \rangle} \quad \text{and} \quad \tau_H = \frac{a(4\pi \langle \rho \rangle)^{1/2}}{B}$$

and the units are in e.m.u.

B is magnetic flux density in gauss,  $\langle \rho \rangle$  is the average mass density in gram/cc.,  $\langle \eta \rangle$  is the resistivity in e.m.u, and a is a characteristic dimension at the plasma in centimeters.

If we choose to look at the voltage and current in Fig. 2 at a time of one microsecond, we find V = 600 volts and I = 5200 amperes. Since the cross section of the plasma is about 2cm x 4cm we can compute  $\langle \eta \rangle$ .

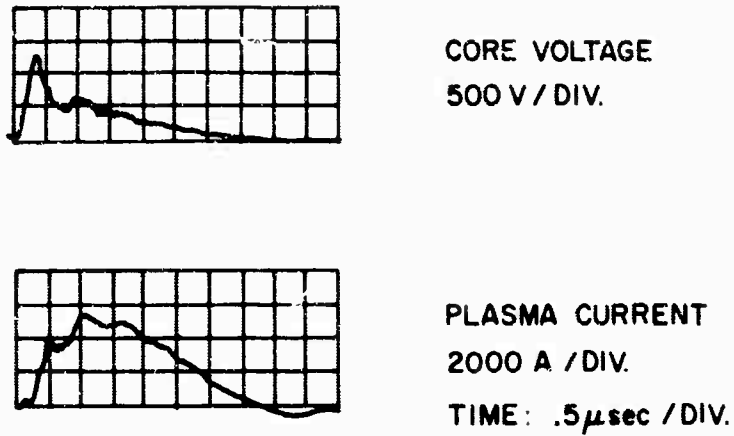


Fig. 2 (1-7)

$$\langle \eta \rangle = \frac{VA}{I2\pi R} \quad \text{where } R \text{ is the average radius of the plasma (5 cm.)}$$

Substituting, we find that

$$\langle \eta \rangle = 2.94 \times 10^{-8} \text{ e.m.u.}$$

When only the inner winding of the toroid is excited, B can be approximated by

$$B = \frac{\mu_0 I}{2\pi R} \times 10^4 \text{ in gauss.}$$

Using the numbers above we have B = 1630 gauss.

From spectrographic analysis of line merging we have a number density of about  $10^{25}$  particle/cc. Therefore  $\langle \rho \rangle = 9.1 \times 10^{-13}$  for the electrons.

Now we assume that a characteristic length of the plasma is half its width or  $a \approx 2$  centimeters for the purpose of calculating  $\tau_R$  and  $\tau_H$ . Then,

$$\tau_R = \frac{4\pi a^2}{\langle \eta \rangle} \approx 2 \times 10^{-6} \text{ seconds and } \tau_H = \frac{a(4\pi \langle \rho \rangle)^{1/2}}{B} \approx 10^{-8} \text{ seconds.}$$

According to the theory, the characteristic time is  $\tau_R^{-3/5} \tau_H^{-2/5}$ . Our values of  $\tau_R$  and  $\tau_H$  yield an e-folding time of .25 microseconds based on the data obtained at one microsecond after the toroidal plasma was initiated. For lower currents or larger resistivity, the e-folding time would be larger. Putting it another way, the growth rate of the instability would be slower.

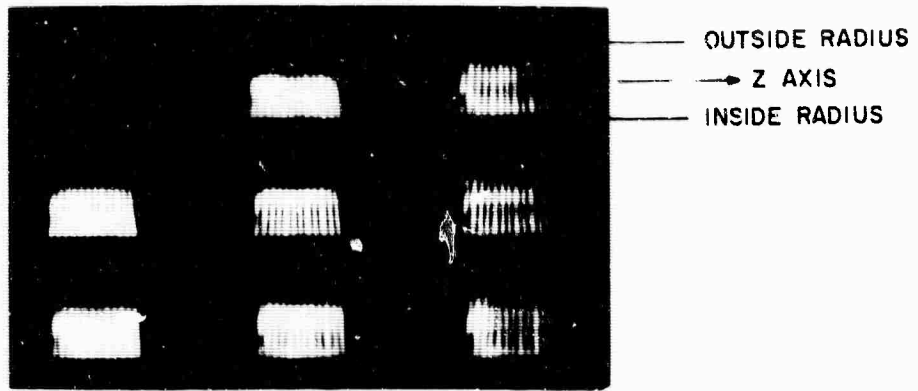
Photographs taken with an S. T. L. image converter camera and shown in Fig. 3 indicate a growth that takes approximately two microseconds for the separation to become comparable with the plasma cross section. This does not appear to be a resistive diffusion process since with the outside winding excited there is no separation of plasma, yet the current, number density, and resistivity are about the same. The significant difference is in the structure of the magnetic field. With the outer winding unexcited, the magnetic field on top of the plasma is weak; however, when this winding is excited the magnetic field is much stronger. It is this difference that determines if the "tearing" mode will be permitted or not.

Recent measurements of axial magnetic field,  $B_z$ , show a null that propagates from the outer radius to the inner radius during a time interval that is consistent with the separation of plasma recorded by the image converter camera.

#### Future Work

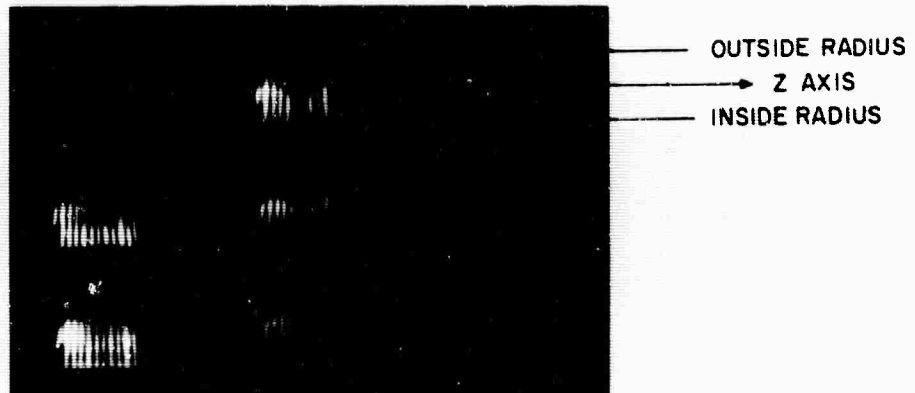
During the next period a complete space and time resolved record of magnetic field and number density will be correlated in order to yield  $\tau_R$  and  $\tau_H$  as functions of time. The exponential growth rate will then be numerically integrated so that the actual motion of the "tearing" mode can be simulated. Also, we shall measure the critical current in the outer winding required for the onset of the instability.

These two results shall either confirm the theory as it now stands or at least indicate what refinements must be made to obtain better agreement between



a. OUTSIDE WINDING EXCITED

TIME ( $\mu$ sec.)	{	0.0	1.5	3.0
		0.5	2.0	3.5
		1.0	2.5	4.0



b. OUTSIDE WINDING NOT EXCITED

TIME ( $\mu$ sec.)	{	0.0	1.5	3.0
		0.5	2.0	3.5
		1.0	2.5	4.0

FIG. 3 (1-8)-FRAMING PHOTOGRAPHS

theory and experiment.

K. Stuart  
Electrophysics Department

References

1. H.P. Furth, J. Killeen, and M.N. Rosenbluth, Phys. Fluids 6, 459 (1963).
2. B. Coppi, J.M. Greene, and J.L. Johnson, AEC Research and Development Report, MATT-326 (March 1965).
3. H.A.B. Bodin, Nuclear Fusion 3 (1963).

1.3 Spectroscopic Study of a Toroidal Discharge

Measurements of the relative intensities of the spectral lines of the Balmen series in atomic hydrogen may be used to compute the temperature of a discharge. A series of oscillograms of the light intensities in different regions of the discharge may be used to compute the discharge temperature as a function of time and position.

If we consider radiative de-excitations from atomic states  $n$  and  $m$ , ( $n$  greater than  $m$ ), to a third state  $i$ , then we can obtain the discharge temperature from the following relationship,

$$KT = \frac{E_n - E_m}{\ln\left[\frac{g_n A_{ni} \lambda_{mi} I_{mi}}{g_m A_{mi} \lambda_{ni} I_{ni}}\right]} \quad (1)$$

where  $K$  is Boltzmann's constant,  $E_n$  and  $E_m$  are the energies of the states  $n$  and  $m$ , measured with respect to the ground state;  $g_n$ ,  $g_m$  are the degeneracies of these states;  $A_{ni}$ ,  $A_{mi}$  are the Einstein transition probabilities for the respective transitions;  $\lambda_{ni}$ ,  $\lambda_{mi}$  are the wavelengths of the lines, and  $I_{ni}$ ,  $I_{mi}$  are the relative intensities of the lines. We shall be dealing with transitions from the third, fourth and fifth levels to the second level.

The underlying assumption behind Eq. (1), and the condition necessary for

it to have any meaning, is that the plasma be in a state of local thermodynamic equilibrium. Considering the plasma as a system of bound and free electron states, this means that there is an equipartition of energy among not only the free states, but at least several of the bound states. Stated alternatively, there is local thermodynamic equilibrium when the Maxwellian energy distribution which characterizes the free electron states extends downward into the bound electron states. In a sufficiently dense laboratory plasma, the collisions between the free electrons tend to randomize their motion and quickly bring about a Maxwellian distribution. The free electrons dominate the electronic excitation rates. In order for the excited states to thermalize, their de-excitation will have to be primarily by collisional effects also. For these states, local thermodynamic equilibrium will exist if the collisional decay rates are much greater than the radiative decay rates. There will then be a balance between collisionally induced de-excitations from still higher levels, and collisional excitations into such levels.

If we take the expression for the collisional decay rate of a level  $n$ , and set it equal to ten times the average radiative decay rate, the following constraint is obtained for  $N_e$ , the free electron density of the hydrogen plasma<sup>1</sup>:

$$N_e \geq \frac{7 \times 10^{18}}{n^{17/2}} \left( \frac{KT}{E_H} \right)^{1/2} \text{ cm}^{-3} \quad (2)$$

$E_H$  is the ionization potential of hydrogen. The following table gives the minimum electron densities allowable for LTE of levels three and four, for two different energies.

KT (ev)	n	$N_e$ (cm <sup>-3</sup> )
1.0	3	$1.7 \times 10^{14}$
1.0	4	$1.5 \times 10^{13}$
0.5	3	$1.2 \times 10^{14}$
0.5	4	$1.1 \times 10^{13}$

Measurements of the electron density will be made on the basis of Stark broadening by obtaining the ratio of the intensities of the beta line with a very wide

monochromator slit and a very narrow one.<sup>1</sup> It is believed presently that the electron density in the plasma under consideration is of the order of  $10^{15} \text{ cm}^{-3}$ . Thus LTE should extend down to at least the fourth, and possibly the third level. Hence our temperature measurements should have meaning.

The above assumes that the plasma is time-independent, which it is not. If we calculate the time necessary for thermalizing conditions between excited states, strictly on the basis of collisions, it is much less than a microsecond. However, since we have an exciting electric field initially ionizing the gas, and driving the plasma, it would probably be best to confine our temperature calculations to times after the current pulse.

At the present time technical difficulties have been eliminated and measurements are being made. The system is being run at a static pressure of about 500 microns. Measurements of the plasma current give us a value of 2900 amperes at the peak of the ionizing current pulse. All of the intensity oscillograms indicate two or more radiation peaks several microseconds apart. The first peak probably corresponds to the excitation and de-excitation of bound electrons, and the second corresponds to the recapture and downward cascading of the free electrons.

While the current pulse lasts for only 4 microseconds, the light seen lasts for at least 20 microseconds, meaning that the plasma lasts for at least that long. This is substantiated by the greater than 20 microsecond duration of the difference coil voltage, which indicates the plasma current.

Reproducibility of data has been a tremendous problem. The system cannot be run for more than an hour and a half at a time due to the slight leak rate, 1 micron per hour, and the fact that by then silicon impurities are probably coming off the walls of the bottle. During each run a complete set of data cannot be obtained. It is found that the static gas pressure is the most critical variable. When the bottle is refilled, the slightest difference in pressure will tremendously change the light intensity oscillograms. Figures 1, 2, 3, and 4 and Table I represent as consistent a set of data as is possible under the present conditions.

PIBMRI-1295.1-65

Oscillograms of the  $\alpha$ ,  $\beta$ ,  $\gamma$  lines of hydrogen

Pressure:  $500 \mu\text{Hy}$

Position:  $3/8''$  from inside of window



$2 \mu\text{sec}/\text{box}$   
 $0.5 \text{ volts}/\text{box}$

$4 \mu\text{sec}/\text{box}$   
 $0.1 \text{ volts}/\text{box}$

$2 \mu\text{sec}/\text{box}$   
 $0.05 \text{ volts}/\text{box}$

$\alpha$



$2 \mu\text{sec}/\text{box}$   
 $0.5 \text{ volts}/\text{box}$

$4 \mu\text{sec}/\text{box}$   
 $0.05 \text{ volts}/\text{box}$

$2 \mu\text{sec}/\text{box}$   
 $0.02 \text{ volts}/\text{box}$

$\beta$



$2 \mu\text{sec}/\text{box}$   
 $0.1 \text{ volts}/\text{box}$

$4 \mu\text{sec}/\text{box}$   
 $0.01 \text{ volts}/\text{box}$

$2 \mu\text{sec}/\text{box}$   
 $0.01 \text{ volts}/\text{box}$

$\gamma$

Note:  
The lower curve in all  
figures is the primary  
current pulse:  
 $145 \text{ amps}/\text{box}$

Fig. 1 (1-9)

PIBMRI-1295.1-65

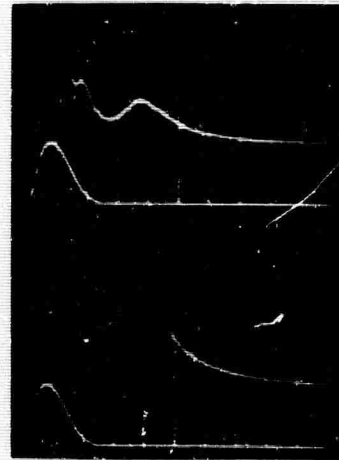
Oscillograms of the  $\alpha$ ,  $\beta$ ,  $\gamma$  lines of hydrogen  
 Pressure: 500 microns Hy  
 Position: 7/8" from inside of window



2 $\mu$ sec/cm  
 1.0 volts/cm

2 $\mu$ sec/cm  
 0.5 volts/cm

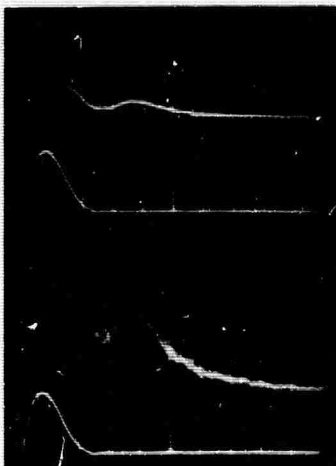
$\alpha$



2 $\mu$ sec/cm  
 0.5 volts/cm

2 $\mu$ sec/cm  
 0.2 volts/cm

$\beta$



2 $\mu$ sec/cm  
 0.1 volts/cm

2 $\mu$ sec/cm  
 0.02 volts/cm

$\gamma$

Note:  
 The lower curve in  
 all figures is the primary  
 current pulse:  
 145 amps/cm

Fig. 2 (1-10)

PIBMRI-1295.1-65

Oscillograms of the  $\alpha$ ,  $\beta$ ,  $\gamma$  lines of hydrogenPressure:  $500 \mu\text{Hy}$ Position:  $9/8''$  from inside edge of window

$2 \mu\text{sec}/\text{box}$   
 $1.0 \text{ volts}/\text{box}$

$2 \mu\text{sec}/\text{box}$   
 $0.5 \text{ volts}/\text{box}$

 $\alpha$ 

$2 \mu\text{sec}/\text{box}$   
 $0.5 \text{ volts}/\text{box}$

$2 \mu\text{sec}/\text{box}$   
 $0.2 \text{ volts}/\text{box}$

 $\beta$ 

$2 \mu\text{sec}/\text{box}$   
 $0.05 \text{ volts}/\text{box}$

$2 \mu\text{sec}/\text{box}$   
 $0.02 \text{ volts}/\text{box}$

 $\gamma$ 

Note:  
 The lower curve in all  
 figure is the primary  
 current pulse:  
 $145 \text{ amps}/\text{box}$

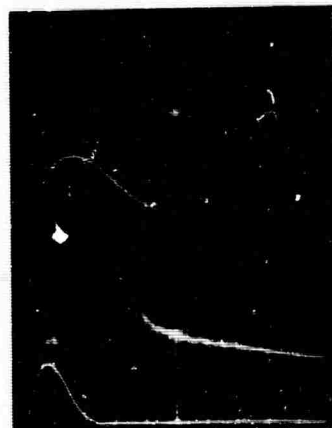
Fig. 3 (1-11)

PIBMRI-1295.1-65

Oscillograms of the  $\alpha$ ,  $\beta$ ,  $\gamma$  lines of hydrogenPressure:  $500 \mu\text{Hy}$ Position:  $11/8''$  from inside edge of window

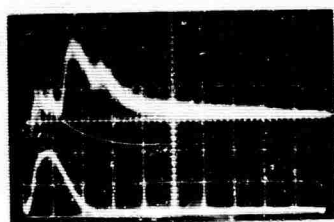
$1 \mu\text{sec}/\text{box}$   
 $0.5 \text{ volts}/\text{box}$

$2 \mu\text{sec}/\text{box}$   
 $0.2 \text{ volts}/\text{box}$

 $\alpha$ 

$1 \mu\text{sec}/\text{box}$   
 $0.2 \text{ volts}/\text{box}$

$2 \mu\text{sec}/\text{box}$   
 $0.05 \text{ volts}/\text{box}$

 $\beta$ 

$2 \mu\text{sec}/\text{box}$   
 $0.02 \text{ volts}/\text{box}$

 $\gamma$ 

Note:  
 The lower curve in all  
 figures is the primary  
 current pulse:  
 $145 \text{ amps}/\text{box}$

Fig. 4 (1-12)

From the oscillograms the temperature has been calculated as a function of time for four different positions across the radius of the bottle. We view the discharge through a flat window of diameter 1-7/8 inches, which is approximately the radius of the toroid. Positions are measured from the inside of the window.

Table I

Time ( $\mu$ sec)	$T_{\alpha\beta}$ ( $10^3$ °K)				$T_{\beta\gamma}$ ( $10^3$ °K)			
	Position (inches)				Position (inches)			
	3/8	7/8	9/8	11/8	3/8	7/8	9/8	11/8
1			4.03				7.42	
2	3.87	6.33	3.66	5.88	3.29	2.46	2.70	
3	3.30	5.98	4.32	3.39	2.46	2.36	2.12	4.22
4	2.98	11.95	7.22	3.10	2.29	1.80	1.98	1.87
5	3.02	4.91	3.99	3.02	2.64	1.99	2.08	2.38
6	3.01	3.45	4.16	3.01	2.56	2.23	2.06	1.68
7	3.05	3.88	4.16	3.01	2.64	2.16	2.04	1.97
8	2.99	5.00	3.46	2.75	2.64	2.02	2.00	2.38
9	3.06	4.40	2.98	2.73	2.30	1.91	2.30	2.46
10	3.01	3.33	2.81	2.88	2.56	2.08	2.15	
11	3.07	3.19	2.77	2.62	2.60	2.05	2.19	
12	2.84	3.04	2.77	2.54	3.39	2.19	2.34	
13	2.84	2.73	2.72	2.73	4.92	2.53	2.58	
14	3.06	2.85	2.67	2.78	4.92	2.89	2.74	
15	3.18	3.11	2.63	2.85		2.46	2.53	
16	2.84	3.19	2.85	2.78		2.53	2.66	

The temperatures given for 1 microsecond should be taken with a grain of salt because the system is obviously not in thermal equilibrium. Also the last two or three temperatures  $T_{\beta\gamma}$  for 3/8" should be read warily due to the great experimental error in reading  $J_Y$  from the oscillograms.

On the basis of our analysis, the beta-gamma temperature should be the more correct one. We see that except for periods late in the decay, it is much less than the alpha-beta temperature. This may indicate that the system is not in a state of LTE until a later time than was expected. More light will be shed on this when the electron density measurements are completed.

The general shape of the oscillograms for 7/8, 9/8, and 11/8 inches agree very well with those obtained by Hinnov and Hirschberg<sup>2</sup> in work done on the stellerator at Princeton, with a plasma confined by a static magnetic field. Note that the initial peak in our photographs occurs later as we move out radially across the bottle. From the photographs we can calculate a diffusion velocity of about  $1 \times 10^6$  cm/sec. Also note that as we move out the second peaks occur earlier. This has not been interpreted yet. Another phenomenon to be interpreted is the fact that at 3/8 inches (also at 5/8 inches, not shown) the peaks of the light intensities occur before the peak of the primary current pulse.

R. M. Eichler  
Electrophysics Department

#### References

1. Griem, Plasma Spectroscopy, McGraw-Hill, 1964, Chapters 6, 13, 14.
2. E. Hinnov, J.G. Hirschberg, "Electron-ion Recombination in Dense Plasmas", Physical Review, Vol. 125, p. 795 (1962).

#### 1.4 Magnetic Probing of a Toroidal Discharge

In order to describe a toroidal plasma and its associated instabilities, it is necessary to have an accurate measurement of the magnetic field about the discharge. The fields are directly related to the plasma current flow and give more information as to the resistive instability process (which visually is the splitting of the glow region into two rings in the z direction) and to the oscillations about the equilibrium position, resulting when an outer winding is present, which is important for the problem of plasma confinement. It is hoped these measurements will substantiate to a large degree the optical measurements that have been and are being

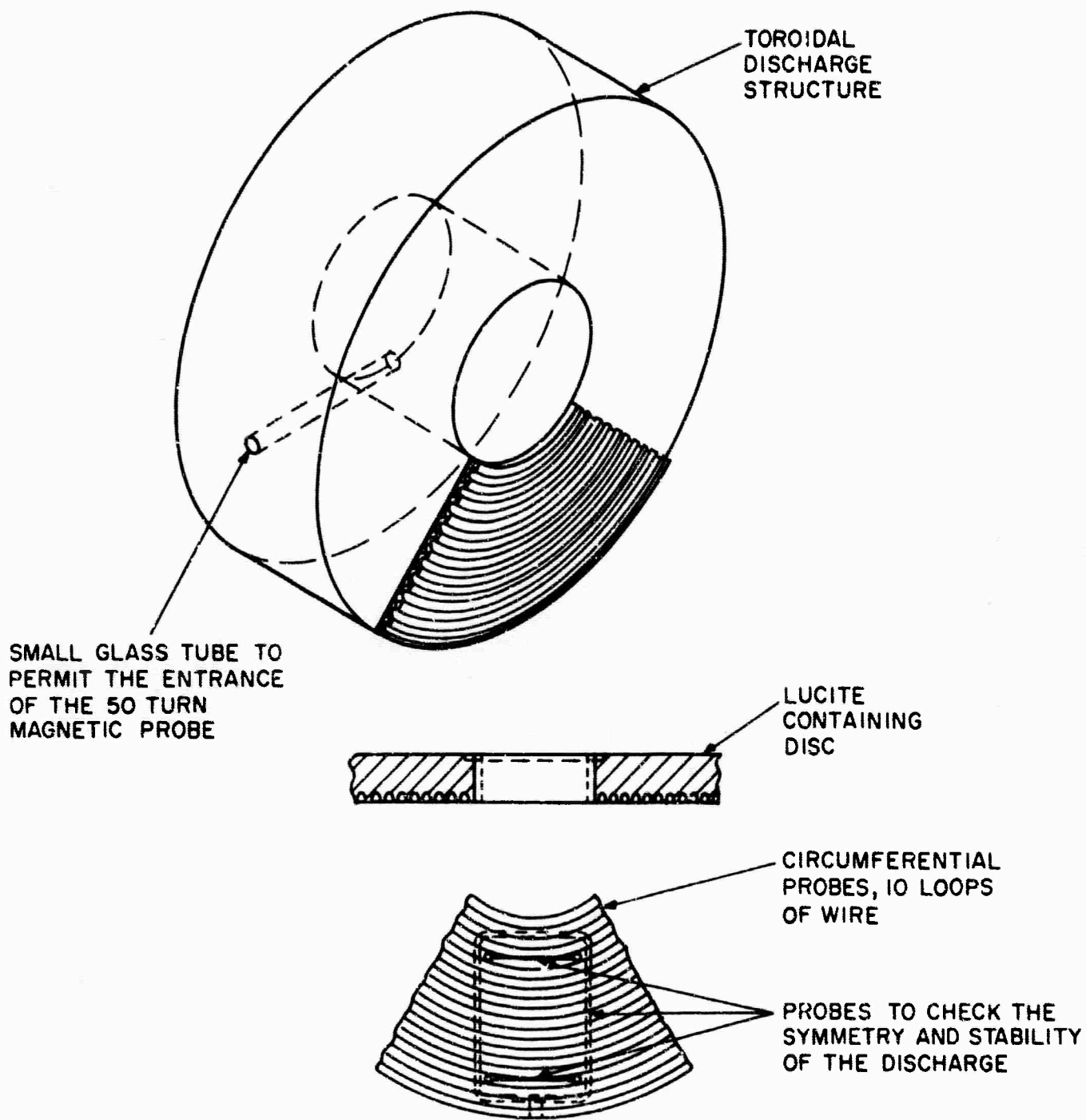


Fig. 1 (1-13) - Sketch of the tube and probe positions. The small pie section cut-out is a portion of a complete disc. (There is one disc on each side of the discharge structure.) The probes on this pie section are repeated around the disc every 90° giving a total of four of these symmetry probe sets to a disc. One set is positioned over the small tube to check the effect it has on the discharge.

performed and the theoretical descriptions which have been presented.

The dynamic response of this plasma created within an electrodeless toroidal discharge tube is being investigated using a 1/16" by 1/16" 50 turn magnetic probe. The probe and its associated circuitry are designed to give the largest noise-free response with the least amount of perturbation to the plasma self fields. The probe is inserted into a small glass tube built into the z-directed center of the discharge structure. The probe can be oriented in the three coordinate directions and gives information on the current distribution. It will also be used to scan the outer surface of the structure.

A difference current transformer measures the total plasma current and there are circumferential probes on the sides of the discharge tube measuring the average z-directed flux as a function of the radial distance and also the electric field. Other magnetic probes are positioned about the discharge tube and give information as to the symmetry and stability of the discharge. These measurements are being carried out at different pressures, voltages, and with and without an outer primary winding. The tube and probe positions are sketched in Fig. 1. The macroscopic motion of the plasma current can be studied by using a parallel outer winding. (To simulate the case of only an inner winding present, a large resistance will be added in series with the outer winding.) Considering the plasma and the windings as being infinitely long and infinitesimally thin concentric right circular cylinders oriented along the z-axis, we may write the equation for the sum of the voltage drops in the loop formed by the two parallel windings (see Fig. 2).

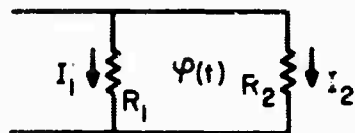


Fig. 2 (1-14)

$$\begin{aligned}
 I_1 R_1 - I_2 R_2 &= - \frac{d}{dt} \Phi \\
 &= - \frac{d}{dt} \mu_0 \pi \left\{ H_1 (r_2^2 - r_1^2) - H_2 (r_2^2 - r_1^2) \right\} \quad (1)
 \end{aligned}$$

where the capital R's represent resistances, the small case r's the radii,  $\phi_{(t)}$  the total flux enclosed and the subscripts 1 meaning inner winding and 2 outer.

Considering a 1 meter length of the model we can obtain an expression for the plasma radius at any instant of time:

$$x \equiv \frac{r}{r_2} = \sqrt{\frac{\int (I_2 R_2 - I_1 R_1) dt}{\mu_0 \pi r_2^2 I_{\text{prim}}} + (1+a^2) \left[ \frac{I_1 - I_2}{I_{\text{prim}}} \right]} \quad (2)$$

where:  $a \equiv \frac{r_1}{r_2}$  and  $I_{\text{prim}} = I_1 + I_2 = \text{Total primary current.}$

The basis for using such an idealized model to obtain the macroscopic motion of the current can be found in reference 2, where Friedman, by other field measurements performed on a similar tube, has found close overall agreement of the experimental fields to those generated by a current sheet model.

These measurements when completed will be used to create a more accurate model for the current flow. Although not all of the measurements are complete, Fig. 3 shows the probe response at different positions within the tube at 6KV and 500 microns of  $H_2$ . It is oriented to obtain the  $B_z$  component of the magnetic field. There is no outer winding for this measurement. It is seen that the values we find are much lower than would be expected from a current sheet whose field is given by

$$B_z = \frac{\mu_0 I}{4\pi d} \left[ \tan^{-1} \frac{z+d}{r} - \tan^{-1} \frac{z-d}{r} \right] \quad (3)$$

where d is the plasma radius and r is the point of the field measurement. If the values of the constants were substituted, it would be seen that the probe should be measuring fields in the 100 gauss range. These low readings may perhaps indicate that the plasma current is split into two almost equal current rings at this pressure. The glow region indeed shows such a splitting. Further measurements are being made to substantiate this assumption.

It has been noticed that at voltages of the order of 3-4 KV and pressures of about 300 microns and higher (500 $\mu$  is the highest pressure we've gone) there

PIBMRI-1295.1-65

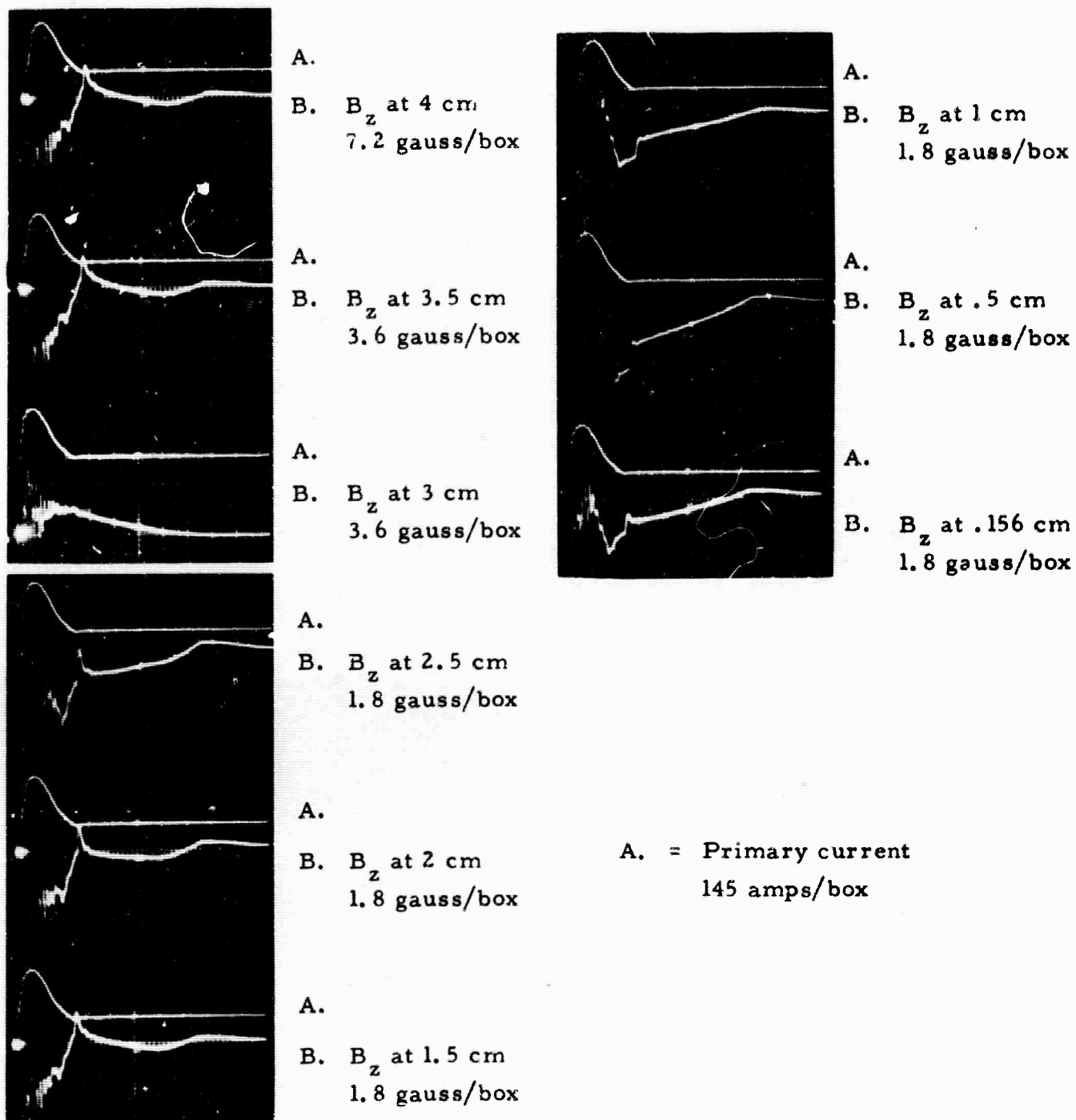


Fig. 3 (1-15) - Probe response ( $B_z$ ) at 6KV and 500 microns of Hydrogen. Time scale -  $2\mu\text{sec}/\text{cm}$ . The distances given are measurements of depth into the tube with .156cm being the outer radius.

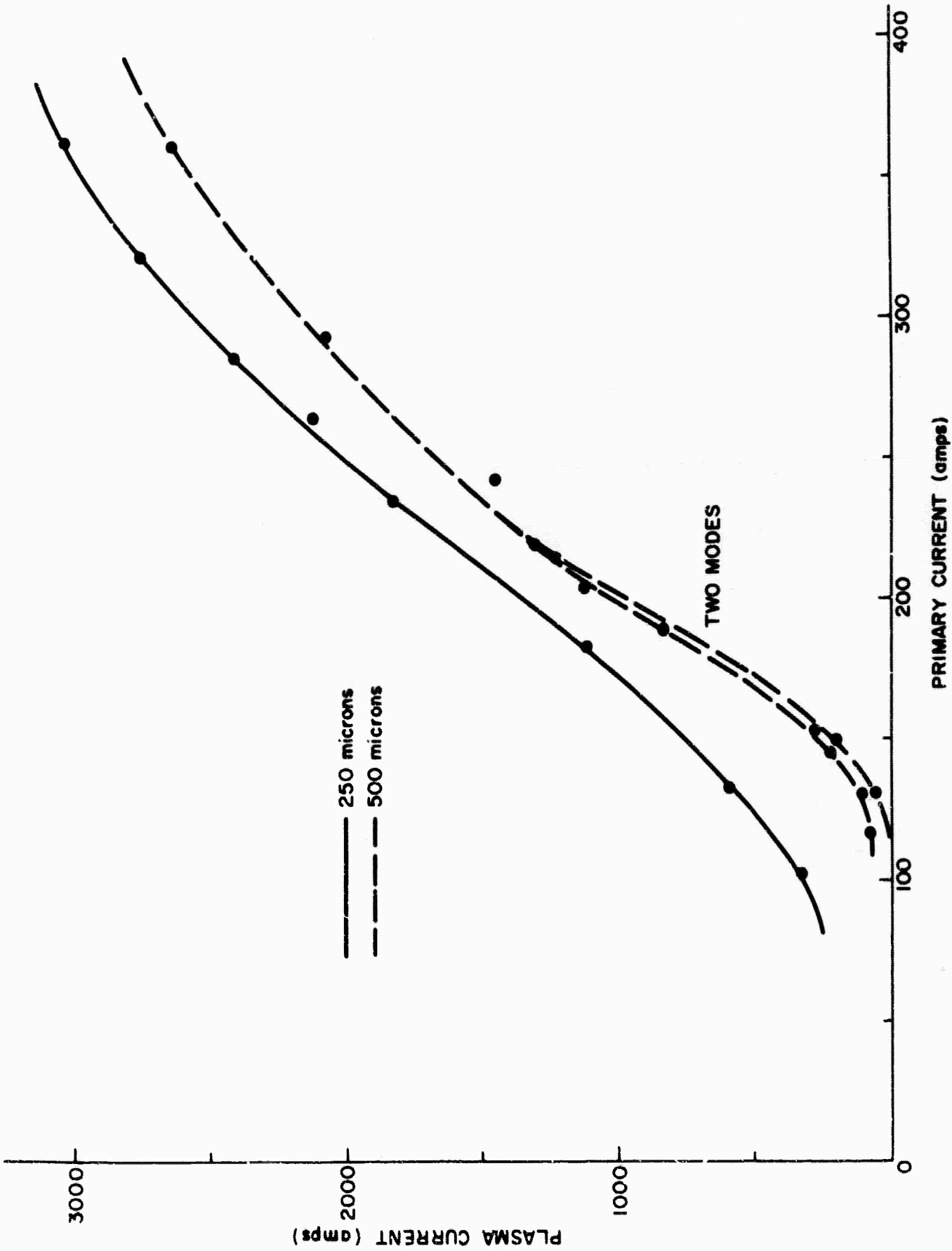


Fig. 4 (1-16) - Plasma current vs. primary current

exist two values for the plasma current for a given primary current and consequently two values for the plasma conductivity. This can represent either two separate and distinct modes of discharge or two possible stable current configurations. It has been noticed that at the lower pressures there exists only one glow ring, while at 300 microns and above, two rings exist. It is proposed that at these pressures and voltages the plasma current can have either a one or two ring configuration, each being equally probable. This is being examined by field measurements. Figure 4 shows the plasma current as a function of the primary current for different pressures of hydrogen. It is seen that the total current is higher at 250 microns than at 500 microns and the two modes may be seen on the lower portion of the 500 micron curve. Both curves seem to follow each other quite well.

The many peaks and zeros seen by the probes as in Fig. 3 are as yet unexplained, but it is hoped that when all the data is correlated, a good idea of the instabilities and their cause will be obtained. This would give us much information on the thermal pressures within the gas discharge and shed new light on the problem of magnetic confinement.

J. Miletta  
Electrophysics Department

#### References

1. J. Freidberg, "Magnetohydrodynamic Stability of a Toroidal Plasma Structure", PIBMRI-1025-62.
2. H. Friedman, "Probing of the Dynamical Response of a Plasma" PIBMRI-1168-63.

#### 1.5 Experimental Study of the Screen Cathode Discharge

(Abstract of an M.S. Thesis)

#### Description of the Screen Cathode Discharge

##### A. The Discharge Structure

This report describes recent work in the continuing study of screen cathode discharges.<sup>1</sup> These discharges are important because they may be used to obtain a

plasma-electromagnetic wave interaction structure with free plasma boundaries.<sup>2</sup>  
 One screen cathode discharge structure currently under investigation is shown in Fig. 1. The discharge structure is enclosed in a large bell jar (1)\*. The anode (2)

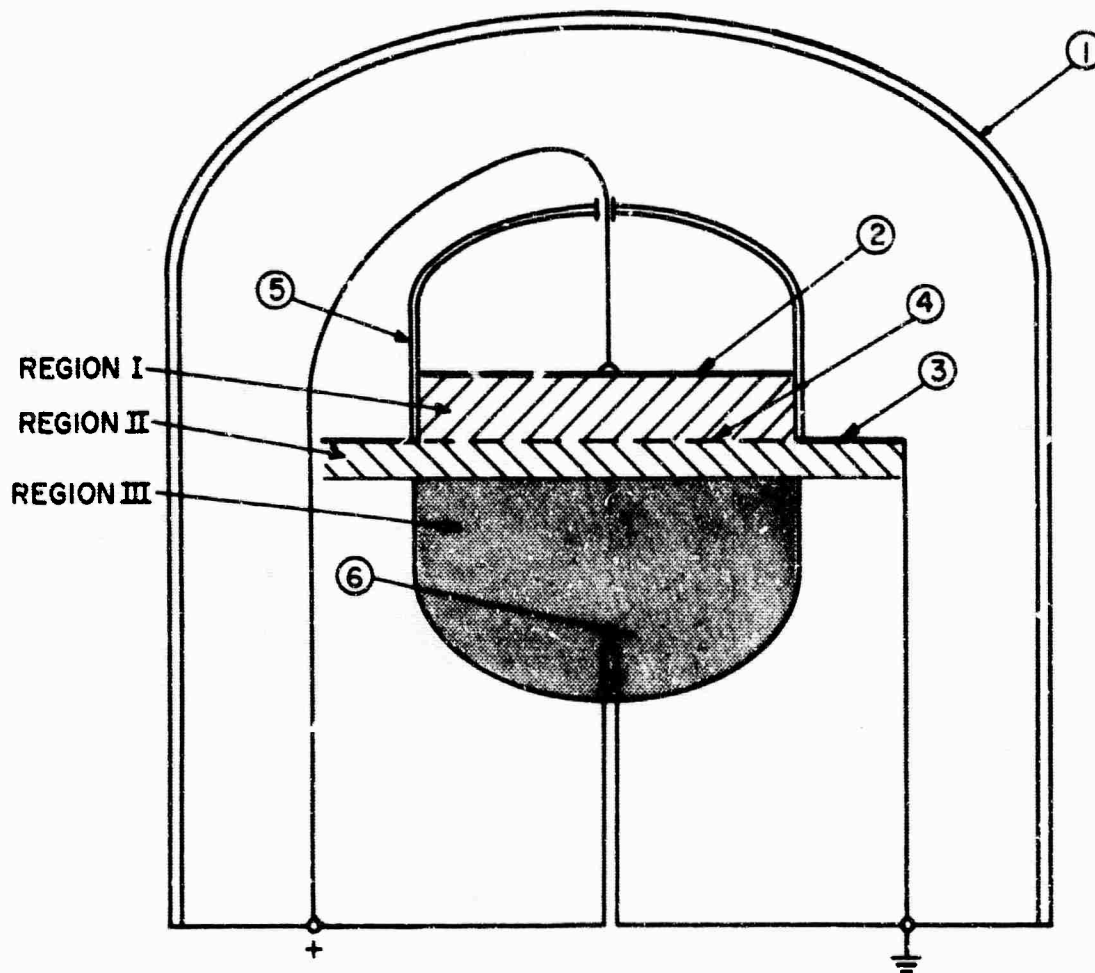


Fig. 1 (1-17) - Screen cathode discharge structure

is a solid stainless steel disk with an  $8 \frac{1}{4}$ " diameter. The cathode consists of a solid stainless steel ring (3) which contains a circular stainless steel screen (4) with a diameter of  $8 \frac{1}{4}$ " within its circular aperture. The screen is composed of

---

\*The numbers in parenthesis refer to the numbered components in Fig. 1.

10 mil wire spaced 15 wires to the inch. For most of the observations the plate to cathode distance was set at 1.45 cm. A smaller pyrex bell jar (5) with an open neck is seated on the junction between the ring and screen of the cathode. A Langmuir probe (6) which can be moved up and down is incorporated in the large bell jar. This 5 mil diameter tungsten probe is bent and has an exposed length of 1 mm.

### B. General Observations

Most of the experimental observations reported below were made by H. Strachman and one should consult his Master's thesis<sup>3</sup> for more detailed information. Two gases were used in the course of the investigation: one was aviation breathing air with a dew point of  $-37^{\circ}\text{F}$ ; the other was tank grade helium. Although a steady discharge could be obtained for currents up to 150 ma, most of the measurements were taken between 20 and 60 ma to avoid excessive cathode heating. The pressure ranges for a stable discharge were quite narrow being only 400 to 500 microns Hg in air and from 2,500 to 3,600 microns Hg in helium. In all the experiments the cathode was grounded and the anode was approximately at 600 volts.

In the screen cathode discharge, as in discharges between solid electrodes, the normal and abnormal glow domains were present. Of most interest is the abnormal glow region which occurs when the discharge current is greater than about 20 ma. Here the screen is entirely covered by the plasma. Further increases in current appear only to increase the plasma light intensity and the depth of plasma penetration below the screen. In this abnormal glow region three separate regions are clearly visible (Fig. 1). Region I is the glow discharge which appears between the electrodes. Striations of lighter and darker regions are visible within this domain. In air, the dominant color of this region is dark blue, while in helium it is greenish blue. Directly below the screen a second region appears with a very diffuse radial boundary which extends to the outer edge of the steel ring on the cathode. It is of pink color in He. In air, region II does not appear; it is merely replaced by a continuation of region III. The thickness of region II was observed to vary from 0.54 cm to 1.34 cm as the discharge current was increased from 20 to 60 ma. Below this thin band of diffuse light is a much longer, parabolic shaped glow, which we call

reg on III. It has a sharp plasma-gas radial boundary extending to the diameter of the screen. The radius of this region and its light intensity diminishes as one moves away from the screen. This region has a reddish-pink color for helium, and an orange color with air.

### Experimental Measurements

#### A. Current-Voltage Characteristics

In the first quantitative data taken, the current-voltage characteristics of the discharge were measured. Although the air discharge was rather erratic in starting, once the discharge was initiated the results were quite reproducible. The current-voltage curves taken in helium all have the characteristic shape associated with volt-ampere characteristics for glow discharges with solid, plane electrodes<sup>4</sup>. The exact empirical equations relating the discharge voltage to the current density and pressure, however, are different from those found for discharges with solid electrodes.

#### B. Total Light Output and Spectrographic Analysis

A photomultiplier tube (RCA 6217) was used to determine the light output as a function of distance below the cathode. A typical result of such a measurement appears in Fig. 2. The peak of the light intensity occurs in region II.

The spectrum of the three regions in the helium discharge was taken and compared to the lines in a helium Geissler tube. It was found that all lines in the anode to cathode region were present in the Geissler tube. Regions II and III however contained spectral lines which did not appear in the helium reference source. They also lacked certain lines which were present in the Geissler tube. The lines which do not appear in the helium spectrum, except for two spectral lines in region III, corresponded to various elements such as chromium which are present in the stainless steel screen cathode. This implies emission of these elements from the cathode. The fact that a number of the characteristic lines do not appear in the region below the screen, and that those which do appear are of varying intensities in the various regions is an indication that different excitation conditions are present in each region. The two lines of the third region which have not as yet been accounted for appear to be the

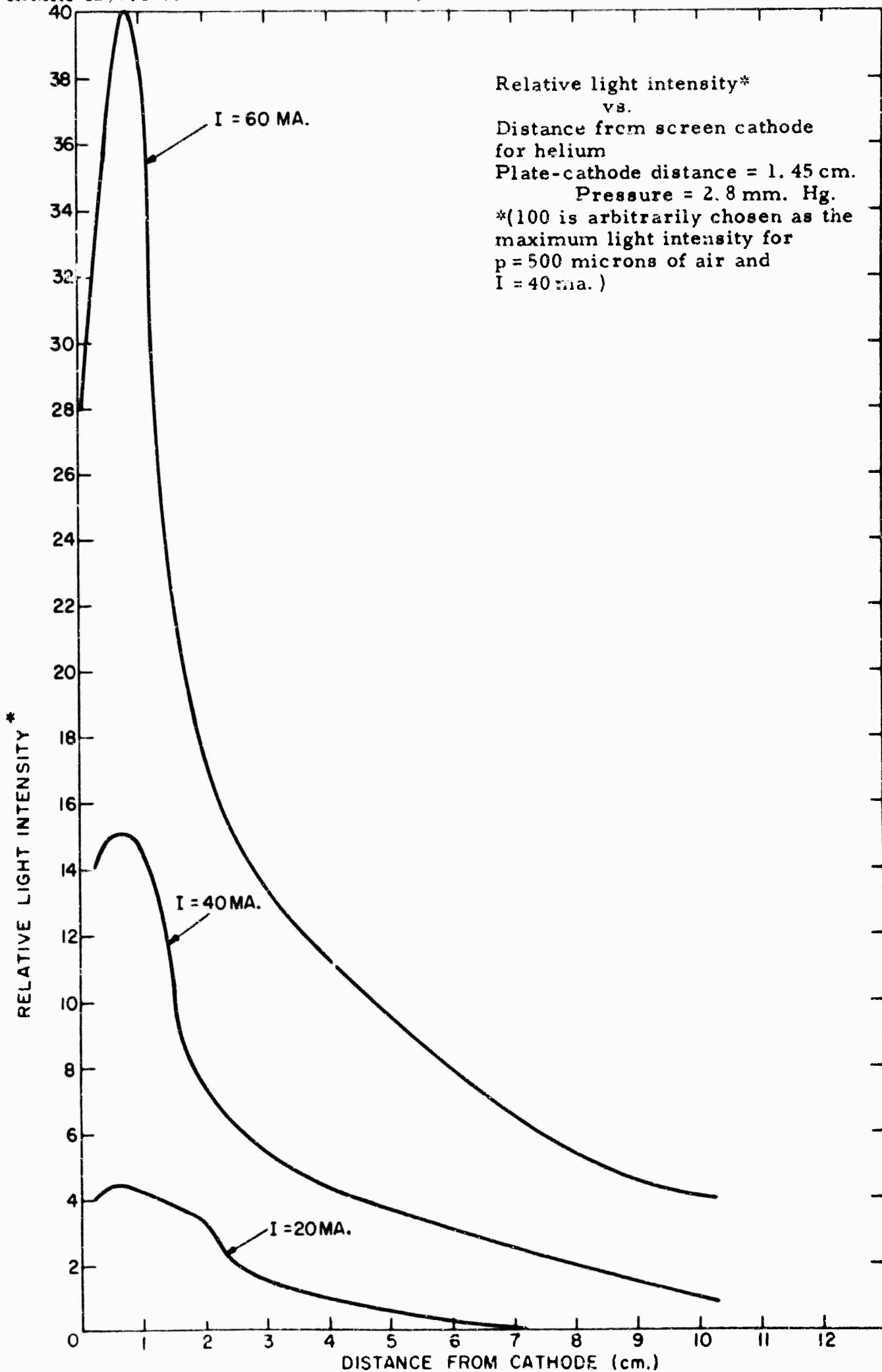


Fig. 2 (1-18)

hydrogen  $\alpha$  and  $\beta$  lines. Their appearance has not yet been satisfactorily explained.

### C. Langmuir Probe Measurements

A tungsten wire probe, with a 5 mil diameter and an exposed length of 1mm, bent at right angles to the glass rod supporting the probe was used to obtain Langmuir probe characteristics of the plasma below the screen. The probe and glass rod was mounted on a shaft with a vacuum seal and could be moved up and down. Earlier floating probe measurements, taken with a flush mounted probe, yielded a peak in the floating potential at a distance of approximately 0.8 cm. from the screen. It is now thought that this maximum does not actually exist but was caused by the small current drawn by the probe. Later, Langmuir probe data indicated a fairly constant floating potential and space potential of approximately 110 volts up to a distance of 6 cm from the screen. There was, of course, a sheath region immediately adjacent to the screen where the potential returned to ground. A preliminary investigation using a Langmuir probe revealed a peak in the electron number density at about 0.7 cm below the screen. Here the electron density was about  $10^{10}$  electron/cm<sup>3</sup> and the electron temperature was close to 10,500°K. Typical Langmuir probe characteristics are shown in Fig. 3.

### Future Work

The investigations described above have greatly added to our knowledge of the screen cathode discharge. They have provided information about stable operating points, light output and spectra, and given an indication of electron number density and temperature. There is also work proceeding on other screen cathode configurations. One example is the discharge described in the article Slot antenna in a plasma appearing in this progress report. However, more research is required to understand the physical processes occurring below the screen. Many interesting questions remain to be answered. Why is the discharge only stable in a relatively narrow pressure range? Why are there two distinct regions below the screen in helium and only one region in air? What is the significance

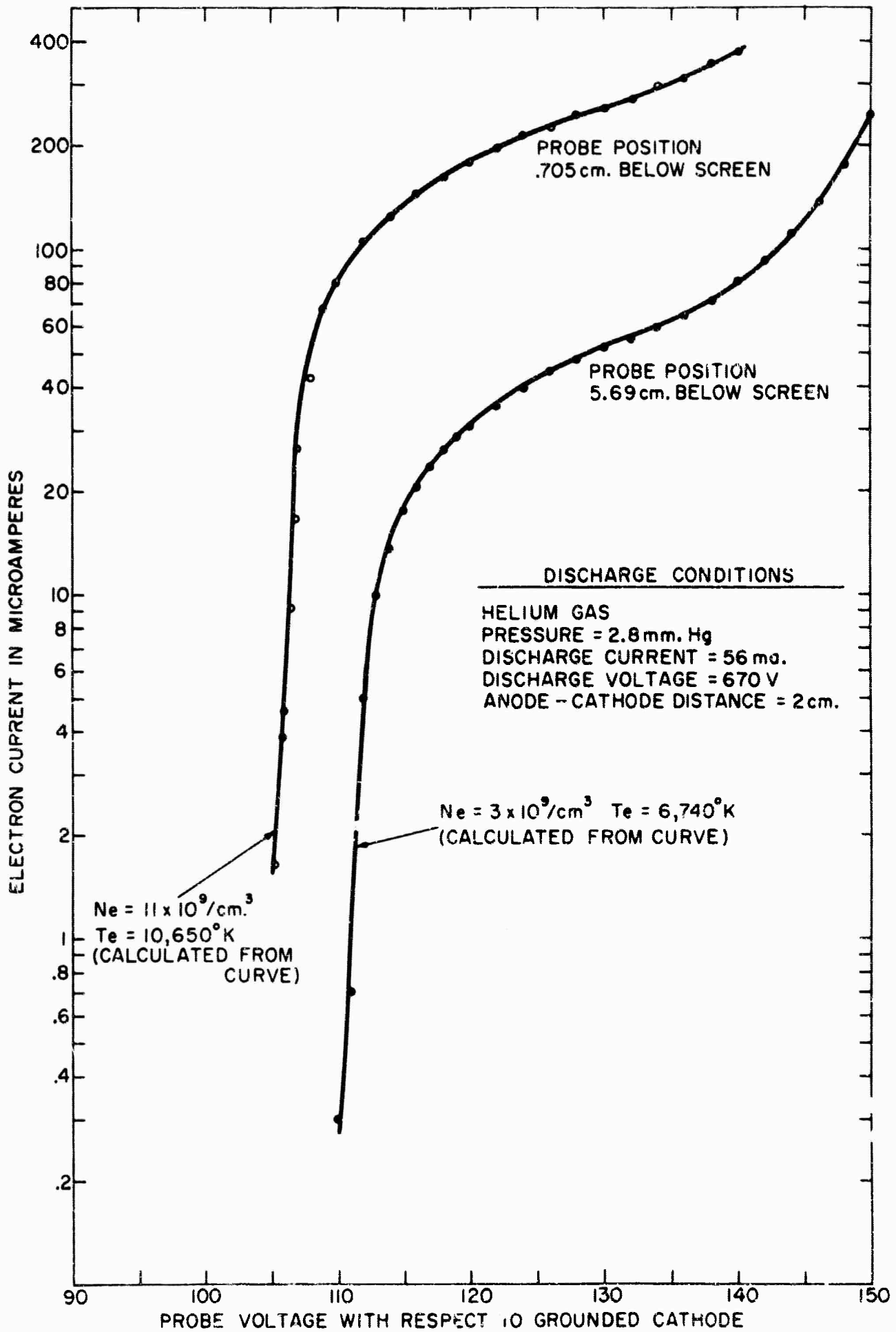


Fig. 3 (1-19) - Langmuir probe characteristics

of the hydrogen  $\alpha$  and  $\beta$  lines in region III? Further Langmuir probe experiments will provide data on electron density, electron temperature, and space potential over a wide range of pressures and currents. It is anticipated that this information together with additional spectrographic study will lead to an increased comprehension of the screen cathode discharge.

H. M. Cronson  
H. L. Strachman  
Electrophysics Department

### References

1. K. T. Lian, "Investigations of Gas Discharge Structures Suitable for Microwave Interaction Studies", PIB Electromagnetics Program, Report to ARPA, Nov. 16, 1964, p. 24.
2. K. T. Lian, "Use of Screen Cathodes to Obtain Plasma/Electromagnetic Wave Interaction Structures with Free Plasma Boundaries", Electronics Letters, 1, 47, 1965.
3. H. Strachman, "Experimental Investigations of the Screen Cathode Discharge", PIB Master of Science (Electrophysics) Thesis, June 1966.
4. G. Francis, "The Glow Discharge at Low Pressure", Handbuch Der Physik, Vol. XXII, Springer-Verlag, Berlin, 1956.

### 1.6 An Air Filled Discharge Chamber

(Abstract of an M.S. Thesis)

#### Purpose of the Work

Scintillation counters using gases as scintillants generally employ noble gases. For good performance, the purity of the gas must be very high.

Nitrogen and Oxygen are considered contaminants; even small quantities of impurities (especially Oxygen) reduce the amount of light emitted, so that great care must be taken to keep scintillation free from contaminants.

On the other hand, air at atmospheric pressure has been extensively used in spark chambers (also called spark counters or discharge chambers).

Such chambers or counters mainly consist of two parallel conducting plates, to which a high voltage pulse is applied whenever a charged particle transverses the gap. A discharge then occurs along the path of the particle, giving a visual indication of the particle track, that may also be recorded on film. The passage of the particle is detected by Geiger counters connected in a coincidence circuit, and the coincidence pulse triggers the high voltage pulse.

In the discharge chamber developed by Cavalleri, et al., and called light chamber, the filling gas is a Penning mixture of Argon and Neon at about atmospheric pressure. The ionizing particle goes between and parallel to two plane electrodes; the scintillation is detected by a photomultiplier and triggers a high voltage pulse (the pulse is actually a high-frequency decaying sinusoid). The electrodes are semitransparent (a conductive, semitransparent coating over a glass plate), and not in contact with the gas.

No spark actually occurs inside the chamber, but only the multiplication of the electrons in the tracks (called gas-amplification). The luminosity of the track, originating from the decay of excited states caused by impact with the electrons, increases as the amplitude of the H. V. pulse increases, up to a value where it can be photographed on sensitive film. The size of the tracks, measured in a direction perpendicular to the applied field (as recorded on the film) is related both to the diffusion coefficient of the electrons in the gas and to the diffusion time.

It is this experiment that we tried to duplicate in our work, except for the use of air as the filling gas. When air is used, a new feature is added; the attachment of electrons plays an important role in the operation of the chamber.

Such a chamber may be a useful device for studying properties of gases, especially if a number of refinements are included. In this work, only the study, construction and operation of a simple chamber are reported. As it is, the apparatus demonstrates the possibility of using air as scintillating gas and of photographing the gas-amplified tracks of  $\alpha$ -particles in air. It also gives an estimate of the diffusion coefficient of energetic electrons in air, and of the value of  $E/p$  necessary for the detachment of electrons from negative molecular Oxygen ions.

All the experiments have been performed at atmospheric pressure; changing the pressure could be one of the steps to be taken to investigate further into the possibilities of the chamber as a tool for research. Unfortunately, lack of time has prevented us from performing such refinements; a number of suggestions are offered to interested researchers in the final chapter of this work.

### Abstract of Report

A discharge chamber is described being filled with ordinary air at atmospheric pressure, and in which the tracks of  $\alpha$ -particles can be photographed. For the operation of the chamber, a photomultiplier detects the primary scintillation due to the passage of an  $\alpha$ -particle and triggers a high-voltage pulse in the chamber. The pulse causes a Townsend multiplication of electrons along the path of the particle, resulting in a great amplification of the luminosity of the track, so that it can be photographed. A number of such photographs are shown.

The size of the tracks is related to the diffusion of the electrons; the diffusion coefficient of the electrons can therefore be estimated, ( $D \approx 0.25 \text{ m}^2 \text{ sec}^{-1}$ ), as well as the mean electronic energy ( $\approx 8.8 \text{ eV}$ ).

A study of the phenomena occurring in the chamber following the passage of an  $\alpha$ -particle, and following the application of the H. V. pulse, is also presented. The study shows that, at the time of application of the H. V. pulse, the electrons liberated by the passage of the  $\alpha$ -particle have become attached to Oxygen molecules, and they must become free again before the multiplication process can take place. There is a minimum intensity for the applied electric field that produces detachment, corresponding to  $E/p$  near  $9 \times 10^4 \text{ V m}^{-1} \text{ mm Hg}^{-1}$ , in agreement with the value found by other experimenters.

The chamber has semi-transparent electrodes through which visible light is 70% transmitted. The photomultiplier is a low noise tube, EMI 9514-S, and the photographic recording is made on Polaroid film, type 410, of sensitivity 10,000 ASA.

The apparatus and circuitry used are described in the text, supplemented by a number of photographs.

G. Gambirasio  
Electrophysics Department

### 1.7 Interaction of High Energy Electron Beams with a Plasma

(Abstract of a report in preparation)

An important, fast developing technique of obtaining experimental information on laboratory plasma systems is by their interaction with high energy electron beams of significant density. A systematic investigation of this problem, using plasma kinetic theory, is under way in which effects due to temperature, finite boundaries, and inhomogeneities are considered.<sup>1</sup>

A paper has recently been submitted for publication in the Journal of Mathematical Physics. The title and abstract follow:

#### Application of the Vlasov Equation to the High Frequency Stability of Finite Relativistic Beam-Plasma Systems

The response of a finite relativistic beam-plasma system to small disturbances is analyzed using the coupled Vlasov-Maxwell equations. It is shown that when  $|\omega - kV_0| \gg \omega_B^2$ , where  $\omega_B$  is the betatron frequency and  $V_0$  the drift velocity of the beam, straight line orbits are sufficiently accurate to describe the beam particle trajectories. Dispersion relations are derived for a finite beam and for both infinite and finite plasma configurations. The effect of a finite but large beam radius is shown to increase the growth rate of the electrostatic instability.

In the above paper the initial equilibrium situation was assumed to be that of an infinitely long electron beam of uniform density penetrating a uniform density plasma, both cylindrical with the plasma radius larger than the beam radius, and the plasma variously confined by a conducting and an insulating wall. The thermal properties were described by uniform Maxwellian distributions.

Current and future research plans constitute a systematic extension of these calculations:

The dispersion relations derived above are being analyzed. A systematic analysis is proceeding in which simple analytical approximations to the solutions of the dispersion relations are being sought in asymptotic regions of parameter space. With these approximations as guides extensive machine calculations are foreseen in order to complete the analysis. The ultimate goal is a complete graphical representation of the effect of temperature, finite radii, etc. on the well-known instabilities as well as on any new instabilities that are uncovered.

The method of the above paper has been extended to the important experimental case of the plasma being finite in length and having a density which decreases with distance along the direction of the beam. The self-consistent field equations have been derived for finite beam radii and zero temperatures. The limit of infinite radii has been fully investigated and has been found to be in complete agreement with a cold plasma theory based upon fluid equations. Future work on this aspect of the beam-plasma problem consists in (1) solving the equations for finite radii and analyzing the solutions for stability criteria, (2) generalizing to finite radii plasmas with confining walls, and (3) including the effects of non-zero temperature. This last aspect is extremely complicated and must probably await the completion of the following analysis.

In the submitted paper and the extension reported above an initial state has been assumed in which the beam and plasma are already in equilibrium. However, the specification of this initial state has merely followed the dictates of convenience and simplicity. A more satisfactory procedure is to specify the beam and plasma properties before they interact (which is just a function of the electron gun device and the plasma producing machine) and then to follow the time development of the system from the first entry of the beam into the plasma. The investigation of this problem has just begun using plasma kinetic theory in which the Boltzmann equation, with a collision term included, is applied. The aim of this investigation is to allow the specification of an equilibrium state (if one really exists) with more confidence. In particular, the extremely interesting case in which the beam itself helps to produce

a substantial part of the plasma from the residual gas can be given a systematic development.

G. Dorman  
Physics Department

### References

1. A list of the important publications on this problem follows:
  - a. S.A. Bludman, K.M. Watson, and M.N. Rosenbluth, *Phys. Fluids* 3, 747 (1960).
  - b. E.A. Frieman, M.L. Goldberger, K.M. Watson, S. Weinberg, and M.N. Rosenbluth, *Phys. Fluids* 5, 196 (1962).
  - c. R.C. Mjolsness, *Phys. Fluids* 6, 1729 (1963).
  - d. R.C. Mjolsness, J. Enoch, and C.L. Longmire, *Phys. Fluids* 6, 1741 (1963).
  - e. S. Weinberg, *J. of Math. Phys.* 5, 1371 (1964).
  - f. H. Singhaus, to be published in the *Physics of Fluids*.

### 1.8 Plasma Sheath Studies

In a gas discharge, the thin region which separates the plasma from any departure from charge neutrality is called the sheath. The space charge density, electric field and potential distributions are all non-zero in the sheath making this region rich in nonlinear phenomena and difficult to analyze. A knowledge of the physical processes in the sheath is essential for the full understanding of many problems in plasma physics such as electromagnetic energy coupling, confinement and diffusion. Although much work has been done to determine the effect of the plasma medium on these processes, the model of the plasma medium itself is not fully understood in regard to the methods by which the cold walls of a vessel actually contain the plasma.

There is some question as to the existence of a d.c. as opposed to time harmonic, steady state sheath surrounding any cold wall. The doubt arises because of a physical contradiction in the boundary condition necessary for a d.c. sheath

derived by Bohm<sup>1</sup>. This Bohm condition requires that the ions reach the beginning of the sheath with a velocity higher than the effective sound speed of the electron-ion plasma. Persson<sup>2</sup> in a study of inertia controlled ambipolar diffusion, shows that there is no plasma diffusion mechanism which can accelerate the ions to this supersonic velocity, and thus the contradiction arises.

In a computer calculation, Allis and Rose<sup>3</sup> have tried to match the plasma region smoothly with the sheath region. Their calculation did not include the ion inertia term, which is by no means negligible at velocities near the sound speed, so they avoided the question completely.

The purpose of this present work is to find the ion velocity transition from sub to supersonic as the ions leave the plasma region and enter the sheath. The method to be used is a perturbation scheme about the state of high velocity ambipolar flow. It will show the effect of non-zero space charge on the ion velocity. This particular perturbation scheme developed by Freidberg<sup>4</sup> differs from conventional analysis in that one searches for the first order correction to a solvable nonlinear differential equation when a small nonlinear term is added.

The analysis begins with the steady state, hydromagnetic equations for an electron-ion system in a neutral gas background:

The continuity equations:

$$\nabla \cdot (n_e \mathbf{v}_e) = n_e v_i \quad (1)$$

$$\nabla \cdot (n_i \mathbf{v}_i) = n_i v_i \quad (2)$$

The momentum balance equation:

$$m_e n_e \mathbf{v}_e \cdot \nabla \mathbf{v}_e + kT_e \nabla n_e = -|e| n_e \mathbf{E} - n_e \mathbf{v}_e m_e (v_m + v_i) \quad (3)$$

$$m_i n_i \mathbf{v}_i \cdot \nabla \mathbf{v}_i + kT_i \nabla n_i = +|e| n_i \mathbf{E} - n_i \mathbf{v}_i m_i (v_m + v_i) \quad (4)$$

where the assumptions of perfect gas law and isothermal conditions have been assumed.

Finally, Poisson's equation:

$$\nabla \cdot \underline{E} = \frac{|e|}{\epsilon_0} (n_i - n_e) \tag{5}$$

The quantities  $\nu_m$  and  $\nu_i$  are constants that approximate the momentum and ionization collision frequencies for charged particle-neutral collisions.

Adding the two momentum equations:

$$m_e n_e \nu_e \cdot \nabla \underline{v}_e + m_i n_i \nu_i \cdot \nabla \underline{v}_i + kT_e \nabla n_e + kT_i \nabla n_i = |e| (n_i - n_e) \underline{E} - m_i n_i \nu_i (\nu_m + \nu_i) - m_e n_e \nu_e (\nu_m + \nu_i) \tag{6}$$

Equation (6) suggests that if the electric field that exists between the electrons and ions is strong enough, the electrons drag the ions along with them as they diffuse. Imposing this physical condition mathematically implies  $n_e = n_i = n_0$  which forces  $\underline{v}_e = \underline{v}_i = \underline{V}_0$  from the continuity relations. Equations (1) and (6) now form a self-consistent set.

$$\nabla \cdot n_0 \underline{V}_0 = n_0 \nu_i \tag{7}$$

$$n_0 \underline{V}_0 \cdot \nabla \underline{V}_0 + a^2 \nabla n_0 = -n_0 \underline{V}_0 (\nu_m + \nu_i) \tag{8}$$

where  $a = \sqrt{\frac{k(T_e + T_i)}{m_e + m_i}}$  is the sound speed for the electron-ion fluid mixture.

In one dimension, Eqs. (7) and (8) can be combined so that  $n_0$  is eliminated, leaving

$$\frac{dV_0}{dx} = \frac{V_0^2 (\nu_m + \nu_i) + a^2 \nu_i}{a^2 - V_0^2} \tag{9}$$

Equation (9) can be integrated to yield  $x$  as a function of  $V_0$ . The plot of  $V_0$  versus  $x$  is shown below, where it has been assumed that the flow starts from the middle of the plasma ( $x=0$ ) with zero velocity ( $V_0=0$ ).

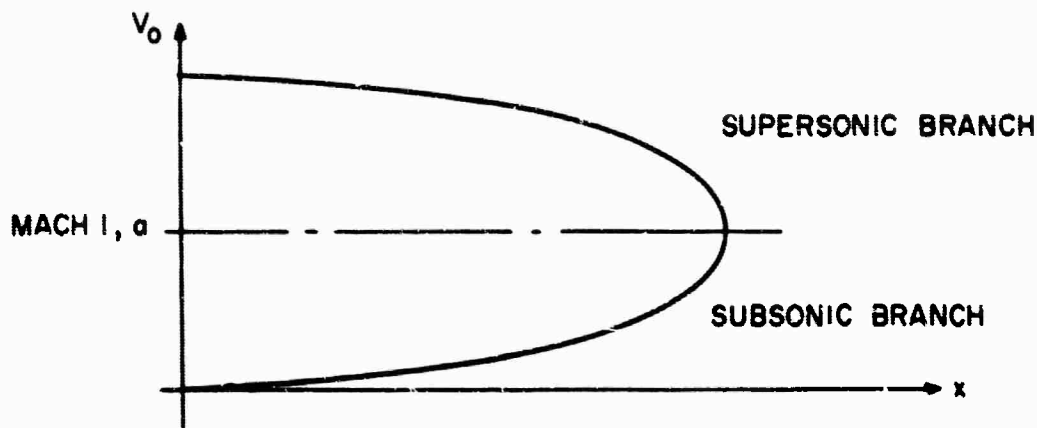


Fig. 1 (1-20)

This curve, obtained also by Persson<sup>2</sup>, has the physical implication that for particles starting from zero velocity, the maximum diffusive velocity possible is Mach 1. Two facts are evident from Fig. 1. The first is that since multivalued solutions are physically impossible, one is always restricted to stay on the branch dictated by initial conditions. Second, there is no method for analytically extending this curve to higher velocities under this neutral fluid model.

In order to find the first order correction to the ion velocity due to a slight deviation from charge neutrality, an expression for the first order charge density is needed. The electron momentum Eq. (3) can be used to find the zeroth order electric field, and the divergence of this electric field yields the first order space charge. The results are

$$E = \frac{V_0}{a^2 - V_0^2} \tag{10}$$

$$(n_i - n_e) = \delta = \frac{(a^2 + V_0^2) [V_0^2 (v_m + v_i) + a^2 v_i]}{(a^2 - V_0^2)^3} \tag{11}$$

The singularity in  $\delta$  seen in Eq. (11) indicates that the assumption of a neutral ambipolar diffusive flow at velocities near Mach 1 is erroneous. Either the

assumptions of isothermal conditions and constant collision frequencies must be abandoned or a perturbation scheme must be derived about a state of high velocity, non-neutral diffusive flow. Some preliminary attempts at imposing energy dependent collision frequencies and adiabatic equations of state fail to remove the singularity.

It will be necessary, therefore, to match a solution in the neutral regime (low velocity) to one in the non-neutral regime (high velocity). This is precisely the approach taken by Allis and Rose<sup>3</sup>; however, they neglected the ion inertia term that must be considered if the high velocity Bohm condition is to be met. Persson's<sup>5</sup> explanation of a phenomenon in his brush cathode is also unsubstantiated. He attributed a discontinuity in light output to the discontinuity in ion velocity at Mach 1. However, the model he used to derive this ion velocity discontinuity was that of a neutral fluid undergoing ambipolar diffusion and since a fluid cannot remain neutral near Mach 1, the existence of the discontinuity is in doubt. To understand the nature of this trans-sonic is the goal of this work.

H. Friedman  
Electrophysics Department

#### References

1. D. Bohm, 'Characteristics of Electrical Discharges', McGraw-Hill, 1949.
2. K. B. Persson, Physics of Fluids, 5, 12, 1962.
3. W. P. Allis and P. J. Rose, Physical Review, 93, 1, 1954.
4. J. Friedberg, To be published.
5. K. B. Persson, NBS Report 8452, p. 22.

#### 1.9 Plasma Boundary Oscillations

(Abstract of PIBAL Report No. 880)

A theoretical investigation is being conducted on the excitation of plasma oscillations in the plasma sheath close to the walls of a plasma. It is well-known that

in the plasma sheath a strong d.c. electric field is found and the electron density at the wall becomes very small compared to the asymptotic value which corresponds to the core of the plasma. As a consequence if an oscillating electric field is applied perpendicular to the wall of the plasma with a frequency smaller than the value of the plasma frequency in the core of the plasma, an oscillation should be excited in a region of the plasma close to the wall. In order to investigate the properties of these possible oscillations, a preliminary analysis has been conducted assuming a plane geometry where the plasma is located in the region  $x \geq 0$ . On the basis of a linear macroscopic approach, the time dependent values of electric field  $E$ , electron density  $n$ , and electron velocity  $u$  satisfy the equations

$$\left. \begin{aligned} \frac{\partial u}{\partial t} &= -\frac{e}{m} E + \frac{a^2}{\gamma} \left( \frac{1}{n_e} \frac{dn_e}{dx} \right) \frac{n}{n_e} - \frac{a^2}{n_e} \frac{\partial n}{\partial x} \\ \frac{\partial n}{\partial t} + \frac{\partial}{\partial x} (n_e u) &= 0 \\ \frac{\partial E}{\partial x} &= -\frac{e}{\epsilon_0} n \end{aligned} \right\} \quad (i)$$

where  $e, m$  are the charge and mass of an electron;  $\epsilon_0$  is the dielectric constant of a vacuum.  $a$  is the speed of sound in the electron gas, and  $\gamma$  is the ratio of specific heats. In Eqs. (1) the effects of collisions have been neglected and the temperature has been assumed constant throughout the plasma.  $n_e$  is the equilibrium electron density which is related to the d.c. electrostatic potential  $\phi$  in the plasma through the equation

$$n_e = n_0 e^{\frac{e\phi}{kT}} \quad (2)$$

where  $k$  is the Boltzmann constant and  $n_0$  is the value of the equilibrium electron density at large distance from the wall. Thus the potential is assumed to be zero in the core of the plasma. If a negligible electron current flows toward the wall, the wall potential is negative and large compared to  $kT/e$ . The local value of  $\phi$  is obtained by solving the equations which govern the electron and ion motion in the d.c. situation.

Assume now a solution of Eqs. (1) of the form  $\exp(i\omega t)$ . The amplitude of the electric field satisfies the equation

$$\frac{d^2 E}{dx^2} - \frac{1}{\gamma} \left( \frac{1}{n_e} \frac{dn_e}{dx} \right) \frac{dE}{dx} + \frac{\omega^2}{a^2} \left( 1 - \frac{\omega_p^2}{\omega^2} \right) E = 0 \quad (3)$$

where  $\omega_p$  is the local value of plasma frequency. The solution of Eq. (3) may be written in the form

$$E = \left( \frac{n_e}{n_0} \right)^{\frac{1}{2\gamma}} y(x) \quad (4)$$

$y(x)$  is a solution of the equation

$$\frac{d^2 y}{dx^2} + \frac{\omega^2}{a^2} \left[ 1 - \frac{\omega_0^2}{\omega^2} \Psi(x) \right] y = 0 \quad (5)$$

where  $\omega_0$  is the value of the plasma frequency at large distance from the wall and

$$\Psi(x) = \frac{1}{2} \left[ \left( 1 + \frac{1}{\gamma} \right) e^{\varphi} + (1-2\varphi)^{-1/2} + \frac{1}{\gamma} (1-2\varphi)^{1/2} - \frac{2}{\gamma} \right] \quad (6)$$

where

$$\varphi = \frac{e\phi}{kT} \quad (7)$$

One observes that  $\Psi = 1$  at  $\varphi = 0$ . As the potential decreases,  $\Psi(x)$  decreases to a minimum value, after which it increases again for large negative values of  $\varphi$ .

Fig. 1 shows the values of  $\Psi$  versus  $\varphi$  for the particular value  $\gamma = 3$ . The minimum value is reached at about  $\varphi \sim -3$ , where  $\Psi_{\min} \sim 1/3$ . Thus a resonance is possible with plasma oscillations confined to a small region close to the wall as long as

$$1 > \frac{\omega}{\omega_0} > \sqrt{\Psi_{\min}} \sim \frac{1}{\sqrt{3}} \quad (8)$$

The reason for the minimum possible value of resonant frequency is the fact that as the electron density  $n_e$  decreases, the d.c. electric field increases. As a consequence

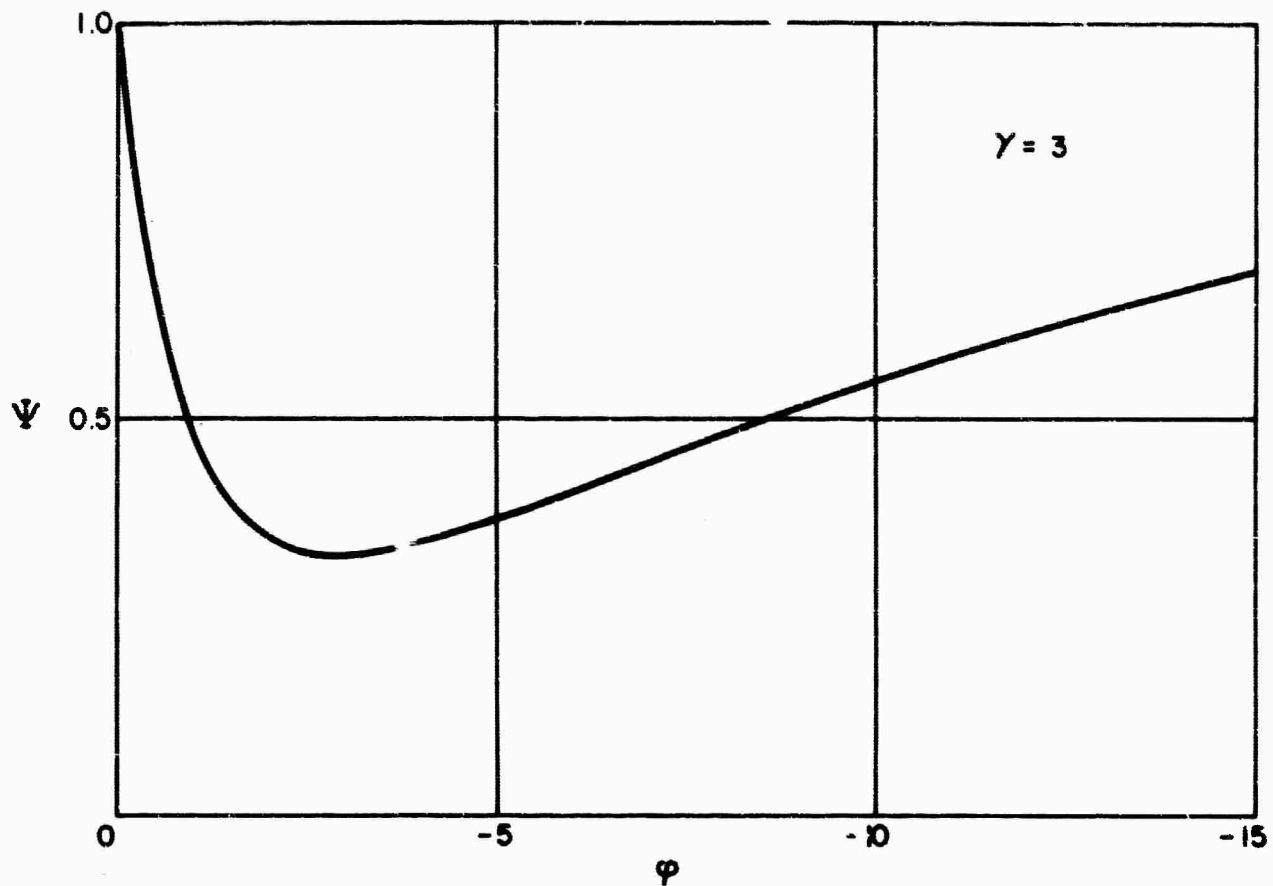


Fig. 1 (1-21) - Function  $\psi$  versus potential in the plasma

a minimum frequency cutoff arises due to the electric field in a way similar to the sound wave properties in an atmosphere which is in equilibrium with a gravitational field. Condition 8 shows that only a relatively narrow range of resonant frequencies close to  $\omega_0$  are possible.

Detailed numerical solutions of Eq. (5) have been conducted. The results are plotted in Fig. 2, where the coordinate  $\xi$  represents the coordinate  $x$  normalized with respect to the Debye length in the core of the plasma. The predicted oscillation is shown, and two resonances are observed at  $\frac{\omega}{\omega_0} = .75$  and at  $\frac{\omega}{\omega_0} = .95$ . Only the former is shown in Fig. 2.

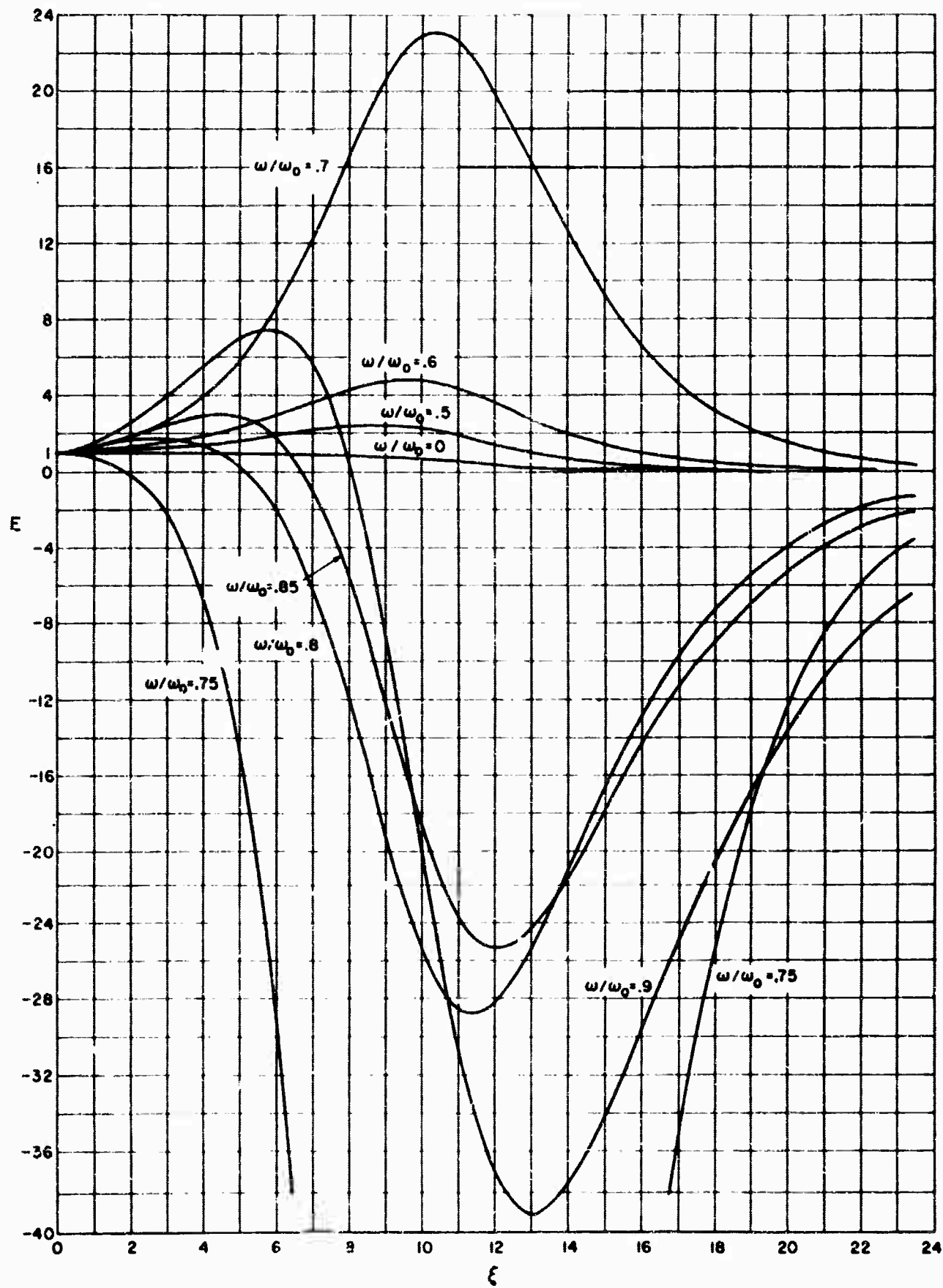


Fig. 2 (1-22) - Electric field distribution as a function of distance from wall

The calculations will be extended to include the effect of electron collisions. Furthermore, a theoretical analysis will be conducted to assess the range of validity of these solutions.

S. Schwartz  
M. H. Bloom  
Dept. of Aerospace Engineering  
and Applied Mechanics

M. Abele  
Electrophysics Department

### 1.10 Perturbation Procedure for Nonlinear Plasma Equations

The study of plasma physics has possibly brought to light more than ever the need of a method for solving nonlinear differential equations. One of the most useful techniques which has evolved is due to Krylov and Bogoliubov<sup>1</sup>, and later refined by Bogoliubov and Mitropolsky<sup>2</sup>. Their perturbation procedures were concerned with solving an ordinary linear differential equation with an additional small nonlinear term. Recently, this technique was extended to cover certain linear, partial differential equations with a small nonlinear term by Montgomery and Tidman<sup>3</sup>. The underlying feature responsible for the success of the above techniques is the removal of secular terms which appear in the expansion procedure.

We have attempted to utilize this feature to solve a class of problems described by an ordinary nonlinear differential equation with an additional small nonlinear term. Motivation for solving this type of an equation has arisen in connection with the following physical problems:

1. The effect of temperature on the propagation of nonlinear waves in an electron plasma.
2. The effect of temperature on the nonlinear stabilization of the electron-ion two stream instability.
3. The nonlinear effects of dispersion and temperature near the upper hybrid resonance.
4. The stability of a class of nonlinear plasma waves.

A more detailed description of these problems will be given later. However, we state that the answer to each of the above problems is contained in the solution of a generalized equation of the form

$$\frac{d^2\varphi}{dt^2} + f(\varphi, \frac{d\varphi}{dt}) = \epsilon g(\varphi, \frac{d\varphi}{dt}) \tag{1}$$

where  $f$  and  $g$  are known functionals of  $\varphi$  and  $\frac{d\varphi}{dt}$ , and  $\epsilon$  is a small parameter.

The essential difference that arises when applying a perturbation procedure to Eq. (1) as compared to the equation treated in references 1, 2 which is of the form

$$\frac{d^2\varphi}{dt^2} + \omega_0^2 \varphi = \epsilon g(\varphi, \frac{d\varphi}{dt}) \tag{2}$$

can be stated as follows. The expansion procedures used to solve Eq. (2) result in a set of linear, inhomogeneous differential equations with constant coefficients while the expansion procedure which we utilize to solve Eq. (1) results in a similar set of equations, except with variable coefficients.

Brief Description of the Expansion Procedure

The four applications given above are concerned with the periodic solutions of Eq. (1). Thus, the first step in the procedure is to define a normalized time variable  $\xi = \omega t$  such that, if periodic solutions do exist, then  $\varphi(\xi) = \varphi(\xi + 2\pi)$ .

Next,  $\varphi(\xi)$  and  $\omega^2$  are expressed as asymptotic series in the parameter  $\epsilon$ , as follows:

$$\varphi = \varphi_0 + \epsilon \varphi_1 + \epsilon^2 \varphi_2 \dots \tag{3}$$

$$\omega^2 = \omega_0^2 (1 + \alpha_1 \epsilon + \alpha_2 \epsilon^2 \dots) \tag{4}$$

In the applications considered, it has been found that even in the simplest problem, the algebra becomes prohibitive after the first correction term. As a result, only this term has been considered, although in principle, the higher order terms could be calculated by continuing the procedure.

The expansions in Eq. (3) and (4) are then substituted into Eq. (1). Upon equating each coefficient of  $\epsilon^n$  equal to zero, there results an infinite set of equations, which are to be solved subject to the initial conditions given by

$$\varphi(0) = A_0 + \epsilon A_1 + \dots \tag{5}$$

$$\frac{d\varphi}{d\xi}(0) = B_0 + \epsilon B_1 + \dots \tag{6}$$

In order for the perturbation procedure to be useful we must assume that the solution to the zeroth order equation, given below, must be known.

$$\omega_0^2 \frac{d^2 \varphi_0}{d\xi^2} + f\left(\varphi_0, \omega_0 \frac{d\varphi_0}{d\xi}\right) = 0 \tag{7}$$

(Clearly it is not feasible to expand about an unknown solution.) The constant  $\omega_0^2$  is determined by the periodicity condition  $\varphi(0) = \varphi(2\pi)$ . Physically, this corresponds to finding either the frequency of oscillation, or the dispersion relation if one is dealing with waves.

With this background, the perturbation problem can now be stated. Given a differential equation of the form of Eq. (1) which has a known zeroth order solution (i. e.  $\epsilon = 0$ ),  $\varphi_0(\xi)$ , satisfying  $\varphi_0(0) = A_0$  and  $\frac{d\varphi_0}{d\xi} = B_0$ , and which is periodic with period  $2\pi$ , then find the first order correction to this solution,  $\varphi_1(\xi)$ , which obeys  $\varphi_1(0) = A_1$  and  $\frac{d\varphi_1}{d\xi}(0) = B_1$ , and which exhibits no secular behavior.

As was previously stated, the equation for  $\varphi_1(\xi)$  is a linear, inhomogeneous differential equation with variable coefficients. In general, an equation of this type cannot be solved. However, in this expansion procedure, the variable coefficients depend on  $\varphi_0(\xi)$  in such a manner that an exact solution for  $\varphi_1(\xi)$  can be obtained. Without performing the steps, the result is

$$\begin{aligned} \varphi_1(\xi) = & -\frac{\alpha_1}{2} \xi \frac{d\varphi_0}{d\xi} + \frac{d\varphi_0}{d\xi} \left[ k_1 + \left( k_2 + \frac{\alpha_1 B_0^2}{2} \right) \int_0^\xi \frac{e^{-\alpha(\xi')}}{(d\varphi_0/d\xi')^2} \right. \\ & \left. + \frac{1}{\omega_0} \int_0^\xi \frac{e^{-\alpha(\xi')}}{(d\varphi_0/d\xi')^2} \int_0^{\xi'} e^{\alpha(\xi'')} \frac{d\varphi_0}{d\xi''} g(\varphi_0, \omega_0 \frac{d\varphi_0}{d\xi''}) d\xi'' \right] \end{aligned} \quad (8)$$

where  $k_1 = \frac{A_1}{B_0}$ ,  $k_2 = B_1 B_0 + \frac{A_1}{2} f(A_0, \omega_0 B_0)$ , and  $\alpha(\xi) = \frac{1}{\omega_0} \int_0^\xi \frac{\partial f(\varphi_0, \omega_0 \frac{d\varphi_0}{d\xi'})}{\partial (d\varphi_0/d\xi')} d\xi'$ .

Secular behavior is clearly exhibited by the first term on the right side of Eq. (8). Since  $\varphi_0(\xi)$  is assumed to be periodic, the term  $k_1 \frac{d\varphi_0}{d\xi}$  exhibits no secular behavior. We have shown that a necessary condition for this perturbation procedure to work (which has been satisfied by all physical problems encountered so far) is that the term

$$\frac{d\varphi_0}{d\xi} \int_0^\xi \frac{e^{-\alpha(\xi')}}{(d\varphi_0/d\xi')^2} \quad (9)$$

be non-secular in behavior. Hence the only remaining term in Eq. (8) which can exhibit secular behavior is the last one, which depends upon the form of the perturbing function  $g(\varphi_0, \omega_0 \frac{d\varphi_0}{d\xi})$ .  $\alpha_1$  is then chosen to eliminate this secular behavior. As a result we obtain the following two conditions:

$$\alpha_1 = \frac{1}{\omega_0 \pi} \int_0^{2\pi} \frac{e^{-\alpha(\xi)}}{(d\varphi_0/d\xi)^2} d\xi \int_0^\xi e^{\alpha(\xi')} \frac{d\varphi_0}{d\xi'} g(\varphi_0, \omega_0 \frac{d\varphi_0}{d\xi'}) d\xi' \quad (10)$$

$$\int_0^{2\pi} e^{\alpha(\xi)} \frac{d\varphi_0}{d\xi} g(\varphi_0, \omega_0 \frac{d\varphi_0}{d\xi}) d\xi = 0 \quad (11)$$

The value of  $\alpha_1$  is the first order correction to  $\omega^2$ , and as is seen from Eq. (10), depends upon the perturbing function  $g(\varphi_0, \frac{d\varphi_0}{d\xi})$ .

Equation (11) should be viewed as a condition on the function  $g(\varphi_0, \frac{d\varphi_0}{d\xi})$

which must be satisfied in order that  $\varphi_1(\xi)$  have periodic solutions. Physically a certain condition on  $g\left(\varphi_0, \frac{d\varphi_0}{d\xi}\right)$  must be expected, or else any arbitrary perturbation term added to the original differential equation would lead to periodic solutions. As an example, periodic solutions would not be expected if  $g\left(\varphi_0, \frac{d\varphi_0}{d\xi}\right)$  corresponded to a frictional loss.

Summarizing, a nonlinear equation with an additional small nonlinear term, whose zero order solution is periodic, will have a first order solution that is periodic if Eqs. (9) and (11) are satisfied and if  $\alpha_1$ , the first order frequency correction is chosen according to Eq. (10). The first order solution,  $\varphi_1(\xi)$ , is given by Eq. (8).

Applications of the Perturbation Procedure

1. The effect of temperature on the propagation of nonlinear waves in an electron plasma.

It has long been known that traveling wave solutions to the cold plasma equations exist obeying a nonlinear dispersion relation given by  $\omega^2 = \omega_p^2$ . Although the physical significance of these solutions is highly questionable, we have attempted to find the first order temperature correction to these equations, primarily to achieve facility with perturbation technique. The equation to be solved can be put in the form

$$\frac{\omega^2}{\omega_p^2} \frac{d^2 u}{d\xi^2} - \left(\frac{1}{u} - 1\right) = - \frac{\epsilon}{2} \frac{\omega^2}{\omega_p^2} \frac{d^2}{d\xi^2} \frac{1}{u^2} \tag{12}$$

where  $\omega_p^2 = \frac{N_o e^2}{m \epsilon_o}$ ,  $\epsilon = \frac{k^2 a^2}{\omega^2}$ ,  $a^2$  = thermal speed,  $u$  = normalized electron velocity in the wave reference frame. Upon applying the perturbation technique to this problem, we have found the first order correction to the dispersion relation, which is given by

$$\frac{\omega_p^2}{\omega^2} = 1 - \frac{k^2 a^2}{\omega^2} \frac{1}{(1-A^2)^{5/2}} \tag{13}$$

where  $A^2$  is a normalized amplitude and  $|A| \leq 1 - \epsilon^{1/4}$ . This result agrees with Wilhelmsson<sup>4</sup> who performed the calculation by a different procedure.

2. The effect of temperature on the two stream instability.

It has been shown<sup>5</sup> that there is a narrow range of wave numbers,  $k$ , for which the electron-ion two stream instability in a cold plasma stabilizes in the non-linear limit. As a result it is desired to determine what effect finite electron and ion temperatures have on this narrow range of stabilization. The nonlinear equations describing the plasma are given by

$$\frac{\omega^2}{\omega_{pe}^2} \frac{d^2}{d\xi^2} \frac{u_e^2}{2} - \left( \frac{a_e}{u_e} - \frac{a_i}{u_i} \right) = - \frac{\epsilon_e}{2} a_e^2 \frac{\omega^2}{\omega_{pe}^2} \frac{d^2}{d\xi^2} \frac{1}{u_e^2} \tag{14}$$

$$\frac{\omega^2}{\omega_{pi}^2} \frac{d^2}{d\xi^2} \frac{u_i^2}{2} + \left( \frac{a_e}{u_e} - \frac{a_i}{u_i} \right) = - \frac{\epsilon_i}{2} a_i^2 \frac{\omega^2}{\omega_{pi}^2} \frac{d^2}{d\xi^2} \frac{1}{u_i^2} \tag{15}$$

where the subscript e(i) stands for electrons (ions), and  $a = 1 - \frac{\bar{nv}}{\bar{n}}$ ,  $\bar{n}$  is the average particle density and  $\bar{nv}$  the average particle flux. The results of this application are not as yet conclusive. However, our calculations indicate that the integrals can be explicitly calculated for this case.

3. Nonlinear effects near hybrid resonance.

If one calculates the power radiated by a single charge moving at a constant velocity in a magnetized plasma, one finds that this power is infinite. To resolve this problem we take into account both temperature and large amplitude effects near the upper hybrid resonance. From the linear theory we know that the former effect introduces coupling between the electromagnetic and the acoustic mode. From other nonlinear problems, we expect the nonlinearities to limit the amplitude of the wave below a certain value above which a collisionless shock forms and all orderly wave energy is rapidly thermalized. The equations describing the behavior near hybrid resonance are given by

$$\frac{\omega^2}{\omega_p^2 + \omega_c^2} \frac{d^2}{d\xi^2} \frac{v^2}{2} + \left( 1 - \frac{1}{v} \right) = \frac{\epsilon_1}{2} \frac{1}{v^5} - \frac{\omega^2}{\omega_p^2 + \omega_c^2} \left[ \frac{d}{d\xi} (u_y \epsilon_y) + \frac{\omega_c}{\omega} \epsilon_y \right] \tag{16}$$

$$\frac{d\epsilon_y}{d\xi} = \epsilon_2 \frac{\omega_p^2 u_y}{\omega^2 v} \tag{17}$$

$$\frac{du_y}{d\xi} - \frac{\omega_c}{\omega} \left(\frac{1}{v} - 1\right) = 0 \tag{18}$$

where  $v$  and  $u_y$  the normalized velocity components  $\perp$  to the magnetic field,  $\omega_c = \frac{eB_0}{m}$ ,  $\epsilon_y$  is the normalized electric field,  $\epsilon_1 = \frac{k^2 a^2}{\omega^2}$ ,  $\epsilon_2 = \frac{\omega^2}{k^2 c^2}$ . This formidable set of nonlinear, coupled differential equations has been solved to first order in  $\epsilon_1$  and  $\epsilon_2$ . Much work has yet to be done to understand the significance of the solutions. However, a great bulk of the calculation has been completed and we present here the nonlinear dispersion relation correct to first order in  $\epsilon_1$  and  $\epsilon_2$ .

$$\frac{\omega^2}{\omega_p^2 + \omega_c^2} = 1 + \frac{\epsilon_1}{(1-A)^{5/2}} - \epsilon_2 \frac{\omega_p^2 \omega_c^2}{(\omega_p^2 + \omega_c^2)^2} (1-A^2) \tag{19}$$

4. Stability of nonlinear plasma waves.

In the preceding three applications we have perturbed about a known period solution to obtain first order corrections. A question that arises is whether or not the zero order solutions are stable solutions about which it is legitimate to perturb. We have performed a stability analysis of the zeroth order solutions of Eqs. (12) and (16). By utilizing certain transformations and the results of the perturbation theory we have shown that these solutions are stable. This result is in agreement with Jackson<sup>6</sup> who considered only Eq. (12) and with Dolph<sup>7</sup> who considered both Eqs. (12) and (16).

J. Freidberg  
 Electrophysics Department

### References

1. N. Krylov and N. Bogoliubov, "Introduction to Nonlinear Mechanics" (1937)
2. N. Bogoliubov and J. Mitropolsky, "Asymptotic Methods in the Theory of Nonlinear Oscillations" Moscow (1958).
3. D. Montgomery and D. Tidman, Phys. Fluids 7, 242 (1964).
4. H. Wilhelmsson, Phys. Fluids 4, 335 (1961).
5. J.P. Freidberg, Phys. Fluids 8, 1051, (1965).
6. E.A. Jackson, Phys. Fluids 6, 753 (1963).
7. C.L. Dolph, J. Math. Anal. and App. 5, 94 (1962).

### 1.11 Kinetic Theoretical Investigations of a Fully Ionized Gas

It is the purpose of the project

- (a) To show that most kinetic theories of fully ionized gases so far published are based on an unfeasible assumption, and
- (b) To propose an alternative theory.

The following PIBAL report on this subject has been prepared and distributed:

PIBAL Report No. 863 - "A Kinetic Theoretical Investigation  
of a Fully Ionized Gas"

Part I - Paradoxes in the B-B-G-K-Y Hierarchy  
(published January 1965)

Part II - Some Aspects of Multiple Collisions  
(published January 1965)

Part III - A Kinetic Theory of Electron Gas  
(published May 1965)

In Part I, we first assume that a constituent particle in an electron gas ( or a fully ionized gas) interacts with more than one particle at the same time and that the mutual interactions among these particles are simultaneously significant. Directing

our attention to the usage of the hypothesis of equal a priori probabilities, we investigate the plausibility of customary methods considering the B-B-G-K-Y hierarchy for the basis of deriving kinetic equations for electron gases. Conditions imposed upon the hierarchy do not seem consistent with the assumption set forth above. Main questions are raised regarding (i) the assumption of characteristic time scales and (ii) the assumption that a set of multiple interactions are, in effect, equivalent to a superposition of binary interactions. The situation is similar regarding other theories advanced hitherto without being based on the hierarchy.

In Part II, the Brownian motion of a test body due to multiple interactions with field particles is investigated within or almost within the framework of Markoff's processes. First, Markoff's processes are studied as presenting such multiple interactions. Based on the study and by means of Markoff's method of random flights, we investigate the Brownian motion of an elastic test body submerged in a rarefied gas constituted of elastic molecules, under the condition that mutual interactions among field particles are negligible. It is shown that there is no difference in effect between temporal repetitions of random binary collisions and multiple collisions (random binary collisions superposed at one moment of time), so far as the friction and diffusion of the test body in momentum space are concerned. The situation is similar when a test body with electric charge is submerged in an electron gas, if the mutual interactions among electrons are ignored. It is not feasible, however, to ignore those mutual interactions of field electrons and to represent electronic multiple interactions by temporal repetitions of random binary interactions, each of which takes place independently: fluctuations of limitlessly large amplitudes in the spatial distribution of electrons, which may possibly take place in this approximation, do not seem realistic, because a limitless concentration of potential energy accompanying a concentration of electrons in a local spot cannot be permitted. Amplitudes of such fluctuations and/or microscopic disturbances must have a certain maximum limit. (The situation does not change even when the interaction force law is of the Debye-Hückel type.) A kinetic theoretical scheme of treating fully ionized gas in the light of the fact is proposed.

In Part III, we develop a kinetic theory of electron gas according to the scheme suggested in Part II. At the first step of approximation, one field electron interacts with the test electron in the sense of Boltzmann's binary collision when those two particles are their mutual nearest neighbors; otherwise the field electron, with the others, exerts a force of the Vlasov type on the test electron. At this stage of approximation, one field electron represents all the field electrons; there is no mutual correlation among the field electrons. In the second approximation, where two electrons represent the field electrons, the pair of field electrons, when they are mutual nearest neighbors, become a source of fluctuating force-field due to their mutual interaction. In the third approximation, three electrons represent the field electrons. As the step of approximation proceeds, the pairs of electrons produce more complex force-fields by their mutual interactions. The kinetic equation of the single-particle distribution function contains interaction terms of the Vlasov type, of the Boltzmann type and of the Fokker-Planck type. There is no difficulty of divergence in the effect.

#### Plans for the next half year interval

Investigation of turbulence in plasma: various correlation functions and their dynamical behaviors will be investigated.

T. Koga  
Dept. of Aerospace Engineering  
and Applied Mechanics

#### 1.12 Kinetic Theory of Plasmas

##### A. Low Frequency Tonks-Langmuir Ion Waves

The work on this project as described in Section 1-3-1-a of the last report has been carried to completion. A paper on this work will appear in the Canadian Journal of Physics (1965).

##### B. Diffusion of a Plasma Column Across a Magnetic Field

(Abstract of PIBMRI-1289-65)

Prigogine-Balescu's method of diagrams, as extended to the case of plasmas

in magnetic fields in the recent work of Haggerty and de Sobrino (Can. J. Phys. 42, p. 1969, 1964), has been applied to the problem of the diffusion in plasmas in a magnetic field. A report of the work has been prepared for circulation prior to publication.

### C. Landau Damping

(Abstract of Report PIBMRI-1280-65)

The classic treatments by Landau and by Van Kampen of the initial value problem of the linearized Vlasov equation are recapitulated, with special reference to the Landau Damping. It is emphasized that the time dependence of the potential, or the density, namely the existence or absence of this Landau damping, is jointly determined by two factors: (1) the form of the "unperturbed" velocity distribution  $F_0(u)$  (i.e. the spatially homogeneous and time-independent part from which the distribution  $F(u)$  is assumed to deviate by small amounts  $f(x, u, t)$ ), and (2) the nature of the initial velocity distribution  $f(x, u, 0)$ . This latter dependence is more explicitly brought out in the Van Kampen treatment in which the velocity distribution is expressed in terms of the normal modes of the plasma, which in general can be described as involving a collective motion arising from the Coulomb interactions between the particles and the streaming motions of the particles. It is the superposition of the streaming motion of the particles on the collective motion (the plasma oscillations) that causes the spatial uniformization of the potential, or the density. This spatial uniformization in the course of time is represented by the Landau damping.

The Landau damping constant  $\gamma$  for the case of a Maxwellian  $F_0(u)$  has been calculated in a "physical" model in which  $\gamma$  is obtained as the transition probability with which an electron having a velocity  $u = \omega/k$  exchanges energy with the collective motion (the plasma oscillation). The transition probability is calculated by the quantum mechanical perturbation theory followed by a passage to the classical limit. The expression obtained for  $\gamma$  is the same as that given by Landau.

### D. Nonlinear Vlasov Equation (Section 1-3-2 of last report)

An attempt is being made to extend the method of stationary solutions of

the linearized Vlasov equation (Van Kampen) to a more general system, namely a two component plasma, and to study the nonlinear Vlasov equation on the basis of some assumptions but without reference to the perturbation method usually employed.

#### E. Homogeneous Plasmas in Magnetic Fields and Inhomogeneous Plasmas

The kinetic equation of a homogeneous plasma in uniform magnetic fields and that of an inhomogeneous plasma having small amplitudes and gradients in the inhomogeneities have been derived on the basis of Bogoliubov's theory. In the former case, the result is equivalent to that of Rostoker (1960) who employs the cluster expansion method instead of Bogoliubov's theory. In the latter case, the result obtained here shows a mathematical similarity to, but differs in implications from, that of Guernsey (1962).

This work will appear in the book now in the course of publication.

T. Y. Wu  
M. J. Haggerty  
D. H. Yee  
Physics Department

## 2. ELECTROMAGNETICS

### Introduction

While a detailed analysis of the processes occurring in the ionized, multiconstituent gas constituted by a plasma is exceedingly complicated, certain macroscopic properties of such a medium may be characterized approximately by an equivalent isotropic or anisotropic dielectric constant and, if temperature effects are included, by an equivalent dynamic pressure. Although the range of validity of this simplified description is limited, (linearized, small signal regime) it is essential to understand properly the influence of such a medium on the propagation of electromagnetic and (or) dynamical waves, on the radiation characteristics of antennas embedded in the medium, and on wave coupling occurring at boundaries and interfaces. These problems have a direct bearing on communication with space vehicles which are surrounded by an ionized plasma shell in the upper atmosphere, here, or which are passing through the (dielectrically anisotropic) ionosphere. Since the vehicle is in motion, the treatment of moving as well as stationary antennas is relevant.

The preceding considerations have furnished the motivation for the theoretical study of a class of propagation, radiation, diffraction, and interface problems in media which simulate a plasma with or without an externally impressed magnetic field. In the "cold plasma" approximation, such media include isotropic and anisotropic dielectrics with appropriate dispersive characteristics, while mechanical deformation is also included in the description of a warm plasma. A systematic study has been in progress with the aim of providing an understanding of the mechanisms of excitation and coupling of various wave types, either in source regions, at boundaries or by continuous inhomogeneities. The approach has been to select mathematically tractable prototype problems which incorporate a sought-after effect in an idealized form, and then to search for procedures which extend the results to more general situations. Major emphasis has been placed not only on formal mathematical solutions but on the extraction of explicit (though approximate) information as well as on a meaningful physical interpretation.

Specific problems investigated so far have included the following:

1. The radiation from arbitrarily prescribed electromagnetic sources in infinite and layered anisotropic cold plasmas. Results have been obtained for the effect of the

anisotropy of the medium on the radiation pattern in an unbounded region, as well as the perturbation introduced by a plane boundary. Interface waves (surface waves, leaky waves, lateral waves) excited by these sources have been studied. An invariant phrasing involving the sophisticated use of ray optics in an anisotropic environment is now being carried out to render the results useful for more general geometrical configurations.

2. The radiation from arbitrarily prescribed electromagnetic or acoustic sources in infinite and layered isotropic warm plasmas. In this instance, one includes in the analysis both the electromagnetic and the dynamical fields which may be coupled in source regions and at boundaries. Several problems in this category are presently under study, with the aim of providing quantitative information of coupling phenomena of various types. One such problem, the diffraction by a semi-infinite plane, has been analyzed for the purpose of yielding the waves excited by structural discontinuities, e. g. an edge, on configurations embedded in a compressible plasma. This study, summarized below, has led to the discovery of novel wave types, for example, electromagnetic-acoustic lateral waves, which are not encountered in a cold plasma environment.

The radiation from sources moving across a plasma interface has also received attention. Emphasis is placed again on interface waves excited by this process, either in a cold or warm plasma; some of these waves have not been considered previously in the technical literature. A brief summary of the status of this investigation is given below.

The coupling between electromagnetic and acoustic waves in a warm cylindrical plasma column has likewise received attention, especially in regard to the resonances which are excited by an impinging electromagnetic field.

3. The effect of continuous inhomogeneities on the processes comprised under 1. and 2. . While the preceding discussion has assumed that the plasma is either wholly or piecewise homogeneous, it is known that there exists on boundaries a plasma sheath wherein the medium properties vary continuously. This variation may influence substantially the wave phenomena predicted on the basis of a sharply bounded interface and therefore merits careful consideration. Selected prototype problems in this category are now being analyzed.

4. Radiation from moving charges in plasmas or passing across plasma boundaries, i. e. effects known as Cerenkov and Transition radiation.

5. Interaction between electron beams and plasmas. An important adjunct to the theoretical investigations is an experimental program which may serve as a check on the validity of the assumptions made in the calculations. Several experiments, described below, are under way and are intended to provide a balanced program.

L. B. Felsen  
Electrophysics Department

### 2.1 Diffraction by a Half Plane in a Compressible Homogeneous Plasma

The coupling of electromagnetic and acoustic waves in a compressible plasma is of interest in such diverse applications as radiation from plasma-clad antennas<sup>1</sup>, wave propagation in the ionosphere<sup>2</sup>, and resonances in ionized columns<sup>3</sup>. Coupling may be produced by continuous stratification, abrupt boundaries, or in electromagnetic source regions. A number of recent investigations have dealt with the effects of various source configurations in an unbounded medium<sup>4</sup>, with selected phenomena due to plane<sup>5</sup>, cylindrical or spherical interfaces separating different homogeneous regions<sup>6</sup>, and also with certain inhomogeneities.<sup>3</sup> The present study is concerned with the influence on the electromagnetic and acoustic wave fields of sharp structural discontinuities which may arise in plasma-clad slot antenna configurations.

The simplest prototype incorporating the above-mentioned structural features and amenable to rigorous analysis is a perfectly conducting half plane. This structure, shown in Fig. 1, is assumed to be immersed in a homogeneous, compressible, isotropic plasma, and is excited by a time-harmonic plane wave (a factor  $\exp(-i\omega t)$  is suppressed). In the (linearized) plasma model adopted here, the electrons are considered mobile and are characterized by a finite temperature, the (stationary) ions produce a neutralizing background, and collisions between electrons and other species are neglected (the latter restriction could readily be eliminated). It is well-known<sup>4</sup> that the fields in such a medium may be separated into an electromagnetic (optical) and a dynamical (acoustic) part, with the former containing all of the magnetic field and the latter all of the charge accumulation. The incident field is either of the optical or acoustic type, with the direction of incidence normal, and the resultant magnetic field parallel, to the edge; the problem is then two-dimensional ( $\partial/\partial x \equiv 0$ ). All of the electromagnetic and dynamical field quantities may be derived from two scalars, the x-component of magnetic field,  $H$ , and the pressure,  $p$ , which satisfy the wave equations,

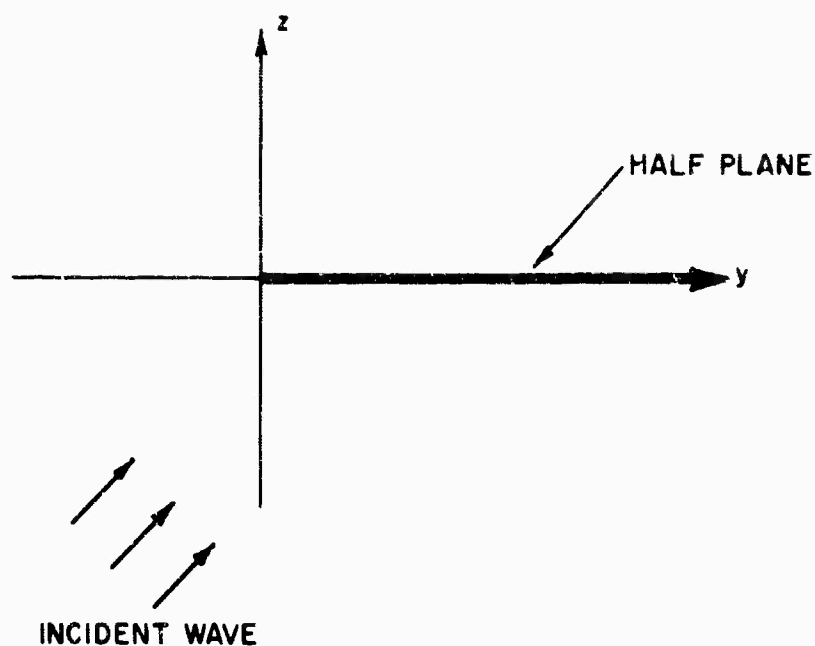


Fig. 1 (2-1) - Physical configuration

$$\left( \frac{\partial^2}{\partial y^2} + \frac{\partial^2}{\partial z^2} + k_o^2 n_p^2 \right) H = 0, \quad k_o = \frac{\omega}{c}, \quad (1a)$$

$$\left( \frac{\partial^2}{\partial y^2} + \frac{\partial^2}{\partial z^2} + k_a^2 n_p^2 \right) p = 0, \quad k_a = \frac{\omega}{a}, \quad (1b)$$

where  $c$  and  $a$  are, respectively, the electromagnetic speed in vacuum and the acoustic speed in the (charge-free) medium, and  $n_p = [1 - (\omega_p / \omega)^2]^{1/2}$  is the plasma refractive index. These equations must be solved subject to a (power) radiation condition at infinity, an edge condition at  $y = z = 0$  (requiring finite stored energy), and the following boundary condition on the half-plane:

$$E_y = 0, \quad v_z = 0, \quad \text{at } z = 0, \quad y > 0, \quad (2a)$$

where  $E_y$  and  $v_z$ , the  $y$ -component of the electric field and the  $z$ -component of the dynamical velocity, are given in terms of  $H$  and  $p$  by:

$$E_y = q \frac{\partial p}{\partial y} + \frac{i}{\omega \epsilon_0 n_p^2} \frac{\partial H}{\partial z}, \quad v_z = -q \frac{\partial H}{\partial y} + \frac{1}{i \omega n_0 m n_p^2} \frac{\partial p}{\partial z} \quad (2b)$$

$q = (1 - n_p^2)/(n_0 e n_p^2)$ , with  $n_0$ ,  $e$ , and  $m$  denoting the electron density, charge and mass, respectively. While some question may be raised concerning the validity of the "perfect reflection" condition  $v_z = 0$ , it has been employed in most previous studies and, because of the lack of a more suitable condition, will also be utilized here.

In view of Eqs. (2a, b), the optical and acoustic fields are coupled at the boundary, and it is convenient to resort to the following Fourier integral representation:

$$H = \frac{1}{2\pi} \int_{-\infty}^{\infty} e^{i\eta y} I_o(\eta, z) d\eta, \quad p = \frac{1}{2\pi} \int_{-\infty}^{\infty} e^{i\eta y} V_a(\eta, z) d\eta, \quad (3a)$$

$$E_y = \frac{1}{2\pi} \int_{-\infty}^{\infty} e^{i\eta y} V_o(\eta, z) d\eta, \quad v_z = \frac{1}{2\pi} \int_{-\infty}^{\infty} e^{i\eta y} I_a(\eta, z) d\eta. \quad (3b)$$

Then from Eqs. (1a, b) and (3a, b), it follows that the Fourier transforms of the field quantities satisfy the following equations:

$$\left( \frac{d^2}{dz^2} + \kappa_o^2 \right) I_o = 0, \quad \left( \frac{d^2}{dz^2} + \kappa_a^2 \right) V_a = 0, \quad (4a)$$

$$V_o = i\eta q V_a - \frac{1}{i \omega \epsilon_0 n_p^2} \frac{dI_o}{dz}, \quad I_a = -i\eta q I_o + \frac{1}{i \omega m n_0 n_p^2} \frac{dV_a}{dz}, \quad (4b)$$

where for real  $\eta$ ,  $\kappa_o$  and  $\kappa_a$  are defined as

$$\kappa_o = +\sqrt{k_o^2 n_p^2 - \eta^2}, \quad |\eta| < k_o n_p, \quad (5a)$$

$$\kappa_o = +i\sqrt{\eta^2 - k_o^2 n_p^2}, \quad |\eta| > k_o n_p, \quad (5b)$$

while for complex  $\eta$ ,

$$\text{Im } \kappa_a > 0 \tag{5c}$$

on the top sheets of the Riemann surfaces corresponding to  $\kappa_o$  and  $\kappa_a$ , respectively.

For the case where the half plane is excited by an optical plane wave, the incident magnetic field and its Fourier transform are given by

$$H_i = \frac{1}{2\pi} e^{i(\eta_i y + \kappa_{oi} z)}, \quad I_{oi} = e^{i\kappa_o z} \delta(\eta - \eta_i), \tag{6a}$$

where

$$\eta_i = k_o n_p \sin \theta_{oi}, \quad \kappa_{oi} = k_o n_p \cos \theta_{oi}, \tag{6b}$$

$\theta_{oi}$  being the angle which the direction of incidence makes with the z-axis. The following forms of  $I_o$  and  $V_a$  satisfy the radiation condition at  $z = \pm \infty$ :

$$I_o = I_{oi} + A_{oo} e^{-i\kappa_o z}, \quad V_a = A_{oa} e^{-i\kappa_a z}, \quad z < 0, \tag{7a}$$

$$I_o = I_{oi} + B_{oo} e^{i\kappa_o z}, \quad V_a = B_{oa} e^{i\kappa_a z}, \quad z > 0. \tag{7b}$$

The function  $A_{oo}(\eta)$  may be regarded as a scattering coefficient from the optical mode to the optical mode, with similar interpretations for the other coefficients in Eqs. (7). Corresponding expressions for  $V_o$  and  $I_a$  are obtained by direct substitution of Eqs. (7) into Eqs. (4).

By imposing the boundary conditions (2a) and the continuity of the field in  $z = 0, y < 0$  on the integral representation (3), a set of coupled, dual integral equations is derived, which is to be solved for the scattering coefficients in Eqs. (7). In solving the integral equations, one makes use of certain function-theoretic arguments to derive two Wiener-Hopf equations which can be factorized to yield results for the unknown field transforms  $I_o(\eta, z)$ , etc. The resulting integral representations constitute the exact solution to the scattering problem, and are tabulated below:

$$H^o = H_i + \frac{1}{2\pi} \int_{-\infty}^{\infty} A_{oo}(\eta) e^{i(\eta y - \kappa_o z)} d\eta, \quad z < 0, \tag{8a}$$

$$p^{\circ} = \frac{1}{2\pi} \int_{-\infty}^{\infty} A_{\circ a}(\eta) e^{i(\eta y - \kappa_a z)} d\eta, \quad z < 0, \quad (8b)$$

$$H^{\circ} = H_i + \frac{1}{2\pi} \int_{-\infty}^{\infty} B_{\circ o}(\eta) e^{i(\eta y + \kappa_o z)} d\eta, \quad z > 0, \quad (8c)$$

$$p^{\circ} = \frac{1}{2\pi} \int_{-\infty}^{\infty} B_{\circ a}(\eta) e^{i(\eta y + \kappa_a z)} d\eta, \quad z > 0; \quad (8d)$$

the superscript  $\circ$  means that the field representations are for the case where the half plane is excited by an optical plane wave, and

$$A_{\circ o}(\eta) = \frac{1}{2} \left[ G_o^-(\eta) - \frac{i \eta q \omega \epsilon_o \eta_p^2}{\kappa_o} F_o^-(\eta) \right], \quad (9a)$$

$$B_{\circ o}(\eta) = -\frac{1}{2} \left[ G_o^-(\eta) + \frac{i \eta q \omega \epsilon_o \eta_p^2}{\kappa_o} F_o^-(\eta) \right], \quad (9b)$$

$$A_{\circ a}(\eta) = \frac{1}{2} \left[ F_o^-(\eta) - \frac{i \eta q \omega m n_o n_p^2}{\kappa_a} G_o^-(\eta) \right], \quad (9c)$$

$$B_{\circ a}(\eta) = -\frac{1}{2} \left[ F_o^-(\eta) + \frac{i \eta q \omega m n_o n_p^2}{\kappa_a} G_o^-(\eta) \right], \quad (9d)$$

The function  $G_o^-(\eta)$  and  $F_o^-(\eta)$  are given by

$$G_o^-(\eta) = -2 \omega \epsilon_o \frac{\sqrt{\kappa_a \eta_p + \eta_i} G_o^+(\eta_i)}{(\eta_i + \eta_{sw}) K^+(\eta_i)} \frac{\sqrt{\kappa_a \eta_p - \eta}}{(\eta - \eta_i)(\eta - \eta_{sw}) K^-(\eta)}, \quad (10a)$$

$$F_o^-(\eta) = -2 \omega m n_o \frac{\sqrt{\kappa_o \eta_p + \eta_i} F_o^+(\eta_i)}{(\eta_i + \eta_{sw}) K^+(\eta_i)} \frac{\sqrt{\kappa_a \eta_p - \eta}}{(\eta - \eta_i)(\eta - \eta_{sw}) K^-(\eta)}, \quad (10b)$$

with

$$G_o^+(\eta_i) = \frac{1}{2\pi i} \frac{\kappa_{oi}}{\omega \epsilon_o n_p^2}, \quad F_o^+(\eta_i) = -\frac{\eta_i q}{2\pi}. \quad (10c)$$

$K^+$  and  $K^-$  in Eqs. (10a,b) are functions which are analytic in the upper and lower halves of the complex  $\eta$ -plane, respectively, and are related to each other by the equation,

$$K(\eta) = K^+(\eta)K^-(\eta) = -\frac{1}{2} \frac{N(\eta)}{\eta_p^2 \eta^2 - \eta_{sw}^2}, \quad (11)$$

and are individually given by<sup>7</sup>

$$\ln K^+(\eta) = \ln K^-(\eta) = -\frac{1}{\pi} \int_{k_o \eta_p}^{k_a \eta_p} \frac{d\xi}{\xi + \eta} \tan^{-1} \left( \frac{\kappa_a |\kappa_o|}{\xi^2 (1 - n_p^2)} \right). \quad (12)$$

In Eq. (11),  $N(\eta)$  has the form

$$N(\eta) = \kappa_o \kappa_a + \eta^2 (1 - n_p^2), \quad (13)$$

and has zeros at (cf. Seshadri<sup>5</sup>)

$$\eta = \pm \eta_{sw} \approx \pm k_a / \sqrt{2 - n_p^2}, \quad k_a / k_o \gg 1, \quad (14)$$

when  $\kappa_o$  and  $\kappa_a$  are defined as in Eqs. (5).<sup>\*</sup>  $N(\eta)$  also has zeros at

$$\eta = \pm \eta_z = \pm (k_o n_p - \delta), \quad 0 < \delta \ll 1, \quad (15)$$

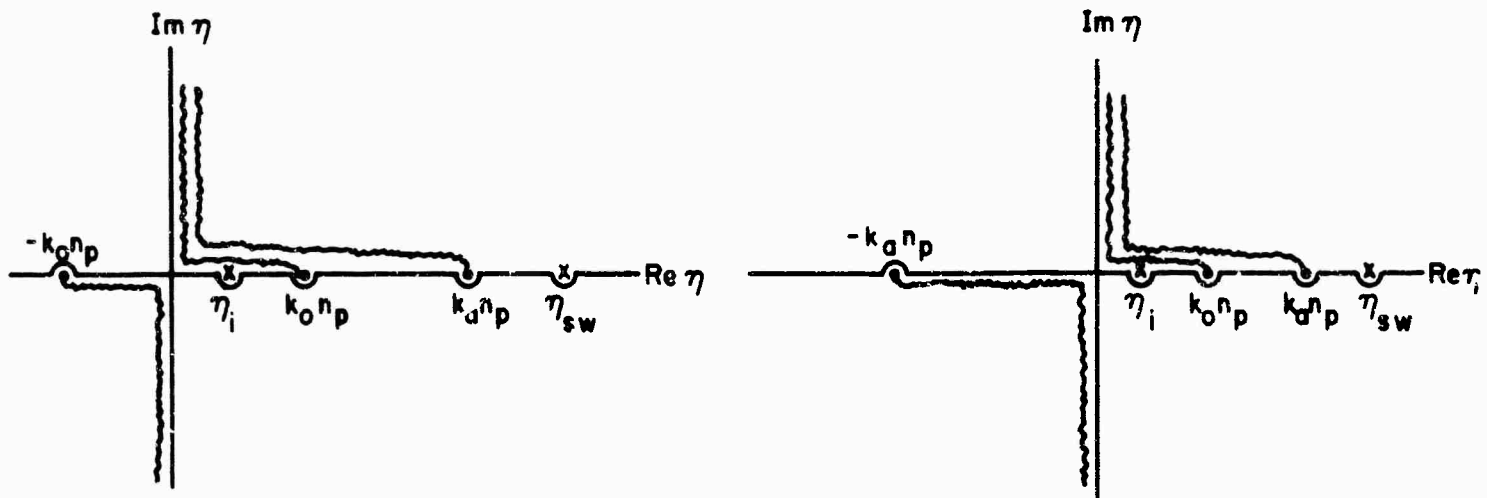
but on the second sheets of the Riemann surfaces defining  $\kappa_o$  and  $\kappa_a$ , respectively.  $\eta = \eta_{sw}$  corresponds to a surface wave pole in Eqs. (10), whereas  $\eta = \eta_z$  corresponds to an improper pole which does not give rise to a residue term in the solution. It is pointed out that  $N(\eta)$  has special physical significance in that it is the denominator of the scattering coefficients  $A_{oo}$  and  $A_{oa}$  for the case where the entire x-y plane is spanned by an infinite, plane, perfect conductor.

The field representations in Eqs. (8) must be accompanied by a specification of the integration path with respect to the singularities. A choice of paths which is

---

\* This result implies that  $K(\eta)$  has no zeros or poles on the top sheet of the Riemann surface defined by Eqs. (5).

consistent with the above discussion is illustrated in Fig. 2. The proper indentations are achieved by introducing small loss into the system and then letting the loss



a) Integration path for H;  $\text{Im } \kappa_o > 0$   
on entire top sheet

b) Integration path for p;  $\text{Im } \kappa_a > 0$   
on entire top sheet

Fig. 2 (2-2)

tend to zero (this is equivalent to imposing the radiation condition in the loss-free case).

For the case where the half plane is excited by an acoustic plane wave the formal solution to the scattering problem may be deduced from Eqs. (8)-(10) by introducing the following changes:  $H \rightarrow p$ ,  $p \rightarrow H$ ,  $o \rightarrow a$ ,  $a \rightarrow o$ ,  $mn_o \rightarrow \epsilon_o$ ,  $\epsilon_o \rightarrow mn_o$ .

To gain an insight into the physical mechanism of the various wave processes which are operative, an asymptotic evaluation of the Fourier integrals has been performed. The results of this analysis, including some numerical data, will be described in detail in a later report. For the present, it suffices to point out that the existence of asymptotic field expressions which may be interpreted as wave types following real ray trajectories is predictable from the refractive index diagrams descriptive of the electromagnetic and dynamical fields. For example, an incident optical wave excites reflected optical as well as acoustic waves. This is depicted in Fig. 3(b) where rays 1, 2, and 3 denote the directions of propagation of the incident optical, reflected optical, and reflected acoustic fields, respectively. These directions may be

determined either analytically or from the refractive index plot in Fig. 3(a). The ray of family 1 which grazes the edge establishes the geometrical shadow boundary

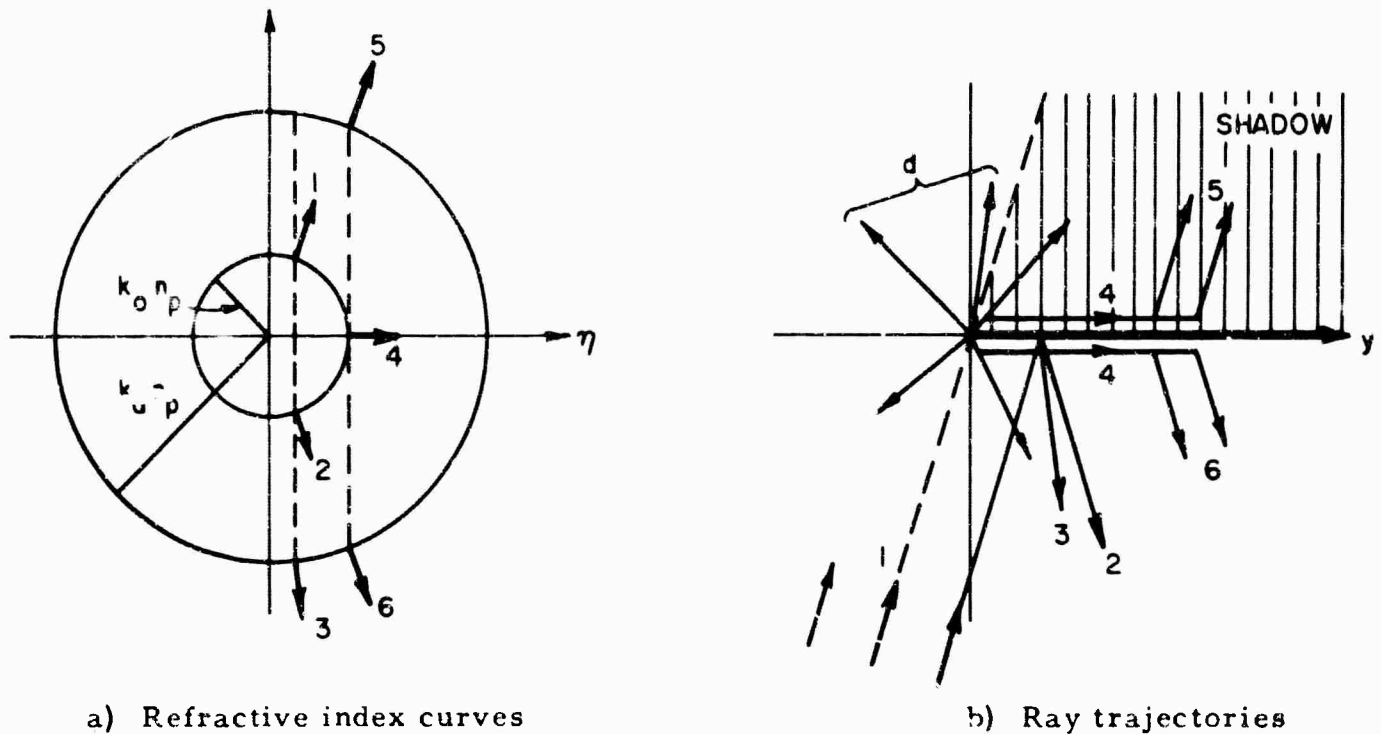


Fig. 3 (2-3)

and also gives rise to a variety of diffraction effects: the radially emerging rays  $d$  which represent either an optical or acoustic cylindrical diffraction field, and the optical lateral rays  $4$  which travel on both sides of the half-plane and shed energy into the acoustic field (rays  $5$  and  $6$ ; see also Fig. 3(a) for the relevant trajectories). Analogous effects arise when an acoustic field is incident.

F. M. Labianca  
 Electrical Engineering Department  
 L. B. Felsen  
 Electrophysics Department

This work was also supported in part by the Air Force Cambridge Research Laboratories under Contract No. AF-19(628)-2357.

### References

1. cf. J. R. Wait, Radio Science (NBS), 68D (1964), p. 1127.
2. H. Poverlein, Phys. Rev., 136 (1964), p. A1605.
3. J. V. Parker, J. C. Nickel, and R. W. Gould, Phys. of Fluids, 7 (1964), p. 1489.
4. M. H. Cohen, Phys. Rev. 123 (1961), p. 711; A. Hessel and J. Shmoys, Proc. Symp. on Electromagnetics and Fluid Dynamics of Gaseous Plasmas (Polytechnic Press, Brooklyn, New York, 1962).
5. A. Hessel, N. Marcuvitz, and J. Shmoys, IRE Trans. AP-10 (1962), p. 48; S. R. Seshadri, IEEE Trans. AP-12 (1964), p. 340.
6. ref. 1; also, S. R. Seshadri, et. al., Can. J. Phys. 42 (1964), p. 465; J. R. Wait, Radio Science (NBS), 69D (1965), p. 247.
7. B. Noble, "The Wiener-Hopf Technique for the Solution of Partial Differential Equations", New York, Pergamon Press, Inc., 1958, p. 6.

### 2.2 Slot Antenna in a Plasma

Here we are concerned with an experimental investigation of slot antennas on plasma clad metal cylinders. The effect of a plasma environment on an antenna has aroused much interest lately. Various theoretical studies have been done on antennas covered by plasma layers.<sup>1, 2</sup> Among approximations often applied in these analyses are: 1) the effect of the non-neutral plasma sheath is negligible; 2) the plasma is incompressible; 3) the assumption of a rigid boundary condition between vacuum-plasma interface and metal-plasma interface. There is really no guarantee that the theoretical results obtained with these and other assumptions will be valid for practical situations.

There have been some laboratory studies of antenna characteristics in the presence of a plasma sheath.<sup>3, 4</sup> In both experiments a dielectric sheet was interposed between the antenna and plasma. On a re-entry vehicle, however, we expect intimate contact between the ground plane of the slot and the plasma. Previously it has been difficult to achieve this close contact in the laboratory. Recently, through the use of screened cathode discharges<sup>5</sup> a plasma clad metal cylinder, designed by Mr. K. T. Lian, has been constructed (see Fig. 1).

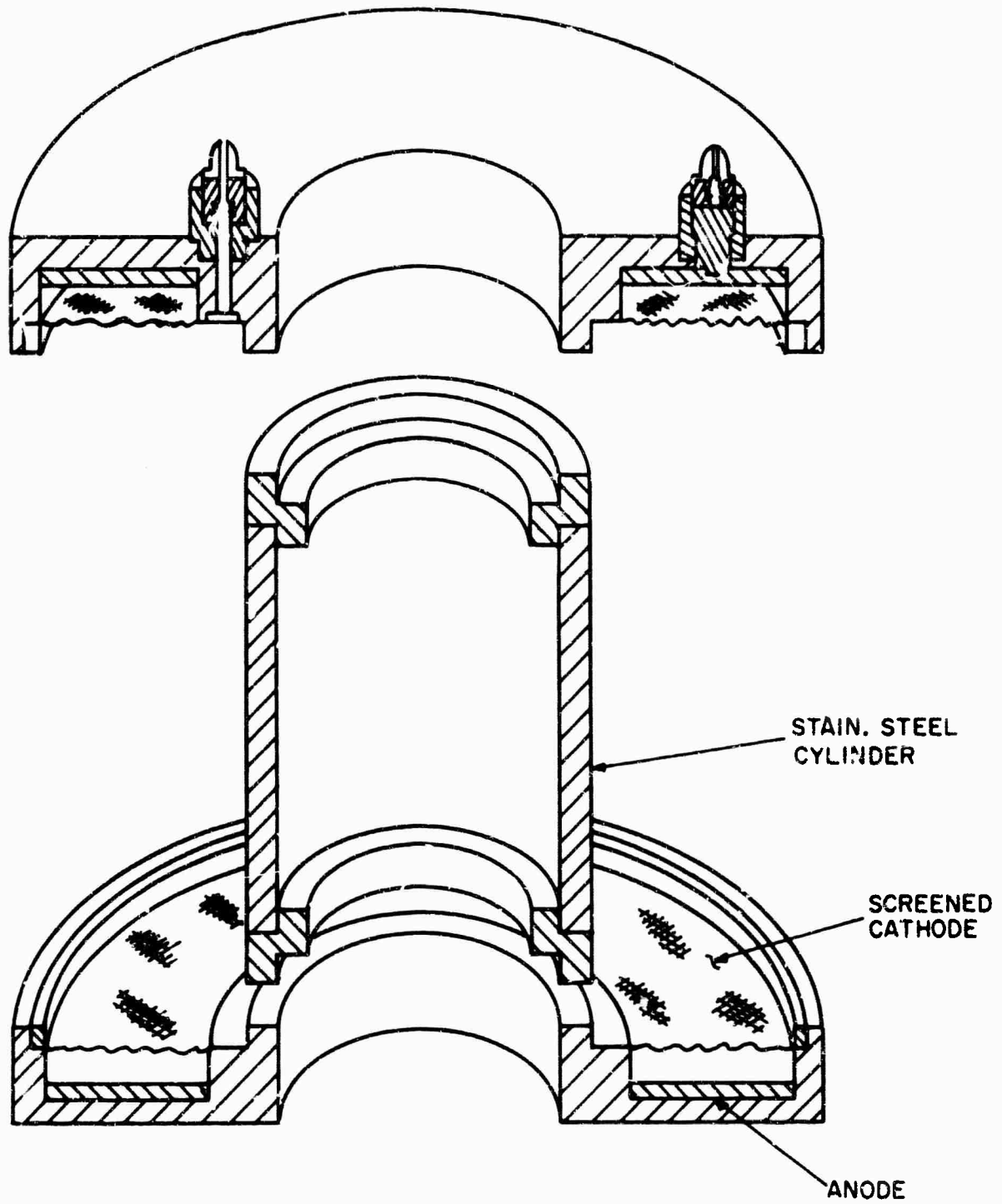


Fig. 1 (2-4) - Discharge configuration for realization of plasma clad metal cylinder

We are currently engaged in an investigation of this discharge under d. c. conditions and plan to determine the electron density and temperature as a function of position with Langmuir probes. Preliminary studies have also been made concerning the design and construction of the microwave circuitry associated with the slot antenna. We hope to begin making impedance and radiation pattern measurements of this plasma clad slot antenna within the next few months.

M. Cronson  
Electrophysics Department

### References

1. Swift, C. T., "Radiation from slotted-cylinder antennas in a re-entry plasma environment", NASA Technical Note TN D-2187, February 1964.
2. Hasserjian, G., "Fields of a curved plasma layer excited by a slot", IEEE Trans. on Antennas and Propagation, Vol. AP-13, May 1965, pp. 389-395.
3. Cloutier, G. C. and Bachynski, M. P., "Antenna characteristics in the presence of a plasma sheath", in Electromagnetic Theory and Antennas, Ed. by E. C. Jordan, (Pergamon Press, New York, 1963), pp. 537-548.
4. Galeis, J. and Mentzoni, M. H., "Waveguide admittance for radiation into plasma layers; theory and experiment", Research Report No. 451, Applied Research Laboratory, Sylvania Electronic Systems, Waltham, Mass.
5. Lian, K. T., "Use of screen cathodes to obtain plasma/electromagnetic wave interaction structure with free plasma boundaries", Electronics Letters, Vol. 1, No. 2, April 1965, p. 47.

### 2.3 Coupling of Acoustic and Electromagnetic Waves

(Abstract of Master of Science Thesis)

In recent years, direct experimental evidence of coupling between electromagnetic and plasma waves was obtained in the phenomenon of Tonks-Dattner resonances.<sup>1, 2</sup> It was found that a cylindrical plasma contained in a dielectric tube resonates when it is immersed in a uniform oscillating electric field; one of these resonances is electromagnetic in nature, while the others are plasma wave resonances. A simple theory<sup>2</sup>, postulating negligible coupling between electromagnetic and plasma waves in an inhomogeneous plasma was found to predict satisfactorily the location of

resonant frequencies. The present investigation was undertaken in order to clarify the nature of coupling between the applied field and plasma waves which, if it is negligible in the body of the plasma, must occur at its boundary. Since the "strength of coupling" has an effect on the sharpness of a resonance, a calculation and a measurement of the  $Q$  of the Tonks-Dattner resonances was undertaken.

The calculation is based on the description of the electron gas by a set of hydrodynamic equations together with Maxwell's equations:

$$\begin{aligned} \nabla \times \underline{E} &= -j\omega \mu_0 \underline{H} \quad , \quad j\omega m n_0 \underline{V} = -\nabla p - n_0 e \underline{E} - \nu n_0 \underline{V} \\ \nabla \times \underline{H} &= j\omega \epsilon_0 \underline{E} - n_0 e \underline{V} \quad , \quad \nabla \cdot \underline{V} = (-j\omega / m n_p a^2) p \end{aligned} \quad (1)$$

where "a" is the acoustic velocity in the plasma. Although the experiment was performed in waveguide, the theoretical calculations assumed no axial variation of fields. This assumption eliminates one loss mechanism, namely radiation along the plasma column (and other directions having a component along the column). This loss mechanism is probably less important in the waveguide geometry used in this investigation than in similar experiments using strip-line geometry. The loss mechanisms remaining within our model are two: internal losses due to collisions, and external losses due to radiation. The calculation of the  $Q$  was performed by first calculating the input impedance of a radial wave emerging from the boundary of the plasma and the impedance looking radially into the plasma column. The resistive component of the former is associated with radiation losses, while the resistive component of the latter results from internal losses. The sum of the two impedances is set equal to zero and the resulting equation is then solved for frequency. The ratio of real to imaginary parts of complex frequency is interpreted as  $2Q$ .

In calculating the impedance looking into the plasma, we were initially forced to assume that the plasma was homogeneous. Under this assumption this impedance has two components - one derived from the electromagnetic wave, the other from the plasma wave. The relationship between these two components is based on the assumed boundary condition at the wall of the tube, namely the vanishing of the normal component of the velocity  $\underline{V}$ .

Since all resonance equations are transcendental, the radius of the plasma

cylinder was assumed to be small compared to the electromagnetic wavelength and large compared to the plasma wavelength. The  $Q$  of the  $n$ th resonance then turns out to be given by

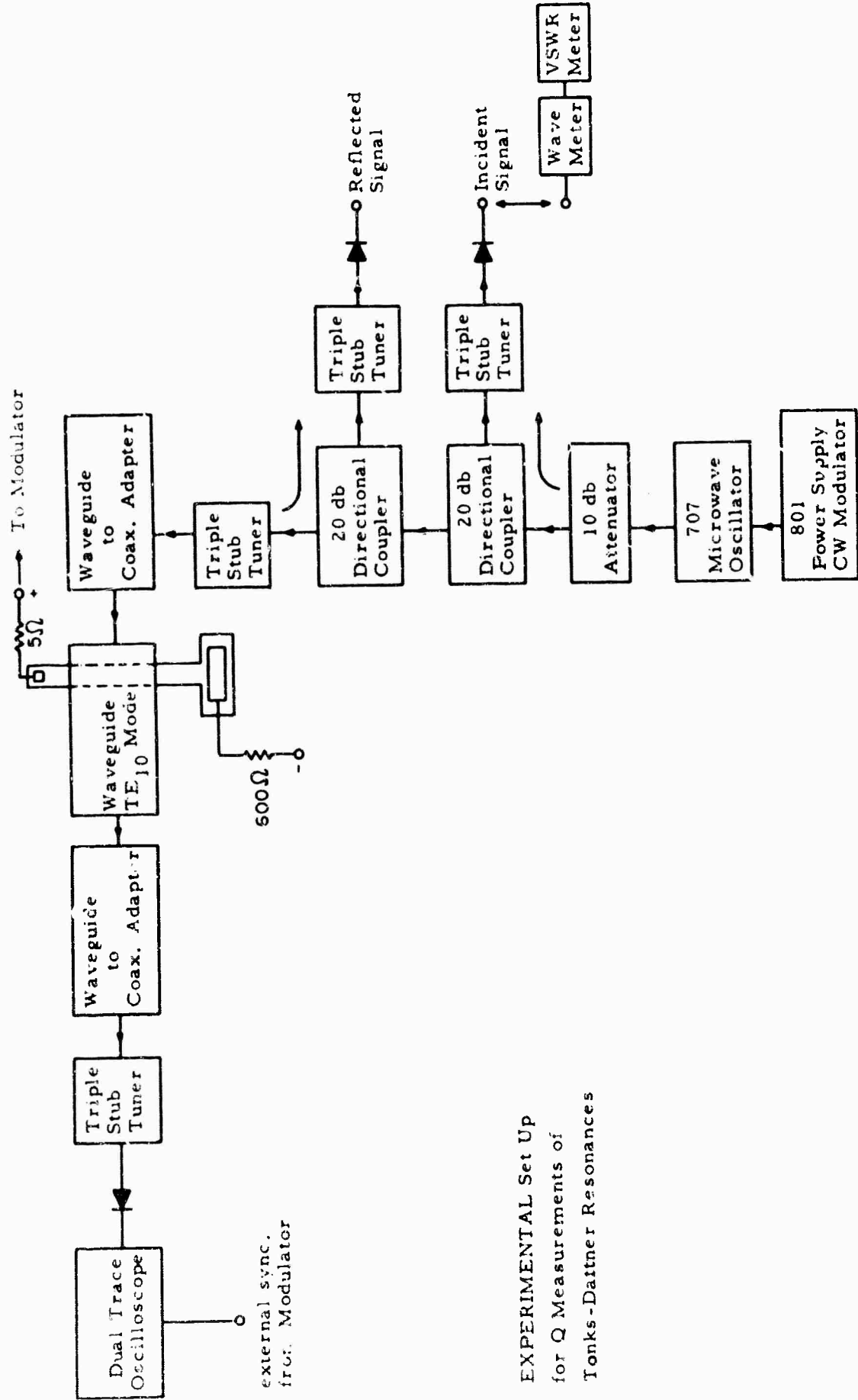
$$\frac{1}{Q} \approx \frac{\pi \omega^2 a^4}{4 c^2 R^2} \left( \frac{3\pi}{4} + n\pi \right)^2 + \frac{\nu}{\omega_p} \quad (2)$$

where  $\omega_p$  is the plasma frequency of the column,  $c$  is the velocity of light,  $\nu$  is the effective collision frequency and  $R$  is the column radius. The first of the two terms in Eq. (2) represents radiation losses while the second one accounts for collision damping. Landau damping has not been taken into account. Under our laboratory conditions, it turns out that radiation damping is negligible.

The homogeneous plasma model is suspect because it is known to predict incorrectly the resonant frequencies of a plasma column. The calculation is therefore being extended to the case of an inhomogeneous plasma. We now assume that there is a homogeneous layer at the outer boundary of the plasma and neglect coupling except at the boundary. Preliminary results obtained for such a model are not very different from those for a homogeneous column. The  $Q$  in the collision dominated case appears to be of the order of  $\nu/\omega$  predicted by Eq. (2).

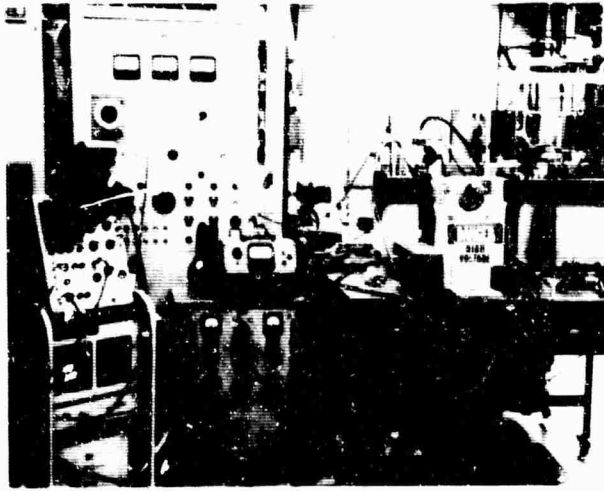
The experimental part of this investigation made use of a pulsed hydrogen discharge in the pressure range 75-150  $\mu$  Hg, in a 1" diameter glass tube. The tube was placed in L-band waveguide and resonances were observed in the 1000-2000 Mc range. The block diagram of the experimental setup is shown in Fig. 1 and photographs of the experimental arrangement are shown in Fig. 2. The resonances were observed in the transmitted signal in the afterglow of the discharge. For a fixed gas pressure and discharge current, the display of transmitted signal vs. time was obtained at a number of frequencies. Typical displays are shown in Fig. 3. The  $Q$  was obtained by observing the frequency change necessary to shift the resonance, as seen on such a display (suitably expanded), by its width. Care was exercised in distinguishing the Tonks-Dattner resonances from surface wave resonances within the waveguide.

Experimental results thus obtained agree qualitatively with the calculation. The measured  $Q$ 's are mostly between 30 and 40. More precise quantitative comparisons cannot yet be made because it was found impossible to measure the effective

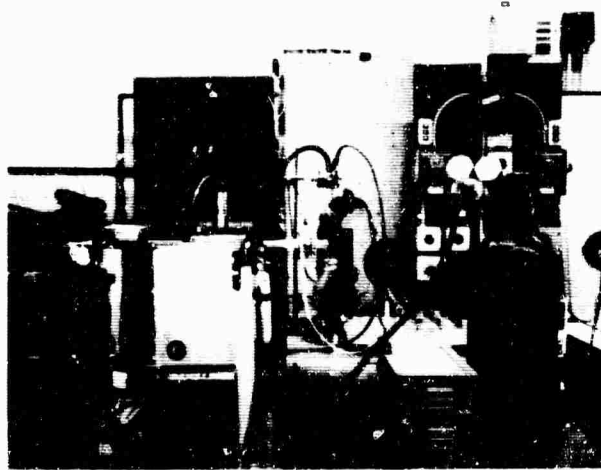


EXPERIMENTAL Set Up  
for Q Measurements of  
Tonks-Dattner Resonances

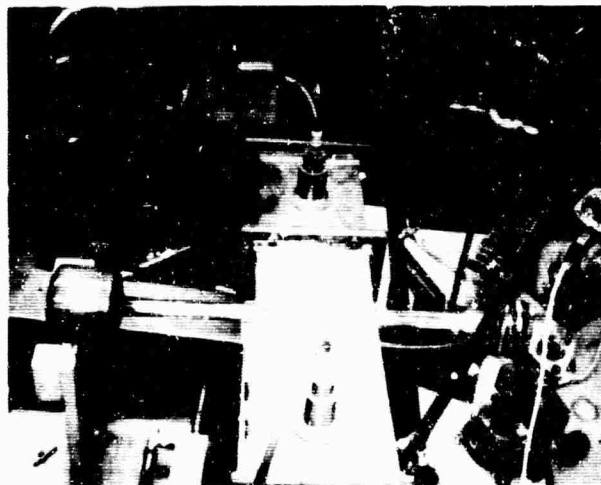
Fig 1 (2-5) - Experimental apparatus for measuring Q of Tonks-Dattner resonances



SIDE VIEW OF  
APPARATUS



END VIEW OF  
APPARATUS



TOP VIEW OF  
DISCHARGE TUBE  
AND WAVEGUIDE

Fig. 2 (2-6) - Experimental equipment in operation

PIBMRI-1295.1-65

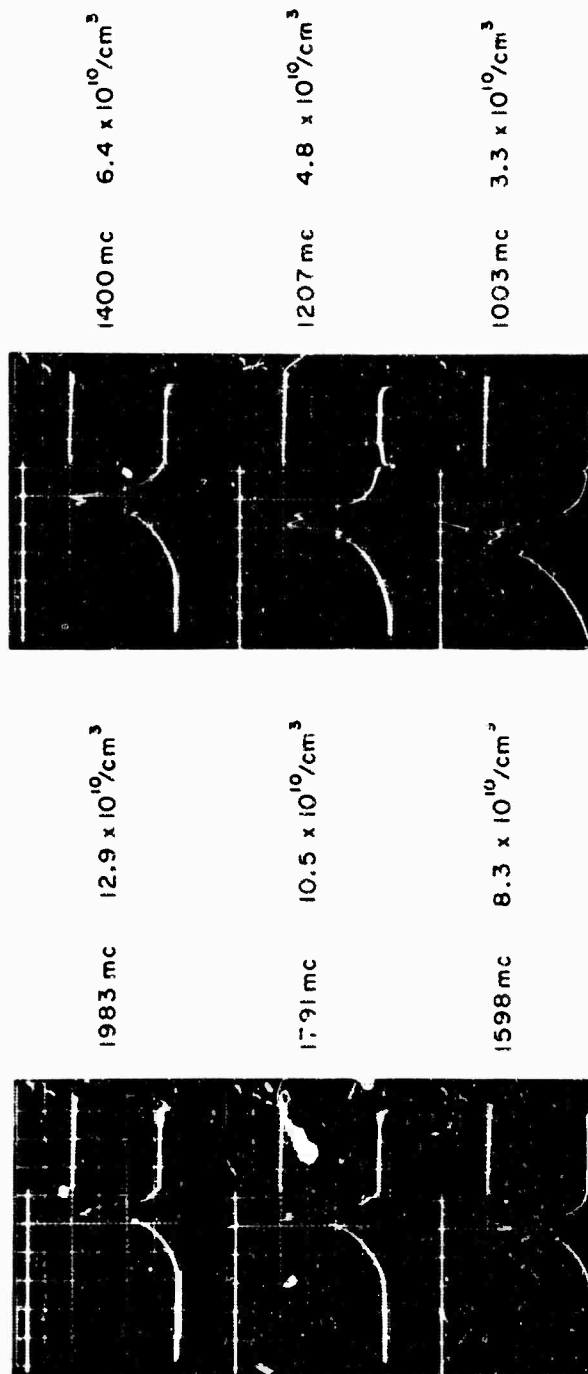


Fig. 3 (2-7) - Series G Run E

collision frequency in the present setup, owing to excessive dissipation in the glass tube. Some runs will be repeated using a teflon tube and then  $Q$  and  $\nu$  will be measured under the same conditions. The above mentioned experiments as well as the theory are described in detail in an Master of Science thesis<sup>3</sup>, and a report will be issued as soon as the above-described current work is completed.

Due to the large difference in the orders of magnitude of radiation and collision damping, the measurement of  $Q$  does not constitute a good test of the validity of the boundary conditions. The present investigation will be extended to the excitation coefficients of these resonances, with the hope that these might be more sensitive to the manner in which electromagnetic waves are coupled to plasma waves at a boundary.

J. Shmoys  
J. Gobler  
Electrophysics Department

#### References

1. A. Dattner, "A Study of Plasma Resonances", Proceedings of the 5th International Conference on Ionization Phenomena in Gases, Vol. 2, p. 1477 (1961).
2. R. Nickel, J. Parker, and R. Gould, "Resonance Oscillations in a Hot Non-uniform Plasma", Physics of Fluids, Vol. 7, No. 9, p. 1489 (1964).
3. J. F. Gobler, "Q Measurements of Tonks-Dattner Resonances", submitted in partial fulfillment of requirements for MS Thesis, Polytechnic Institute of Brooklyn. June 1965.

#### 2.4 Group Velocity and Power Flow Relations for Surface Waves in Plane-Stratified Anisotropic Media

Two aspects of power flow associated with electromagnetic waves in plane-stratified, lossless, linear, dispersive, anisotropic media were studied in application to surface wave propagation. One aspect is the relation between group velocity and the velocity of energy transport of surface waves in such media. It is shown that the group velocity of surface waves is equal to the ratio of the real part of the complex Poynting vector, integrated over the coordinate of stratification, to the corresponding

integral of the stored energy density. The second aspect is the relation between the dyadic surface impedance representing either a slab of plane-stratified medium above a perfectly conducting plane or a semi-infinite region (the latter for the case of evanescent fields) and the power flow in the respective structures.

Let us consider first the relation between the group velocity and the velocity of energy transport of surface waves. It is well known that in homogeneous anisotropic media, the velocity of energy transport of plane waves is equal to the plane wave group velocity, which is the gradient in wave number space of the frequency.<sup>1, 2</sup> An analogous relation holds for the case of surface waves in plane-stratified anisotropic media in that the group velocity, which is now the gradient of the frequency in the transverse wave number plane, is equal to the integral (over the coordinate of stratification) of the real part of the complex Poynting vector, divided by the corresponding integral of the energy density.

We assume all space to be filled with a plane-stratified, anisotropic medium whose interaction with monochromatic fields can be described in terms of a Hermitian dielectric tensor  $\underline{\epsilon}$  and a Hermitian permeability tensor  $\underline{\mu}$ <sup>2, 3, 4</sup>. The medium is taken to be independent of  $x$  and  $y$  so that the only space coordinate on which  $\underline{\epsilon}$  and  $\underline{\mu}$  will depend is  $z$ . The tensors  $\underline{\epsilon}$  and  $\underline{\mu}$  are continuous functions of  $z$  except for a possibly denumerable number of finite jumps. They are analytic functions of  $\omega$  whose  $z$  dependence is such that the medium supports surface waves that propagate transversely to  $z$ . Such surface waves are those solutions of the source-free Maxwell equations

$$\left. \begin{aligned} \nabla \times \underline{H} &= j\omega \underline{\epsilon} \cdot \underline{E} \\ \nabla \times \underline{E} &= j\omega \underline{\mu} \cdot \underline{H} \end{aligned} \right\} \quad (1)$$

which have the form

$$\left. \begin{aligned} \underline{E}(\underline{r}; \underline{k}_t, \omega) \\ \underline{H}(\underline{r}; \underline{k}_t, \omega) \end{aligned} \right\} = \left\{ \begin{aligned} \underline{e}(z; \underline{k}_t, \omega) \\ \underline{h}(z; \underline{k}_t, \omega) \end{aligned} \right\} e^{-j\underline{k}_t \cdot \underline{r}} \quad (2)$$

where  $\underline{e}$  and  $\underline{h}$  are such that  $\lim_{|z| \rightarrow \infty} \left( \frac{\underline{e}}{\underline{h}} \right) = 0$ . The  $e^{j\omega t}$  time dependence has been

suppressed in Eqs.(1) and (2). We also require that the integral of the stored energy density  $w$  and of the real part of the Poynting vector,  $\underline{s} = \text{Re}(\underline{e} \times \underline{h}^*)$ , from  $z = -\infty$  to  $z = +\infty$  be finite. Furthermore, since the field components transverse to  $z$ ,  $\underline{e}_t$  and  $\underline{h}_t$ , must be continuous across any jump in  $\underline{\epsilon}$  or  $\underline{\mu}$ , they must be continuous functions of  $z$ .

For any particular medium that can support surface waves, solutions of the form given in Eq. (2) that satisfy the above requirements will exist only for those values of  $\underline{k}_t$  and  $\omega$  satisfying the surface wave dispersion relation

$$D_s(\underline{k}_t, \omega) = 0 \tag{3}$$

of the medium. Taking the neighboring sets of values  $(\underline{k}_t, \omega)$  and  $(\underline{k}_t + d\underline{k}_t, \omega + d\omega)$  so as to satisfy Eq. (3), the surface wave fields at  $(\underline{k}_t + d\underline{k}_t, \omega + d\omega)$  can be expressed, to first order, in terms of the fields and their derivatives, with respect to  $k_x, k_y$  and  $\omega$ , at  $(\underline{k}_t, \omega)$  as

$$\left. \begin{aligned} \underline{E}(\underline{r}; \underline{k}_t + d\underline{k}_t, \omega + d\omega) &= \underline{E}(\underline{r}; \underline{k}_t, \omega) + \delta \underline{E}(\underline{r}; \underline{k}_t, \omega) \\ \underline{H}(\underline{r}; \underline{k}_t + d\underline{k}_t, \omega + d\omega) &= \underline{H}(\underline{r}; \underline{k}_t, \omega) + \delta \underline{H}(\underline{r}; \underline{k}_t, \omega) \end{aligned} \right\} \tag{4}$$

where the variation  $\delta$  symbolizes the differential operator

$$\delta = d\underline{k}_t \cdot \nabla_{\underline{k}_t} + d\omega \frac{\partial}{\partial \omega} \tag{5}$$

with

$$\nabla_{\underline{k}_t} = \underline{x}_0 \frac{\partial}{\partial k_x} + \underline{y}_0 \frac{\partial}{\partial k_y}$$

The differential equations satisfied by  $\delta \underline{E}$  and  $\delta \underline{H}$  can be found by operating with  $\delta$  on Maxwell's equations. Since  $\underline{\epsilon}$  and  $\underline{\mu}$  are independent of  $\underline{k}_t$ , this operation gives

$$\left. \begin{aligned} \nabla \times \delta \underline{H} &= j \frac{\partial \omega \underline{\epsilon}}{\partial \omega} \cdot \underline{E} + j \omega \underline{\epsilon} \cdot \delta \underline{E} \\ \nabla \times \delta \underline{E} &= -j \frac{\partial \omega \underline{\mu}}{\partial \omega} \cdot \underline{H} - j \omega \underline{\mu} \cdot \delta \underline{H} \end{aligned} \right\} \tag{6}$$

In order to find the relation between group velocity and the velocity of energy transport, we consider the quantity  $\nabla \cdot (\delta \underline{E} \times \underline{H}^* + \underline{E}^* \times \delta \underline{H})$ . By expanding the divergence of the cross products, substituting from Eqs. (1) and (4) and using the fact that  $\underline{\epsilon}$  and  $\underline{\mu}$  are Hermitian, it is possible to show that

$$\nabla \cdot (\delta \underline{E} \times \underline{H}^* + \underline{E}^* \times \delta \underline{H}) = -j d\omega (\underline{E}^* \cdot \frac{\partial \underline{\epsilon}}{\partial \omega} \cdot \underline{E} + \underline{H}^* \cdot \frac{\partial \underline{\mu}}{\partial \omega} \cdot \underline{H}) \quad (7)$$

If  $\underline{E}$  and  $\underline{H}$  are taken to be Rms quantities,  $\underline{E}^* \cdot \frac{\partial \underline{\epsilon}}{\partial \omega} \cdot \underline{E}$  and  $\underline{H}^* \cdot \frac{\partial \underline{\mu}}{\partial \omega} \cdot \underline{H}$  are recognized to be twice the time average electric and magnetic energy densities, respectively.<sup>2, 4, 5</sup> Their sum is twice the time average energy density  $w$ .

If we first operate with  $\delta$  on the fields as given in Eq. (1), which results in the expressions

$$\left. \begin{aligned} \delta \underline{E} &= (\delta \underline{e} - j d\underline{k}_t \cdot \underline{f} \underline{e}) e^{-j \underline{k}_t \cdot \underline{f}} \\ \delta \underline{H} &= (\delta \underline{h} - j d\underline{k}_t \cdot \underline{f} \underline{h}) e^{-j \underline{k}_t \cdot \underline{f}} \end{aligned} \right\} \quad (8)$$

and then substitute these expressions for  $\delta \underline{E}$  and  $\delta \underline{H}$  into the left-hand side of Eq. (7), the equality becomes, upon rearranging,

$$w d\omega - d\underline{k}_t \cdot \underline{s} = j \frac{1}{2} \frac{\partial}{\partial z} z_0 \cdot (\underline{e}_t^* \times \delta \underline{h}_t + \delta \underline{e}_t \times \underline{h}_t^*) \quad (9)$$

taking due account of the relation  $\nabla \cdot \underline{s} = 0$ , which holds for a lossless medium.

By assumption,  $(\underline{k}_t, \omega)$  and  $(\underline{k}_t + d\underline{k}_t, \omega + d\omega)$  satisfy Eq. (3) so that to first order

$$d\omega = d\underline{k}_t \cdot \nabla_{\underline{k}_t} \omega(\underline{k}_t)$$

where  $\omega(\underline{k}_t)$  is the solution of Eq. (3). Using this expression for  $d\omega$  in Eq. (9) gives

$$d\underline{k}_t \cdot (w \nabla_{\underline{k}_t} \omega - \underline{s}) = j \frac{1}{2} \frac{\partial}{\partial z} z_0 \cdot (\underline{e}_t^* \times \delta \underline{h}_t + \delta \underline{e}_t \times \underline{h}_t^*) \quad (10)$$

The term on the right-hand side of Eq. (10) does not vanish identically so that, in general,  $\nabla_{\underline{k}_t} \omega \neq \underline{s}/w$  and hence the group velocity  $\nabla_{\underline{k}_t} \omega$  cannot be interpreted as a local

energy transport velocity. In order to eliminate the right-hand side of Eq. (10), this equation is integrated from  $z = -\infty$  to  $z = +\infty$ . Since  $\underline{e}_t$  and  $\underline{h}_t$ , and also  $\delta\underline{e}_t$  and  $\delta\underline{h}_t$ , are continuous functions of  $z$ , the integral of the right-hand side reduces to the end point contributions at  $z = \pm\infty$  which are zero since  $\underline{e}_t = \underline{h}_t = 0$  there. Thus defining

$$\underline{S} = \int_{-\infty}^{\infty} \underline{s} dz \quad (11)$$

and

$$W = \int_{-\infty}^{\infty} w dz \quad , \quad (12)$$

upon integration Eq. (10) becomes

$$d\underline{k}_t \cdot (W \nabla_{\underline{k}_t} w - \underline{S}) = 0 \quad . \quad (13)$$

Because  $s_z$  is zero for the surface wave,  $\underline{S}$  has no  $z$  component, and as  $d\underline{k}_t$  is arbitrary, Eq. (13) implies that

$$\nabla_{\underline{k}_t} w = \underline{S} / W \quad . \quad (14)$$

Although  $\underline{s}$  can vary in magnitude and direction with  $z$ , the total real Poynting vector  $\underline{S}$  is independent of  $z$  and represents the total surface wave power flow across a strip, normal to  $\underline{s}$ , infinite in  $z$  and of unit width. The term  $W$  represents the total stored energy of the surface wave fields in an infinite cylinder, parallel to  $z$ , whose  $x$ - $y$  cross section has unit area. Equation (14) thus states that the group velocity is equal to the velocity of energy transport  $\underline{S} / W$  of the surface wave as a whole. This statement for the surface waves is analogous to the relation  $\nabla_{\underline{k}} w = \underline{s} / w$  for plane waves in homogeneous, anisotropic media and should prove useful in developing a ray model for the surface wave fields radiated by a point source.

If instead of filling the entire space, a plane-stratified medium of the type described above fills the half space above a perfectly conducting plane at  $z = 0$ , it is possible to show that the surface waves in this configuration are such that Eq. (14) is satisfied, provided that in the definitions of  $\underline{S}$  and  $W$  the lower limit is replaced by zero.

Another aspect of power flow in a plane-stratified medium is the relation between energy transport in a slab of such a medium above a perfectly conducting plane and the reactive dyadic surface impedance representing the slab.

When formulating electromagnetic problems involving fields of the form given in Eq. (2) in a lossless, plane-stratified, anisotropic medium above a perfectly conducting plane at  $z=0$ , it is sometimes convenient to represent the effect of the structure below a plane  $z=d > 0$  on the fields above this plane by a dyadic surface impedance  $\underline{\tilde{Z}}$  defined at  $z=d$  by requiring that the relation

$$(\underline{e}_t)_{z=d} = \underline{\tilde{Z}} \cdot (\underline{z}_0 \times \underline{h}_t)_{z=d} \tag{15}$$

holds for all possible fields of the form given in Eq. (2). If one now wishes to solve for fields of the form given in Eq. (2), in the region  $z > d$ , relation Eq. (15) may be used as a boundary condition at  $z=d$  and will insure that the transverse fields connect continuously to valid fields in the region  $0 < z < d$ . That is, if  $\underline{e}$  and  $\underline{h}$  in the region  $z > d$  are such that Eq. (15) is satisfied, and if  $\underline{h}_d$  is taken as  $(\underline{h}_t)_{z=d^+}$ , the corresponding  $\underline{e}$  in the region  $0 < z < d$  will be such that  $(\underline{e}_t)_{z=d^-} = (\underline{e}_t)_{z=d^+}$ .

Let us define

$$W_d = \int_0^d w \, dz \tag{16}$$

and

$$\underline{S}_d = \int_0^d \underline{s} \, dz \tag{17}$$

which is a transverse vector. The term  $W_d$  represents the stored energy in the slab per unit area in the  $x$ - $y$  plane and  $\underline{S}_d$  is the power flow through a strip, of unit width and height  $d$ , that is normal to  $\underline{S}$ . Employing Eqs. (16) and (17), it has been shown that the connections between the dyadic surface impedance and the power flow and stored energy in the slab take the forms

$$\left. \begin{aligned} j \frac{1}{2} \left[ (\underline{z}_0 \times \underline{h}_t^*) \cdot \frac{\partial \underline{\tilde{Z}}}{\partial \underline{k}_x} \cdot (\underline{z}_0 \times \underline{h}_t) \right]_{z=d} &= \underline{S}_{dx} \\ j \frac{1}{2} \left[ (\underline{z}_0 \times \underline{h}_t^*) \cdot \frac{\partial \underline{\tilde{Z}}}{\partial \underline{k}_y} \cdot (\underline{z}_0 \times \underline{h}_t) \right]_{z=d} &= \underline{S}_{dy} \end{aligned} \right\} \tag{18}$$

and

$$-j \frac{1}{2} \left[ (\underline{z}_0 \times \underline{h}_t^*) \cdot \frac{\partial \underline{\tilde{Z}}}{\partial \omega} \cdot (\underline{z}_0 \times \underline{h}_t) \right]_{z=d} = W_d \tag{19}$$

Since Eqs.(18) and (19) hold for arbitrary  $\underline{k}_t$  and  $\omega$ , they are valid, in particular, for values of  $\underline{k}_t$  and  $\omega$  that correspond to a surface wave and thus furnish an alternative way of calculating those portions of the surface wave power and energy that are in the slab.

The relation between power flow and the derivatives of  $\underline{Z}$  with respect to  $k_x$  and  $k_y$  given in Eq. (18) does not appear to have been previously recognized. While the connection between stored energy and  $\partial \underline{Z} / \partial \omega$ , to the best of our knowledge, has not been shown to hold explicitly for surface impedances, the connection between stored power and the impedance matrix of a lossless junction is well known. <sup>(6)</sup>

Relations (18) and (19) can also be shown to hold for the surface impedance representing a semi-infinite, plane-stratified, lossless medium below the plane  $z = d$  for values of  $\underline{k}_t$  and  $\omega$  so that the fields are evanescent at  $z = -\infty$ . In this case

$$\underline{S}_d = \int_{-\infty}^d \underline{s} dz \quad \text{and} \quad W_d = \int_{-\infty}^d w dz .$$

H. L. Bertoni  
A. Hessel  
Electrophysics Department

### References

1. W. P. Allis, S. J. Buchsbaum and A. Bers, "Waves in Anisotropic Plasmas", John Wiley and Sons, New York (1962), pp. 103-106.
2. T. H. Stix, "The Theory of Plasma Waves", McGraw-Hill Book Company, New York (1962), pp. 45-51.
3. L. D. Landau and E. M. Lifshitz, "Electrodynamics of Continuous Media", Pergamon Press, New York (1960), p. 331.
4. A. Tanning, "A Contribution to the General Theory of Linear Networks", Norwegian Defense Research Establishment, Report No. 28 (1959), pp. 13-23.
5. Reference 3, pp. 253-256.
6. C. G. Montgomery, R. H. Dicke and E. M. Purcell, "Principles of Microwave Circuits", McGraw-Hill Book Company, New York (1948), pp. 151-153.

### 2.5 Diffraction by a Transparent Elliptical Cylinder

Several recent papers on the classical theory of diffraction have presented verifications of the geometrical interpretation of diffraction phenomena for smooth obstacles of continuous curvature. The work of Keller and Levy<sup>2</sup> is an example for the cases of the parabolic and the elliptical cylinders. In their discussion the surfaces of the cylinders are considered to be either perfectly rigid or perfectly free with respect to acoustic waves.

Diffraction by a transparent obstacle also may be treated as a formal boundary-value problem to show the validity of the geometrical theory of diffraction. In the case of a surface of constant curvature results based on the classical theory of diffraction have been obtained for the circular cylinder<sup>1</sup> and the sphere.<sup>1,4</sup> For surfaces of variable curvature the classical method of separation of variables can be applied only for a few coordinate systems. Moreover, in each of these instances fundamental difficulties arise in conjunction with the boundary conditions because of the absence of any orthogonality relations between the solutions outside and inside the surface.

In the present contribution we resolve the difficulty with the boundary conditions for the case of a transparent elliptical cylinder through the use of perturbation theory. The solution to the formal boundary-value problem for an impulsive source can thus be given in terms of asymptotic expansions.

A line source is located at  $\underline{r} = \underline{r}_1$  exterior to the cylinder and parallel to its axis. The unbounded medium exterior to the cylinder is characterized by the wave velocity  $v_1$  and the interior of the cylinder by the velocity  $v_2$ . It is assumed that a Laplace transformation with respect to time exists for all quantities; in terms of notation:  $\bar{\varphi}(s) = \mathcal{L}\{\varphi(t)\}$ . The mathematical formulation of the problem requires that the time transforms of the exterior and interior solutions  $\bar{\varphi}_i(\underline{r}, \underline{r}_1; s)$  satisfy the wave equation:

$$(\nabla^2 - k_i^2) \bar{\varphi}_i(\underline{r}, \underline{r}_1; s) = -\delta(\underline{r} - \underline{r}_1), \quad k_i = s/v_i, \quad i = 1, 2 \quad (1)$$

The subscripts 1 and 2 refer to the exterior and interior regions, respectively. The time transform variable is  $s$ . If  $\bar{\varphi}_1$  is decomposed into the incident and scattered waves,  $\bar{\varphi}_1 = \varphi_1^i + \bar{\varphi}_1^s$ , then  $\bar{\varphi}_1^i$  is given by

$$\bar{\varphi}_1^i(\underline{r}, \underline{r}_1; s) = \frac{1}{2\pi} K_0(k_1 R), \quad R = |\underline{r} - \underline{r}_1|, \quad (2)$$

where  $K_0(k_1 R)$  is a Bessel function of the third kind. The scattered wave  $\bar{\varphi}_1^s$  must satisfy the radiation condition

$$\bar{\varphi}_1^s(\underline{r}, \underline{r}_1; s) = O\left(\left(\frac{\pi}{2k_1 r}\right)^{1/2} e^{-k_1 r}\right) \text{ for } r \rightarrow \infty, \quad (3)$$

and  $\bar{\varphi}_2(\underline{r}, \underline{r}_1; s)$  must remain finite as  $r \rightarrow 0$ . In addition, the boundary conditions

$$a_1 \bar{\varphi}_1(\underline{r}, \underline{r}_1; s) \Big|_{\underline{r}=\underline{r}_0} = a_2 \bar{\varphi}_2(\underline{r}, \underline{r}_1; s) \Big|_{\underline{r}=\underline{r}_0}, \quad (4)$$

$$b_1 \frac{\partial}{\partial n} \bar{\varphi}_1(\underline{r}, \underline{r}_1; s) \Big|_{\underline{r}=\underline{r}_0} = b_2 \frac{\partial}{\partial n} \bar{\varphi}_2(\underline{r}, \underline{r}_1; s) \Big|_{\underline{r}=\underline{r}_0}, \quad (5)$$

on the surface of the cylinder must be satisfied.  $a_1, a_2, b_1,$  and  $b_2$  are constants appropriate to the boundary conditions and the media involved.

The separation of the wave equation Eq. (1) in elliptic cylinder coordinates

$\xi, \eta$

$$x = c \cosh \xi \cos \eta, \quad (6)$$

$$y = c \sinh \xi \sin \eta, \quad (7)$$

( $c$  being one-half the interfocal distance) leads to the angular and radial differential equations)

$$\left\{ \frac{d^2}{d\eta^2} + (\lambda + 2h_1^2 \cos 2\eta) \right\} A(\eta, \nu, h_1) = 0, \quad (8)$$

$$\left\{ \frac{d^2}{d\xi^2} - (\lambda + 2h_1^2 \cosh 2\xi) \right\} R(\xi, \nu, h_1) = 0, \quad (9)$$

( $\lambda$  being the separation constant,  $\nu$  the order, and  $h_1 = \frac{1}{2} k_1 c$ ). The solutions to these ordinary differential equations are Mathieu functions<sup>3</sup>.

From the fact that the region surrounding the cylinder is multiply connected

$$\bar{\varphi}_i(\xi, \eta, \xi_1, \eta_1; s) = \bar{\varphi}_i(\xi, \eta + 2n\pi, \xi_1, \eta_1; s), \quad n = 1, 2, \dots, \quad (10)$$

the source term may be written as

$$\delta(\underline{r} - \underline{r}_1) = c^{-2} (\cosh 2\xi - \cos 2\eta)^{-1} \delta(\xi - \xi_1) \sum_{m=-\infty}^{\infty} \delta(\eta - \eta_1 + 2m\pi) \tag{11}$$

and the solution as

$$\bar{\varphi}_1(\xi, \eta, \xi_1, \eta_1; s) = \sum_{m=-\infty}^{\infty} \bar{\varphi}_{i_0}(\xi, \eta + 2m\pi, \xi_1, \eta_1; s) \tag{12}$$

This operation is equivalent to the introduction of a helical Riemann surface with an infinite number of sheets; on the zeroth sheet  $\bar{\varphi}_1 = \bar{\varphi}_{i_0}$ ,  $0 \leq \xi < \infty$ ,  $0 \leq \eta \leq 2\pi$ .

The periodicity condition in Eq. (10) requires that the Mathieu functions be of integral order. Eigenfunction expansions in terms of the fundamental solutions  $\theta^{(1)}$ ,  $\theta^{(2)}$ ,  $R^{(1)}$ , and  $R^{(2)}$  to Eqs. (8) and (9) can be used to represent the solutions in both regions. The expression for the incident and scattered waves in the exterior region are

$$\bar{\varphi}_1^i(\xi, \eta, \xi_1, \eta_1; s) = \sum_{n=-\infty}^{\infty} A_n \theta^{(1)}(\eta, n, h_1) \theta^{(2)}(\eta, n, h_1) R^{(1)}(\xi_1, n, h_1) R^{(2)}(\xi, n, h_1), \tag{13}$$

$$\bar{\varphi}_1^s(\xi, \eta, \xi_1, \eta_1; s) = \sum_{n=-\infty}^{\infty} B_n \theta^{(1)}(\eta, n, h_1) \theta^{(2)}(\eta_1, n, h_1) R^{(1)}(\xi_1, n, h_1) R^{(2)}(\xi, n, h_1), \tag{14}$$

and the wave in the interior region is  $\xi < \xi_1$ ,  $\eta < \eta_1$ ,

$$\bar{\varphi}_2(\xi, \eta, \xi_1, \eta_1; s) = \sum_{n=-\infty}^{\infty} C_n \theta^{(1)}(\eta, n, h_2) \theta^{(2)}(\eta, n, h_2) R^{(1)}(\xi_1, n, h_2) R^{(2)}(\xi, n, h_2). \tag{15}$$

The coefficients are determined by the expansion of Eq. (2) in elliptic cylinder coordinates; the coefficients  $B_n$  and  $C_n$  are as yet unknown. If the inequalities are reversed, the arguments of the corresponding functions are to be interchanged.

Application of Green's theorem to the unbounded region enclosing the cylinder leads to a fundamental difficulty due to the boundary conditions Eqs. (4) and (5).

Unlike the cases of the circular cylinder and the sphere where the angular functions

are independent of wave number, different wave numbers appear in the angular functions of the respective eigenfunction expansions for the exterior and interior regions. Therefore, each coefficient of the expansion for one region must contain an infinite series of coefficients associated with the other region.

Furthermore, the eigenfunction expansions in Eqs. (13), (14), and (15) cannot be applied conveniently for the examination of the nature of the discontinuity at the wave front because they converge too slowly for large values of the transform variable  $s$ . The relationship between the transform variable and the time after the arrival of the wave front is shown by the Tauberian theorem<sup>8</sup>,

$$\lim_{s \rightarrow \infty} s \bar{f}(s) e^{-s R_g / v} = \lim_{t \rightarrow R_g / v} f(t - R_g / v) \quad (16)$$

where  $t_g = R_g / v$  is the time of onset for the pulse and  $R_g$  is the geometrical ray path length.

In order to obtain rapidly converging series expansions in accordance with Eq. (16), it is necessary to make use of the asymptotic behavior of the angular and radial Mathieu functions as a function of their order<sup>6</sup>. Proceeding as in the case of the perfectly rigid acoustic elliptical cylinder,<sup>5</sup> a Trugall-Watson transformation

$$\frac{1}{2i} \int_{C_1 + C_2} \cot v \pi f(v) dv = \sum_{n=-\infty}^{\infty} f n \quad (17)$$

is applied to the eigenfunction expansions for the solutions  $\bar{\Phi}_1$  and  $\bar{\Phi}_2$ .  $C_1 + C_2$  is a contour in the complex order plane enclosing the real axis (see Fig. 1).

For large values of the time transform parameter in keeping with Eq. (16), the angular solutions for the exterior and interior regions are nearly orthogonal, even for moderate wave velocity ratios, i. e.,  $\frac{v_1}{v_2} = \frac{4}{3}$ . Thus the transformation matrix between the two angular functions is nearly diagonal; the evaluation of the integral

$$\int_0^{2\pi} g^{(1)}(\eta, v, h_1) g^{(2)}(\eta, v, h_2) d\eta = \delta_{vv} g(v, h_1, h_2) \quad (18)$$

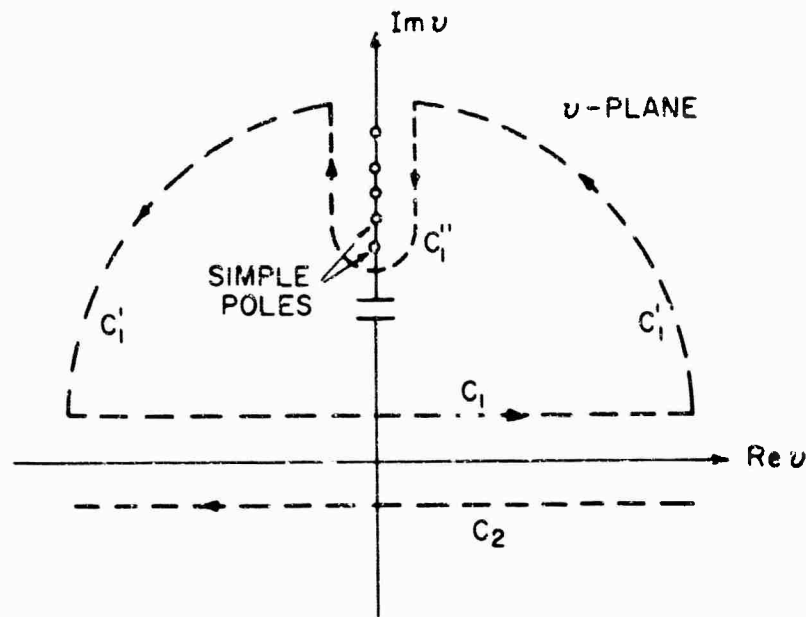


Fig. 1 (2-8)

can be carried out as a perturbation calculation for a two parameter differential equation.<sup>7</sup> In this instance the parameters are the order,  $\nu$  and the quantity,  $h$ .

With the aid of the expansions in Eq. (18), the coefficients  $B(\nu)$  and  $C(\nu)$  of the eigenfunction expansions in Eqs. (14) and (15) can be determined through the boundary conditions Eqs. (4) and (5). The resulting expression for the solution  $\bar{\varphi}_1$ ,

$$\bar{\varphi}_1(\xi, \eta, \xi_1, \eta_1; s) = \frac{1}{i} \int_{C_1} A(\nu) \varrho^{(1)}(\eta, \nu, h_1) \varrho^{(2)}(\eta_1, \nu, h_1) R^{(1)}(\xi_1, \nu, h_1) R^{(2)}(\xi, \nu, h_1) \cdot g(\nu, h_1, h_2) a_2 b_2 \frac{d_1^i(\xi_0, \nu, h_1) - d_1^s(\xi_0, \nu, h_1)}{a_1 b_2 d_2(\xi_0, \nu, h_2) - a_2 b_1 d_1^s(\xi_0, \nu, h_1)} d\nu \quad (19)$$

can be treated in a manner analogous to transparent circular cylinders.<sup>1</sup> The quantity  $d$  in Eq. (19) is defined by the relation

$$\frac{\partial}{\partial \xi} \bar{\psi}_i(\xi, \eta, \xi_1, \eta_1; s) \Big|_{\xi = \xi_0} = d_i(\xi_0, \nu, h_i) \bar{\psi}_i(\xi, \eta, \xi_1, \eta_1; s) \quad (20)$$

where

$$\bar{\varphi}_1^i(\xi, \eta, \xi_1, \eta_1; s) = \frac{1}{i} \int_{C_1} A(\nu) \bar{\psi}_1^i(\xi, \eta, \xi_1, \eta_1; s) d\nu \quad (21)$$

Only the contour  $C_1$  is retained since the integrand is an even function of the order  $\nu$ ; the summations in Eqs. (13), (14) and (15) have been replaced by contour integrals as in Eq. (21).

If the path of integration  $C_1$  is deformed as shown in Fig. 1, there is no contribution to Eq. (19) from the large hemicircle  $C$  since the integrand of Eq. (19) vanishes as  $|\nu| \rightarrow \infty$ . The region surrounding the cylinder is divided into illuminated and shadow zones by the two lines from the source which are tangent to the cylinder (Fig. 2). In the shadow zone the integrand of Eq. (19) has simple poles along the imaginary axis of the order plane (Fig. 1). The resulting residue series arising from the evaluation of Eq. (19) along path  $C$  corresponds to the diffracted rays shown in Fig. 2. In addition, Eq. (19) yields an infinite series of terms which account for the internal reflections in the cylinder.

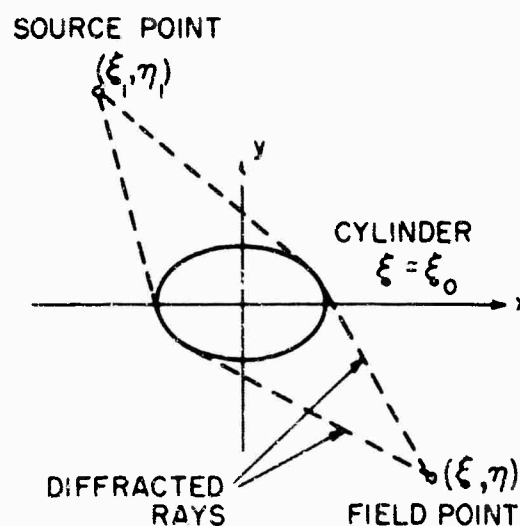


Fig. 2 (2-9)

In the illuminated zone the integrand of Eq. (19) also possesses two saddle points. Evaluation of the integral along the path of steepest descent yields the incident and reflected rays. Present also in the illuminated zone are, of course, all of the terms found in the shadow zone; the passage of the diffracted ray an infinite number of times around the cylinder is expressed by Eq. (12). The inversion of  $\bar{\phi}$  into the time domain shows that only the diffracted wave has a wave front distinctly different from that of the incident wave; it has no discontinuity at the wave front. The expressions obtained from the asymptotic evaluation of the exact solutions may be rewritten according to the geometrical theory of diffraction to show the influence of variable curvature.

L. D. Porter  
Department of Aerospace Engineering and  
Applied Mechanics

#### References

1. Franz, W., "Theorie der Beugung elektromagnetischer Wellen", Springer-Verlag (1957).
2. Keller, J. B. and Levy, B. R., "Decay exponents and diffraction coefficients for surface waves on surfaces of nonconstant curvature", IRE Trans. Ant. and Prop. AP-7 (1959), p. S52-S61.
3. Meixner, J. and Schafke, F. W., "Mathiesche Funktionen und Sphäroidfunktionen", Springer-Verlag (1954).
4. Nussenzweig, H. M.: to appear.
5. Porter, L. D., "The diffraction of a circular pulse by an elliptical cylinder" Ph. D. dissertation U. C. L. A. (1961).
6. Porter, L. D., "Asymptotic solutions to Mathieu's equation for complex order", to appear.
7. Titchmarsh, E. C., "Eigenfunction expansions associated with second order differential equations", Oxford University Press, Part I (2nd edition) (1962), Part II (1958).
8. Van der Pol, B. and Bremmer, H., "Operational Calculus", Cambridge University Press (1953).

## 2.6 Cerenkov Radiation in Dielectric Media

It is planned to carry out experimental and theoretical studies of the Cerenkov effect in a plasma medium; specifically it is intended to study this effect in a plasma filled cavity and if possible utilize the effect for the study of fluctuation phenomena in plasmas.

The program is proceeding in steps. First, theoretical investigations of the Cerenkov effect in a dielectric wave were carried out and are reported below. For the purpose of familiarizing the students with the problem, the classical problem of Cerenkov radiation in an infinite dielectric medium was treated. The method was then extended to discuss the case of a finite train of bunched electrons passing through a dielectric filled cavity. The results will be compared with an experiment as a check on the experimental technique. After agreement between theory and experiment has been established as expected, disagreements between experiments and computations for the case of a plasma filled cavity might be then more justifiably attributed to assumptions about the plasma medium. Thus the Cerenkov effect may become a diagnostic tool for the study of real plasmas.

Preliminary studies on Cerenkov radiation in idealized plasmas are described in 2.7 and preparatory work for experimentation is described in 2.9.

### 2.6.1 Dielectric Filled Infinite Space, One Electron

This classical problem was solved using Maxwell's equations in cylindrical coordinates

$$\nabla \times \vec{E} = - \frac{\partial \vec{H}}{\partial t} \quad (1)$$

$$\nabla \times \vec{H} = \vec{J} + \epsilon_0 \epsilon \frac{\partial \vec{E}}{\partial t} \quad (2)$$

Where  $\epsilon$  is the relative dielectric constant, and  $\vec{J}$  is the current of a single electron moving in the  $z$  direction

$$\vec{J} = \frac{qv}{2\pi r} \delta(z-vt) \vec{u}_z \quad (3)$$

$v$  is the velocity of the electron. The Fourier transforms in  $t$  and  $z$  are taken, then the  $E$  and  $H$  fields can be found. When Cerenkov radiation is possible, i. e.,  $v > c_r$ , the inverse transforms in  $z$  yield

$$\hat{H}_\phi(\omega, r, z) = -\frac{j\omega\gamma}{4c_r} q H_1^{(2)}\left(\frac{\omega\gamma r}{c_r}\right) e^{-j\frac{\omega}{v}z} = \hat{H} e^{-j\frac{\omega}{v}z} \quad (4)$$

$$\hat{E}_z = -q \frac{\mu_0 \gamma^2 \omega}{4} H_0^{(2)}\left(\frac{\omega\gamma r}{c_r}\right) e^{-j\frac{\omega}{v}z} = \hat{E} e^{-j\frac{\omega}{v}z} \quad (5)$$

where  $c_r = \frac{1}{\sqrt{\mu_0 \epsilon \epsilon_0}}$  the speed of light in the dielectric

$$\gamma = 1 - \frac{c_r^2}{v^2}$$

The power radiated is

$$P = \int \vec{E} \times \vec{H} \cdot d\vec{A}$$

where the integration is performed over a cylinder infinitely long in the  $z$  direction with vanishingly small radius so that the contribution at the ends can be neglected

$$P = \int_0^{2\pi} \int_{-\infty}^{\infty} r dz d\theta \frac{1}{(2\pi)^2} \int_{-\infty}^{\infty} d\omega d\omega' \hat{E}(\omega) \hat{H}(\omega') e^{-j\frac{z}{v}(\omega+\omega')}$$

carrying out the integration over  $\theta$  and  $z$  yields

$$P = v r \int_{-\infty}^{\infty} d\omega d\omega' \delta(\omega+\omega') \hat{E}(\omega) \hat{H}(\omega')$$

$$= 2 v r R_e \int_0^{\infty} \hat{E}(\omega) \hat{H}^*(\omega) d\omega \quad (6)$$

For this problem Eq. (6) gives

$$P = \frac{q^2 \gamma^2 \mu_0 v}{8\pi} \int_0^{\infty} \omega d\omega \quad (7)$$

This shows the divergence of power at infinite frequencies which would disappear if a real dielectric were chosen whose relative dielectric constant would approach 1 for

sufficiently high frequencies.

2.6.2 Dielectric Filled Infinite Space, Finite Train of (N+1) Electrons

This problem is approached in the same manner as the previous one with the previous  $\vec{J}$  replaced by

$$\vec{J} = \frac{qv}{2\pi} \frac{\delta(\mathbf{r})}{r} [\delta(z-vt) + \delta(z-z'-vt) \dots \delta(z-nz'-vt)] \vec{u}_z$$

where  $z'$  is the spacing between electrons. The fields can be solved by replacing  $q$  by

$$q \sum_{n=0}^N e^{jn \frac{z'x}{v}}$$

in the single electron solution. The fields are found to be

$$\hat{H}_\phi = \frac{-j\omega\gamma}{4c_r} q e^{-j \frac{z'x}{v}} \sum_{n=0}^N e^{j \frac{nz'x}{v}} H_1^2 \left( \frac{\omega\gamma r}{c_r} \right) \tag{8}$$

$$\hat{E}_z = -q \frac{\mu\gamma^2}{4} e^{-j \frac{z'x}{v}} \sum_{n=0}^N e^{j \frac{nz'x}{v}} H_0^2 \left( \frac{\omega\gamma r}{c_r} \right) \tag{9}$$

The power radiated using Eq. (6) is

$$P = \frac{q^2 \mu_o \gamma v}{4\pi} \int_0^\infty r dr \left[ (N+1) + \sum_{n=1}^N 2(N+1-n) \cos \left( \frac{z'n x}{v} \right) \right] \tag{10}$$

The first term in the brackets represents the radiation from (N+1) independent electrons, the second term represents the interaction term. In order to get a large enhancement of radiation the cosine term must be close to one. Therefore,  $\frac{z'n x}{v} = m\pi$  where  $m$  is an integer. For a specific  $x$  enhancement of radiation is possible; however, since  $x$  is a continuous variable there cannot be any great increase in  $P$  except when  $z' = 0$ . This corresponds to all the electrons being coincident for this case

$$P = (N+1) \cdot P(\text{one electron}) \tag{11}$$

This is the result that is expected since the power radiated varies as the square of the charge.

2.6.3 Dielectric in Cylindrical Waveguide, One Electron

This problem can be solved by replacing the radiation condition at infinity by the condition that  $E_z = 0$  at the waveguide wall. The fields then become

$$\hat{E}_z = \frac{\mu_0 q^2 \gamma^2 \omega}{4} \left\{ H'_0 \left( \frac{\omega \gamma r}{c_r} \right) - \frac{H'_0 \left( \frac{\omega \gamma r_0}{c_r} \right) J_0 \left( \frac{\omega \gamma r}{c_r} \right)}{J_0 \left( \frac{\omega \gamma r_0}{c_r} \right)} \right\} e^{-j \frac{\omega z}{v}} \quad (12)$$

$$\hat{H}_\phi = \frac{j q \omega \gamma}{4 c_r} \left\{ H'_1 \left( \frac{\omega \gamma r}{c_r} \right) - \frac{H'_1 \left( \frac{\omega \gamma r_0}{c_r} \right) J_1 \left( \frac{\omega \gamma r}{c_r} \right)}{J_1 \left( \frac{\omega \gamma r_0}{c_r} \right)} \right\} e^{-j \frac{\omega z}{v}} \quad (13)$$

where  $r_0$  is the waveguide radius. The power can be found by a pole residue integration to give

$$P = \frac{\mu_0 q^2 v \gamma c_r}{4 r_0} \sum_{\ell=1}^{\infty} \frac{\omega_\ell N_0 \left( \frac{\omega_\ell \gamma r_0}{c_r} \right)}{J_1 \left( \frac{\omega_\ell \gamma r_0}{c_r} \right)} \quad (14)$$

where the  $\omega_\ell$ 's are the roots of

$$J_0 \left( \frac{\omega_\ell \gamma r_0}{c_r} \right) = 0 \quad (15)$$

For  $\frac{\omega_\ell \gamma r_0}{c_r} \gg 1$  the roots of Eq. (15) are

$$\omega_\ell = \pi \left( \ell - \frac{1}{4} \right) \frac{c_r}{v r_0} \quad (16)$$

Using the asymptotic forms for  $N_0(x)$  and  $J_1(x)$  Eq. (14) becomes

$$P \approx \frac{\mu_0 \pi q^2 v c_r^2}{4 r_0^2} \sum_{\ell=1}^{\infty} \left( \ell - \frac{1}{4} \right) \quad (17)$$

The power up to the  $n^{\text{th}}$  mode is

$$P_n = \frac{\pi \mu_o q^2 v c_r^2}{8 r_o^2} \ell \left( \ell + \frac{3}{4} \right) \quad (18)$$

The power in the infinite dielectric up to  $\omega_\ell$  is after using Eq. (16)

$$P_N = \frac{\pi \mu_o q^2 v c_r^2}{8 r_o^2} \left( \ell - \frac{1}{4} \right)^2 \quad (19)$$

The two answers are approximately equal because the fields radiated go slower than the electron; physically there should be almost no reaction of the field reflected from the guide walls on the electron. This is borne out by the equations.

2.6.4 Dielectric in Cylindrical Waveguide, Finite Train of (N+1) Electrons

Once again the field solutions can be obtained by replacing  $q$  by

$$q \sum_{n=0}^N e^{j \frac{n z' w}{v}} \quad \text{A pole integration gives the power}$$

$$P = \frac{\mu_o q^2 v c_r v}{4 r_o} \sum_{\ell=1}^{\infty} \omega_\ell \frac{N_o \left( \frac{\omega_\ell \gamma r_o}{c_r} \right)}{J_1 \left( \frac{\omega_\ell \gamma r_o}{c_r} \right)} \left[ N+1 + \sum_{n=1}^N 2(N+1-n) \cos \frac{z' n \omega_\ell}{v} \right] \quad (20)$$

The asymptotic forms of  $N_o(x)$  and  $J_1(x)$  and Eq. (16) yield for the power up to the  $L^{\text{th}}$  mode

$$P_L = \frac{\mu q^2 \gamma c_r^2 v \pi}{4 r_o^2} \left[ L \left( L + \frac{3}{4} \right) (N+1) + \sum_{\ell=1}^L \sum_{n=1}^N \left( \ell - \frac{1}{4} \right) 2(N+1-n) \cos \frac{z' n}{v} \frac{\pi c_r}{\gamma r_o} \left( \ell - \frac{1}{4} \right) \right] \quad (21)$$

The last term in the bracket can be made very large because the  $\omega$ 's are discrete.

For instance if  $\frac{z' c_r \left( \ell - \frac{1}{4} \right)}{v \gamma r_o} = 2m$  (integer) for a particular  $\ell$ , then the last term is equal to  $N(N+1) \left( \ell - \frac{1}{4} \right)$ . This power is  $N(N+1)$  times the power one electron emits

in a waveguide. It is also  $N(N+1)/(\epsilon - \frac{1}{4})$  times the total power radiated up to frequency  $\omega$ , by one electron in the infinite dielectric.

2.6.5 Dielectric Filled Cavity, One Electron

Using a similar but more lengthy analysis than in the previous case the fields are found to be

$$\hat{H}_\phi = \sum_{n=1}^{\infty} \frac{-q \kappa_n j}{8 J_0(\kappa_n r_0)} \left[ -H_1^{(1)}(\kappa_n r) H_0^{(2)}(\kappa_n r_0) + H_1^{(2)}(\kappa_n r) H_0^{(1)}(\kappa_n r_0) \right] \times \left[ F_n(\omega) \cos \beta_n z - j G_n(\omega) \sin \beta_n z \right] \tag{23}$$

$$\hat{E}_z = \frac{-q \mu_0 c^2 r}{8 \omega} \sum \frac{\kappa_n^2}{J_0(\kappa_n r_0)} \left[ H_0^2(\kappa_n r) H_0'(\kappa_n r_0) - H_0'(\kappa_n r) H_0^2(\kappa_n r_0) \right] \times \left[ F_n(\omega) \cos \beta_n z - j G_n(\omega) \sin \beta_n z \right] \tag{24}$$

where  $\beta_n = \frac{n\pi}{2z_0}$ ,  $2z_0$  is the length of the cavity,

$$\kappa_n^2 = \frac{\omega^2}{c^2} - \beta_n^2$$

$$F_n(\omega) = \frac{\sin\left(\frac{\omega}{v} + \beta_n\right) z_0}{\left(\frac{\omega}{v} + \beta_n\right) z_0} + \frac{\sin\left(\frac{\omega}{v} - \beta_n\right) z_0}{\left(\frac{\omega}{v} - \beta_n\right) z_0} \text{ for } n \text{ even,}$$

$$= 0 \text{ for } n \text{ odd,}$$

$$G_n(\omega) = \frac{\sin\left(\frac{\omega}{v} - \beta_n\right) z_0}{\left(\frac{\omega}{v} - \beta_n\right) z_0} - \frac{\sin\left(\frac{\omega}{v} + \beta_n\right) z_0}{\left(\frac{\omega}{v} + \beta_n\right) z_0} \text{ for } n \text{ odd,}$$

$$= 0 \text{ for } n \text{ even.}$$

Since the structure is not uniform in the z direction any longer, and the electron's radiation will be a function of time, the previous expression for power

is no longer useful. The total energy radiated by the electron in transversing the cavity is more meaningful and can be shown to be

$$\text{Energy} = \int_{-z_0/v}^{z_0/v} dt \int \vec{J} \cdot \vec{E} \, dv \quad (25)$$

where the second integration is performed over the volume of the cavity.

The expression for  $\hat{E}_z$  in Eq. (24) substituted in Eq. (25) yields

$$\text{Energy} = \frac{q^2 v^2 \mu_0 c^4}{z_0 r_0} \sum_{n, \ell} \frac{\kappa_{n\ell}^3}{[\omega^2 - (\beta_n v)^2]^2} \frac{N_0(\kappa_{n\ell} r_0)}{J_1(\kappa_{n\ell} r_0)} \left( a_e \sin^2 \frac{\omega z_0}{v} + a_o \cos^2 \frac{\omega z_0}{v} \right) \quad (26)$$

The values of  $n$  and  $\ell$  in the sum are such as to keep  $\kappa_{n\ell}$  real. Where  $\kappa_{n\ell}$ 's are the roots of  $J_0(\kappa_{n\ell} r_0) = 0$

$$\begin{aligned} a_e &= 1 && \text{for } n \text{ even.} \\ &= 0 && \text{for } n \text{ odd.} \\ a_o &= 0 && \text{for } n \text{ even.} \\ &= 1 && \text{for } n \text{ odd.} \end{aligned}$$

For large  $n$  the main contribution to the sum will occur near  $\omega^2 - (\beta_n v)^2 = 0$ . At that point the numerator also goes to zero. If the asymptotic form for  $N_0(x)$  and  $J_1(x)$  are substituted the expression for energy radiated becomes

$$\text{Energy} = \frac{\pi \mu_0 q^2 c^2 z_0}{4 r_0^2} \sum_{\ell=1}^{\infty} \left( \ell - \frac{1}{4} \right) \quad (27)$$

This expression which is  $\frac{2z_0}{v}$  times the radiation of one electron in a waveguide is equal to the energy which one electron radiates in a distance  $2z_0$  of the waveguide. Therefore the average power radiated in the two cases is equal.

2.6.6 Dielectric Filled Waveguide, Finite Train of (N+1) Electrons

To solve this problem  $q$  can again be replaced by  $q \sum_{n=0}^N e^{j \frac{n z' \omega}{v}}$

to get the E and H fields. These fields can be substituted into Eq. (25) to get the energy radiated. If the same approximations as stated in the last section are applied, the energy can be shown to be

$$\text{Energy} = \frac{q^2 u_0^2 c^2 \pi z_0}{4 r_0^2} \sum_{\ell=1}^{\infty} \left( \ell - \frac{1}{4} \right) \left[ N+1 + \sum_{n=1}^N 2(N+1-n) \cos \frac{z' n \omega_{\ell}}{v} \right] \quad (28)$$

Enhancement of radiation is possible by choosing

$$\beta_n = \frac{\omega}{\left( \frac{n \pi}{2 z_0} \right)} = v \quad (29)$$

$$\left( \frac{\omega}{z'} \right) = v \quad \text{and} \quad (30)$$

$$\sqrt{\frac{\omega^2}{c_r^2} - \beta_n^2} r_0 = \alpha_n \quad (31)$$

where  $\alpha_n$  is the  $n$ th root of  $J_0(x) = 0$ .

If these conditions are satisfied the radiation at  $\omega$  is the same as that emitted in a waveguide.

Conclusion Concerning Cerenkov Radiation in Dielectrics

The power emitted by one electron is approximately the same in the three different geometries. The only difference is that the radiation in the waveguide and cavity occurs at discrete frequencies, while in infinite space there is a continuous spectrum. The  $N+1$  electrons change the frequency spectrum of radiation in the infinite dielectric case but the total power emitted is not very much different from  $(N+1)$  electrons emitting independently. For the other two cases the radiation increases significantly if appropriate values of  $r_0$ ,  $z'$  and  $z_0$  are chosen.

R. Sasiela  
 R. Hutter  
 Electrophysics Department

7 Cerenkov Radiation in an Infinite Magneto-Plasma

In the last few years several articles<sup>1-3</sup> have appeared dealing with Cerenkov radiation in a plasma. These authors have found the same conditions - although in different forms - for the ranges of  $\omega$  as functions of plasma frequency ( $\omega_p$ ), cyclotron frequency ( $\omega_c$ ) and velocity ( $v$ ) in which Cerenkov radiation may occur. Below is shown how these conditions come naturally from the Allis (C. M. A.) diagram<sup>5</sup> from a method suggested by Felsen<sup>4</sup>, McKenzie<sup>6</sup> and G. Deschamps.

In order for Cerenkov radiation to occur a wave which has the same phase velocity as the particle must occur in the medium. Expressed mathematically this condition for a particle traveling in the  $z$  direction is

$$\frac{\omega}{k_z} = v \tag{1}$$

where  $k_z$  is the wavenumber in the  $z$  direction. In each of the regions in Fig. 1  $n = \frac{kc}{\omega}$  vs.  $\theta$  is plotted for the two modes. The  $z$  direction is towards the top of the page and  $\theta$  is measured with respect to the  $z$  axis. The dotted circle ( $n = 1$  curve) represents a wave moving at the speed of light. The curves outside the circle are slow waves; those inside are fast. For Cerenkov radiation

$$n = \frac{kc}{\omega} = \frac{k_z}{\cos \theta} \frac{c}{\omega} = \frac{1}{\beta \cos \theta} > 1$$

Therefore, Cerenkov radiation is possible only in regions 3, 6, 7 and 8 because these are the only regions in which slow waves occur. Each of these regions will be examined in turn.

Region 3

In region 3 all values of  $k_z$  are possible, therefore Cerenkov radiation can occur at any velocity. For instance for the value of  $\frac{k_z c}{\omega}$  shown in Fig. 2, the operating point would be at 1. The group velocity is the perpendicular to the curve shown. In this region the waves are forward in the radial direction.

Region 6

in region 6 there are points such as 1 in Fig. 3 where  $v$  is too small and no

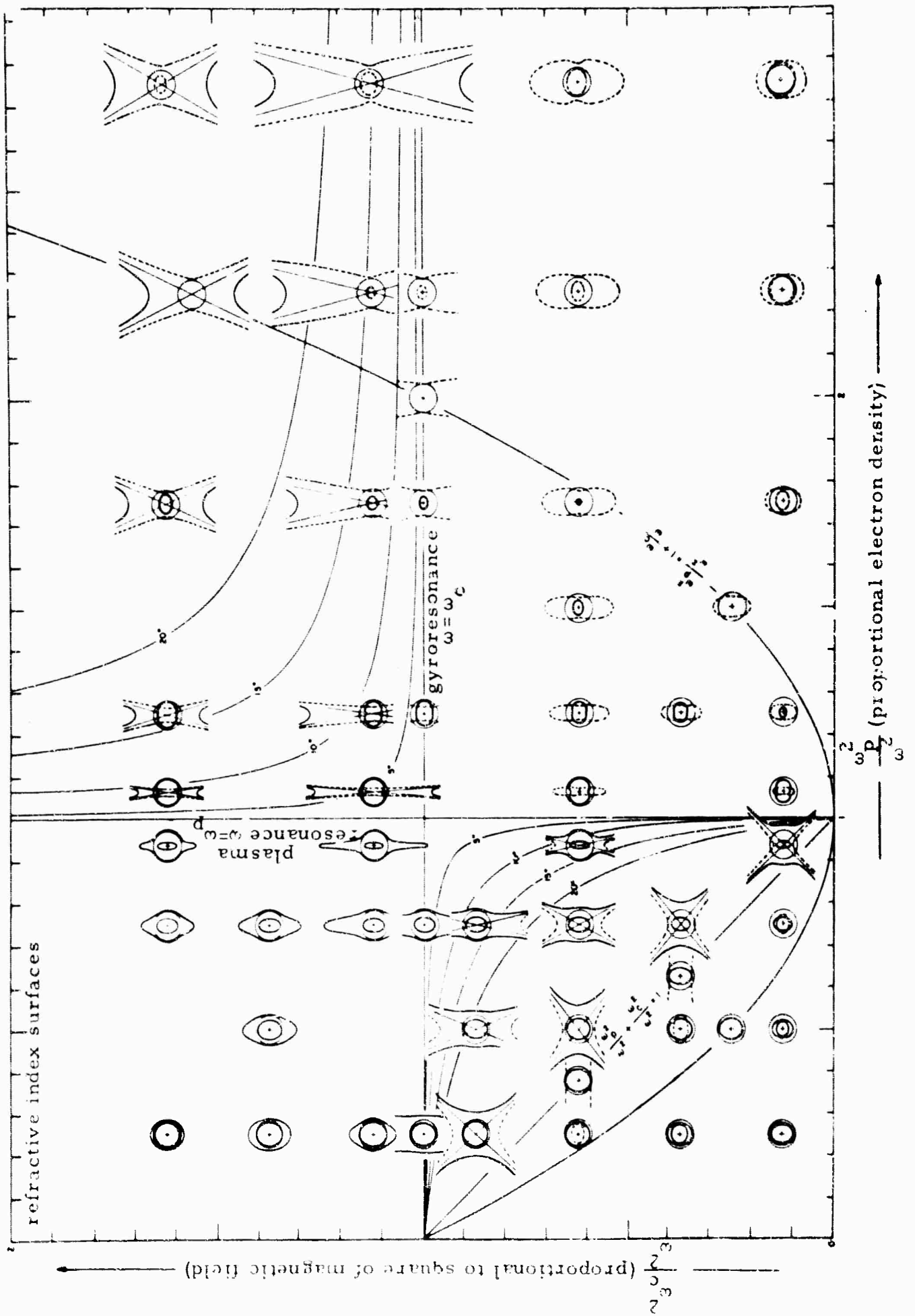


Fig. 1 (2-10)

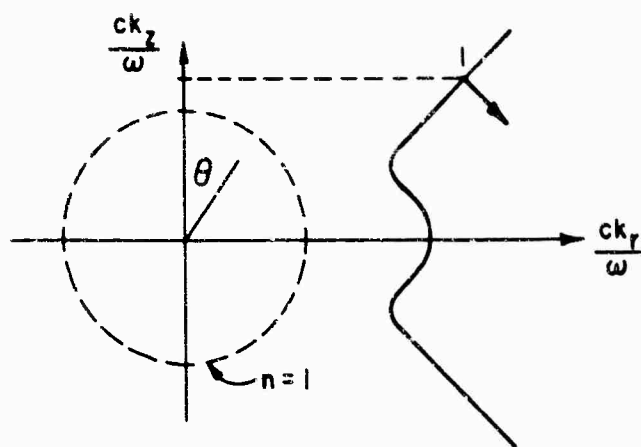


Fig. 2 (2-11)

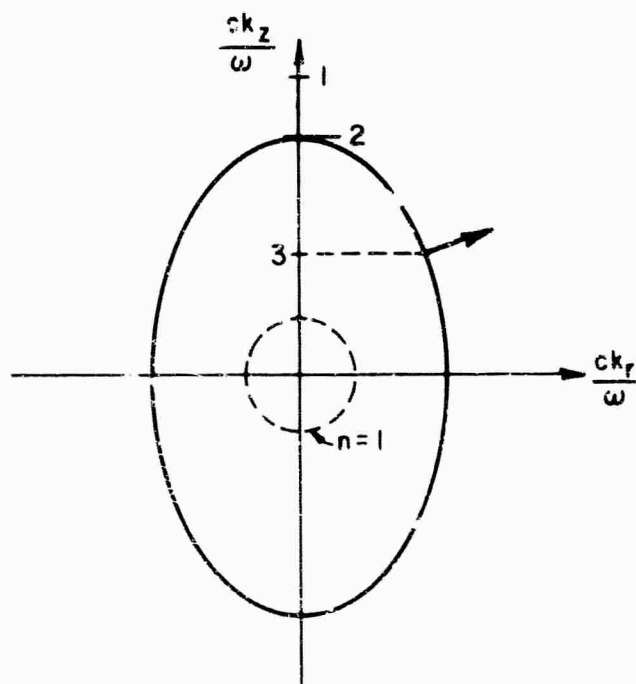


Fig. 3 (2-12)

Cerenkov radiation occurs. At points like 3 Cerenkov radiation is possible and the radiation is emitted as a forward wave as is seen by the direction of the normal. The dividing point is 2. At this point  $k_r = 0 = \theta$ . The equation of this dividing point can be obtained from the dispersion formula<sup>5</sup>

$$\tan^2 \theta = \frac{-P(n^2 - R)(n^2 - L)}{(S_n^2 - R_L)(n^2 - P)} \quad (3)$$

where

$$P = 1 - \left(\frac{f_p}{f}\right)^2, \quad (3a)$$

$$R = 1 - \left(\frac{f_p}{f}\right)^2 \frac{1}{1 - \left(\frac{f_c}{f}\right)^2}, \quad (3b)$$

$$L = 1 - \left(\frac{f_p}{f}\right)^2 \frac{1}{1 + \left(\frac{f_c}{f}\right)^2}, \quad (3c)$$

and

$$S = \frac{1}{2} (R + L). \quad (3d)$$

At point 2,  $\theta = 0$

$$\therefore n = \frac{1}{\beta}$$

The roots of the dispersion curve are

$$n^2 = R = \frac{1}{\beta^2} \quad (4)$$

$$n^2 = L = \frac{1}{\beta^2} \quad (5)$$

These two give the same curve

$$\left(\frac{f_c}{f}\right)^2 = \left[1 + \frac{\beta^2}{(1 - \beta^2)} \left(\frac{f_p}{f}\right)^2\right]^2 \quad (6)$$

This curve divides the region where Cerenkov radiation occurs from the one where it does not occur.

It can be shown that  $\left(\frac{f_c}{f}\right)^2$  must be less than the expression on the right of Eq. (6) for Cerenkov radiation to occur.

Regions 7 and 8

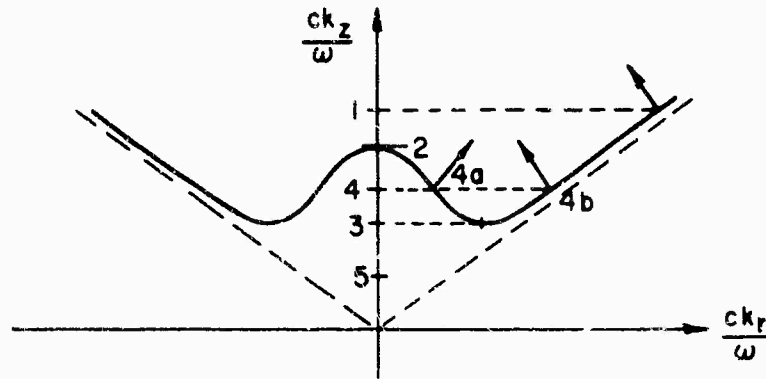


Fig. 4 (2-13)

In regions 7 and 8 the  $n$  vs.  $\theta$  is shown in Fig. 4. At a point such as 1, one wave is possible and it is a backward wave. At 4 there are two waves possible, 4a being a backward wave, the other, 4b, being a forward wave. At 5 the velocity is too high for Cerenkov radiation to occur. Point 2 represents the boundary between the case of one root and two roots. This point is characterized by  $\theta = 0$  and  $n = \frac{1}{\beta}$ . The dividing curve is just an extension of Eq. (6) into regions 7 and 8. For this region,

however,  $\left(\frac{f_c}{f}\right)^2$  must be greater than the expression on the right of Eq. (6).

The dividing curve between two roots and none is point 3. This point is characterized by a double root of the dispersion equations with  $n = \frac{1}{\beta \cos \theta}$ . This condition can be shown to be

$$\left(\frac{f_c}{f}\right)^2 \geq \frac{4\beta^2}{(1-\beta^2)^2} \left[ \left(\frac{f_p}{f}\right)^2 - 1 \right]$$

When all the conditions are plotted Fig. 5 is obtained.

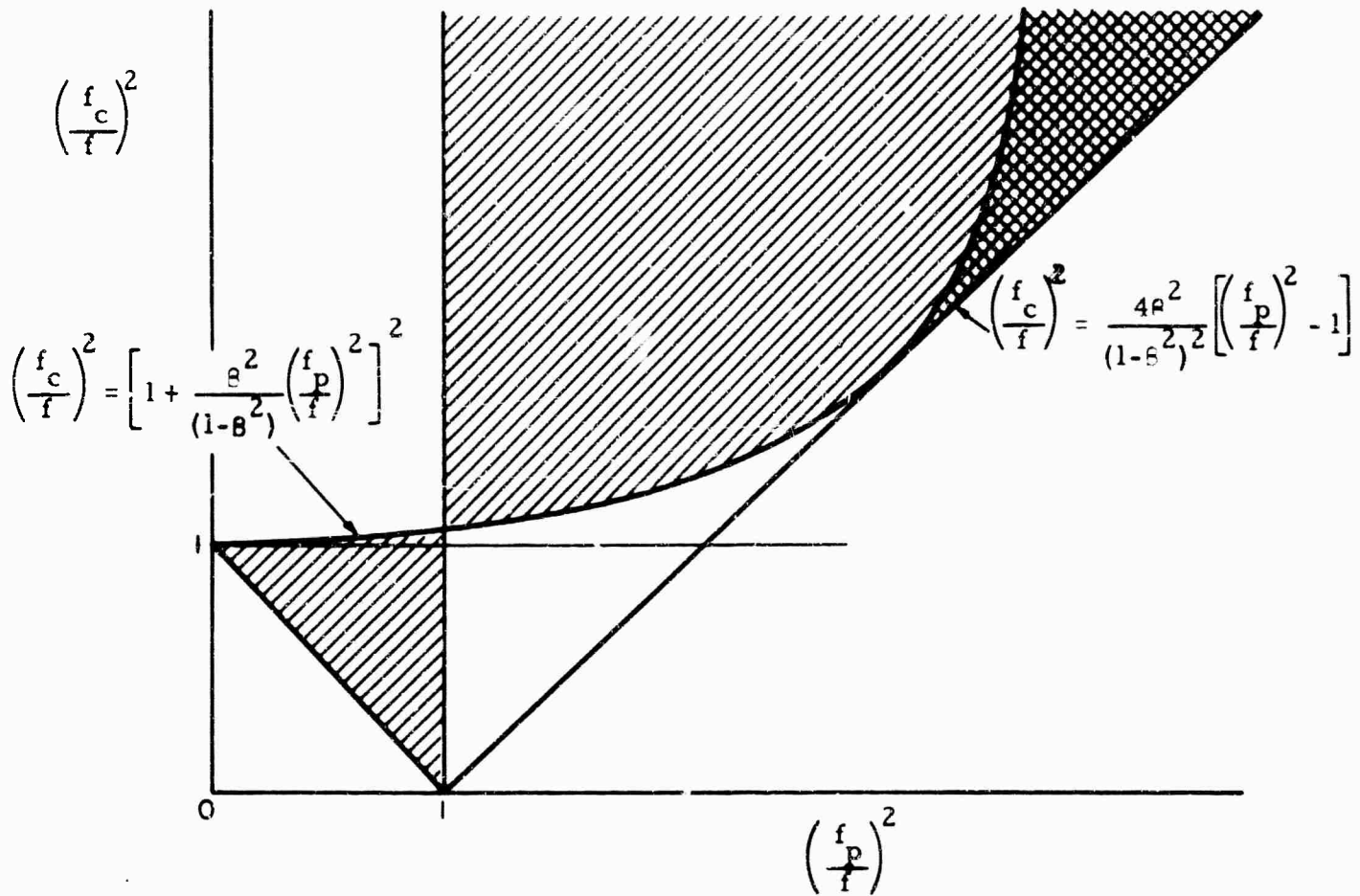


Fig. 5 (2-14)

R. Sasiela  
 R. Hutter  
 Electrophysics Department

References

1. Kenyon, Richard Jay, "Cerenkov Radiation from an Anisotropic Plasma", Technical Documentary Report, ASD-TDR-62-643, Ultramicrowave Section, Electrical Engineering Research Laboratory, University of Illinois.

2. Kikuchi, Hiroshi, "Cerenkov Radiation in a Plasma", Symposium on Quasi Optics, Polytechnic Institute of Brooklyn, 1964.
3. Sollfrey, W. and Yura, H. T., "Cerenkov Radiation from Charged Particles in a Plasma in a Magnetic Field", Physical Review, 139, A48(1965).
4. Felsen, L. P., "On the Use of Refractive Index Diagrams for Source-Excited Anisotropic Regions", Radio Science Journal of Research, Vol. 69D, 155, (Feb. 1965).
5. Stix, T. H., "The Theory of Plasma Waves", McGraw-Hill Book Company, New York, 1962.
6. McKenzie, J. F., "Cerenkov Radiation in a Magneto-Ionic Medium", Phil. Trans. Roy. Soc. London, 255, Ser. A, p. 585-606.

2.8 Transition Radiation

When a charged particle crosses a change in medium parameters, electromagnetic radiation is emitted. This phenomenon is fundamentally unlike either Bremsstrahlung or the Cerenkov effect in that the charge need not either accelerate or move faster than the speed of light in the medium in order that radiation be emitted.

A study of transition radiation is now under way. So far, three problems have been considered:

Dielectric Half-Space:<sup>†</sup>

The problem is to find the fields produced by the current density  $\underline{J} = Qv \delta(x) \delta(y) \delta(z - vt) \underline{z}_0$  in an infinite space in which the dielectric constant  $\epsilon(\omega)$  is  $\epsilon_-$  for  $z < 0$ , and  $\epsilon(\omega) = \epsilon_+$  for  $z > 0$ , and  $\mu = \mu_0$  throughout. (See Fig. 1.) The

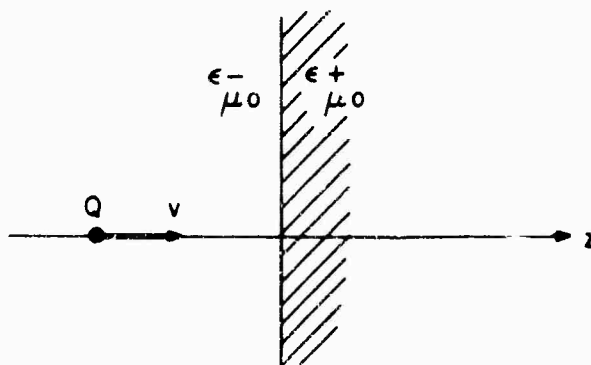


Fig. 1 (2-15) - Transition radiation in dielectric

analysis is carried out in the frequency domain, and formal expressions for the fields are derived via a Hankel transform in the variable  $\rho = \sqrt{x^2 + y^2}$ . The result for the z-component of electric field is

$$\phi_z(z, \rho, t) = \frac{1}{\pi} \int_{-\infty}^{+\infty} e^{i\omega t} E_z(z, \rho, \omega) d\omega \tag{1}$$

$$E_z(z, \rho, \omega) = \frac{1}{\pi} \int_{-\infty}^{+\infty} q J(q\rho) e_z(z, q, \omega) dq \tag{2}$$

$$e_z(z, q, \omega) = \left\{ \begin{array}{l} \frac{\frac{i\omega Q}{2\pi\epsilon_+ v^2} (1-v^2\mu_0\epsilon_+)}{\omega^2\mu_0\epsilon_+ - \frac{\omega^2}{v^2} - q^2} e^{i\frac{\omega}{v}z} \\ + \frac{Qq^2}{2\pi i\omega\epsilon_-} e^{i\sqrt{\omega^2\mu_0\epsilon_+ - q^2}z} A_+, \text{ for } z > 0 \\ \\ \frac{i\omega Q(1-v^2\mu_0\epsilon_-)}{\omega^2\mu_0\epsilon_- - \frac{\omega^2}{v^2} - q^2} e^{i\frac{\omega}{v}z} \\ + \frac{Qq^2}{2\pi i\omega\epsilon_+} e^{-i\sqrt{\omega^2\mu_0\epsilon_- - q^2}z} A_-, \text{ for } z < 0 \end{array} \right\} \tag{3}$$

$$\text{wh. re } A_{\pm} = \left[ \frac{1}{\sqrt{\omega^2\mu_0\epsilon_{\pm} - q^2} - \frac{\omega}{v}} - \frac{\sqrt{\omega^2\mu_0\epsilon_{\mp} - q^2} - \frac{\epsilon_{\mp}\omega}{\epsilon_{\pm}v}}{\omega^2\mu_0\epsilon_{\pm} - q^2 - \frac{\omega^2}{v^2}} \right] \div$$

$$\left[ \sqrt{\omega^2\mu_0\epsilon_+ - q^2} + \frac{\epsilon_+}{\epsilon_-} \sqrt{\omega^2\mu_0\epsilon_- - q^2} \right]$$

The integral Eq. (2) is then evaluated asymptotically in the far field. This parallels previous research by certain Russian authors.<sup>1,2</sup> The previous workers, however, found only saddle point contributions to Eq. (2). Besides the saddle point we include contributions from the branch point and pole singularities of Eq. (3).

Vacuum-Plasma Interface:

The situation is shown in Fig. 2. The half-space  $z > 0$  is filled with a col-

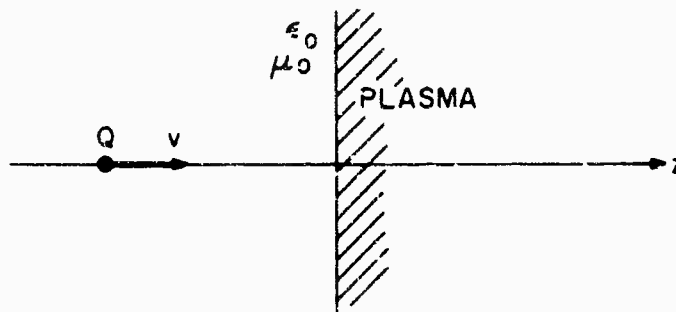


Fig. 2 (2-16) - transition radiation in plasma

lisionless warm electron plasma which is assumed to have fluid-like behavior. Small-signal linearized equations are used. The analysis of this problem is similar to that discussed in †. Again formal expressions for the field quantities are derived in terms of integrals which are evaluated asymptotically. As in problem †, previous solutions of this problem<sup>3</sup> have not taken branch point and pole contributions into account.

It is found that temperature effects are particularly important when the frequency is near the plasma frequency or when the velocity of the incident charge is near the acoustic velocity of the plasma. Results indicate that the transition radiation effect could be used in plasma diagnostics.

Transient Solution:

We consider the case where the point charge is replaced by a line charge (i. e.  $\underline{J} = \delta(x) \delta(z - vt) Qv \underline{z}_0$ ). Instead of concentrating on the harmonic components of the fields, the Fourier inversion of Eq. (1) is attempted. In the case where  $\epsilon_+$  and  $\epsilon_-$  are frequency independent, it appears that an exact solution is obtainable. These aspects are presently under study.

E. Ott  
 J. Shmoys  
 Electrophysics Department

### References

1. V. L. Ginzberg and I. M. Frank, "Radiation of a Uniformly Moving Electron Due to its Transition from One Medium Into Another", *Journal of Physics* 9, 353 (1945).
2. G. M. Garibian, "Contribution to the Theory of Transition Radiation", *J. E. T. P.* 6, 1079 (1958).
3. Yakovenko, "Transition Radiation with Account of Temperature", *J. E. T. P.* 14, 278 (1962).

### 2.9 Radiation by a Uniformly Rotating Line Charge in a Plasma

(Abstract of PIBAL Report No. 873)

The current interest in radio communication with space vehicles and other phenomena associated with vehicles reentering the earth's atmosphere has stimulated the study of wave propagation in a plasma. Such a study is of importance in providing a knowledge of both the possible wave types which the plasma admits and their means of excitation.

#### Summary:

A theoretical investigation is conducted for the radiation produced by a linear distribution of electric charge executing circular motion both inside and outside a cylindrical plasma column. The analysis includes the effects of compressibility and anisotropy of the plasma upon the radiation characteristics of the charge distribution.

In the incompressible isotropic case, a dipole resonance phenomenon is exhibited for the first harmonic of the angular frequency of rotation of the charge when the charge moves at non-relativistic velocities. If the charge moves at extremely small velocities, the resonance becomes a singularity. The influence of compressibility upon these radiation characteristics is discussed and is shown to be negligible. In the case of the presence of a magnetic field, i. e. for an anisotropic plasma, the dipole resonance is shifted. Moreover, a multiple resonance is possible for a sufficiently higher order harmonic. Furthermore, in a frequency range just above this multiple resonance Cerenkov radiation contributes to the existent Bremsstrahlung for a single harmonic in the neighborhood of the singularity of the index of refraction. Thereafter, the radiation contributions of the remaining harmonics is negligible.

S. Gianzero  
Department of Aerospace Engineering and  
Applied Mechanics

## 2.10 Experimental Work in Connection with Cerenkov and Transition Radiation

### 2.10.1 The Rebatron

The purpose of the project is to set up a facility for using a relativistic, very strongly bunched electron beam to study Cerenkov and transition radiation in gaseous plasmas. Studies of interactions between such beams and dielectrics, periodic circuits and metallic foils are also possible.

The parts for a rebatron were obtained from Professor Coleman at the University of Illinois. During the past year a table and vacuum station were constructed, the rebatron and associated modulators were assembled, and the necessary trials were carried out to make the device operative. At the present time a beam of approximately 1 Mev and several milliamperes pulse current is available; the pulses may be from 1 to 2 microseconds duration and at a repetition rate up to about 200 per second.

Figure 1 is a photograph of the rebatron. The accelerating cavity is

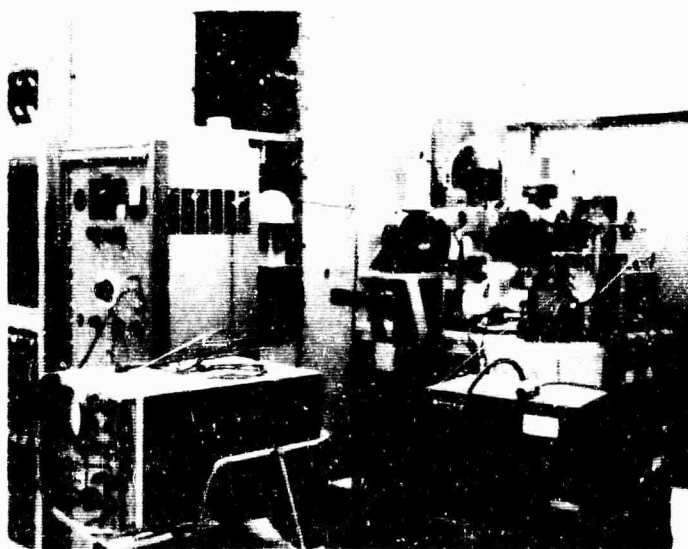


Fig. 1 (2-17)

a circular cylinder 4 cm long by 8.13 cm diameter. The beam enters and leaves the cavity through small holes on the axis. The rf power enters through two oppositely placed apertures on the cylindrical surface which provide optimum coupling from the waveguides. The two waveguides and the two magnetrons are visible in the photograph. The electron pulse enters the cavity after the rf pulse has had time to fill the cavity and the electrons see an accelerating field of approximately constant amplitude. This field accelerates and bunches approximately 30% of the electrons, those which enter during a favorable phase interval, and these bunches are expelled through the exit hole at the magnetron frequency. Any harmonic can be generated so long as its wavelength is greater than the length of the bunch. Above about the tenth harmonic it is necessary to excite a prebunching cavity in order to produce shorter bunches. This is done with a signal of appropriate phase and amplitude tapped off the line from one of the magnetrons.

#### 2.10.2 Beam Measurements

The beam consists of high energy electrons in bunches about 1mm diameter and from 1 to 5 mm long. The velocity spectrum, the shape and stability of the bunches, and the average current and voltage of the beam depend on the operating parameters such as magnetron current and frequency and the excitation of the pre-bunching cavity. It would be desirable to determine these relationships experimentally.

The velocity spectrum and the average velocity or voltage will be measured with a magnetic analyzer which can be seen in the photograph. This is being tested at the present time and will be in use during the next half year.

The shape of the bunches is very difficult to measure but it is closely related to the harmonic content of the beam current. At this time we are preparing to measure the amplitude of the fifth harmonic by shooting the beam through RG 91 waveguide and measuring the radiated power. Later we will measure higher harmonics by the same and possibly some other methods.

#### 2.10.3 Planned Experiment with Plasma

The group has been interested in radiation from electrons moving in anisotropic plasmas and some members have been calculating the radiation into modes in waveguides and resonant cavities filled with plasma. An experiment is being planned

to measure the radiated power from the rebatron beam in a plasma-filled cavity. The first step will be to measure the radiation into a dielectric-filled cavity. This is so much easier to do that it is worthwhile doing it as a calibration experiment and as a test of the correspondence between theoretical and experimental results.

Cold tests are being carried out on a configuration similar to that which will contain the plasma. The development of the plasma-filled cavity proceed as described below.

#### 2. 10. 4 Screen Discharge

To measure radiation from the beam into a plasma-filled cavity it is necessary to develop a discharge which accurately realizes this situation. Previous work done in our laboratory led us to try to use a screen cathode discharge to achieve this. Figures 2 and 3 are a photograph and a sketch of a configuration that is being tested at this time. This resembles the Penning discharge except that in the case of the Penning the central cylinder is positive and can be filled with a fairly uniform plasma provided a strong magnetic field is present. In the case of the screen cathode an apparently uniform plasma can be achieved even without a magnetic field. Also the screen cathode is more easily adaptable to the function of being a resonant cavity. Some development work remains to be done on this discharge.

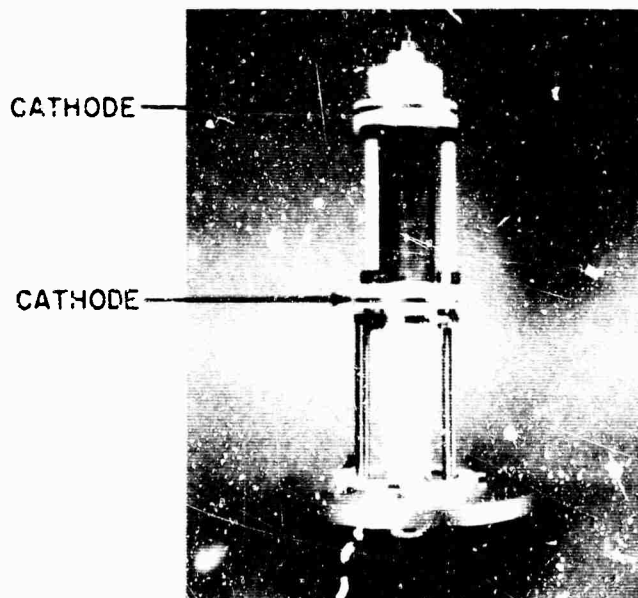


Fig. 2 (2-18) - Photograph of cavity screen discharge

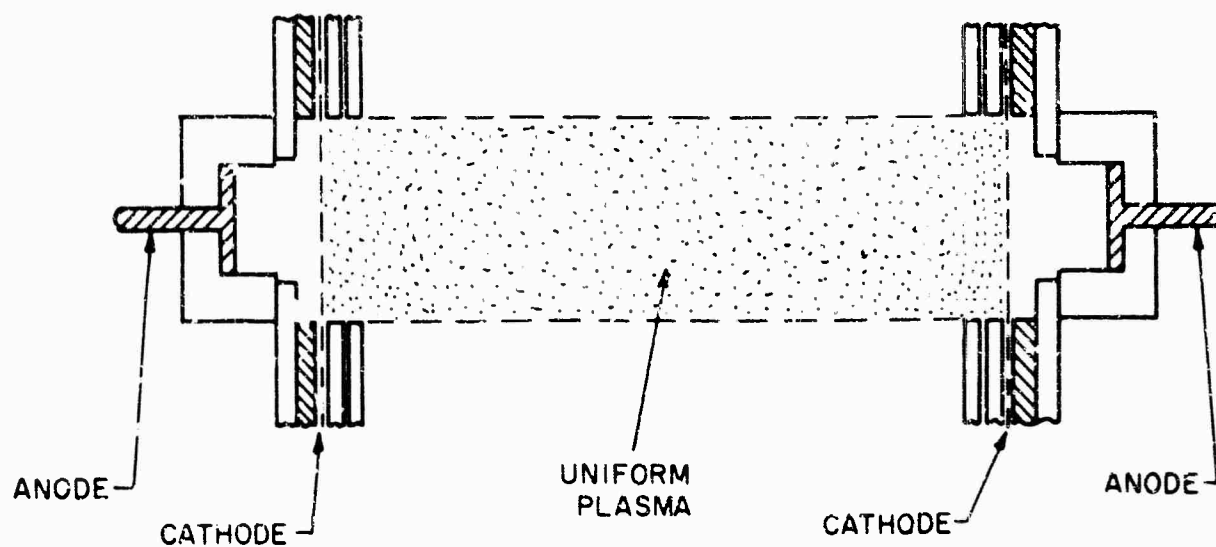


Fig. 3 (2-19) - Schematic of cavity screen discharge

R. Pepper  
R. Hutler  
Electrophysics Department

## 2.11 Propagation of Waves in Plasma Waveguides

### Purpose of the Project

We investigate the nonquasistatic solutions for the propagation of waves in waveguides completely or partially filled by plasma. We shall extend our research to high-power electron beam-plasma interactions. The ultimate objective of this research is to examine the feasibility of utilizing electron beam-plasma systems for new types of microwave amplifiers, microwave generators, and for the heating of plasmas at the expense of the d. c. energy of an electron beam.

### Accomplishments

We have formulated the solution for the following beam-plasma system: the plasma contains electrons neutralized in the unperturbed state by ions of finite mass. The unperturbed density of the electrons and the ions is not uniform. The beam electrons drift along the axis of uniformity of the waveguide. Their unperturbed charge densities and velocities are not uniform. Furthermore, a uniform, finite, axial, magnetostatic field along the axis of uniformity of the waveguide was assumed to exist.

The formulation of the solution for the above mentioned system is a generalization of the solution for the case with uniform beam and plasma densities and uniform beam velocity.

For the case of a partially filled waveguide we must consider the boundary conditions between beam and plasma and also between plasma and free space inside the waveguide. The usual procedure is the introduction of equivalent surface charges and surface currents. This method is valid only under the assumption that the variation of the total electric field at the perturbed boundary is very small. It came out that this is not the case for neutral plasmas. We have started the investigation of the formulation of more satisfactory approximate boundary conditions between neutral plasmas and free space inside a waveguide.

Another part of our research was the formulation of an approximate method for the investigation of dispersion relations for plasma waveguides, by coupling of empty-waveguide modes and quasistatic modes. This method has given very satisfactory results for the symmetric mode of propagation inside a completely filled plasma waveguide. Currently we apply the same technique for the investigation of the following two cases:

- a) Propagation of the mode with one azimuthal variation inside a completely filled circular cylindrical plasma waveguide.
- b) Wave propagation inside a partially filled circular cylindrical plasma waveguide.

### Plans

During the next half-year interval we plan to complete the following dispersion diagrams:

- a) Quasistatic solution for the partially filled plasma waveguide.
- b) Direct solution for the partially filled plasma waveguide.
- c) Coupling of modes for the partially filled plasma waveguide.
- d) Coupling of modes for the case of one azimuthal variation inside a completely filled circular cylindrical waveguide
- e) Coupling of modes for the electron beam-plasma interaction.

P. E. Serafim  
Electrical Engineering Department

G. Pisane  
Electrophysics Department

### 3. FLUID DYNAMICS

#### Introduction

The observable characteristics associated with the very high speed flight of vehicles within the atmosphere is intimately related to the flow field characteristics of the vehicles. The electrons and excited states of the chemical species in these flows are somewhat in the nature of stains or traces which are contained in the masses of gas which act as a carrier in more detail. There are some couplings between the chemical behavior of the flow and its dynamics. However, much information about the energy distribution and the basic gas dynamic configuration can be obtained without the consideration of the chemical influences. With this in mind, fluid dynamical studies of the near-wake structure of conical shapes has been carried on in the heated (1500<sup>o</sup>K stagnation temperature) hypersonic blowdown wind tunnel. The initial results of these experiments were obtained under Air Force sponsorship and are described below. Extensions of this work leading toward the investigation of effects of angle of attack on the near wake structure have been initiated under ARPA-ONR sponsorship and are now under way.

The scattering characteristics of these flow fields are significantly dependent upon the nature of the fluctuations in the flows. A powerful tool in the investigation of these fluctuations is the hot wire anemometer. A description of the anemometer equipment being activated for fluctuation diagnostics is likewise described here. The electron distributions generated by the chemical or photo-ionization behavior of the hypersonic flows of interest is also under study in several of its many facets. In particular, diagnostic techniques employing microwave resonant cavities have been developed and are under further development. The major tools in these developments are based on fluid dynamic behavior as generated in shock tubes and a shock tunnel. In their initial form, the cavities are constructed to resonate as an effective dielectric represented by plasma flows through the cavity or stagnates against a cavity. In this way the presence of a limited

electron density band can be perceived. However, several experiments must be run if one wishes to survey a wide electron density range which corresponds to a large plasma frequency band. To overcome this disadvantage and to permit a continuous time-resolved measurement of electron densities by means of resonant cavity techniques, an interesting diagnostic device based upon the plasma tuning of a klystron oscillator has been devised.

The explanation of certain phenomena which have been perceived by radar, has hinged upon the hypothesis that there is a significant electron density level upstream of the shock layer surrounding a vehicle. This phenomenon is termed precursor ionization. Detailed measurements of this type of precursor ionization have been made with the use of resonance cavity methods which are described in greater detail herein. The use of these cavity techniques in the investigation of chemical kinetics phenomena, are now under consideration. Their application in this context appears to be promising under conditions where electron reactions are coupled to vibrational relaxations. Promising cavity configurations of several kinds are under study as described here.

Chemical kinetic studies involving the scattering of ion beams is employed to determine inter-molecular potential energy functions of gaseous species. These experiments to be described are significant in the determination of thermodynamic and transport properties of gases pertinent to the observable problem. Finally, in the context of exploring methods for providing high energy streams of fluid for gas dynamic and chemical testing purposes, the magnetohydrodynamic behavior of certain channel flows has been explored. New types of solution for this magnetohydrodynamic flow configuration have been evolved.

The work to be described here has been carried out completely under the ARPA-ONR program except for the initial work on the fluid dynamics of the near wake which was started under an Air Force program subsequently terminated.

M. Bloem  
Dept. of Aerospace Engineering  
and Applied Mechanics

### 3.1 Resonant Cavity Techniques for Measurement of Electron Density and Collision Frequency of Hypersonic Flows

#### 3.1.1 General Data

Resonant microwave cavity techniques are being used for plasma diagnostics of hypersonic flows of low density gases in three facilities including a 5' diameter shock tunnel, a 6" shock tube and a 2" shock tube all at the Long Island Graduate Center. Objectives include special cavity diagnostics for non-uniform flows encountered at shock discontinuities of models, investigation of shock wavefront characteristics and calibration of the shock front facilities. The primary effort to date has been in the latter two areas.

Specific accomplishments during this period include:

- (a) Preliminary testing of microwave diagnostics of 4 millisecond hypersonic shocks produced in 5' shock tunnel. A brief report indicates sufficient sensitivity for experimentation. Further refinement of instrumentation techniques as well as shock reproducibility is being pursued prior to interpretation of cavity data so far obtained.
- (b) A T.M. smooth bore cavity has been constructed for microwave diagnostics in a 6" shock tube. An assembly drawing is shown in Fig. 1.
- (c) Design data for smooth bore cavities has been experimentally determined. A detailed report of this work is given later.
- (d) Quantitative electron density measurements have been made using a diagnostic cavity partially filled with a field induced plasma. This work is reported in detail.

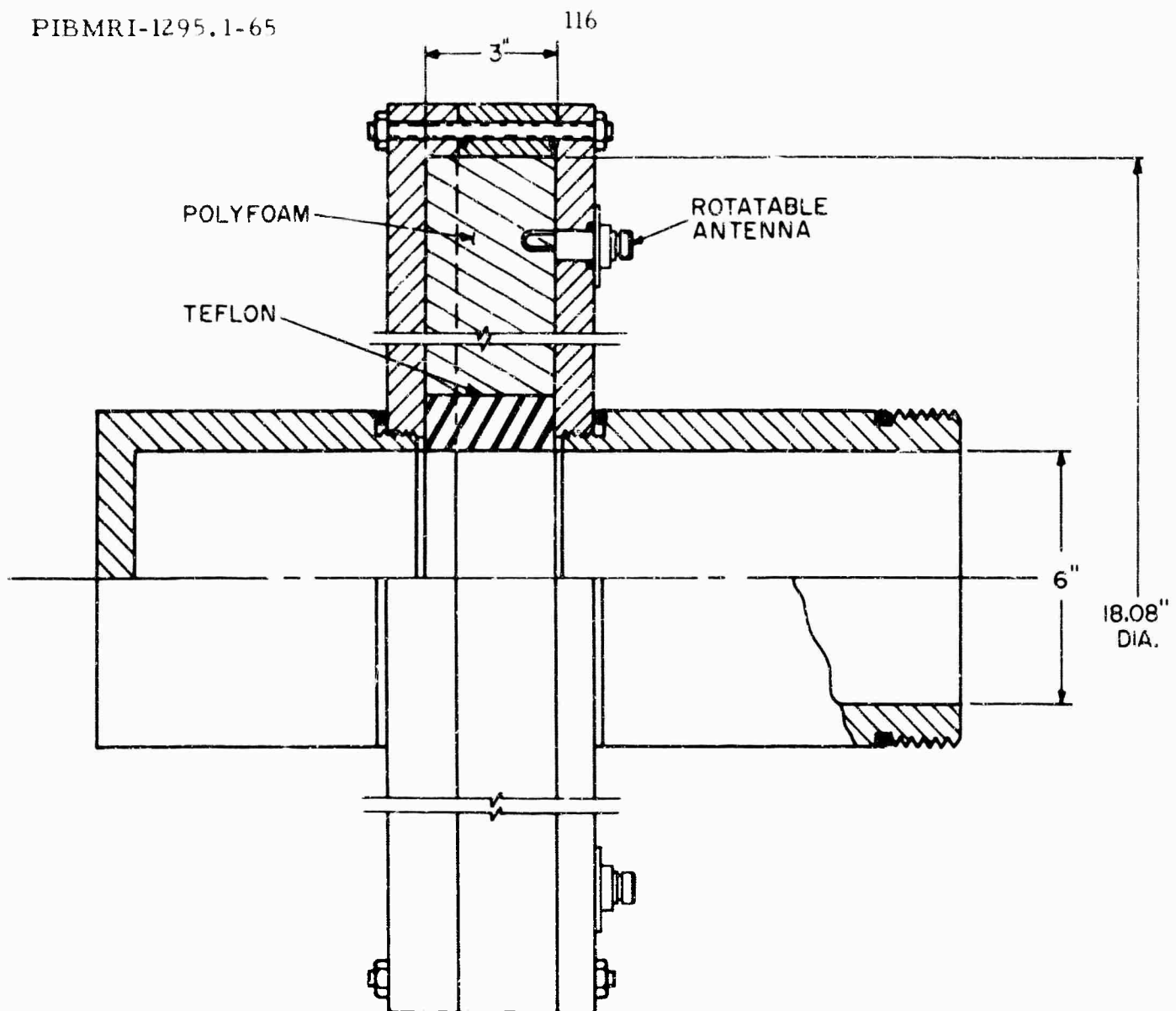


Fig. 1 (3-1) - Assembly drawing for TM diagnostic cavity (6" shock tube)

#### Plans for Next Period

Further microwave diagnostics on shock flows will be carried out utilizing expanded and improved shock facilities. Smooth bore cavities for the 5' shock tunnel will be designed. New electronic means for continuously reading electron density will be investigated. The application of diagnostics to non-uniform plasma flows will be further investigated.

J. Griemsmann  
 D. Jacenko  
 E. Malloy  
 Electrophysics Department

S. Lederman  
 Dept. of Aerospace Engineering  
 and Applied Mechanics

3.1.2 Preliminary Data on Cavity Measurement of Electron Density  
in the 5' Shock Tunnel

Using the cavities shown schematically in Figs. 2 and 3 electron density measurements have been made in hypersonic shocks produced in the

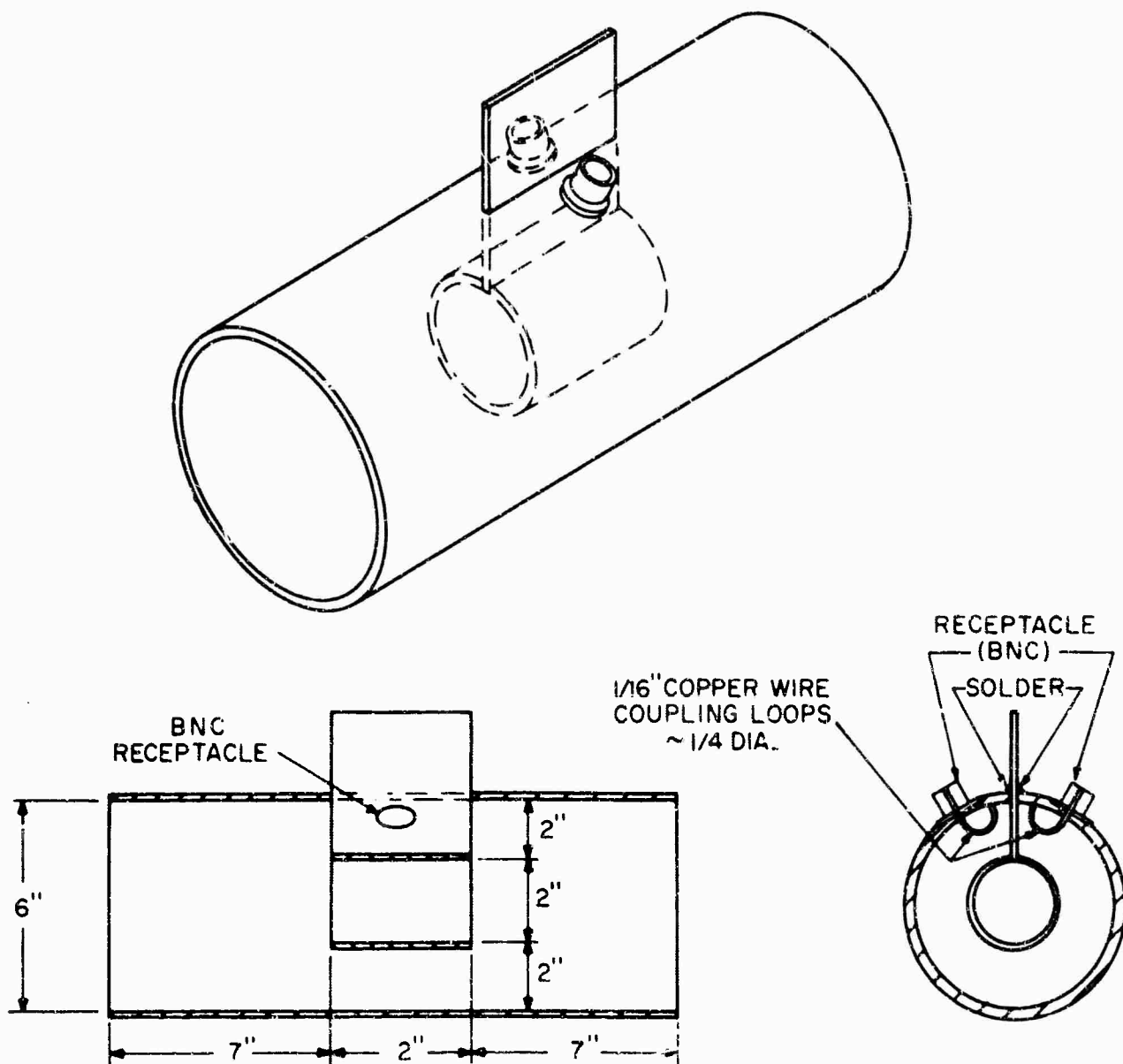


Fig. 2 (3-2) - Schematic of open resonant cavity (center ring construction)

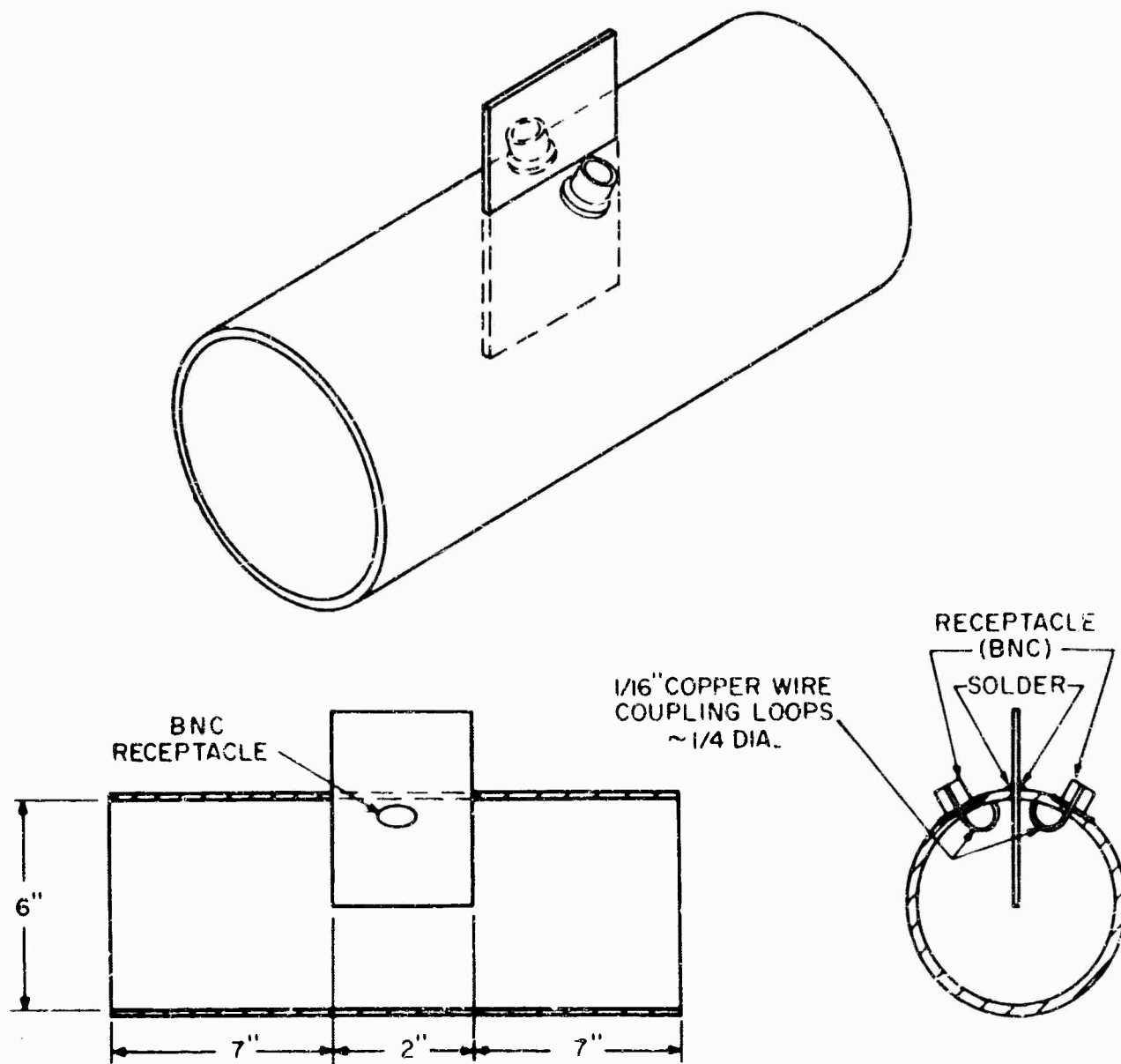


Fig. 3 (3-3) - Schematic of open resonant cavity (fir construction)

5' shock tunnel at the Long Island Graduate Center of the Polytechnic Institute of Brooklyn. Preliminary testing has indicated adequate sensitivity of the cavities and test equipment but also further tests must be made to insure quantitative interpretation of the test data.

Testing to date has been done by arranging for the cavities to have greater electrical transmission when the shock flow is in the cavity. This is done by presetting the frequency at a value higher than the measured resonant frequency under vacuum conditions. Shown in Fig. 4 are oscilloscope traces designed primarily to show the sensitivity of the cavities. The upper curve is for the cavity of Fig. 3 which was preset at a frequency 1 megacycle higher than the 567 megacycle resonant frequency. The lower trace is for the cavity of Fig. 2 with the frequency set at the upper half power point. This second frequency setting would be sensitive to a lower electron density and accordingly reacts earlier and returns later to the quiescent state. The time scale is 1 millisecond per major division. Other instrumentation planned includes locking an oscillator to the resonant

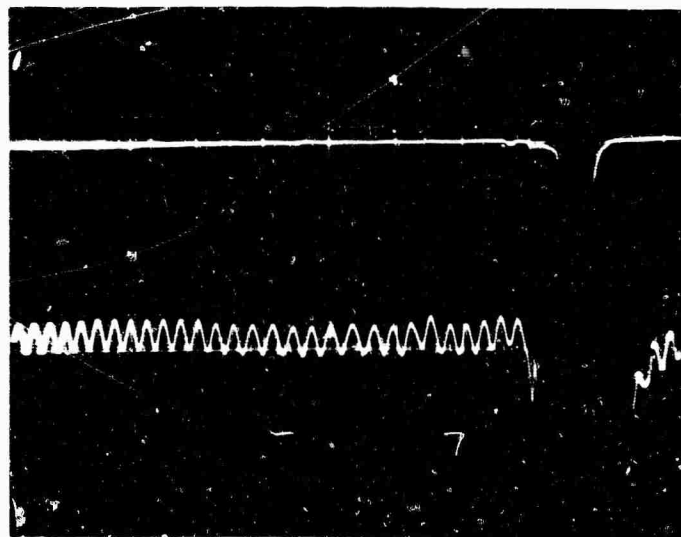


Fig. 4 (3-4) - Sensitivity check on diagnostic cavities

frequency of the cavity so as to get a continuous measure of electron density in terms of frequency for the period of the shock. Rapidly sweeping the preset frequency is also a technique being explored.

Among the aerodynamic effects to be studied are the perturbations in electron density that are produced by the instrument itself particularly relating to the obstructions contained in the flow channel. One test includes a tandem connection of the cavities of Figs. 2 and 3.

J. Griemsmann  
E. Malloy  
Electrophysics Department

S. Lederman  
Dept. of Aerospace Engineering  
and Applied Mechanics

### 3.1.3 Design Data for Smooth Bore T. M. Diagnostic Cavities

#### Summary

Measured design data has been obtained which will make possible improved "smooth bore" T.M. diagnostic cavities, particularly for electron densities lower than  $10^8$  electrons per cubic centimeter. Besides the unobstructed cylindrical channel provided for the air flow, the design data provides the means for reduction in size and weight and improved overall aerodynamic shaping. The design data will permit good engineering estimates of range of electron densities that can be measured for a given design.

#### Introduction

Shown schematically in Fig. 5 is a form of cavity which has been used in shock tube diagnostics where the dimension  $d$  is that of the internal diameter of the shock tube. Part of the cavity is noted to be a teflon dielectric cylinder which provides for the physical continuity of the cylindrical channel and also serves as part of the dielectric of the cavity. For diagnostics in a 1" shock tube, microwave resonant cavities operating at about 3 gigacycles have been previously used to measure electron densities of about  $10^{10}$  electron per cubic centimeter.

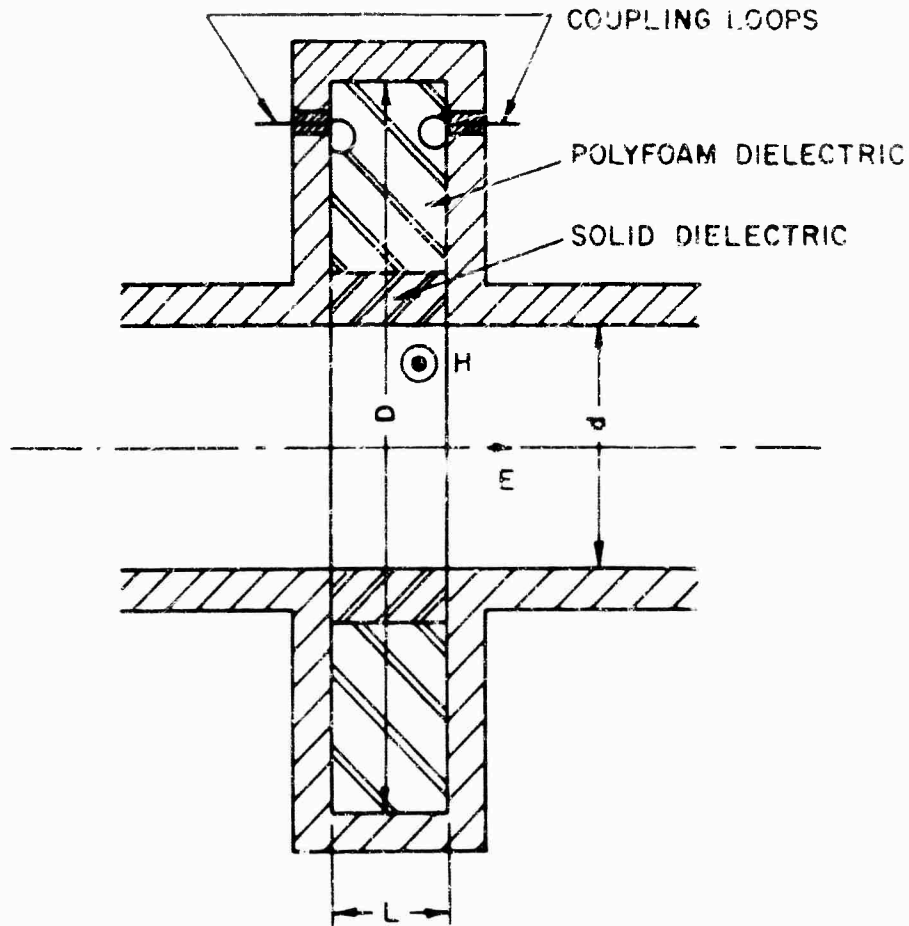


Fig. 5 (3-5) - Cross-section of TM smooth bore cavity

More recently a microwave cavity (see Fig. 1) has been built for diagnostics in a 6" shock tube. This was a scaled model of that for the 1" shock tube. This cavity is operated at about .5 gigacycles and is designed to measure electron densities of about  $10^7$  electrons per cubic centimeter. The overall diameter is 20". One method of obtaining a smaller construction which has been used is to build the resonant cavity internal to the bore as illustrated in Fig. 2. Another method of design is shown in Fig. 6. This design preserves the smooth bore feature of the design of Fig. 1. The structure external to the bore, however, is a coaxial line structure and permits smaller overall diameter as well as better aerodynamic shaping.

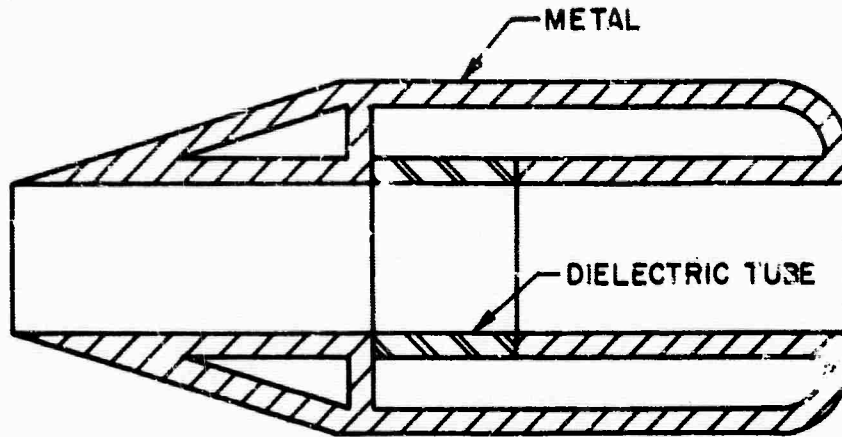


Fig. 6 (3-6) - Cross section of TM - coax cylindrical cavity

One difference between the smooth bore cavities of Figs. 1 and 6 and that of Fig. 2 is that for the smooth bore cavities the plasma to be measured flows through only part of the cavity and it is correspondingly less sensitive to dielectric changes in the bore. One objective of this experiment is to measure the decrease of this sensitivity in particular as a function of the ratio  $L/d$ .

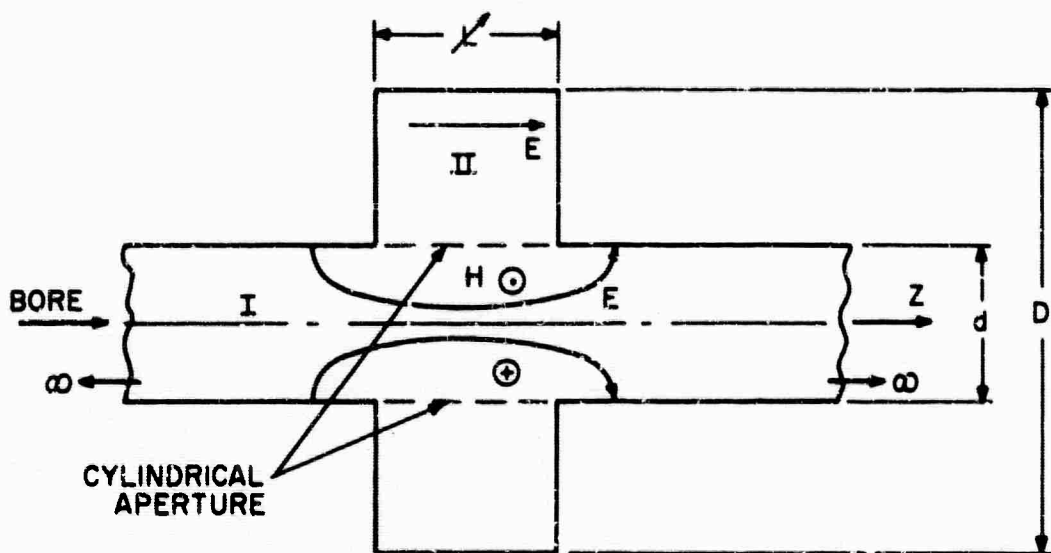
Another objective is to provide the information necessary for the design of different reactance structures external to the bore. This can be done by making the assumption that for a given  $L/d$  the field distribution in the cylindrical dielectric aperture looking into the bore is substantially independent of reasonable changes in the structure external to the bore. Under these circumstances the field internal to the bore is independent of the external structure and designs can be formulated in terms of relatively simple equivalent circuits.

#### Analysis and Circuit Representation

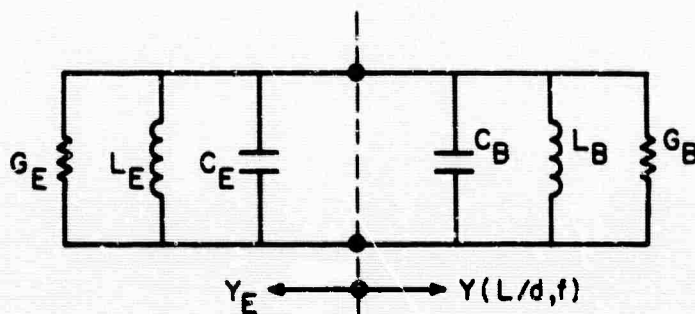
For convenience of reasonable size and availability of precision test equipment, measurements were performed at about 5000 megacycles per second on a cavity of the type shown in Fig. 1. The internal dimensions were  $D = 1.8''$ ,  $d = .6''$  and  $L = .10''$ ,  $.15''$ ,  $.20''$ ,  $.25''$ ,  $.30''$  and  $.35''$ . The variations in  $L$  were obtained by inserting rings of internal diameter  $D$  in the outer barrel of the cavity. For separating out the design information, pieces of foamed dielectric were machined so as to independently fill the bore of the cavity on that part external

to it. Dielectric constants of about 1.03 and 1.075 were used. The measurements made were the resonant frequency for all values of  $L$  using an air cavity and various combinations of dielectric filling.

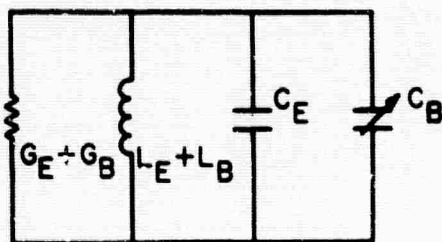
The basis for the measurements and their interpretation are best explained through the use of Figs. 7 and 8. In Fig. 7(a), the internal cross-section of the cavity of Fig. 1 is reproduced. The T.M. mode used is characterized by circular magnetic field lines in planes perpendicular to the axis. In the region external to the bore, region II in Fig. 7, the electric field is substantially uniform in the  $z$ -direction. In the region II near the cylindrical aperture into the bore some deviation from uniformity takes place. For the purposes of this investigation the deviation from uniformity is assumed negligible. Typical electric field lines in the bore, region I, are illustrated in Fig. 7(a). For the operating frequencies chosen for diagnostic cavities the tube of diameter  $d$  is well below cut-off for all modes and the field decays rapidly away from the aperture. Under these circumstances the field distribution in the bore is fixed once a given frequency is specified and a uniform field in the aperture is assumed. The wave admittance or E-type dominant mode radial line admittance is then specified and can be represented at one frequency and one value of  $L/d$  by the right hand part of the circuit shown in Fig. 7(b). The admittance  $Y$  is arbitrarily chosen to be represented in terms of the capacitance  $C_B$ , representing the energy stored in the electric field in the bore (I) and  $L_B$  representing the energy stored in the magnetic field in the bore.  $G_B$  represents the energy dissipated in the bore or on the metallic walls of the bore. For diagnostic purposes it is assumed that introducing materials into the bore which have dielectric constants only a few percent different from 1.0 will not change the field configuration in the bore. As a consequence only the capacitance  $C_B$  will change as the result of introducing a tenuous dielectric into the bore. For the following measurements the circuit to the left of the line in Fig. 7(b) represent the short circuited radial line structure. In design this structure could be any structure which realizes the same reactance,  $Y_E$ , looking outward from the aperture. In Fig. 7(c) is shown the equivalent resonant frequency circuit used for diagnostic



a) Line diagram of internal cavity cross-section



b) Equivalent circuit at aperture



c) Equivalent circuit for measurements

Fig. 7 (3-7) - Cavity cross-section and equivalent circuits

and calibrating measurements. The sensitivity of the cavity is seen to be dependent on the ratio of  $C_B$  to  $C_E$ . The ratio of  $C_B$  to  $C_E$  is obtained below by measuring the resonant frequency with air and with one other known dielectric.

It should be emphasized that the equivalent circuit representations of Fig. 7 are valid only for the frequencies very close to that at which the measurements of the susceptance looking into the bore are made. The use of the measured data would then be limited to design of cavities at the same frequency or scaled versions thereof. When the diameter  $d$  however is far below cut-off for the cavity mode as it has been for previous designs primarily electric energy will be stored in the bore and this field configuration will not differ much from the field configuration to be found at zero frequency ( $D = \infty$ ). In view of this, a good approximate representation for this admittance at frequencies equal to or below those represented by the measurements is an open-circuited radial transmission line as shown in Fig. 8. This circuit was chosen to present the data obtained from the measurements using the quantity  $a$ . This quantity is that which will give the same resonant frequency as that of measured cavity of Fig. 7(a) when region II is the same for both cavities. The rigorous alternative to this approximate approach is to obtain data for different values of  $D$  and different values of frequencies over the range of interest.

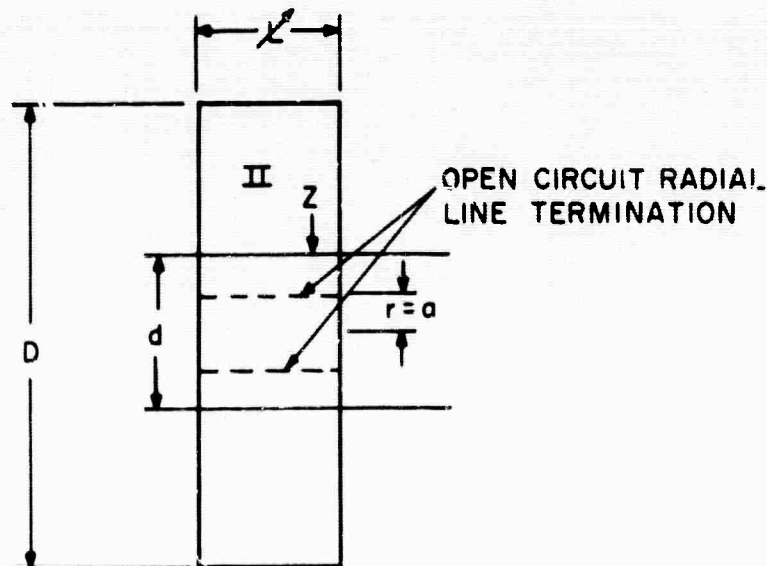


Fig. 8 (3-8) - Equivalent TM radial line representation

### Experimental Data

Shown in Fig. 9 are the resonant frequencies for the cavity of Fig. 7(a) plotted as a function of  $L$  for the cavity air filled and for the cavity filled with each of two dielectrics. These measurements provide reference points for measuring the geometric calibrating factor  $C_B/C_E$  and also some to measure the dielectric constants of the two foam materials. With the exception of the points for  $L = .10$ , all the values of dielectric constant calculated from the smooth curves are quite precise. For the dielectric #1 a specification of the dielectric constant as  $1.035 \pm .0025$  covers all conditions. The same specification for dielectric #2 is  $1.077 \pm .003$ .

For perspective, two special resonant frequencies are indicated. When  $L/d$  is mentally conceived to be large the resonance should be expected to approach that of T.M. cylindrical cavity, since electrical energy stored in the bore becomes less and less significant. The resonant frequency of the air cavity should approach the 5000 megacycle value indicated. When  $L/d$  becomes very small the impedance seen looking into the bore is very large compared to radial line characteristic impedance such that the ultimate condition is virtually a normalized open circuit at the aperture. For very small  $L/d$  the resonant frequency for the air cavity should approach the 6000 megacycle value indicated in Fig. 9.

The data sought for the design of improved cavities is presented in Fig. 10 in terms of open circuit radial equivalent of the T.M. modal fields in the bore as already considered in the analysis. The aperture length,  $L$ , is the height of the equivalent radial line. The quantity  $a$  is the position for the open circuit of the radial line equivalent. The range of  $L/d$  is given by,  $.25 \leq L/d \leq .58$ . The equivalent circuit is quite precise for  $d/\lambda = .27$  and is adjudged to be a good approximation for any value below this where  $\lambda$  is the T. E. M. wavelength in the medium of the homogeneously filled cavity.

Shown in Fig. 11 is the change in resonant frequency of the cavity from the condition of air filling the bore to that of the indicated dielectric filling the

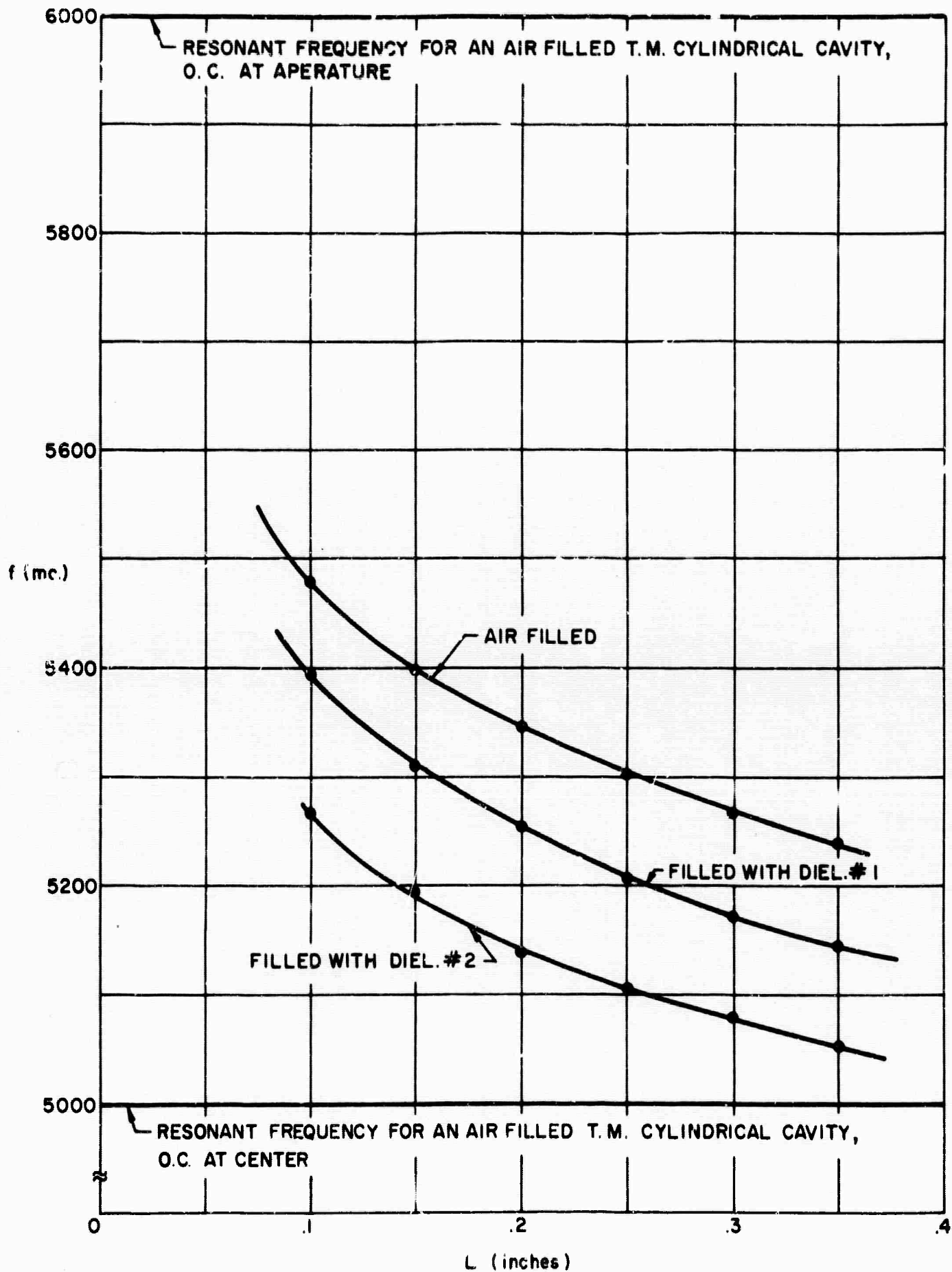


Fig. 9 (3-9) - Resonant frequencies for filled cavities

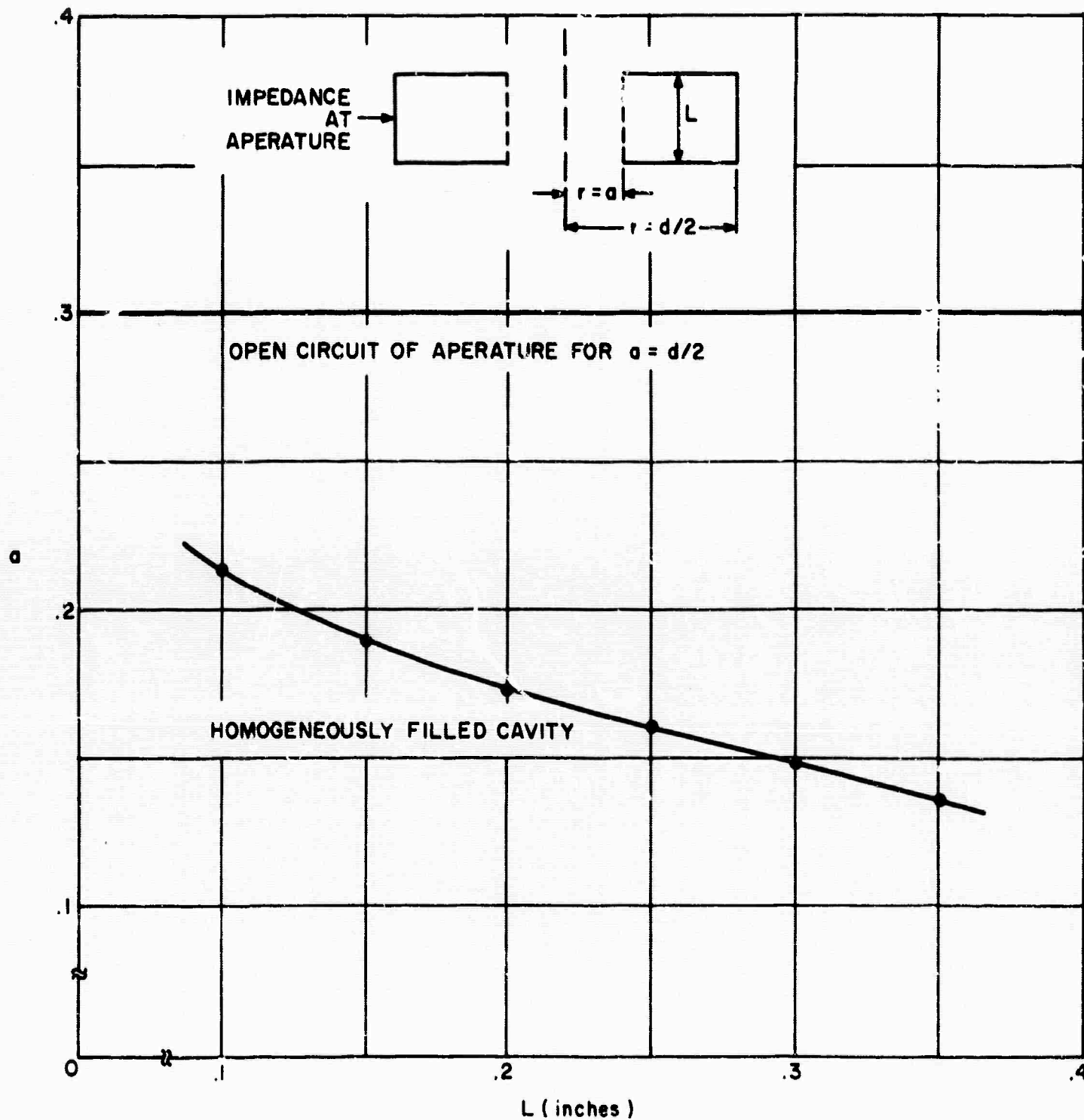


Fig. 10 (3-10) - Inner radius for equivalent open-circuited radial line

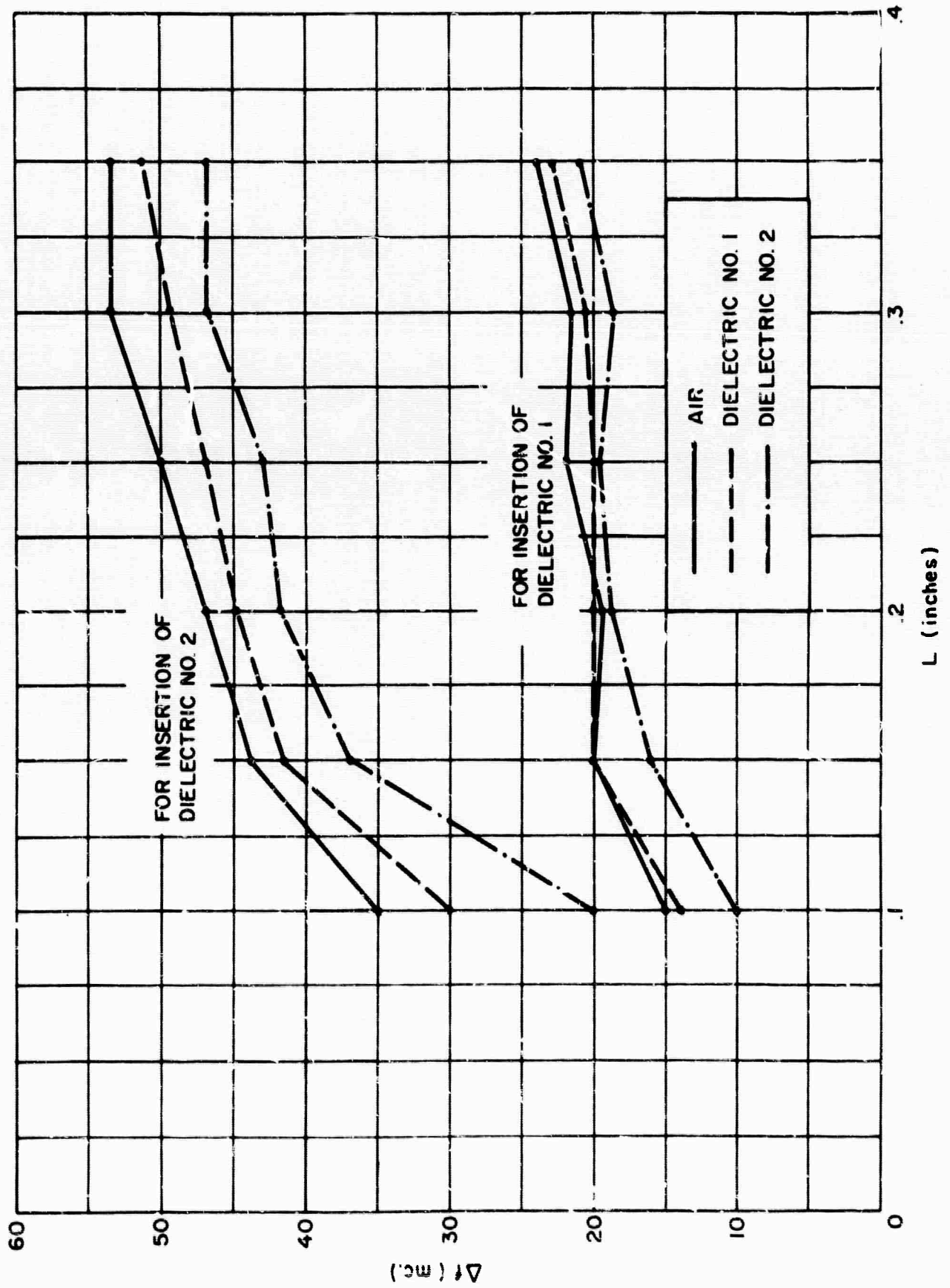


Fig. 11 (3-11) - Resonant frequency charges caused by dielectric inserts

bore. For additional checks the curves are also shown with dielectrics #1 and #2 filling that part of the cavity external to the bore. The shift in these instances is expected to be less by virtue of the larger value of  $C_E$  in the equivalent circuit of Fig. 7(c). Since the sensitivity of the cavity is seen to depend upon the ratio of  $C_B$  to  $C_E$ , the  $\frac{C_B}{C_E}$  ratio can be defined as the "calibration constant" of the cavity. It can readily be obtained from the equivalent circuit in Fig. 7(c) and is:

$$\frac{C_B}{C_E} = \frac{\left(1 - \frac{\omega_1^2}{\omega_2^2}\right)}{\left(K_c \frac{\omega_1^2}{\omega_2^2} - 1\right)}$$

where  $\omega_1$  - resonant frequency of the cavity when cavity is completely filled with dielectric.

$\omega_2$  - resonant frequency of the cavity when only the outer portion of the cavity is filled with dielectric.

$K_c$  - dielectric constant of the dielectric insert.

In Table I are shown the calibration constants for cavities of various lengths  $L$ . They are computed from the measured data using the above formula. As shown, these data were obtained for the cases when the external portion of the cavity was filled with various dielectrics and inserts built from various dielectrics were introduced into the bore of the cavity.

Figure 12 shows the average calibration sensitivity of the cavity vs. length obtained from the data in Table I. In this case, average calibration constants were computed for each "L" of the cavity.

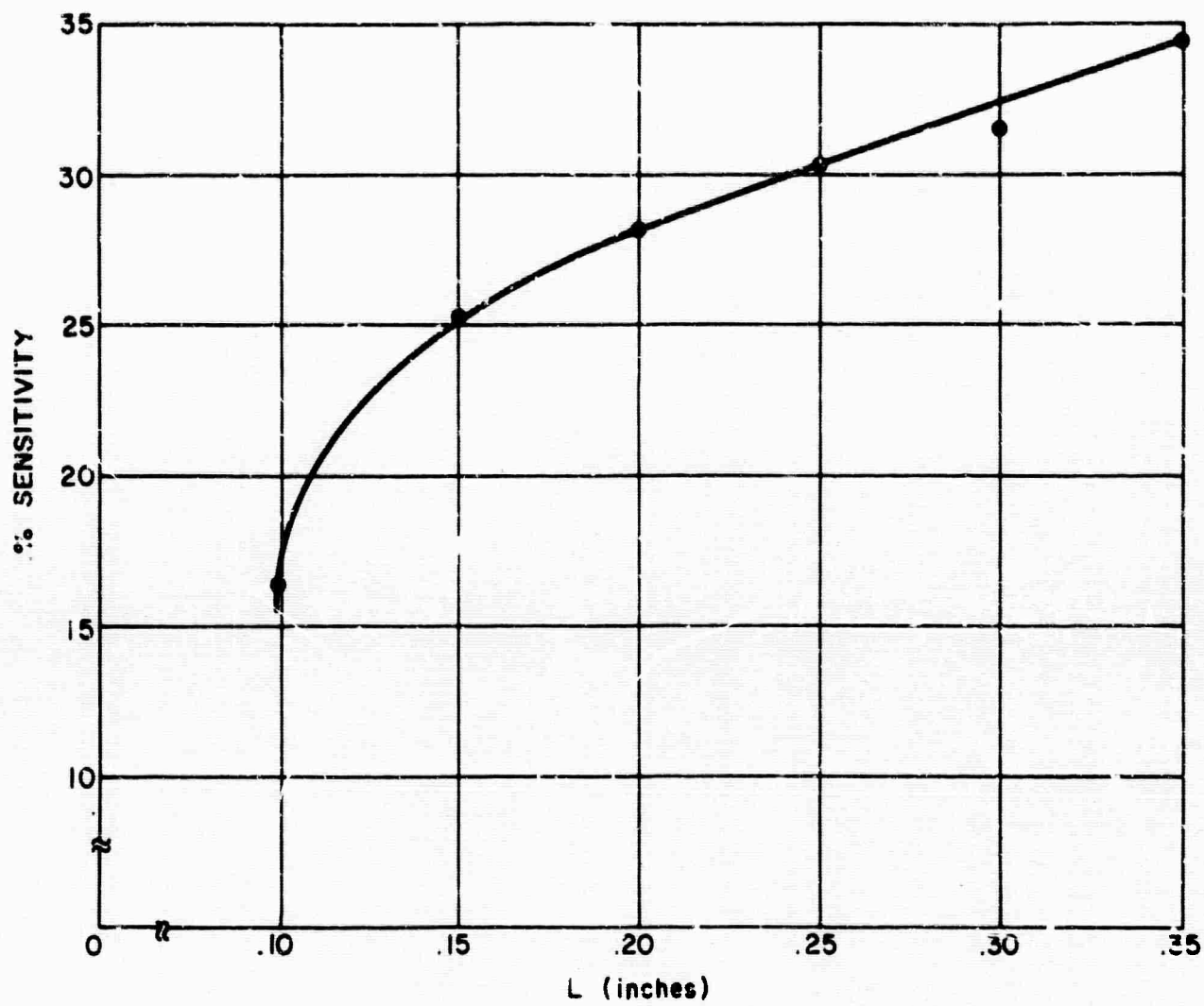


Fig. 12 (3-12) - Sensitivity calibration constants of cavities

Length "L" of the cavity (inches)	D#1 Insert Cavity filled up with			D#2 Insert Cavity filled up with		
	air	D#1	D#2	air	D#1	D#2
.35	.361	.345	.314	.368	.358	.321
.30	.309	.294	.270	.365	.336	.314
.25	.314	.282	.306	.331	.297	.299
.20	.275	.280	.266	.300	.289	.269
.15	.256	.275	.216	.274	.261	.298
.10	.287	.183	.122	.194	.170	.110

Table #1 Calibration constants of the cavity

J. Griemsmann  
D. Jacenko  
Electrophysics Department

#### 3.1.4 Measurement of Electron Density and Collision Frequency of a Field Induced Plasma

As a check on the resonant cavity techniques, the electron density of a plasma produced by a d. c. periodically pulsed voltage inside a one inch circular glass tube was measured using the 6" diameter cavity designed originally for electron density measurement in the 5' shock tunnel.

A schematic diagram of measuring cavity arrangement is shown in Fig. 13. For calibration purposes two identical 1" hollow circular glass tubes were made so that they would extend through the total length of the cavity. One was fitted with electrodes so as to provide the plasma. The other was open-ended. Foam dielectric rod sections having a dielectric constant of 1.075 were machined so as to fill this second one inch tube. The replacement of the air dielectric constant by the known foam dielectric constant provides the cavity calibrations.

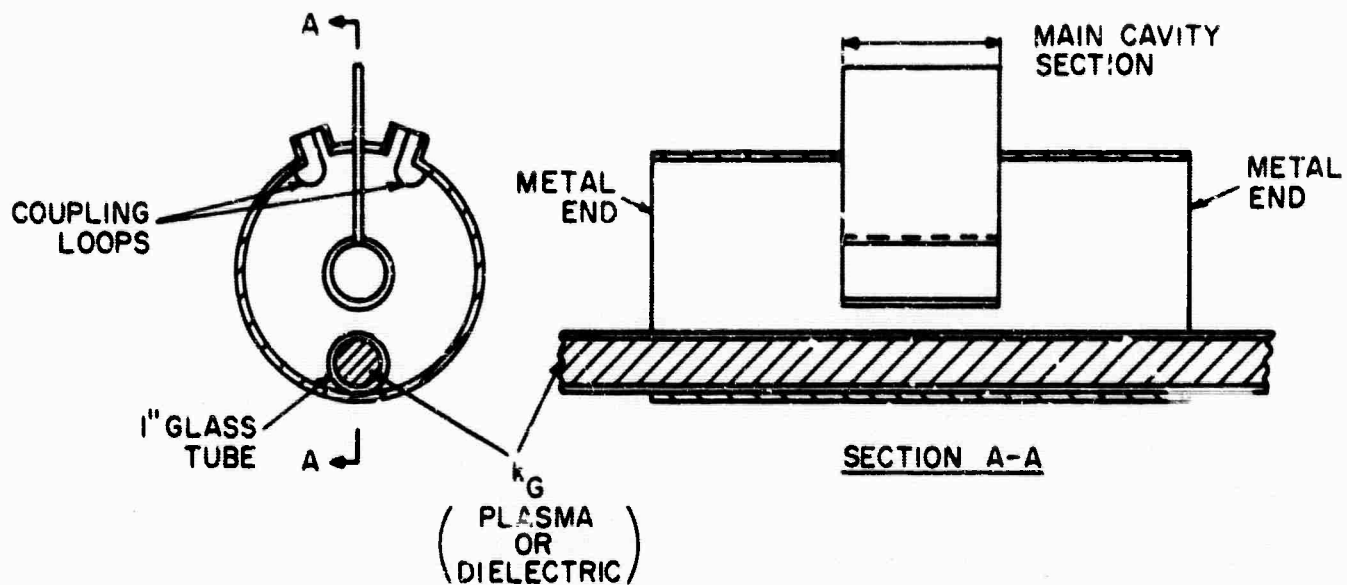


Fig. 13 (5-13) - Partially filled cavity - hydrogen plasma

One determination of electron density requires three electrical measurements. Each consists of the measurement of resonant frequency and  $Q$  of the cavity under the following conditions:

- (a) Plasma filling a 1" glass tube
- (b) Air filling a 1" glass tube
- (c) Polyfoam filling a 1" glass tube.

For the measurement the assumption is made that neither the dielectric constant of the polyfoam nor that of the plasma deviates sufficiently from 1.00 so as to cause a significant change in the field pattern from that obtained for the empty glass tube. Under these circumstances the cavity may be represented in the neighborhood of the resonant frequency by the equivalent circuit shown in Fig. 14. Here  $L_C$  represent the total relative magnetic energy stored in the cavity and  $G_C$  represents the relative losses in the cavity when the air filled glass tube is in the cavity. The total relative electric energy stored in the cavity is considered to be represented by the capacitance

$$C_T = C_C + C_X = C_C + K \cdot k'_e \quad (1)$$

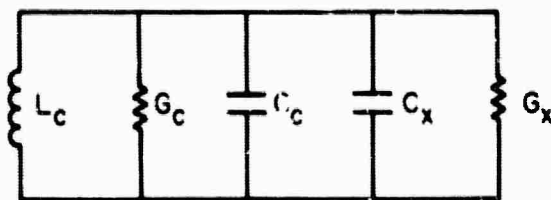


Fig. 14 (3-14) - Equivalent circuit for measurements

where  $C_x$  represents the relative electric energy stored inside the glass tube and  $C_c$  the electric energy storage elsewhere in the cavity. This equivalent circuit may be completely evaluated. If losses inside the glass tube are due to electric field they may be taken into account by using a complex dielectric constant  $k_{\epsilon}^* = k_{\epsilon}' - jk_{\epsilon}''$ . In this instance the capacitance inside the glass tube may be represented as some geometric factor  $K$  times the real part of the relative dielectric constant  $k_{\epsilon}'$  as indicated in Eq. (1). The losses are then represented by

$$G_x = K \cdot \omega k_{\epsilon}'' \tag{2}$$

The complex relative dielectric constant of the plasma may be written in the form

$$k_{\epsilon}^* = k_{\epsilon}' - jk_{\epsilon}'' = 1 - \frac{p^2}{1 + q^2 p^2} - j \frac{qp^3}{1 + q^2 p^2} \tag{3}$$

where

$$p = \frac{\omega}{\omega_p}, \quad q = \frac{\nu}{\omega p} \tag{4}$$

The quantity  $\omega$  equals the angular frequency of the field,  $\nu$  is the collision frequency.

The plasma angular frequency is given by

$$\omega_p^2 = \frac{ne^2}{m\epsilon_0} \cong (18\pi)^2 n \tag{5}$$

where  $n$  is the electron density,  $e$  the electronic charge,  $m$  the mass of the electron and  $\epsilon_0$  the absolute dielectric constant of free space.

For determination of the electron density only the values of resonant frequencies under each of the above conditions are required. Assuming the inductance of the equivalent circuit to be invariant yields

$$\omega_{rp}^2 (C_C + K k'_{\epsilon p}) = \omega_{ra}^2 (C_C + K) = \omega_{re}^2 (C_C + K \cdot k_{\epsilon o}) \quad (6)$$

where  $\omega_{rp}$ ,  $\omega_{ra}$ ,  $\omega_{re}$  are respectively the measured angular resonant frequencies of the cavity with plasma, air and polyfoam dielectrics. The latter dielectric may be considered to be lossless with  $k_{\epsilon o}$  being the relative dielectric constant. The calibration constant,  $\frac{K}{C_C}$ , for the cavity may be obtained from the second two equations of (6) and is found to be

$$\frac{K}{C_C} = \frac{\left(\frac{\omega_{ra}}{\omega_{re}}\right)^2 - 1}{k_{\epsilon o} - \frac{\omega_{ra}^2}{\omega_{re}^2}} \quad (7)$$

The real part of the relative dielectric constant of the plasma obtained from the first two equations of (6) is then

$$k'_\epsilon = \left(\frac{\omega_{ra}}{\omega_{rp}}\right)^2 - \left(\frac{C_C}{K}\right) \left[1 - \left(\frac{\omega_{ra}}{\omega_{rp}}\right)^2\right] \quad (8)$$

Identifying this value of  $k'_\epsilon$  with that of Eq. (3) permits solving for the electron density by using Eq. (5). Analytically a simple subsidiary relation is found to be

$$\frac{\left(\frac{\nu_p}{\omega}\right)^2}{1 + \left(\frac{\nu}{\omega_p}\right)^2 \left(\frac{\nu_p}{\omega}\right)^2} = 1 - k'_\epsilon = \frac{1 - \left(\frac{\omega_{ra}}{\omega_{rp}}\right)^2}{\left(\frac{\omega_{ra}}{\omega_{re}}\right)^2 - 1} [k_{\epsilon o} - 1] \quad (9)$$

For determination of collision frequency the "Q" of the cavity is measured with plasma present and with air dielectric. Let these values be respectively  $Q_p$  and  $Q_a$ . In terms of the equivalent circuit we have

$$Q_p = \frac{1}{\omega_{rp} L_T (G_C + G_X)} \quad (10)$$

and

$$Q_a = \frac{1}{\omega_{ra} L_T G_C} = \frac{\omega_{ra} C_C \left(1 + \frac{K}{C_C}\right)}{G_C} \tag{11}$$

Identifying  $G_X$  of Eq. (10) with that of Eq. (2) permits solving for the imaginary part of plasma dielectric constant, namely,

$$k''_e = \left(\frac{1 + C_C/K}{Q_a}\right) \left(\frac{\omega_{rp}}{\omega_{ra}}\right) \left(\frac{\omega_{ra} Q_a}{\omega_{rp} Q_p} - 1\right) \tag{12}$$

This expression explicitly contains only measured quantities except for the calibration constant,  $C_C/K$ , which in turn is given in terms of measured quantities by Eq. (7). From Eq. (3) the collision frequency is determined through the relation

$$k''_e = \frac{qp^3}{1 + q^2 p^2} \tag{13}$$

The above equations are exact for the assumed equivalent circuit. Under conditions of high Q (say > 500) and for measurements at frequencies sufficiently above plasma and collision frequency considerable simplification of the above expressions can be obtained through approximations.

Experimental Results

In the physical arrangements shown in Fig. 13 measurements of electron density were made on hydrogen plasmas operating at about 40 microns pressure and currents of .6, 1 and 5 milliamperes. The measured values are shown in the following data:

Plasma Measurements

<u>Current (ma.)</u>	<u>f<sub>rp</sub>(MC.)</u>	<u>Q<sub>p</sub></u>
.6	521.80+.07	— *
1.0	521.80+.10	— *
5.0	521.80+.73	640

\* Measurement accuracy was not sufficient to measure reliably the small reduction in Q noted.

Zero Current Measurements (Air Equivalent)

$$f_{ra} = 521.80 \quad Qa = 949$$

Measurements With Polyfoam Dielectric ( $k_{\epsilon 0} = 1.075$ )

$$f_{rc} = 521.80 - .450$$

Computed Data

1. Calibration Constant  $-K/C_C = .0235$
2. Electron Density

<u>Plasma Current (ma)</u>	<u>Electron Per cc</u>	$\frac{k'}{\epsilon}$	$\frac{\omega}{\omega_p}$
.6	$1.0 \times 10^8$	1.0117	9.25
1.0	$1.43 \times 10^8$	1.0167	7.73
5.0	$1.04 \times 10^9$	1.122	2.87

3. Collision Frequency (5 ma. plasma)

$$\nu = 5.4 \times 10^8 \text{ collisions/sec. } (k''_{\epsilon} = .022, \nu/\omega_p = .518)$$

4. The plasma  $Q = \frac{k'_{\epsilon}}{k''_{\epsilon}} = 51$

Discussion of Results and Conclusions

The measured values of average electron density in the plasma values are found to agree in order of magnitude with those calculated for the plasma from the measured currents and pressures.

Experimentally the limitation on the smallest electron density that could be measured in the plasma tube was found to be about  $10^8$  electrons/cc and this was primarily a consequence of the frequency resolution of the equipment used. It should also be noted that the energy stored in the plasma was approximately 1/40 of the total energy stored in the cavity. When the cavity is applied to

flow diagnostics the plasma will fill the cavity. Electron densities as low as  $2.5 \times 10^6$  should then be readily measured for those instances in which the influence of collision frequency can be neglected.

Experimentally the limitation on the highest electron density that could be measured in the plasma tube was found to be the loss of Q of the cavity. For the plasma tube having a 5 ma. current the collision frequency is quite high, just about 1/2 of the plasma frequency - the Q of the plasma itself is noted to be only 50. Such a plasma would not have been measurable had it filled the cavity. For flow diagnostics the collision frequency would have to be at least 40 times less or less than  $\nu = 1.35 \times 10^7$  collisions/sec. in order that an electron density as high as  $10^9$  electrons/cc could be measured. Collision frequencies as high as  $10^7$ /sec are not anticipated for the intended shock tunnel application. In any case the maximum electron density of  $10^8$  electrons/cc was the upper limit designed for the cavity.

The 5 ma. current experiments introduces several points that could bear further investigation. Measurements were made at a frequency of electric field only 2.87 times the plasma frequency. How close to the plasma frequency is Eq. (3) of the text and its associated plasma model valid? For no collisions ( $\nu = 0$ ,  $q = 0$ ) the equation (3) would violate the Kronig-Kramer condition since it postulates loss for any variation of dielectric constant with frequency. An experimental check could be made on the equation by measuring the collision frequency and electron density of the same plasma at two different frequencies using two different cavities. One of these cavities would be operated at a frequency close to the plasma frequency being a partially filled cavity as in the above experiments. The other cavity would be operated at a frequency sufficiently above the plasma frequency to insure satisfaction of the previous restrictions.

Other experimental conditions that require further checking are the non-uniform electron density distribution in the plasma and conditions for radiation through the ends of the cavity. In the above tests no significant difference in the

measurements resulted from covering the open ends with copper foil.

J. Griemsmann  
E. Malloy  
Electrophysics Department

### 3.2 Microwave Resonant Cavity Measurement of Shock Produced Electron Precursors

Experimentalists working with shock tubes have noticed a variety of electrical signals appearing on different types of probes in the region well ahead of the advancing shock front. These signals seem to assume various forms, shapes, polarities and apparent velocities of propagation, depending on the external circuitry and position of the probes relative to the shock tube. Some signals appear to propagate effectively with the speed of light and are presumably produced by photoionization effects. Other signals, however, propagate with velocities of the order of the shock speed. The latter type of signal has been attributed to a large scale diffusion of electrons upstream through the shock front.

In theoretical treatments of the problem, a variety of flow conditions have been considered. These yield electron precursor effects which are attributed mainly to diffusion in some cases and to photoionization in others. Supporting experimental observations are cited in both instances. However, the experimental evidence in these cases suffers from a common shortcoming, namely, the difficulty in interpretation of the signals obtained from probes, whether they are immersed in the flowing medium or placed external to the shock tube. To avoid the difficulties and uncertainties of interpretation of the different probe signals, means other than probes were selected for use in the present investigation. In particular, microwave resonant cavities are principal diagnostic devices used here. For the problem at hand, the advantages of microwave techniques outweigh the shortcomings. Their unique suitability here is related to the fact that at no time is there any interaction between the flowing medium and the probing microwave signal, which is negligibly small; the interpretation of the

recorded signals is straightforward and theoretically as well as experimentally well-founded; and finally the signals recorded are free from spurious effects, unlike the signals obtained from probes.

This investigation is being carried out in a 0.89-inch diameter shock tube. The schematic diagram of this shock tube is shown in Fig. 1. Figure 2 presents a photographic view of the experimental setup. As can be seen from these figures, two S-band cavities are inserted in tandem at the end of the shock tube. In front of these cavities a microwave antenna is inserted about six inches downstream. This antenna is designed to excite a  $TE_{11}$  mode at a frequency of about 9 kmc. The signal excited in the shock tube serves to determine the shock front velocity and the relative shock front position.<sup>1</sup>

The cavities (Fig. 3) operated in the S-band frequencies provide the means of measuring the precursor electron density. The microwave cavity is designed to operate in the  $TM_{010}$  mode. The operating mode to the microwave cavity is dictated by the electric and aerodynamic properties of such a cavity. A resonant cavity operated in the  $TM_{010}$  mode can be built into the shock tube with the center portion of the cavity constituting a part of the shock tube (see Fig. 1); the gas flow is left undisturbed by the presence of the cavity and at the same time the center portion of the cavity, exposed to the flow, has the maximum concentration of the electric field and is thus the most sensitive to perturbation (the perturbation level, of course, being the degree of ionization of the flowing medium). The frequency of operation of the cavity is dictated by the size of the shock tube.

With an operating frequency of about 2.7 kmc and a cavity Q of about 3000, an electron density level of  $5 \times 10^7$  to  $10^{10}$  el/cm<sup>3</sup> can be measured<sup>2, 3, 4</sup>. It is thus possible with such an arrangement to obtain an electron density profile of the precursor as a function of the distance from the moving shock front. A second S-band cavity, tuned to the same resonant frequency as the first and mounted about ten inches behind the first, provides the means of obtaining the velocity of the electron precursor. Efforts are being made to experimentally assess the relative

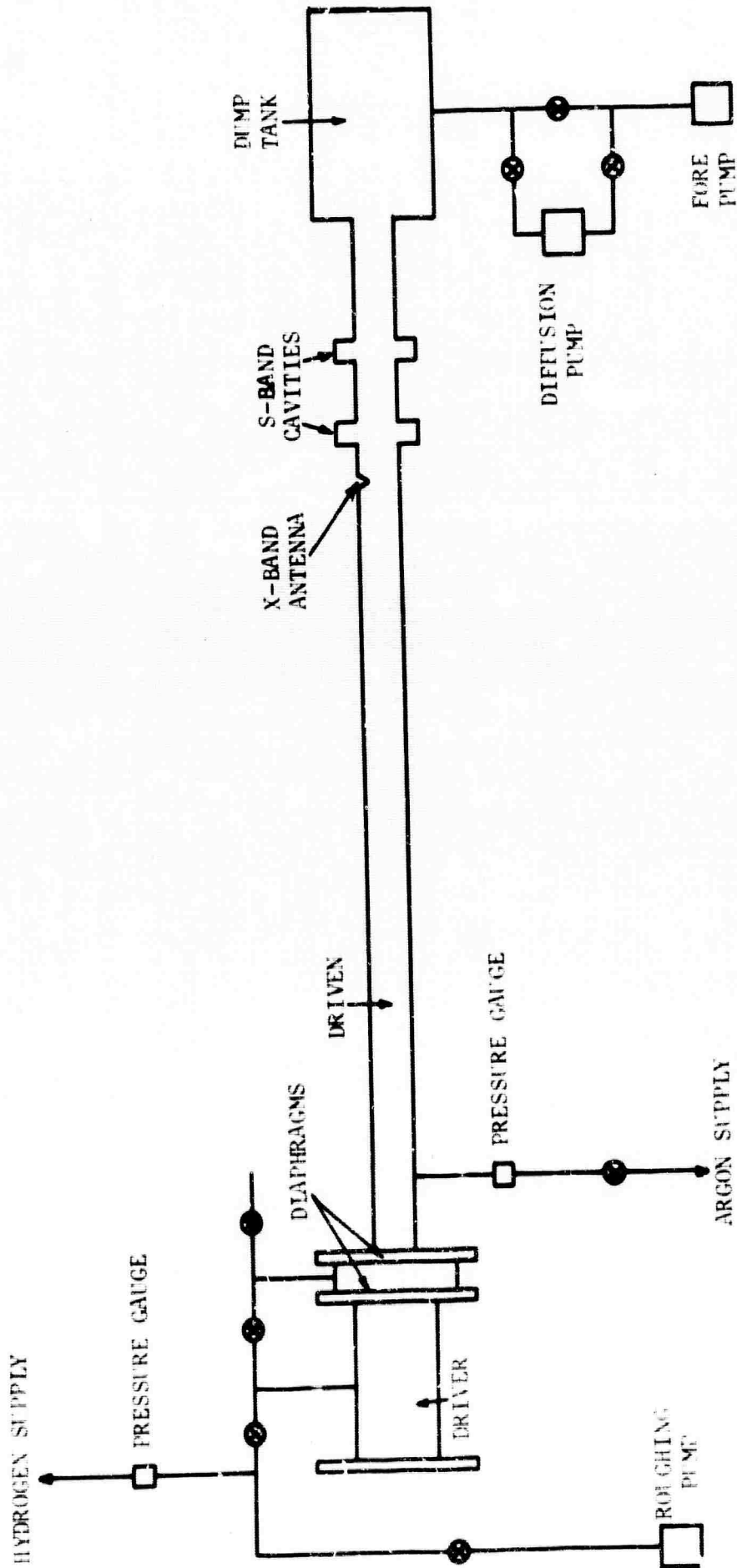


Fig. 1 (3-15) - Schematic diagram of shock tube

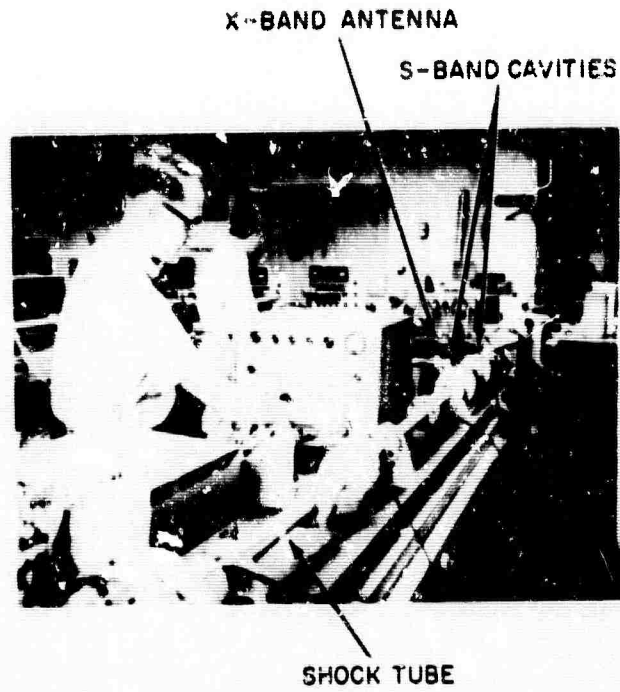
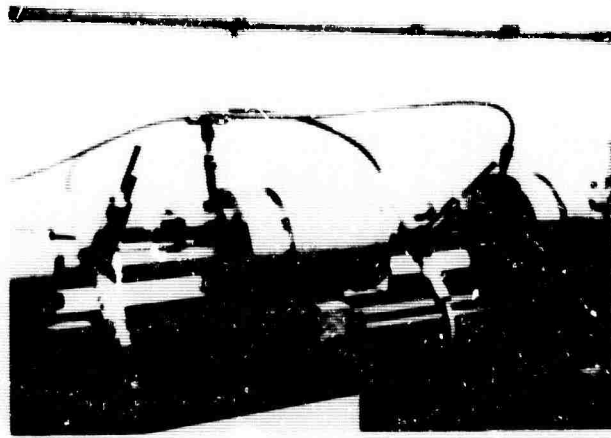
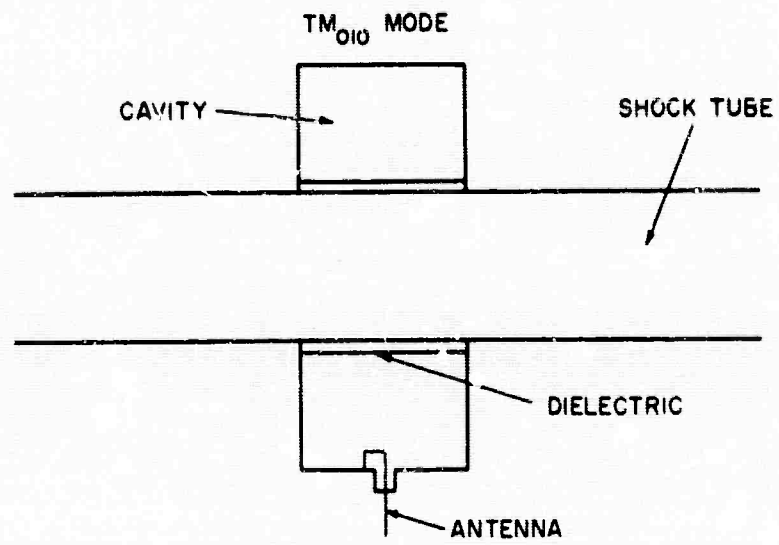


Fig. 2 (3-16) - Photograph of experimental setup



A. PICTURE OF S-BAND CAVITY



B. SCHEMATIC OF S-BAND CAVITY

Fig. 3 (3-17) - S-Band cavity

importance of diffusion and radiation in the precursor structure as a function of shock velocity. A typical recording obtained by the cavity method is shown

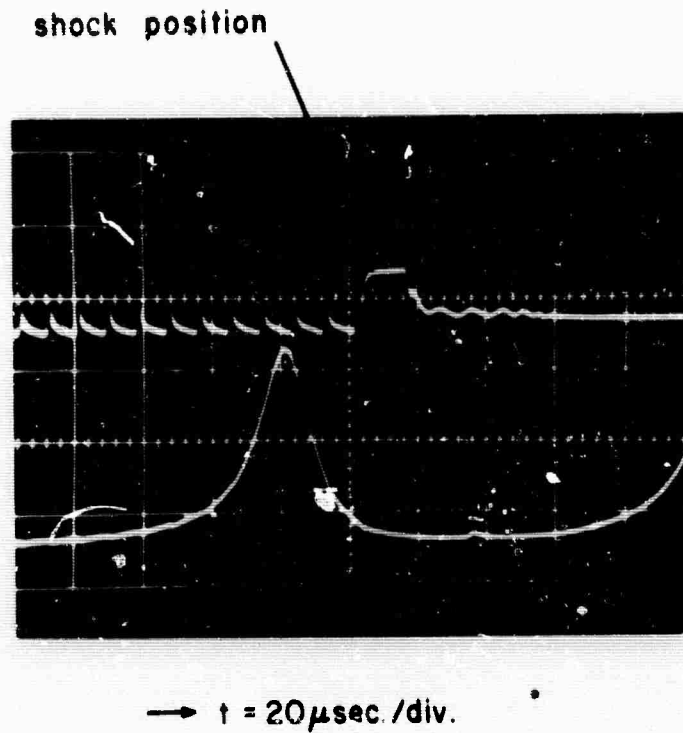


Fig. 4 (3-18) - Upper trace - shock velocity measurement  
Lower trace - S-Band cavity response (precursor measurement)

Note: The S-Band cavity responds before the arrival of the shock front.

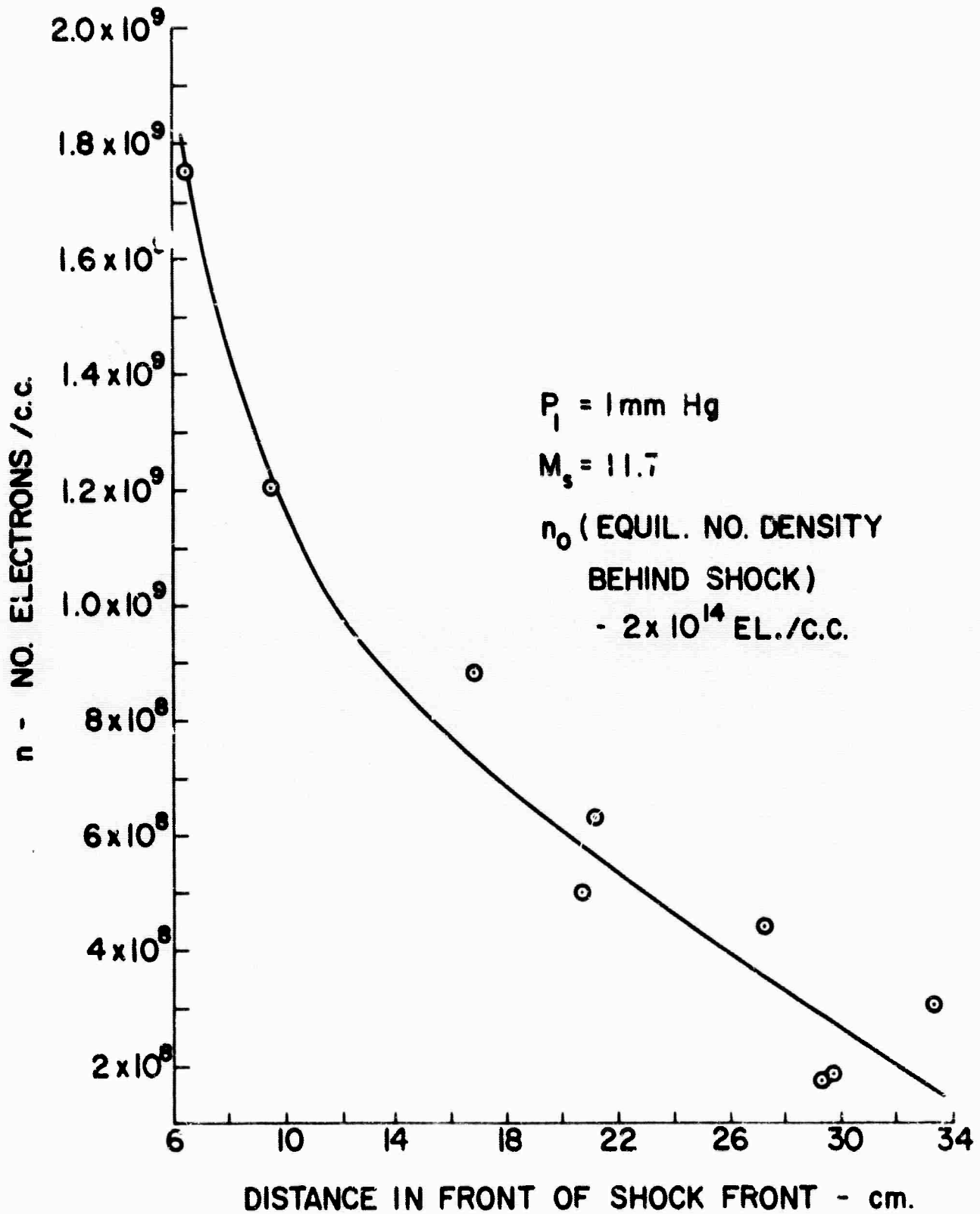


Fig. 5 (3-19) - Preliminary precursor electron density profile in argon in a pressure driven shock tube

in Fig. 4, as well as a preliminary electron density profile of the precursor as a function of distance from the shock front in Fig. 5.

S. Lederman  
D. S. Wilson  
Dept. of Aerospace Engineering  
and Applied Mechanics

### References

1. Lederman, S., "Preliminary Experimental Investigation of the Ionized Gas in Front and Behind a High Velocity Shock in Argon", PIBAL Report No. 780, March 1963; also, RADC TDR 63-267, August 1963.
2. Lederman, S., Abele, M. and Visich, M. Jr., "Microwave Techniques Applicable to Shock Tube Measurements", PIBAL Report No. 857, September 1964.
3. Lavitt, M. and Herlin, M. A., "Application of the Resonant Cavity Method to the Measurement of Electron Densities and Collision Frequencies in the Wake of Hypervelocity Pellets", Massachusetts Institute of Technology, Lincoln Laboratory Report No. TR-248, October 1961.
4. Cahill, W. P., Dueterhoeft, W. C. and Dean, A. P., "Analysis of Resonant Cavity Techniques for Measurement of Effective Electron Density in a Plasma Stream", University of Texas, Report No. S-48, June 1961.

### 3.3 Electron Density and Relaxation Time Measurement Behind a Reflected Shock

In a shock tube samples of gas may be rapidly heated to temperatures of the order of  $10^4$ °K. There may, however, be some delay in raising the internal energy of the molecules to produce dissociation and ionization. Initial ionization is usually attributed to collisions between molecules but as the electron density increases, collisions between electrons and neutral particles may also become important or even dominant in the ionization process. The resulting time lag between heating of the neutral gas by the shock and attainment of the equilibrium electron density may best be studied in a shock tube. This lag or

relaxation time depends on the efficiency of molecular collision processes, on the physical properties of the particular gas under investigation, on the density of the gas and on its purity. Determination of these relaxation times is of importance for understanding combustion and other rapid chemical reactions.

Several methods have been used to measure this delay time. In this investigation an attempt is being made to apply a microwave resonant cavity technique to measure this relaxation time behind a reflected shock in a shock tube. One particular cavity arrangement well-suited for this measurement is an "end wall" cavity operated in the  $TE_{011}$  mode. Fig. 1 shows the schematic of this

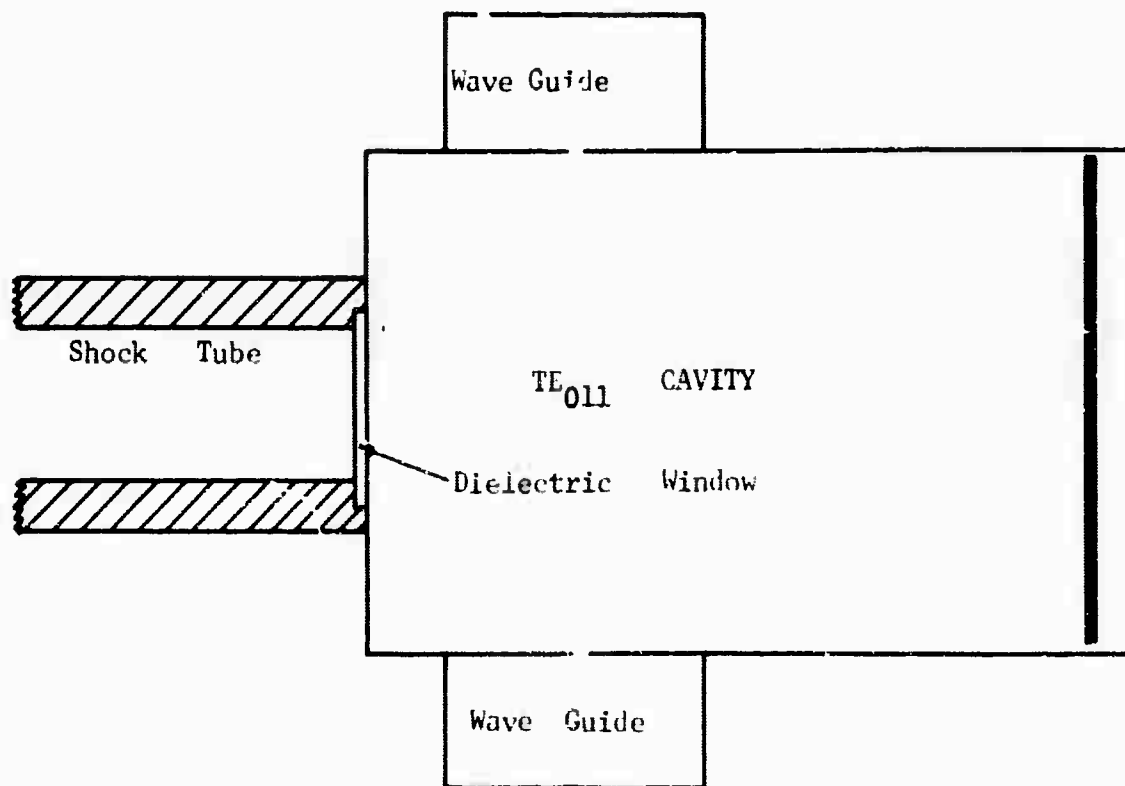


Fig. 1 (3-20) - Schematic of end wall cavity

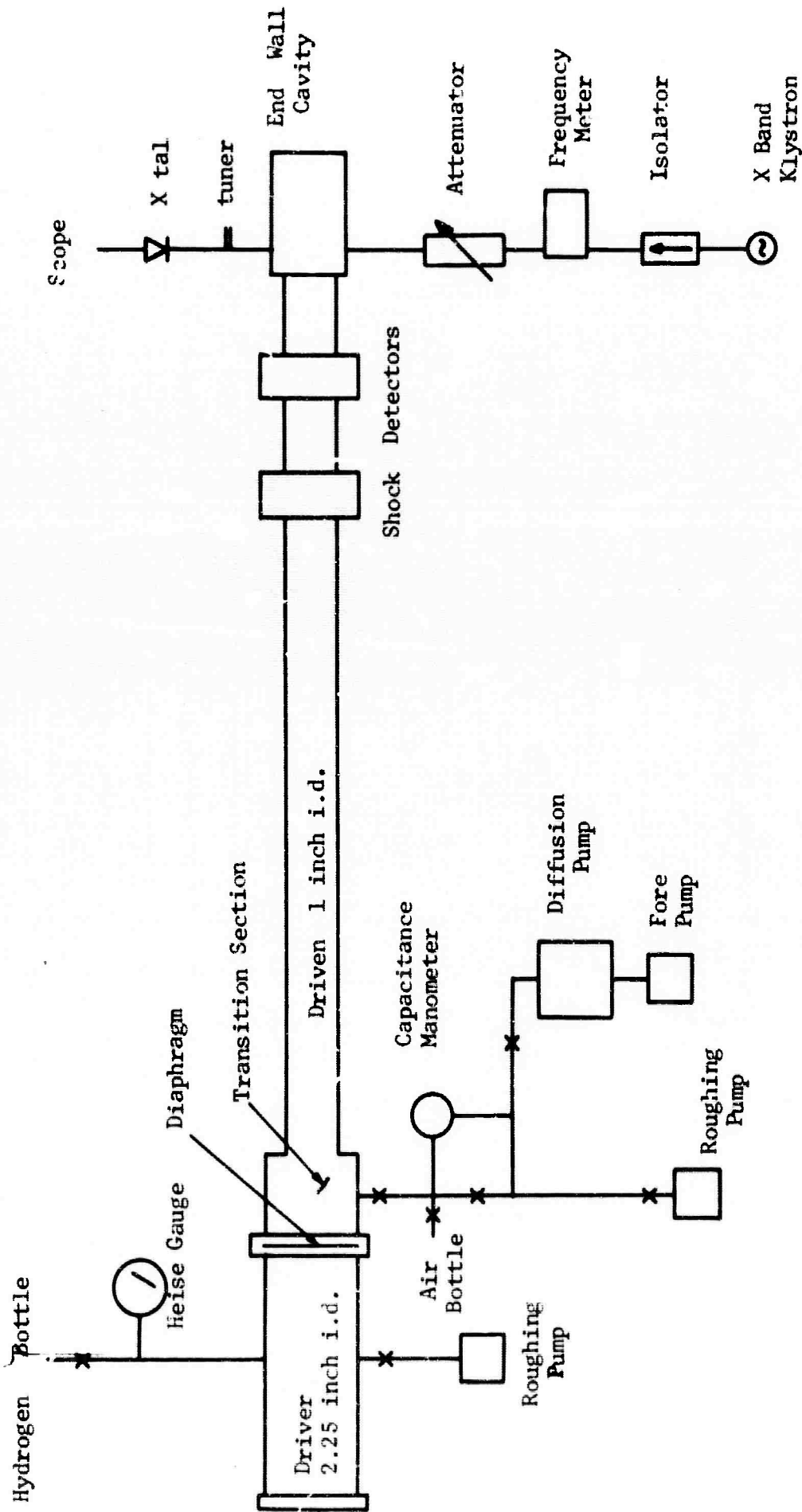


Fig. 2 (3-21) - Schematic of shock tube and instrumentation

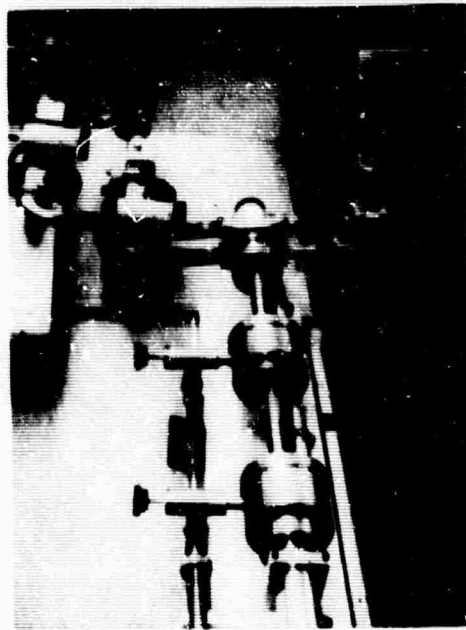
type of a resonant cavity. Fig. 2 shows a schematic representation of the experimental apparatus including the cavity. In Fig. 3, a photographic view of the equipment is shown. As can be seen from Fig. 1, a dielectric window forms the end of the shock tube and separates the cavity from the shock tube. This is a very important detail. When the incident shock is reflected from the dielectric window, the ionized gas behind the reflected shock forms a conducting wall which completes the cylindrical cavity. The depth of penetration of the cavity field into the plasma depends on the electron density at the wall. Since the resonant frequency of the cavity depends on its size and therefore on the penetration depth, the measurement of the resonant frequency may be used to determine the electron density. The change in resonant frequency as a function of electron density is given by

$$\frac{\Delta\omega}{\omega_0} \sim -K \frac{\omega_0}{\omega_p} \left(1 - i \frac{\nu}{\omega_0}\right),$$

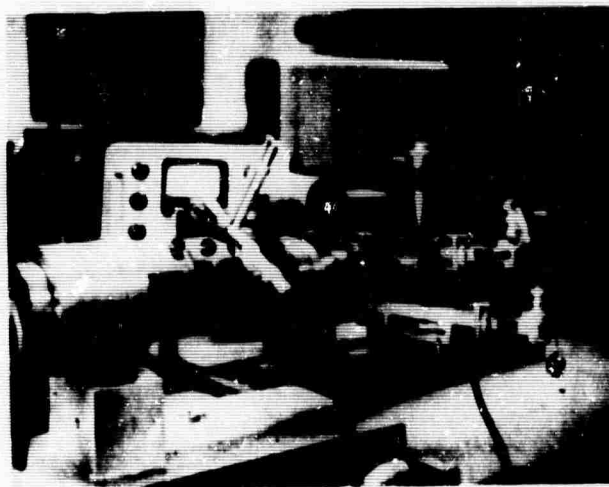
where  $\omega_0$  is the resonant frequency of the cavity with a metallic wall adjacent to the dielectric diaphragm,  $\omega_p$  is the plasma frequency,  $\nu$  is the collision frequency, and  $K$  is a configuration constant easily obtained through calibration<sup>1</sup>.

In making measurements, two microwave signals are applied simultaneously to the cavity. The two signals are displaced below the resonant frequency  $\omega_0$  by amounts  $\Delta\omega_1$  and  $\Delta\omega_2$ , of the order 10-20 mc. The difference between the two frequencies may also be of the order of 10 mc at an operating frequency of 9 kmc. The cavity then will resonate for each signal when the corresponding electron density forms in front of the dielectric window. By repeating a number of closely controlled tests, and shifting the frequency applied to the cavity, it is possible to obtain an electron density profile behind the reflected shock as a function of time. A typical signal obtained from this cavity is shown in Fig. 4. Four resonant conditions are clearly visible. The first two correspond to the buildup of ionization and the latter two to the decay.

This work, as mentioned above, is being conducted in a one inch i. d. shock tube. The driven gas is dry air at an initial pressure of 1 mm Hg. The



END WALL CAVITY



END WALL CAVITY

Fig. 3 (3-22) - Top and side views of end wall cavity on shock tube

Resonant frequency of cavity closed by a metallic piston

$$f_0 = 8782 \text{ mc}$$

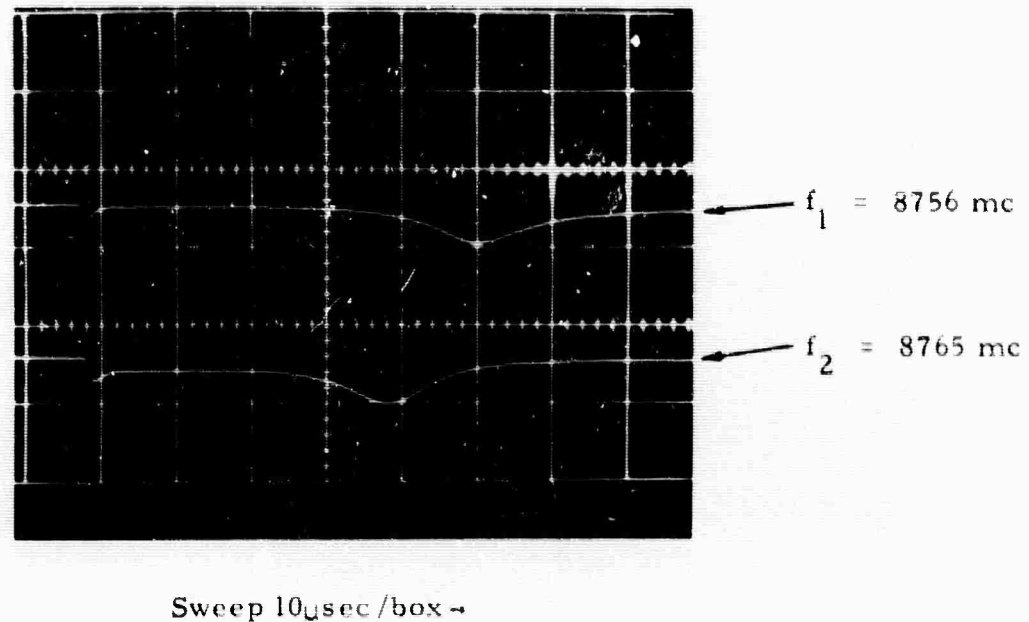


Fig. 4 (3-23) - Typical data trace showing end wall cavity response

driver gas is hydrogen at 120 psia. The incident shock Mach number was maintained at  $9.2 \pm 0.2$  S. D. Some preliminary results obtained are shown in Fig. 5. As expected, the ionization relaxation time was found to be very short, on the order of  $2 \mu \text{ sec}$ . The equilibrium electron density was found to be about  $4 \times 10^{13} \text{ el/cm}^3$ . As can be seen in Fig. 5, the decay is much slower than the buildup. The measured rise time is found to be in good agreement with the data reported by Manheimer and Low<sup>2</sup>. It was also found that the end wall cavity technique may yield information on the boundary region between the end wall and the plasma. The measurements shown in Fig. 5 were conducted with a boron nitrate window on the cavity. Tests, using a mylar window on the cavity, were also conducted and they indicated a somewhat lower equilibrium electron density behind the reflected shock. The measured relaxation time remained the same, however. The reason for this effect is not

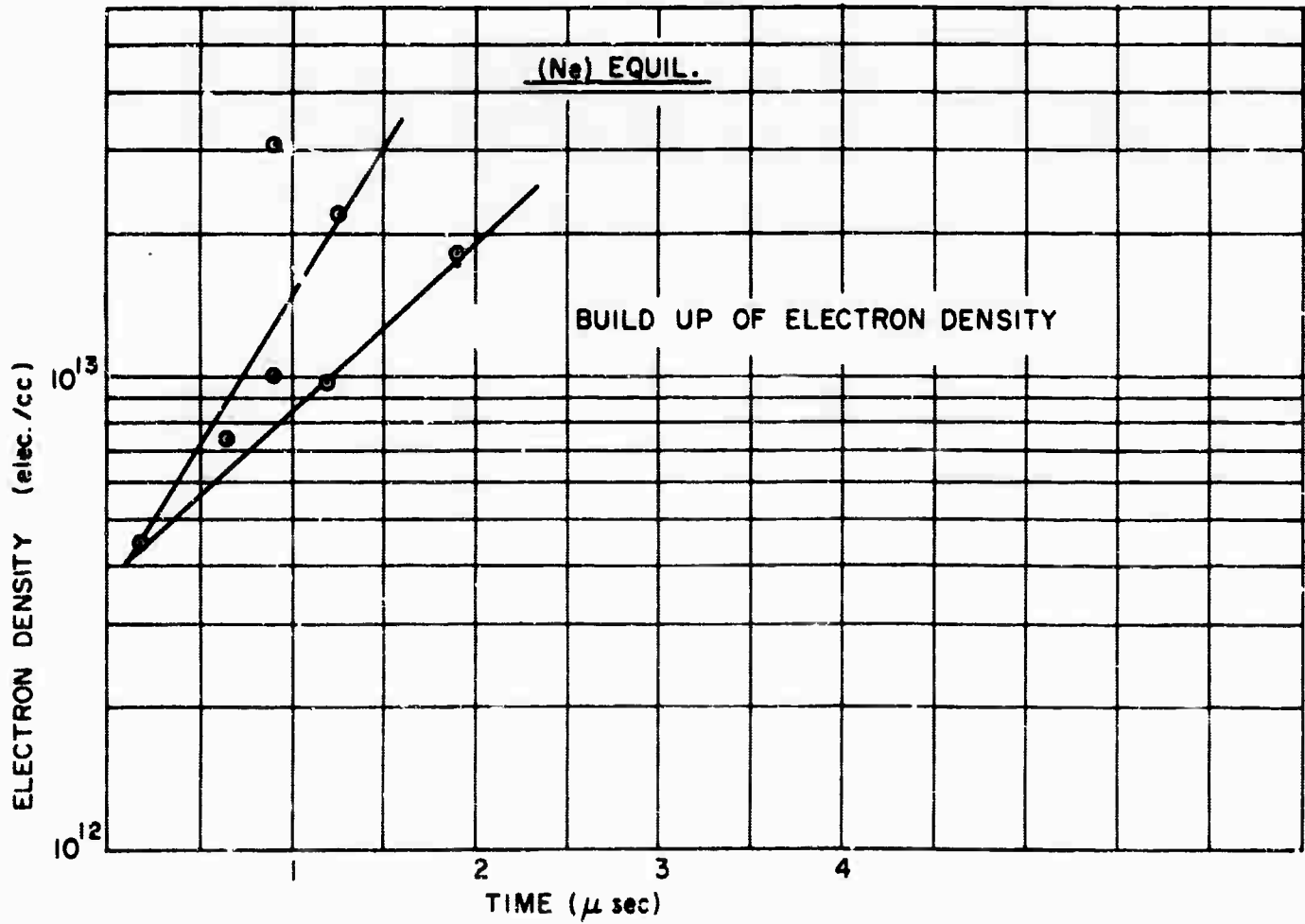
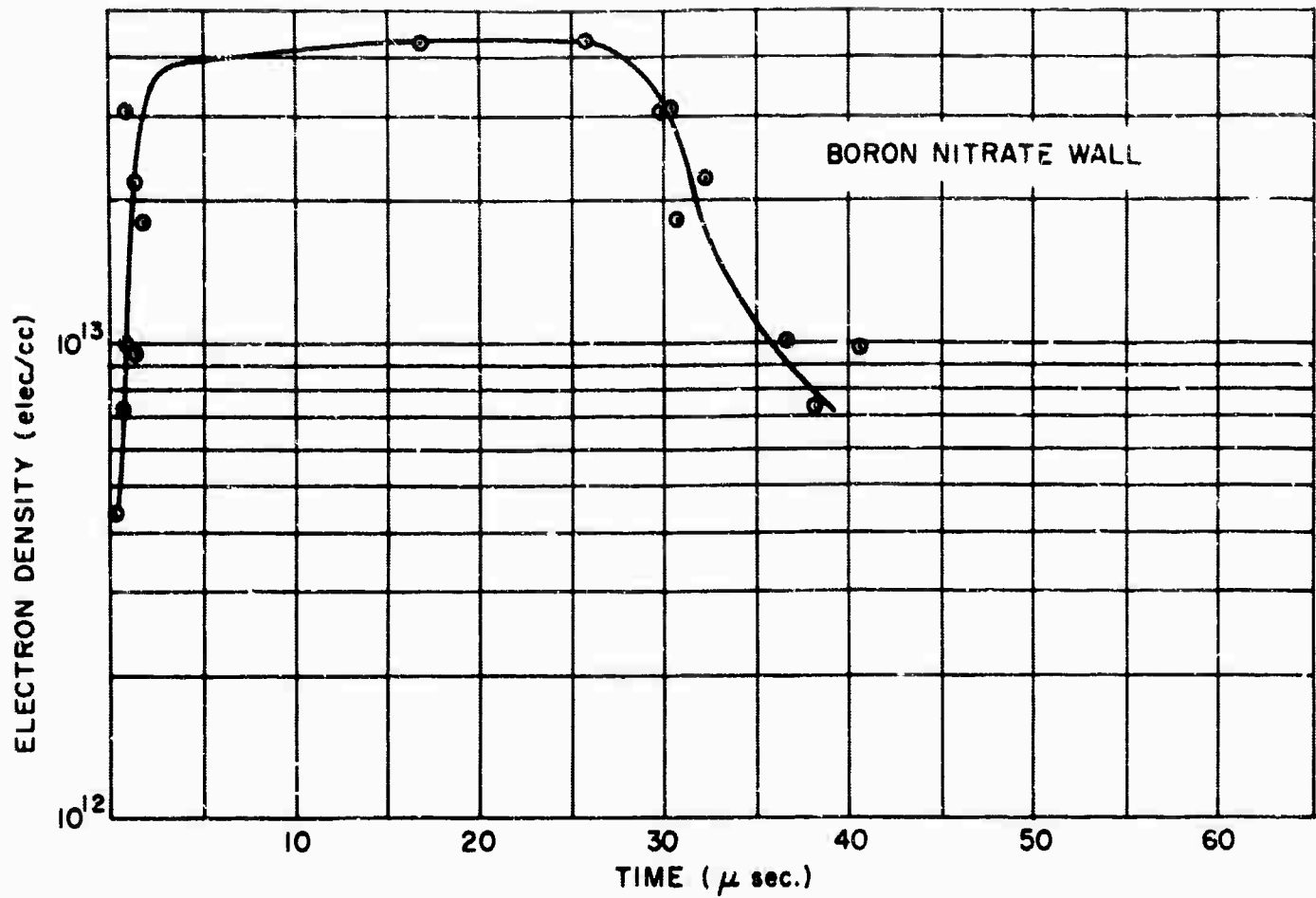


Fig. 5 (3-24) - Electron density as a function of time behind a reflected shock in air  $M_{si} = 9.2$

quite clear at this time and an investigation into the cause of the discrepancy should be undertaken.

S. Lederman  
E. Dawson  
Dept. of Aerospace Engineering  
and Applied Mechanics

### References

1. Lederman, S., Abele, M., and Visich, M. Jr., "Microwave Techniques Applicable to Shock Tube Measurements", Polytechnic Institute of Brooklyn, PIBAL Report No. 857, September 1964.
2. Manheimer, Y. and Low, W., "Electron Density and Ionization Rate in Thermally Ionized Gases Produced by Medium Strength Shock Waves", J. Fluid Mech., 6, pp. 449-461, 1951.

### 3.4 Measurement of Time-Resolved Electron Density

The measurement of time-resolved electron densities in a plasma specimen or plasma flow, with the use of microwave resonant cavities, requires a certain number of reproducible tests if the electron density varies over a wide range. Present measurements yield discrete values or at most continuous values in a narrow range of electron densities. Techniques of this kind are described, for example, in reference 1. This note describes a method for obtaining a continuous time-resolved electron density measurement over a wide range of values.

As reported recently in the literature, fast electronic tuning over a wide frequency band can be accomplished by the addition of an external, plasma filled cavity to an otherwise conventional reflex klystron (Fig. 1). It is pointed out here that this principle can be utilized in an inverse fashion for the measurement of time-resolved electron densities.

The basic scheme is indicated in Fig. 2. It consists of a conventional reflex klystron or externally tuned microwave triode, an external cavity tunable

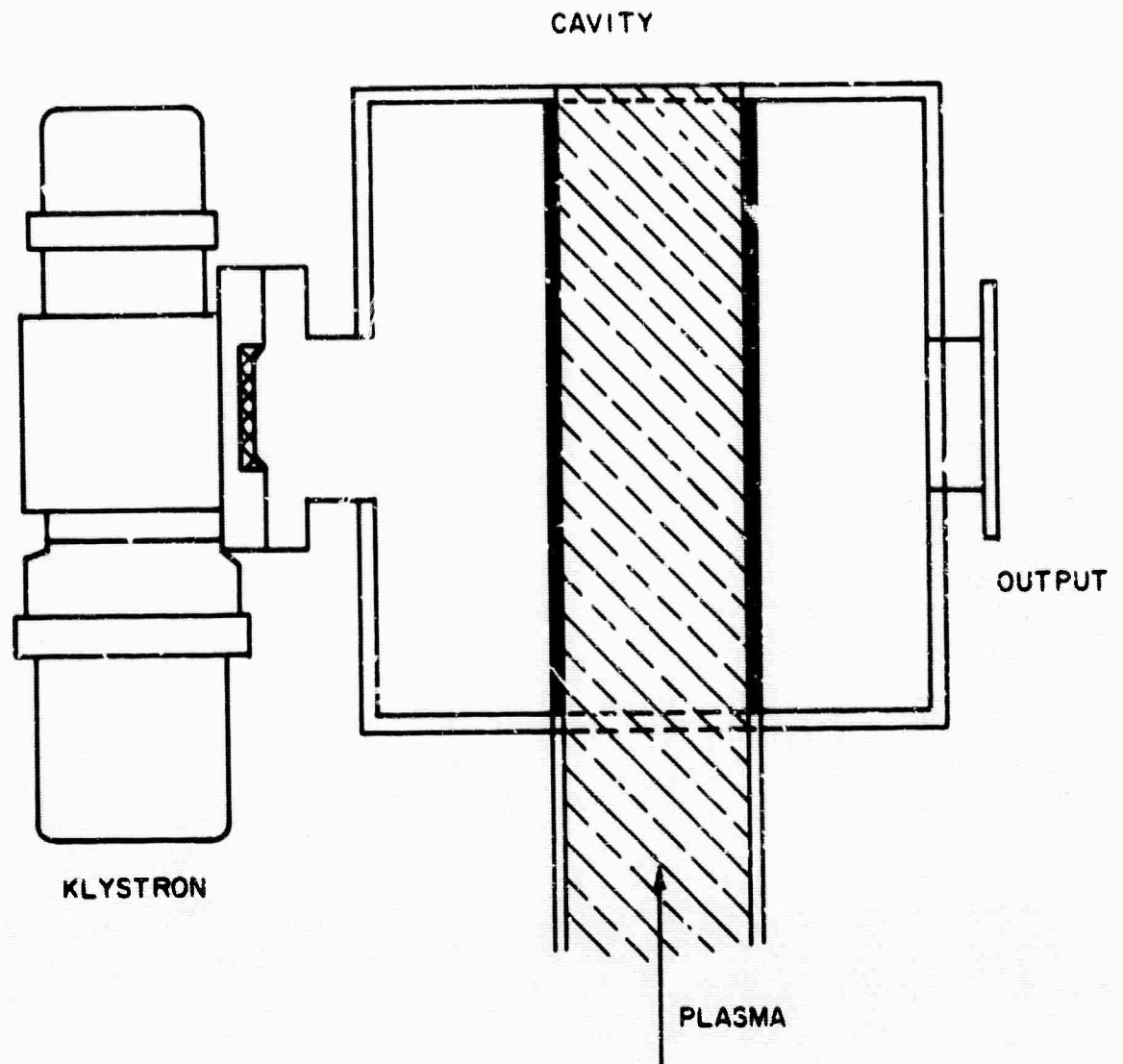


Fig. 1 (3-25) - Schematic of the plasma tuned klystron oscillator

by an ionized flow through it, a second microwave signal source, a crystal mixer, a FM detection system, and a recorder. The system operation is the following: the klystron or microwave triode, in conjunction with the external cavity without a plasma, is generating a signal of a frequency  $f_0$ . When an ionized flow is introduced into the cavity, the signal changes to a new frequency  $f$ . In the case of a time varying electron density, the frequency of the klystron oscillator varies accordingly. The result is an equivalent frequency modulated carrier. This

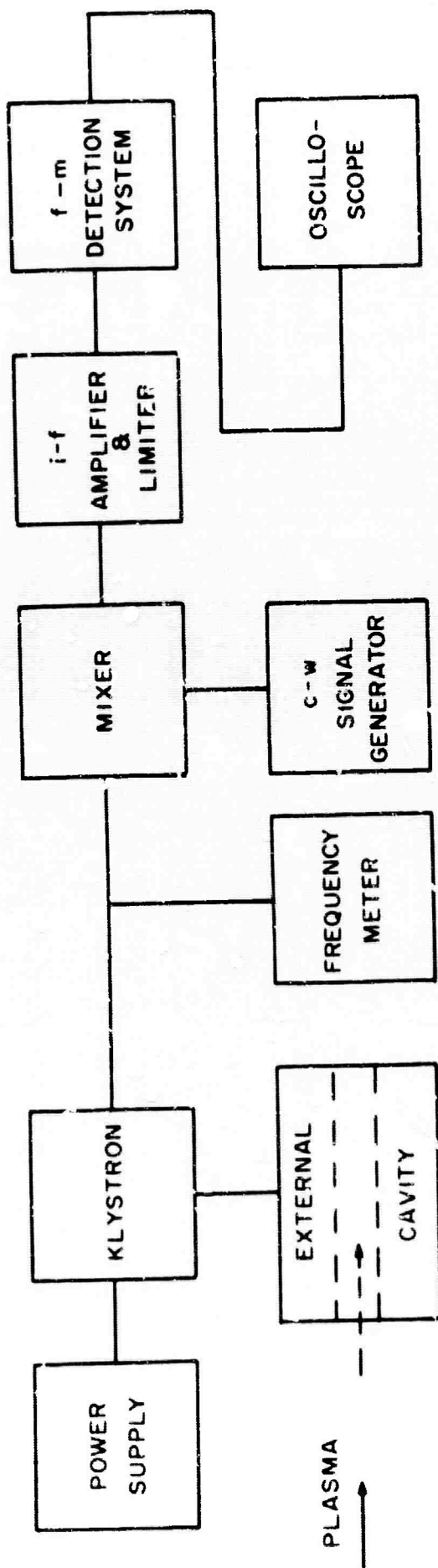


Fig. 2 (3-26) - Schematic diagram of the time-resolved electron density measurement method

signal is then mixed with a signal from the second generator and the resulting i-f signal is applied to the detection system. The output of the detector is then recorded on an oscilloscope. It is thus possible to obtain a time-resolved electron density distribution. The absolute value of the number density is obtained by a standard calibration method. This system can be applied not only to conditions generated in shock tunnels or tubes, but also for any specimen to which cavity diagnostics can be employed.

S. Lederman  
Dept. of Aerospace Engineering  
and Applied Mechanics

### References

1. Lederman, S., Abele, M., and Visich, M. Jr., "Microwave Techniques Applicable to Shock Tube Measurements", Polytechnic Institute of Brooklyn, PIBAL Report No. 857, September 1964.

### 3.5 An Experimental Investigation of the Near Wake of a Slender Cone at

$$\underline{M_{\infty} = 8 \text{ and } 12}$$

Under Air Force\* sponsorship, various experimental data have been obtained in the near wake region of a  $10^{\circ}$  angle ( $5^{\circ}$  half-angle) sharp cone at free stream Mach numbers of 8.0 and 11.8. The tests were conducted in a blow-down type tunnel using fine wires to support the model. The Mach 8.0 tests were conducted at free stream Reynolds numbers of  $0.3 \times 10^6$  and  $1.7 \times 10^6$  per foot; laminar and turbulent boundary layers were obtained on the cone surface at these respective Reynolds numbers. Data obtained include radial profiles of temperature, pressure, and Mach number at axial locations between one and three base diameters downstream of the model. Heat transfer and pressure distributions on the model base were also obtained.

\* This work was carried out under USAF Contract No. AF 33(616) - 7661 Project No. 7064 and Task No. 7064-01 and USAF Contract No. AF 49(638)-1391 Project-Task 9781-01 PE 1405014.

The Mach 11.8 tests were conducted at a free stream Reynolds number of  $0.6 \times 10^6$  per foot and the surface boundary layer for all these tests was laminar. Data obtained include centerline distributions of Mach number, pressure, and temperature for a distance between one and four base diameters downstream of the model. Centerline temperatures were also obtained in the recirculation region for model wall to stagnation temperature ratios of 0.06 and 0.47. In addition, total temperature profiles were obtained downstream of the rear stagnation point.

R. J. Cresci  
Dept. of Aerospace Engineering  
and Applied Mechanics

Under ARPA/ONR sponsorship the program of near wake studies has been continued with the objective of examining the near wake of a  $20^\circ$  angle ( $10^\circ$  half-angle cone) at an angle of attack.

Up to the present time the boundary layer measurements over the body have been made. Moreover, the near wake measurements at zero angle of attack at Mach 8 have been carried out. These are described in detail in PIBAL Report No. 893 entitled "An Investigation of Hypersonic Flow Around a Slender Cone" by E. M. Schmidt and R. J. Cresci.

### 3.6 Utilization of Hot-Wire Anemometer

The hot-wire anemometer unit being used at the Polytechnic Institute of Brooklyn Aerospace Laboratories (PIBAL) is a Model CCB two-channel system manufactured by Flow Corporation (see Fig. 1). Unit is self-contained and features separate constant current supply and controls for each of two hot-wire probes, and separate d. c. bridge circuits for each of two probes. The system's Sum-Difference control unit permits reading signal A, signal B,  $A + B$ , or  $A - B$ . Present capability includes gas stream turbulence measurements for subsonic and supersonic flows with high or low stream temperatures; specifically, measurements of the intensity and scale of longitudinal and transverse turbulent components may be accomplished.

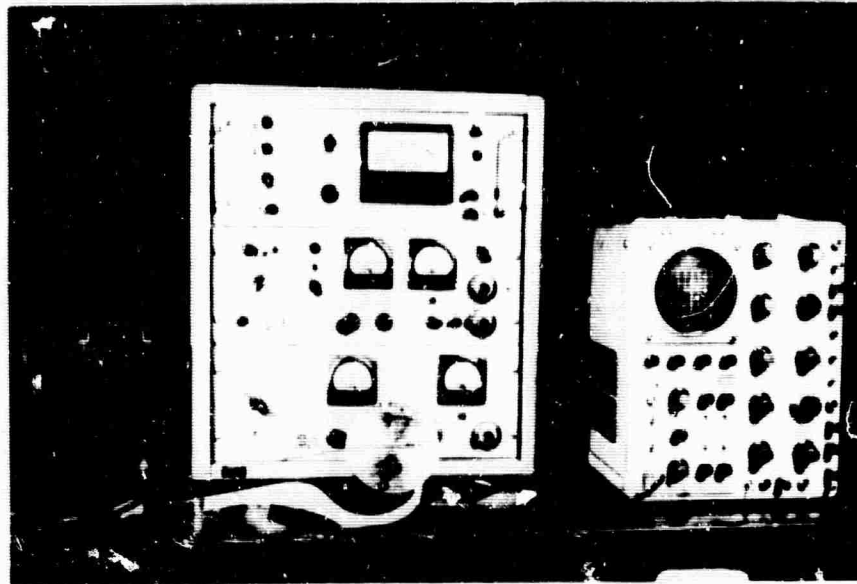
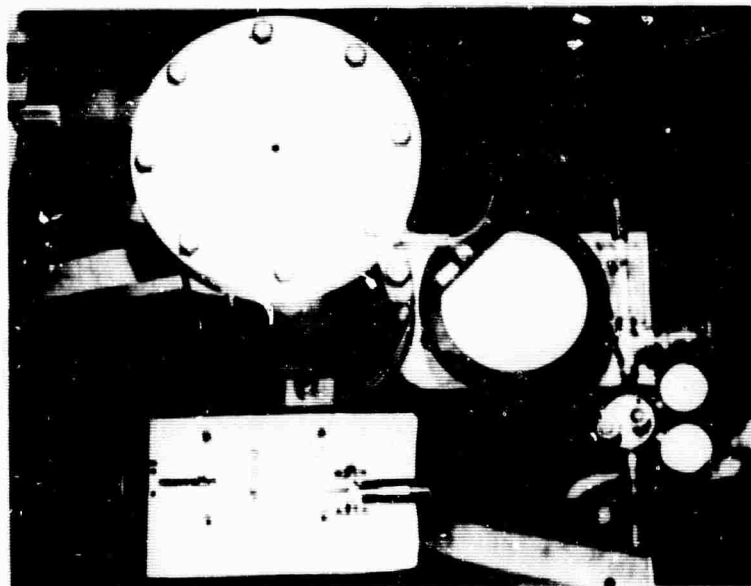


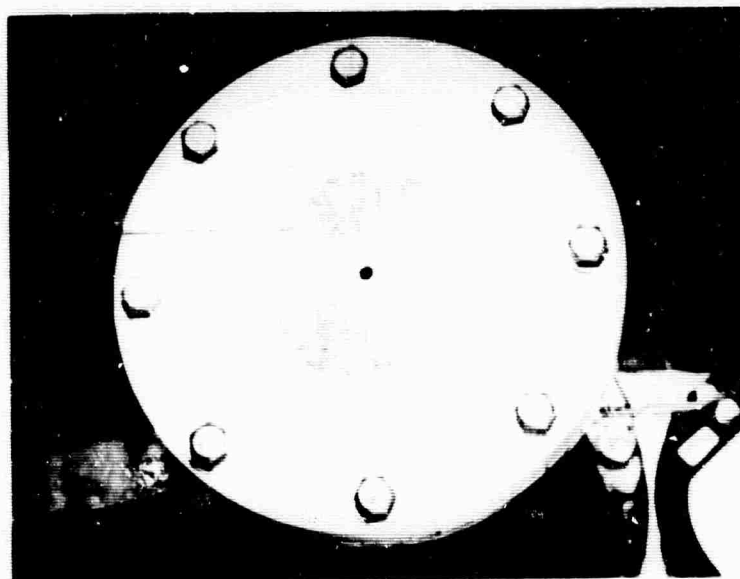
Fig. 1 (3-27) - Flow corporation constant current hot-wire anemometer and associated equipment

At the present time a free-jet calibration tunnel has been put in operation wherein flow conditions are subsonic and stream temperatures up to  $2000^{\circ}\text{R}$  are obtainable (see Fig. 2). Experimental investigation of the structure of the turbulent flow of three-dimensional free jets will commence immediately following the present calibration program. A typical orifice for generating these jets and the associated pitot probe and hot-wire probe for these studies is shown in Fig. 3.

The CCB Hot-Wire system will also be used in the experimental investigation of flow properties in the near wake of a slender hypersonic vehicle. Of particular interest is the assessment of the nature of the free shear layer between the rim of the cone and the rear stagnation point. Free-mixing flows such as this are characterized by their instability hence it is of great interest to determine if



a) Free-jet calibration tunnel and hot-wire probe



b) Hot-wire probe and axisymmetric orifice plate

Fig. 2 (3-28)

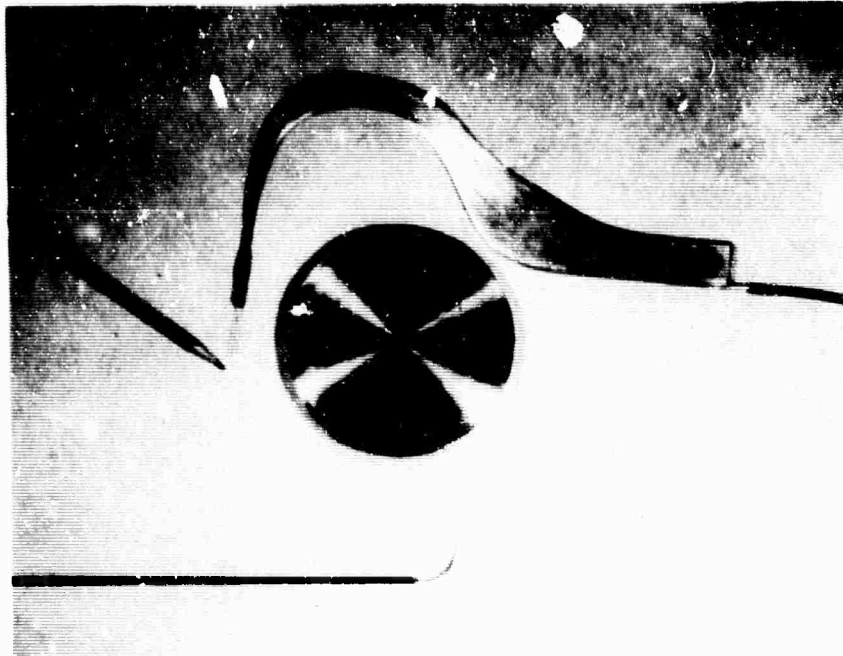


Fig. 3 (3-29) - Orifice plate for generating three-dimensional jets with calibration pitot probe (top) and hot-wire probe (bottom)

the laminar boundary layer on the body (at  $M \approx 12$  and roughly 150,000 ft. altitude) will suffer transition to turbulent flow after expansion at the base of the body. If such is the case, then a study of the turbulent structure of this flow and the ability to obtain an approximate eddy viscosity expression is highly important.

Attached herewith is a data sheet indicating the operating range and characteristics of the hot-wire system being used at PIBAL.

DATA SHEET FOR MODEL CCB  
HOT WIRE ANEMOMETER

Model CCB

.25  $\mu$  V noise level;  $\tau$  denotes the normal time constant of the wire.  
2 cps - 100 kc

Hot Wire Filaments

<u>Mat</u>	<u>dia</u>	<u>App. Resist(<math>\Omega</math>)</u>	<u>Max Wire (<math>T^{\circ}F</math>) Temp</u>	<u><math>\tau</math></u>
W1 Tungsten	.00015"	8.0	600	.0004 sec
W3 Tungsten	.00035"	1.5	600	.0016 "
W5 Tungsten	.0005"	.7	600	.003 "
P15 { 20% Rhodium 80% Platinum }	.0005"	2.3	2000	.003 "

Two types of electrical circuiting have been used with hot wire instruments, namely, "constant current" operation and "constant temperature" operation.

In the constant current system, the wire heating current is kept constant and the voltage across the hot-wire is examined. In this system, the response of the hot-wire to a velocity fluctuation is modified by its own internal heat capacity, therefore it is necessary to include a compensating circuit in the amplifier which automatically corrects for this internal heat capacity.

In the constant temperature type of instrument, a feedback circuit maintains constant resistance, and therefore constant temperature, through the hot-wire. The energy input of the hot-wire must then go entirely into the air stream, and the internal heat capacity of the hot-wire is no longer of importance because its temperature is constant. Consequently this energy input is a measure of the instantaneous air velocity.

While the constant-Temperature system presents apparent theoretical advantages it is subject to serious limitations. The upper frequency limit of the feedback amplifier must be more than twice the useful frequency range of the instrument, so that to match the performance of the best constant current systems requires excessively high frequency operation with associated problems of stability. Noise levels are generally higher and drift in the high gain d. c.

amplifier must be carefully controlled. High capacity power supplies must be regulated to better than .001%, which implies great expense and bulk.

P. M. Sforza  
Dept. of Aerospace Engineering  
and Applied Mechanics

### 3.7 Ion Beam Collision Studies

#### Purpose of the Project

Collisions of ions and neutral atoms and molecules using ion beams in the energy range 200-2,000 e.v. are being investigated by means of scattering experiments.

When a hypersonic object enters earth's atmosphere, a shock wave is formed in front of it, and the air in front of it is heated to high temperatures. In the high temperature range encountered, 3000 to 8000<sup>o</sup>K the thermal conductivity and viscosity coefficients (as well as other transport properties) are not directly measurable by laboratory techniques. The results of small angle scattering measurements can be used to obtain information about the intermolecular potential over a range of 0.2 to 20 e.v.

In turn the intermolecular potential energy function obtained from scattering experiments can be used in the appropriate theoretical equations of statistical mechanics and statistical thermodynamics to obtain the equation of state of the high temperature gases, and the transport properties such as viscosity, thermal conductivity and diffusion coefficients.<sup>2,3</sup>

#### Accomplishments since January, 1965.

A universal cross electron beam ionizer was constructed and installed for the purpose of measuring the flux of high velocity neutral molecules which result from charge-exchange collisions and other inelastic processes.

The electron beam ionizer was patterned after a mass spectrometer ion

source proposed by Doctoroff, et al.<sup>4</sup> for a high sensitivity residual gas analyzer. In this arrangement the electron and ion beams move coaxial with the axis of the atomic or molecular beam. Electrons accelerated from a hot tungsten filament pass through a wire mesh grid, and are brought to a focus in the vicinity of a voltage defining slit. Beyond this slit they diverge. Ions formed in this region of the source by collisions of electrons with molecules are accelerated into the sector field of the mass spectrometer, and detected by a secondary electron multiplier.

In addition, a sector wheel chopper was installed for modulating the beam and a lock-in amplifier added to distinguish the modulated beam from the unmodulated background.

To date it has not been possible to detect ions resulting from the interaction of the electron beam with the high speed neutrals produced by charge exchange in the ion source, because of the large ion current produced by electron ionization of the residual gas in the vacuum chamber. It is hoped that careful application of retarding potentials and magnetic analysis will eventually allow detection of the small signals.

In addition, considerable time was spent in various modifications of the arc discharge ion source to eliminate electrical breakdowns in the ion source which limit the maximum attainable beam energy.

#### Plans for the Following Period

##### Ion scattering cross sections.

It is planned to measure the total scattering cross section for scattering of energetic helium ions from helium and other neutral gases. In addition, the charge exchange cross section will be measured. The variation of the cross section with beam energy will be used to determine the intermolecular potential energy.

Previous attempts to measure these cross sections produced cross sections much larger than expected. This was traced to a charging effect in which the beam caused insulating layers to form on metal surfaces, and the static electric fields caused ions to be deflected out of the beam. A modification of the vacuum pumping system is planned which will include a bakeable molecular sieve trap to

eliminate back-streaming of diffusion pump oil.

The arc discharge ion source produces an ion beam in which the ions can have excited electronic states. Future work will be concerned with designing an ion source in which the ions are produced by collision of gas molecules with electrons having well defined energies. Scattering experiments using such a source would eliminate possible errors in cross sections caused by excited ions.

N. C. Peterson  
E. Fonder  
Chemistry Department

### References

1. Wray, K. L. in "Hypersonic Flow Research", Academic Press, New York, 1962, p. 181.
2. Hirschfelder, J. O., Curtis, C. F. and Bird, R. B., "Molecular Theory of Gases and Liquids". Wiley, New York, 1954.
3. Amdur, I. and Mason, E. A. Phys. Fluids, 1, 370 (1958).
4. Doctoroff, M., Grossel, S., Oblas, D. W., Proceedings of the Second International Congress on Vacuum Techniques, Pergamon Press, London, 1961.

### 3.8 Similar Solution of the Steady Incompressible MHD Flow in a Slender Channel (Abstract of a paper in preparation)

The classical Jeffrey-Hamel problem in ordinary hydrodynamics has been extended to include the case of the flow of an electrically-conducting fluid in the presence of a magnetic field. The solution of the problem is not only of theoretical interest, but may also be applied to magnetohydrodynamic flows in diffusers and nozzles. Exact solutions have been obtained independently by Axford<sup>1</sup> and Vatazhin<sup>2</sup> for small values of the magnetic Reynolds number.

In this paper, we seek similar solutions to the equations of magneto-hydrodynamics using the boundary layer approximation for the equations of motion. The resulting equations then describe the flow at moderate or high Reynolds

numbers in a slender channel, i. e., the characteristic length of the channel,  $l$ , is much greater than the half-height,  $r$ .

In Section 2 of this paper, we obtain the governing equations with the boundary layer approximation. The boundary conditions to be satisfied at the walls are also given. In Section 3, we show that these equations can be reduced to two ordinary differential equations, one of which may be integrated and then combined with the other one to form an equation of the third order. Solutions are sought for flows between two divergent plane walls. The results are compared with the exact solution in reference 1 for a magnetic Reynolds number  $^{12}M$  (Axford's notation) of 0.01. It is found that for the magnetic interaction parameter  $N$  less than  $2/3$  the magnetic field and wall angle effects interact to give a good approximation to the exact solution in the velocity profile and the maximum wall angle to avoid flow separation for wall angles at which the boundary layer approximation breaks down. This result is fortuitous. The discrepancy in the magnetic field distribution, however, increases steadily as the wall angle increases. This limits the applicability of the similar solutions to wall angles equal to or less than ten degrees.

W. Mak

M. H. Bloom

Dept. of Aerospace Engineering  
and Applied Mechanics

#### References

1. Axford, W. I., "The Magnetohydrodynamic Jeffrey-Hamel problem for a weakly conducting fluid". *Quar. Journ. Mech., Appl. Math.*, Vol. 14, 335, 1961.
2. Vatazhin, A. B., "On the flow in a diffuser in the presence of a magnetic field". *Jour. Appl. Math. & Mech.*, Vol. 24, 765, 1960.

#### 4. COMMUNICATIONS AND PATTERN RECOGNITION

##### Introduction

In this section a number of studies are reported that are either basic or related to the problem of detection and recognition of objects moving at hypersonic speeds. The problem of detection can be considered a problem in communications where a transmitter transmits a signal which is reflected from a time varying channel. The Electrical Engineering Department is involved in a program of studying time varying channels and optimum transmitters. Basic studies in pattern recognition are carried out in the Electrophysics Department.

In Section 4.2 a fading channel simulator is described. This channel simulator can be used to study the ionosphere, troposphere, or a rapidly moving target.

In Section 4.3 the response of an F.M. discriminator to a fading signal in additive Gaussian noise is investigated both theoretically and experimentally. To perform the experimental work an electronic channel simulator was constructed.

Studies of the response of a phased locked loop receiver are described in Section 4.1. This receiver is used whenever threshold techniques are necessary. The report shows how it is possible to extend the phase locked loop threshold further by following the loop by a non-linear filter rather than by a linear filter. The response of a phase locked loop demodulator to a fading signal has been calculated and experimental work will begin shortly. The results of this threshold extension procedure will be applied to the fading problem.

An estimation procedure to determine the characteristics of a signal transmitted through a fading channel is discussed in Section 4.4.

In Section 4.5 optimum analog detectors and approaches used in making them realizable are described. Some experimental work has been started to determine the degradation of performance resulting from the application of realizability conditions.

In the last section, 4.6, a sketch of an approach to the theory of pattern recognition is given.

As mentioned in the general introduction to this report the work contained in Section 4 will be continued under different sponsorship for the reasons stated there.

D. Schilling  
Electrical Engineering Dept.

#### 4.1 Extending the Phase Locked Loop Threshold

When estimating an F. M. signal embedded in noise most investigators use a phase locked loop receiver or a frequency demodulator with feedback. The devices are used as they extend threshold considerably over the more conventional F. M. demodulator.

When threshold is reached in each of these devices sharp spikes are seen at the output of the device. In the F. M. demodulator, this spike is caused by the input noise causing a phase rotation of  $2\pi$  radians in a short interval of time. The F. M. demodulator with feedback has spikes caused by this F. M. detector and also by the loop falling out of synchronization.

The phase locked loop has only one type of spike. This spike is due to the phase locked loop falling out of synchronization. When this happens, the phase moves  $2\pi$  radians to the next stable point. The time required for this  $2\pi$  shift in phase is the inverse of the loop gain. The larger the loop gain the smaller the time required to make the transition. Since the device is a frequency demodulator, a large spike is observed having a width the inverse of the loop gain and an area of  $2\pi$ . This spike can be mathematically represented by a delta function and the number of spikes per second has been calculated.

A minimum number of spikes is obtained by using a very wideband system. Even when this minimum number is obtained one can further reduce the effect of these spikes on the output signal to noise ratio. This is done by following

the phase locked loop by a nonlinear filter. When the spike occurs, it is sensed and the nonlinear filter holds the output at the level obtained just prior to this spike. In this manner, spikes can be eliminated, but distortion of the signal is introduced.

Calculations are now underway to determine exactly how much extension is possible. A 6db further extension of threshold is estimated. Experimental work is also underway.

D. L. Schilling  
Electrical Engineering Dept.

#### 4.2 Fading Channels and Communication Through Fading

An electronic probability machine has been constructed, packaged, and tested. A report has been written outlining its operation and its limitations. A paper describing its construction and operation has been submitted to the IEEE Transactions on Instrumentation and Measurement.

Work is now proceeding that will result in a catalog of the various types of probability densities that may be generated within our water tank fading channel simulator. This catalog will also contain information as to available center frequencies and bandwidths as well as limitations as to the available fading spectrum for any given probability density function. To aid in the experimental work connected with the generation of desirable fading spectra a 0-5,000 hertz low frequency spectrum analyzer has been obtained and a narrow band high frequency spectrum analyzer is being obtained.

A program of limiter circuit and fast acting AGC circuit design and construction is well underway. When completed this program will yield a supply of "known parameter" blocks for use in constructing and testing various proposed "anti fading" communication schemes. They should also allow experimental verification or modification of various theoretical "ideal" limiter results.

Mr. Edward Nelson, a PIB instructor and PhD candidate has a single channel, electronic fading channel simulator in operation. He is investigating the transmission of F. M. signals through this system. While this circuit is not as versatile as the water tank simulator it has several advantages of its own. These advantages include the relative ease with which the fading rate and the fading spectrum may be controlled and the fact that by employing a loop of tape recorded noise as the "fading" generator one may not just apply statistically similar fading to different signals but may actually apply identical fading to these different types of signals. This ability to apply identical fading to different types of signals may be important in exploring the fine structure of various antifading circuitry.

K. K. Clarke  
Electrical Engineering Dept.

4.3 Analysis of an F. M. Discriminator With Fading Signal Plus Additive Gaussian Noise

The problem to be handled is shown by the diagram below.

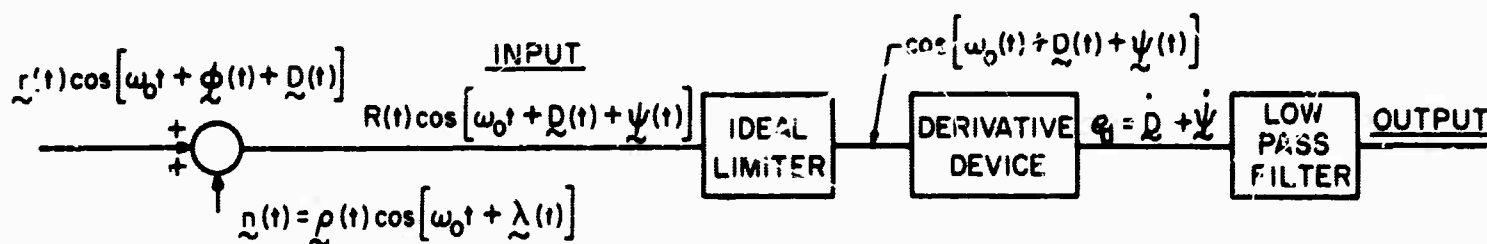


Fig. 1 (4-1)

It is desired to compute the ratio of signal to noise ratio at output  $\frac{(S_o)}{(N_o)}$  to that at the input  $\frac{(S_i)}{(N_i)}$  and estimate the discriminator threshold both theoretically and experimentally. To do this one must compute the power spectrum at the output of the derivative device. Thus, the initial undertaking will be a computation of the correlation function at  $e_d$ , specifically  $R_{\dot{D}}(\tau)$ .

The fading signal is achieved by the following means.

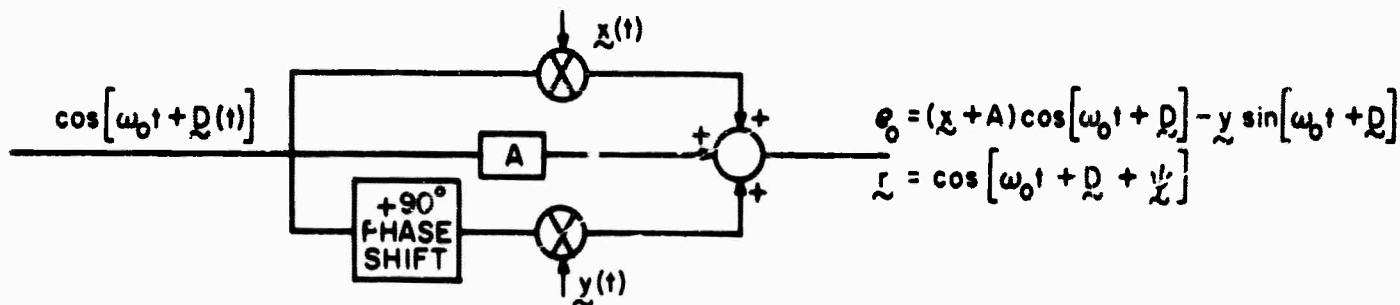


Fig. 2 (4-2)

$x(t)$  and  $y(t)$  are two independent low pass Gaussian processes with the same autocorrelation function  $R_x(\tau) = R_y(\tau)$ .  $r(t)$  is Ricean, or Rayleigh if  $A = 0$ . The fading device has a bandwidth greater than 200KC. The center frequency ( $f_0$ ) is taken as 455KC. A description of the device appeared in the Microwave Research Institute Progress Report No. 26, 1 April 1964 through 30 September 1964. The only modification is that the low pass processes are now obtained from a Zener diode by filtering and amplifying. The measured power spectrum of the Zener diode is flat from 1/2 cps, the limit of the Quantech low frequency wave analyzer (Model 304). The amplifiers are a.c. coupled with low frequency breaks of .1 cps. In particular  $G_x(f) \approx \frac{n/2}{\{1 + (f/f_e)^2\}}$  where  $f_e = 10$  cps. The envelope statistics were measured by means of two probability density machines, one consisting of a phototube and the other completely electronic. The results were quite good. Furthermore, the power spectrum of the envelope ( $A = 0$ , Rayleigh) was also measured and found to be consistent with the theory. Supervisor was provided by Professor K. K. Clarke who was also responsible for the development of both probability density machines.

Returning to the problem, one notes that with no additive noise  $R_{\phi}$  has already been determined, from which  $G_{\phi}(f)$  was computed by numerical methods. Lawson and Uhlenbeck handles this for the case where  $G_x(f)$  is bandlimited white noise, whereas Rice in "Sine Wave plus Random Noise" does it for  $G_x(f)$  a

Gaussian spectrum. The spectrum of  $\dot{\phi}$  will be measured and compared with the theoretical results of Rice and Lawson and Uhlenbeck. Exact agreement is not to be expected since the experimental spectrum has a double pole. Also, an attempt will be made to measure the statistics of  $\phi(t)$ . With  $A = 0$  (Rayleigh) one expects a uniform probability density.

With additive noise  $R\dot{\psi}$  will be found theoretically first for the case of no modulation. When modulation is included  $D(t)$  will be considered as  $\underline{a} + \underline{\theta} \sin(\omega t + \underline{\gamma})$  where  $\underline{a}$  and  $\underline{\gamma}$  are independent and uniform in  $(0, 2\pi)$ . In practice one never knows the phase of the signal exactly. The inclusion of  $\underline{a}$  and  $\underline{\gamma}$  also makes the process stationary.

This work is being carried on under the guidance of Professors K. K. Clarke and D. Schilling.

E. Nelson  
Electrical Engineering Dept.

#### 4.4 Optimum Demodulation Using Bayes Criterion In Random Channels

Recent studies have been concerned with the detection of phase and frequency modulated signals corrupted by additive Gaussian white noise in deterministic channels under the optimizing condition that the Bayes risk be minimized. This work has been extended to include the effects of a randomly fading channel. Fading behavior can be broadly categorized according to whether the channel fluctuations are rapid or slow as compared to data observation intervals, and also according to whether there are amplitude and phase variations or simply amplitude changes.

The simplest case to be considered is that of the transmission of a discrete phase angle through a fading channel whose transmission amplitude is a Gaussian random variable and whose phase fluctuations are neglected. Received signals (including additive white Gaussian noise) are of the form

$$\underline{v}(t) = \underline{A} S_0 \cos(\omega_0 t + \underline{\theta}) + \underline{n}(t), \quad 0 \leq t \leq T$$

where  $A$  has a mean of unity and a variance of  $\sigma_A^2$ . The optimum Bayes demodulator for this type of received signal has been found and its block diagram representation is shown below.

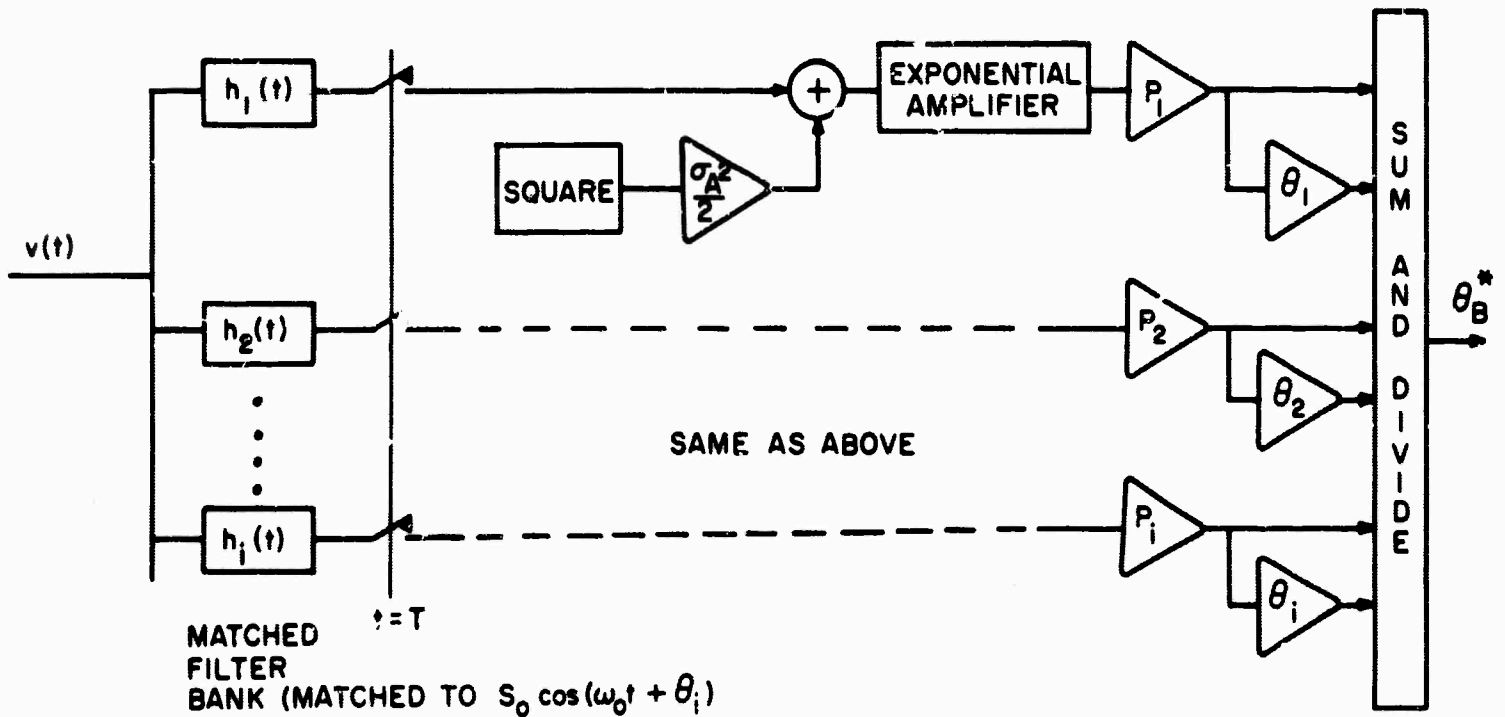


Fig. 1 (4-3)

In the limit as the variance,  $\sigma_A^2$ , of amplitude fluctuations approaches zero (that is, as the channel becomes deterministic) the implementation approaches that which has been previously derived for non-random channels.

A further degree of complexity is introduced by including phase fluctuations as well as amplitude fluctuations. Received signals may then be represented in the form

$$\underline{v}(t) = \underline{x} \cos(\omega_0 t + \underline{\theta}) + \underline{y} \sin(\omega_0 t + \underline{\theta}) + \underline{n}(t), \quad 0 \leq t \leq T$$

where  $\underline{x}$  and  $\underline{y}$  are Gaussian random variables. Only when  $\underline{x}$  or  $\underline{y}$  has a non-zero mean value can phase information be extracted from the received signal; furthermore, it can be shown that a fairly simple realization can be effected in this case.

A third class of problems is concerned with the estimation of a random process  $\underline{a}(t)$  which appears in the following phase modulated signal:

$$\underline{v}(t) = \underline{x} \cos [\omega_0 t + a(t)] + \underline{y} \sin [\omega_0 t + a(t)] + \underline{n}(t), \quad 0 \leq t \leq T$$

Special cases of this include Gaussian, Rayleigh, and Ricean amplitude variation, and for each of these, estimator implementations have been found which are approximate to first order.

In forthcoming months this work will be extended to include the effects of rapidly fading channels. In addition, former work will be generalized to include the spaced-antenna diversity problem, wherein the data is composed of many independent received signals.

The present work is being carried out under the supervision of Professor D. Schilling.

P. Crepeau  
Electrical Engineering Dept.

#### 4.5 Realizable Approximations to Optimum Analog Demodulators

(Abstract of a report in preparation)

We consider here the problem of continuously estimating an analog signal which has been used to modulate a carrier and then is contaminated by additive noise and fading. An early solution is provided by the work of Wiener<sup>1</sup> who has established a procedure for finding a linear filter that yields a lower mean-squared error than any other linear filter. A second approach is that of Youla<sup>2</sup>. Using a maximum a posteriori performance criterion he finds a set of integral equations describing the desired results. Van Trees<sup>3</sup> allows the form of these equations suggest real-time receiver structures containing feedback loops and non-linearities

as well as unrealizable components (realizable with sufficient delay).

The first part of this work is concerned with the realization of the above receiver without delay. Since most of these receivers include some form of a phase-locked loop which constantly loses lock, it is intended to investigate the effects of this transient condition. We then seek the "optimum" receiver for continuous estimation without delay and where data acquisition starts at some fixed time (after lock is restored). This problem (with a mean-squared error criterion) reduces to the original Wiener problem but for a growing-memory filter. This problem is solved here. Comparisons with the performance of optimum stationary filter indicate little difference, hence the latter filter being simpler to implement is preferred.

A criticism of the above solution to date is the ambivalence towards a performance criterion. Specifically both maximum a posteriori (MAP) and minimum variance criteria are used somewhat interchangeably. In this work we establish a performance measure for the MAP criterion and try to develop the connection between the two criteria. Work on this topic shall continue.

Most of the above, and subsequent work, is restricted to the linear region of the receiver's operation. Following Viterbi<sup>4</sup> we use Fokker-Planck techniques to investigate the non-linear performance of these receivers. Further experimental and theoretical work in this regard is in progress. Briefly we find the presence of "clicks" (jumps in phase) adds to the system error and tends to question the suitability of the performance criterion. It is possible that a better receiver design would result from a compromise between reducing the frequency of clicks and the design in the linear region. As indicated above, work in this area is progressing.

The latter section of this effort deals with the effects of fading on system performance and design. We first consider A. M. (or baseband) signals (with fading) and find the optimum linear filter. (This is an extension of Wiener's work to include fading). We find that as the carrier-to-noise ratio is increased the error instead

of reducing to zero (as in the non-fading case) approaches a constant due to the fading. To investigate whether this (fading) error can be reduced by a non-linear filter we extend the Cramer-Rao (lower) Bound to include fading and find that the fading error does disappear. Schwartz<sup>5</sup> has extended the work of Youla and found the MAP receiver in the presence of fading. We next evaluate the performance of this receiver for slow fading and find that again the fading error disappears. Finally we evaluate the performance of P.M. receivers in a fading environment.

As indicated above the following areas are still being investigated:

- 1) non-linear performance and subsequent modification of design (by Raymond Stroh, a full-time Masters student); 2) performance measures for MAP and comparison with minimum variance (by Walter Devensky, a part-time Masters student).

R.R. Boorstyn  
Electrical Engineering Department

#### References

1. Wiener, N., "Extrapolation, Interpolation, and Smoothing of Stationary Time Series", MIT Technology Press and John Wiley and Sons, Inc., New York (1950).
2. Youla, D.C., "The use of maximum likelihood in estimating continuously modulated intelligence which has been corrupted by noise," IRE Trans. on Information Theory, Vol. IT-3, pp. 90-105, March 1954.
3. Van Trees, H.L., "Detection, Estimation and Modulation Theory" (to be published)
4. Viterbi, A.J., "Phase-locked loop dynamics in the presence of noise by Fokker-Planck techniques", Proc. IEEE, pp. 1737-1753, December 1963.
5. Schwartz, M., "Maximum a posteriori demodulation of analogue-type signals through random fading media", Polytechnic Institute of Brooklyn, PIBMRI 1244-64, December 1964.

#### 4.6 Pattern Recognition Theory

The following is a sketch of an approach to the theory of pattern recognition which aims to answer certain fundamental questions posed in a previous

report<sup>1</sup>. The basic problem of pattern recognition is to classify an unknown object, signal, or set of signals to one of several categories. The signals might be radar returns, emission spectra, etc.; the set of categories might be {target and noise, noise alone}, {natural object, harmless man-made object, threatening object} etc. If the signal statistics are known for each category, then the problem is easy. A more usual case is not even to know the form of the distributions involved, e.g. it may not be known that they are Gaussian. The material presented is abstract and not applied, but it is believed that further work in applying the basic ideas would be valuable.

General

In the following a pattern will be defined as an  $r$ -component real vector which can belong to one of  $k$  classes. It will be assumed that  $d$  sample patterns of known class are provided from each of the  $k$  classes, these differing from each other even within the same class because of random perturbations. The sample patterns will be denoted by  $\xi_{ji}^{(\nu)}$  where  $j$  is the class,  $i$  the component ( $1, 2 \dots r$ ) and  $\nu$  the individual sample index ( $1, 2 \dots d$ ). The task is to classify or recognize the  $k(d+1)$ 'st pattern ( $x_i$ ) according to some criteria to be developed below. A pattern recognizer will be defined as a function  $\Gamma(\xi, \underline{x}, j)$  such that for every  $(\xi, \underline{x})$  combination  $\Gamma = 0$  for some  $j$  and  $\Gamma = 1$  for all other values of  $j$ . As an example, consider

$$\Gamma(\xi, \underline{x}, j) = \begin{cases} 0 & j = j_0 \\ 1 & j = 1, 2, \dots, j_0 - 1, j_0 + 1, \dots, k \end{cases} \tag{1}$$

where  $j_0$  minimizes  $\sum_{i=1}^r \left[ \frac{1}{d} \sum_{\nu=1}^d \xi_{ji}^{(\nu)} - x_i \right]^2$

Here will be said that  $\underline{x}$  is recognized as belonging to class  $j_0$  after the recognizer is calibrated by the samples  $\xi$ . The choice of patterns (by "nature" or some external process) is assumed to be made according to a probability density  $P$  defined as follows:  $P(\xi, \underline{x}, j) d\xi d\underline{x}$  is the probability of having the calibration patterns in the volume element  $d\xi$ , the unknown pattern in the volume element

$d\underline{x}$ , and the unknown pattern chosen from class  $j$ . The probability of misclassifying the unknown pattern is given by

$$Q = \sum_{j=1}^k \int_{-\infty}^{\infty} \int_{-\infty}^{\infty} \Gamma(\xi, \underline{x}, j) P(\xi, \underline{x}, j) d\xi d\underline{x} \quad (2)$$

If the function  $P$  is known there is no difficulty in finding an optimum pattern recognizer:

$$\begin{aligned} \Gamma(\xi, \underline{x}, j) &= 0 \quad \text{if } j \text{ maximizes } P(\xi, \underline{x}, j) \text{ with fixed } \xi, \underline{x} \\ \Gamma(\xi, \underline{x}, j) &= 1 \quad \text{otherwise} \end{aligned} \quad (3)$$

Similarly, for a fixed pattern recognizer  $\Gamma$  there is no difficulty finding a probability density  $P$  which causes a large error probability  $Q$ : simply choose any function  $P(\xi, \underline{x}, j)$  which does not depend on the last argument (i. e., all chosen distributed identically). Then

$$\int_{-\infty}^{\infty} \int_{-\infty}^{\infty} P(\xi, \underline{x}, j) d\xi d\underline{x} = \frac{1}{k} \quad (4)$$

and since it will always be true that

$$\sum_{j=1}^k \Gamma(\xi, \underline{x}, j) = k-1 \quad (5)$$

it follows that

$$Q = 1 - \frac{1}{k} \quad (6)$$

An even larger error can be obtained if it is assumed that the statistics are such as to "deliberately mislead" the pattern recognizer during calibration. A pathological  $P$  which results in a probability of error of 1 can be defined as follows: divide the vector space into  $k$  disjoint regions  $J_1, J_2, \dots, J_r$  such that

$$\begin{aligned} P(\xi_1, \xi_2, \dots, \xi_k, \underline{x}, j) &= 0 \\ \text{unless } \xi_\beta \in J_\beta \quad (\beta = 1, 2, \dots, r) \text{ and } \underline{x} \notin J_j. \end{aligned} \quad (7)$$

The best recognizer with this distribution would, according to Eq. (3), result in

$$\Gamma(\xi, \underline{x}, j) = 1 \text{ for } \underline{x} \in J_j$$

and therefore in  $Q = 1$ . Of course, the latter situation could not arise if calibration samples and the unknown to be recognized are generated statistically independently, but assuming this independence would exclude time-dependent processes and other useful cases.

The problem which arises in practice is that a pattern recognizer must be designed without knowing the density function  $P$ . It cannot be expected to arrive at a  $\Gamma$  which will cope with all  $P$ 's, since as was shown above, if  $\Gamma$  is fixed there exists a  $P$  which allows  $\Gamma$  to do no better than random guessing (or even a  $P$  which results in error all the time). However, such  $P$ 's which cause such poor performance regardless of the way the recognizer is designed can either be said to have low probability or excluded altogether. These two possibilities will now be explored.

Average Optimization

The probability density functions  $P$  are assumed known except for certain parameters  $\underline{a}_1, \underline{a}_2 \dots \underline{a}_k$ , each of which might be an  $n$ -component real vector or an integer (in which case the integrals below would be sums). These parameters are described by a density function  $A(\underline{a}_1, \underline{a}_2 \dots \underline{a}_k)$ . If some parameters (such as variances) are the same for all classes, this will be indicated by a degeneracy in the function  $A$ . The error probability  $Q$  is now a random variable depending on the values of the random variables  $\alpha$ :

$$Q(\underline{a}_1, \underline{a}_2 \dots \underline{a}_k) = \sum_{j=1}^k \int_{\infty}^{\infty} \int_{\infty}^{\infty} \Gamma(\xi, \underline{x}, j) P(\xi, \underline{x}, j, \alpha) d\xi d\underline{x} \quad (8)$$

The criterion for optimizing the pattern recognizer will now be defined as the minimization of the expected value of  $Q$ :

$$\bar{Q} = \int_{\infty}^{\infty} \int_{\infty}^{\infty} \dots \int_{\infty}^{\infty} Q(\underline{a}_1, \underline{a}_2 \dots \underline{a}_k) A(\underline{a}_1, \underline{a}_2 \dots \underline{a}_k) d\underline{a}_1 d\underline{a}_2 \dots d\underline{a}_k \quad (9)$$

By combining the above two equations, it can be seen that the desired pattern recognizer is defined by:

$$\Gamma(\underline{\xi}, \underline{x}, j) = 0 \text{ if } j \text{ maximizes } \int_{-\infty}^{\infty} P(\underline{\xi}, \underline{x}, j, \underline{\alpha}) A(\underline{\alpha}) d\underline{\alpha} \quad (10)$$

$$\Gamma(\underline{\xi}, \underline{x}, j) = 1 \text{ otherwise}$$

These equations can be made more explicit and easily visualized if some additional assumptions are made:

$$P(\underline{\xi}, \underline{x}, j, \underline{\alpha}) = \prod_{\ell=1}^k P(\xi_{\ell}; \underline{\alpha}_{\ell}) p(\underline{x}; \underline{\alpha}_j) p_j \quad (11)$$

$$A(\underline{\alpha}_1, \underline{\alpha}_2, \dots, \underline{\alpha}_k) = A_1(\underline{\alpha}_1) A_2(\underline{\alpha}_2) \dots A_k(\underline{\alpha}_k) \quad (12)$$

Physically these assumptions are that the parameters  $\underline{\alpha}_j$  are statistically independent for the different classes, that once the  $\underline{\alpha}$  are chosen the calibration samples  $\xi_{\ell}$  for the different classes are statistically independent, and the samples and  $\underline{x}$  are statistically independent. The pattern recognizer now becomes

$$\Gamma(\underline{\xi}, \underline{x}, j) = 0 \text{ if } j \text{ maximizes } p_j \frac{\int_{-\infty}^{\infty} P(\xi_j; \underline{\alpha}) p(\underline{x}; \underline{\alpha}) A_j(\underline{\alpha}) d\underline{\alpha}}{\int_{-\infty}^{\infty} P(\xi_j; \underline{\alpha}) A_j(\underline{\alpha}) d\underline{\alpha}} \quad (13)$$

$$\Gamma(\underline{\xi}, \underline{x}, j) = 1 \text{ otherwise.}$$

Still further simplification results if it is assumed that the different samples of the same class are statistically independent,

$$P(\xi_{\ell}; \underline{\alpha}_{\ell}) = \prod_{v=1}^{\lambda} p(\xi_{\ell}^{(v)}; \underline{\alpha}_{\ell}) \quad (14)$$

that the A functions are constant to very large arguments, and that the r components of each pattern vector are independent Gaussian random variable with means and variances  $(M_j, \sigma_j^2) = \underline{\alpha}_j$ . The pattern recognizer now becomes

$$\Gamma(\underline{\xi}, \underline{x}, j) = 0 \text{ if } j \text{ maximizes } p_j \prod_{i=1}^r \frac{1}{D_{ji} \left[ 1 + \frac{1}{d+1} \left( \frac{x_i - M_{ji}}{D_{ji}} \right)^2 \right]^{\frac{d-1}{2}}} \quad (15)$$

$$\Gamma(\underline{\xi}, \underline{x}, j) = 1 \text{ otherwise}$$

where

$$M_{ji} = \frac{1}{d} \sum_{v=1}^d \xi_{ji}^{(v)} \text{ and } D_{ji}^2 = \frac{1}{d} \sum_{v=1}^d \left[ \xi_{ji}^{(v)} \right]^2 - M_{ji}^2$$

The quantities  $M_{ji}$  and  $D_{ji}^2$  will be recognized as the sample means and variances, and if  $d$  is large the quantity minimized above is equivalent to

$$p_j \prod_{i=1}^r \frac{1}{D_{ji}} e^{-\frac{1}{2} \left( \frac{x_i - M_{ji}}{D_{ji}} \right)^2} \quad (16)$$

so that the usual method of pattern recognizer calibration by parameter estimation is seen to be approximately optimum in the present sense.

Minimax Optimization

The idea here is to consider the situation as a two person zero sum game between the designer who chooses  $\Gamma$  to minimize  $Q$  and nature who chooses  $P$  to maximize  $Q$ . As was explained above, nature would always win this game by making  $P$  independent of  $j$ , by multinode densities for small  $d$ , or by other pathological distributions, unless the class of  $P$ 's which are allowed is restricted. From here on it will be assumed that  $P$  belongs to some set  $\mathcal{P}$  of probability densities, but that  $\Gamma$  is any allowable pattern recognizer function. Let  $Q[\Gamma, P]$  be the probability of error when recognizer  $\Gamma$  is used with probability density  $P$ , and let the expression

$$\Lambda[\Gamma] = \text{Max}_{P \in \mathcal{P}} Q[\Gamma, P] \quad (7)$$

denote the maximum value of  $Q$  with  $\Gamma$  fixed and with  $P$  ranging over the set  $\mathcal{P}$ . The minimax optimum pattern recognizer will be defined as that value of  $\Gamma$  which minimizes the above expression. If the class  $\mathcal{P}$  is too restricted it means that

the pattern recognizer can behave very poorly if the assumed class does not include the actual distribution. For example, if  $\mathcal{P}$  consists of independent Gaussian distributions, the actual distributions could be highly dependent, have unsymmetrical density functions, etc. On the other hand, there can be difficulties in naively making  $\mathcal{P}$  too general, as the following indicates: it is reasoned that there are unreasonable  $P$ 's for which no recognizer can be expected to work well, so why not exclude all those  $P$ 's from  $\mathcal{P}$  for which no recognizer can achieve an error probability less than some arbitrary maximum tolerable error  $Q_m$ ? In other words, why not define  $\mathcal{P}$  as the set of  $P$ 's such that at least one  $\Gamma$  exists which makes

$$Q[\Gamma, P] \leq Q_m \quad (18)$$

The answer is that this leads to the uninteresting conclusion that all pattern recognizers are equally good, since it can be shown that

$$\Lambda(\Gamma) = Q_m$$

for  $\mathcal{P}$  defined as above. This is easily proved by assuming the contrary: assume  $\Lambda(\Gamma) = q < Q_m$  for some  $\Gamma$ , say  $\Gamma_a$ . There must then be a pair  $\Gamma_a, P_b$  such that  $Q[\Gamma_a, P]$  is maximized at value  $Q = q$  for some  $P$  in  $\mathcal{P}$ , say  $P_b$ . Now denote a distribution defined by Eq. (7) by  $P_c$ , and note that

$$P = (1-\delta) P_b + \delta P_c \quad (19)$$

is a valid density function for  $0 \leq \delta \leq 1$ . Substituting this  $P$  in Eq. (2):

$$Q = (1-\delta)q + \delta$$

which is larger than  $q$  and not larger than  $Q_m$  if

$$0 < \delta \leq \frac{Q_m - q}{1 - q} \quad (20)$$

This violates the assumption that  $P_b$  maximizes  $Q[\Gamma_a, P]$ , and in fact shows that distribution described by Eqs.(19) and (20) should belong to  $\mathcal{P}$ . Note finally that  $q$  could not have been greater than  $Q_m$ , since by Eqs.(17) and (18),  $\Lambda(\Gamma) \leq Q_m$  for  $P \in \mathcal{P}$ . Therefore, if  $\mathcal{P}$  is defined as the set of all densities such that some

recognizer gives an error probability of  $Q_m$  or less, then the function defined in Eq. (17) becomes independent of the recognizer  $\Gamma$ .

The above discussion shows that the minimax approach can be usefully employed only if suitable set of possible distributions  $\mathcal{P}$  is defined in a sufficiently restrictive way. Let  $G$  be the set of permissible pattern recognizers as defined by Eq. (1). Then it is always true that

$$\text{Max}_{P \in \mathcal{P}} \text{Min}_{\Gamma \in G} Q[\Gamma, P] \leq \text{Min}_{\Gamma \in G} \text{Max}_{P \in \mathcal{P}} Q[\Gamma, P] \quad (21)$$

The equality holds if and only if the  $\Gamma, P$  space contains one or more saddle points. The pair  $\Gamma_\sigma, P_\sigma$  will be defined as a saddle point if

$$\text{Max}_{P \in \mathcal{P}} Q[\Gamma_\sigma, P] \text{ occurs at } P = P_\sigma$$

and

$$\text{Min}_{\Gamma \in G} Q[\Gamma, P_\sigma] \text{ occurs at } \Gamma = \Gamma_\sigma$$

The common value of both sides in Eq. (21) will then be  $Q[\Gamma_\sigma, P_\sigma]$ . There may be several saddle points, in which case the  $Q$  function must have the same value at each. The optimum pattern recognizer can then be defined as any of the  $\Gamma_\sigma$  if saddle points exist. In game theory, if no saddle points existed a randomized strategy would be adopted, i. e., the choice of  $\Gamma$  would be made among several with certain probabilities. Discussions of the applicability and reasonableness of such strategies tend to get very involved,<sup>3</sup> but it seems best here to always use the optimum  $\Gamma$  determined by Eq. (17). There is a considerable literature for problems of this type where the regions  $G$  and  $\mathcal{P}$  are polyhedral, i. e., the constraints on  $\Gamma$  and  $P$  are linear inequalities. However, the techniques for solving these "constrained matrix games" such as linear programming<sup>2</sup> seem to be suitable for numerical computer solutions rather than analytic paper solutions.

A. E. Laemniel  
Electrophysics Department

References

1. Marcuvitz, N., et al., "The Polytechnic Institute of Brooklyn Electromagnetics Program", 16 November 1964.
2. Kuhn, H.W. and Tucker, A.W. (eds.), "Linear Inequalities and related systems", Princeton U. Press, Princeton, New Jersey, 1956.
3. Luce, R.D. and Raiffa, H., "Games and Decisions", John Wiley and Sons, New York, 1957.
4. Laemmel, A.E., "Final Report on Pattern Recognition and Detection by Machines", Polytechnic Institute of Brooklyn, Report PIBMRI-1130-63, 8 March 1963.

5. EDUCATION, PARTICIPATION IN COMMITTEES,  
REPORTS AND PUBLICATIONS

5.1 Education

One of the major aims of the program which is supported by ARPA is to educate students in the subject areas relevant to Project DEFENDER.

In addition to "general background courses" there are special courses, introductory in nature, in the field of plasmas. Some of these are:

1. Plasma dynamics I and II, presently taught by Professor N. Marcuvitz
2. Thermodynamics of real gases, Professor V. Agosta
3. Ionization phenomena in gases, Spring 1966, Dr. R. Pepper
4. Introduction to magneto-hydrodynamics, Spring 1966, Professor D. Wilson.

In addition to these regular courses, there have been a number of special courses:

1. Kinetic theory of gases, Professor T. Wu
2. Wave propagation in plasmas, Visiting Professor H. Motz
3. Collision processes and chemical reaction, Professor N. Peterson.

There will be other special topics courses, such as

4. Stability of plasma waves, Professor J. Freidberg.

The plasma laboratory facilities, briefly described in the body of this report, are under the supervision of Professor H. Farber. Through general laboratory courses, students are being instructed in experimental techniques and measurements in the field of vacuum, gas discharge and microwave technology.

Furthermore, there were a great many formal seminars and informal discussion groups; a partial listing is given here:

October, 1964

Radiation in Anisotropic Media (two sessions)	S. Rosenbaum
Jahn-Teller Effect	J. Pearlman

November, 1964

Molecular Beam Scattering	N. C. Peterson
Tonks-Dattner Resonances	J. Shmoys and J. Gobler
Electron Tunneling Through Thin Films	T. Nakayama
Molecular Beam Scattering	N. G. Peterson
Langmuir Probes	D. Wilson and S. Schwartz

Photoinduced Chemisorption on Insulators	P. Mark
Eigen (Network) Approach to Wave Propagation in Plasmas	N. Marcuvitz
Turbulent Fluctuations as Related to Microwave Scattering from Plasma	M. Bloom
Molecular Beam Scattering	N. C. Peterson

December 1964

Ion Sound Waves Experiments for Low Pressure Discharges - Predictions of Plasma Kinetic Theory	M. Haggerty
Shock Tunnel Studies	S. Lederman
Tools of Experimental Plasma Research	K. Lian
Electron Beam - Plasma Interaction	P. Serafim
Radiation in the Presence of a Gyrotropic Plasma Half Space	H. Bertoni
Landau Damping	J. Freidberg
Peculiar Effect in Infrared Spectra	P. D'Antonio
Synchronous Coupling of Harmonic Waves in Parametric Interactions	E. Cassedy

January 1965

Electroacoustic Resonances in Plasmas	H. J. Schmitt Sperry Rand Research Center Sudbury, Massachusetts
Collisionless Damping	D. Yee
Electrically Driven Shock Tubes and Tunnels for Planetary Entry Studies	W. Warren General Electric Company Valley Forge, Pa.
Strain Fields as Determined by Moiré Techniques	G. Oster
On Bogoliubov's Kinetic Theory as a Theory of Fully Ionized Gas	T. Koga
Microwave and Plasma Research at the University of Sheffield	A. L. Cullen University of Sheffield Sheffield, England
Plasma Electron Temperature in an Inhomogeneous Electric Field	H. Cronson

February 1965

Landau Damping	T. Y. Wu
Propagation and Scattering Characteristics of a Sinusoidally Stratified Dielectric Slab	H. C. Wang
Scattering by a Sinusoidally Stratified Dielectric Half Space	H. C. Wang

Diffraction by a Half Plane in an Anisotropic  
Medium

S. Rosenbaum

Coupling of Magneto-hydrodynamic Waves

H. Poeverlein  
Air Force Cambridge Research  
Laboratories, Bedford, Mass.

March 1965

Review of Ionospheric Measurement Techniques

S. Gross  
Airborne Instruments Lab.  
Melville, N. Y.

Generation and Propagation of Waves in a  
Partly Ionized Gas

B. S. Tanenbaum  
Case Institute of Technology  
Cleveland, Ohio

On Transition Functions Occurring in the Theory  
of Diffraction in Inhomogeneous Media

L. Levey

April 1965

Scattering of Kilovolt Atomic Beams

N. C. Peterson

Analysis of Propagation Along Warm Plasma  
Columns

P. Diament  
Columbia University, N. Y. C.

Microwave Propagation in Laboratory Plasma;  
Finite Temperature Effects

S. P. Schlesinger  
Columbia University, N. Y. C.

Physical Origin to Internal Rotation About  
Single Bonds

R. G. Parr

Interpretation of Moiré Patterns

C. Chung

May 1965

Plasma Activities at Oxford University

H. Motz

Beam Plasma Amplifier Research

P. Chorney  
Microwave Associates  
Burlington, Mass.

Electron Density and Internal Rotation  
Barriers

R. E. Wyatt

June 1965

Landau Damping

H. Motz

Diffraction by an Opaque Convex Cylinder

L. D. Porter

Incoherent Scattering of Radio Waves from the  
Upper Atmosphere

H. Motz

Diffraction by a Half Plane in a Compressible  
Homogeneous Plasma

F. Labianca

Landau Damping

T. Y. Wu

October 1965

Induced Spectra and Quasi-Electronic Transitions

S. Ukeles

Participation at outside meetings relevant to the program included the following talks:

a) First International Congress on Instrumentation in Aerospace Simulation Facilities held in Paris, France in September, 1964:

Microwave Techniques Applicable to Shock Tube Measurements	M. Visich and S. Lederman
---	------------------------------

b) 19th Anti-Missile Research Advisory Council Meeting, sponsored by ARPA and held in Washington, D. C. in April, 1965:

The Polytechnic-ARPA ONR Program	N. Marcuvitz
----------------------------------	--------------

Hypersonic Flows	M. Bloom
------------------	----------

Electromagnetic Phenomena in Anisotropic, Dispersive Media	L. B. Felsen
---	--------------

Time Varying Communication	A. E. Laemmel
----------------------------	---------------

Channels and Pattern Recognition	D. L. Schilling
----------------------------------	-----------------

c) Electrochemical Society Meeting, San Francisco, California, May 1965:

Electrical Properties of Oxide Films on Silicon	F. C. Collins
---	---------------

d) Seminar at the State University of New York, Dept. of Mechanics, Stony Brook, L. I., N. Y. in May, 1965:

Some Confusions in the Kinetic Theory of Plasma	T. Koga
---	---------

e) Professional Technical Group on Antennas and Propagation Meeting held in Washington, D. C. in August-September, 1965:

Group Velocity and Power Flow Relations for Sur- face Waves in Stratified Anisotropic Media	H. Bertoni
--	------------

f) IEEE Globe Communications Conference, Boulder, Colorado in June, 1965.

An Information Theory Approach to Radar Detection and Parameter Esti- mation	C. L. Temes
---	-------------

## 5.2 Participation in Committees

Professor N. Marcuvitz is a member of the Ballistic Missile Defense Advisory Committee for the period of three years from July 1965 to June 1968. He is also a member of the Atomic and Molecular Physics Panel of the Institute for Defense Analyses.

Professor R. Hutter has taken part informally in meetings and project

reviews of the ARPA-ECM Electronic Components Subcommittee, headed by Col. Benjamin I. Hill of ARPA.

Professor M. Bloom has attended the meetings of the Wake Panel as well as the meetings of the Atomic and Molecular Physics Panel of the Institute for Defense Analyses.

### 5.3 Reports and Publications

#### 5.3.1 Reports

- S. Lederman, M. Abele and M. Visich, Jr., "Microwave Techniques Applicable to Shock Tube Measurements", PIBAL Report No. 857 dated September 1964.
- T. Koga, "A Kinetic Theoretical Investigation of a Fully Ionized Gas - Part I: Paradoxes in the E-B-C-K-Y Hierarchy. Part II: Some Aspects of Multiple Collisions. Part III: A Theory of Electron Gas", PIBAL Report No. 863 Parts I and II dated January 1965, Part III dated May 1965.
- S. C. Gianzero, Jr., "Radiation by a Uniformly Rotating Line Charge in a Plasma", PIBAL Report No. 873 dated June 1965.
- L. D. Porter, "Diffraction by a Transparent Elliptical Cylinder", PIBAL Report No. 874 (in preparation).
- S. H. Schwartz, "Oscillations in the Plasma Sheath", PIBAL Report No. 880 dated July 1965.
- E. Schmidt, "An Investigation of Hypersonic Flow Around a Slender Cone", PIBAL Report No. 893 (in preparation).
- C. L. Temes and D. Schilling, "An Analysis of Radar in Terms of Information Theory and Physical Entropy", PIBMRI-1270-65 dated June 1965.
- D. D. H. Yee and T. Y. Wu, "Landau Damping", PIBMRI-1280-65 dated June 19, 1965.
- M. J. Haggerty, "On the Kinetic Theory of Diffusion of a Plasma Column Across a Magnetic Field", PIBMRI-1289-65 dated August 10, 1965.
- H. Bertoni and A. Hessel, "Group Velocity and Power Flow Relation for Surface Waves in Plane Stratified Anisotropic Media", PIBMRI-1293-65 (in preparation).
- H. Bertoni and A. Hessel, "Surface Waves on a Uniaxial Plasma Slab; Their Group Velocity and Power Flow", PIBMRI-1294-65 (in preparation).

### 5.3.2 Published papers

- T. Koga, "Conductivity of a Warm Plasma to an Oscillating Electric Force in the Presence of a Strong Magnetic Field", *Il Nuovo Cimento, Series X, Vol. 34*, pp. 987-1009, November 1964.
- T. Koga, "Reconsideration of the Collision Model Proposed by Bhatnagar, Gross and Krook", *Il Nuovo Cimento, Series X, Vol. 36*, pp. 174-188, March 1965.
- C. L. Temes, "An Information Theory Approach to Radar Detection and Parameter Estimation", *IEEE Annual Communications Conference, Convention Record*, June 1965.
- A. E. Laemmel, "Pattern Recognition of Time Varying Systems", *IEEE Annual Communications Conference, Convention Record*, June 1965.
- F. C. Collins, "Electrochemical Behavior of Grown Oxide on Silicon", *Journal of Electrochemical Society, Vol. XII*, p. 786, August 1965.
- T. Y. Wu, "Kinetic Equation of Gases and Plasmas", Addison-Wesley Publishers (in preparation).

## DOCUMENT CONTROL DATA - R&amp;D

(Security classification of title, body of abstract and indexing annotation must be entered when the overall report is classified)

1. ORIGINATING ACTIVITY (Corporate author) Polytechnic Institute of Brooklyn Graduate Center, Route 110 Farmingdale, L. I., N. Y.		2a. REPORT SECURITY CLASSIFICATION Unclassified	
		2b. GROUP	
3. REPORT TITLE Research on Electromagnetics for Project DEFENDER			
4. DESCRIPTIVE NOTES (Type of report and inclusive dates) Semi-Annual Technical Summary for period ending 30 September 1965			
5. AUTHOR(S) (Last name, first name, initial) Coordinator: Hutter, Rudolf G. E.			
6. REPORT DATE 30 September 1965		7a. TOTAL NO. OF PAGES 200	7b. NO. OF REFS 90
8a. CONTRACT OR GRANT NO. Nonr-839(38)		9a. ORIGINATOR'S REPORT NUMBER(S) PIBMRI-1295.1-65	
b. ARPA Order No. 529			
c. Program Code No. 5730		9b. OTHER REPORT NO(S) (Any other numbers that may be assigned this report.)	
d.			
10. AVAILABILITY/LIMITATION NOTICES Qualified requestors may obtain copies of this report from DDC. Other persons or organizations should apply to the Clearinghouse for Federal Scientific and Technical Information (CFSTI), Sills Bldg., 5285 Pt. Royal Rd., Springfield, Va.			
11. SUPPLEMENTARY NOTES		12. SPONSORING MILITARY ACTIVITY Advanced Research Projects Agency and Office of Naval Research, Washington, D.C.	
13. ABSTRACT In this semi-annual report progress on a fairly large number of projects is described. In general, these projects deal with electromagnetic phenomena in plasmas and plasma-like media, such as the properties of antennas, excitation of electromagnetic waves in plasmas, coupling of acoustic and electromagnetic waves, propagation through time varying, random media, electron densities in shock waves, basic kinetic theory of ionized media, instabilities in plasmas, properties of laboratory type plasmas, etc. A smaller group of projects deals with characteristics of transmitters and receivers for communication through randomly time varying media and with the problem of pattern recognition.			